University of Sussex

Engineering and Characterisation of Novel Protein Covalent Linkages in Horseradish Peroxidase (HRP): Effect on structure and function

By

Falah Al-Fartusie

(فلاح سموم الفرطوسي)

A thesis submitted for the degree of
Doctor of Philosophy (Biochemistry)
At the University of Sussex

September 2011

Declaration

I hereby declare that this thesis has not been and will not be submitted, in whole or in part, to another University for the award of any other degree.

Signed ……..

Falah Al-Fartusie

Acknowledgment

I would like to express my gratitude to all those who gave me the possibility to complete this thesis. First of all, I am deeply indebted to Prof. Andrew T. Smith whose guidance, constant support, stimulating suggestions and encouragement helped me in all the time of the research, even after he left Sussex University.

I am really grateful to and would like to thank Dr. Alaa Abdul-Sada for his help, advice and support throughout this work. During some of my darkest moments, Ali was always there for me and provided endless encouragement when it was needed most. Also, I wish to thanks Dr. Iain Day for his help during the writing of this thesis.

I would like to present my deepest gratitude to Dr. Wendy Doyle for her kind support and help. Wendy's wide knowledge and her logical way of thinking have been of great value to me. Her understanding and personal guidance have provided a good basis for the present thesis.

My gratitude is also expressed to Dr. Mark Roe and Dr. Darren Thompson, who directed me during X-ray crystallographic studies. Their assistance and guidance have been of great value to this study. I would also like to thank all members of the Smith lab group, past and present, especially Usen, Sarah, Maria and Elodie.

Finally, I would like to thank my family: mother, brothers and sisters. Really, without their support, prayer and supplication I could never have completed this stage of my life. To them and to the souls of my father and young brother (Salah) I dedicate this thesis.

Falah Al-Fartusie

SUMMARY

Both mammalian and bacterial peroxidases contain novel covalent linkages. In the former a sulfonium linkage to a critical Met residue is thought to modify the normal planarity of the haem affecting the functional properties. Following on from the work of Metcalfe *et al.*, 2004 which showed that such links could be engineered in ascorbate peroxidase, horseradish peroxidase (HRP) has been used as convenient model system to try and understand the structural and electronic effects of engineered covalent linkages. Previous work in the group (Cali, 2008) had shown that mutation of Ser167 to Met in HRP-C* resulted in autocatalytic cross-linking on incubation with hydrogen peroxide. In this thesis, two additional HRP variants, S167Y and S167W were studied and a new novel structural linkage discovered.

The UV/Vis spectrum of the S167Y variant suggested a more 6-coordinate high spin character. The molar extinction coefficients were markedly increased, 180 mM^{-1} cm^{-1} for S167Y and 135 mM^{-1} cm^{-1} for S167W, compared to 100 mM^{-1} cm^{-1} for the WT enzyme, consistent with a more 6 coordinate high spin character normally seen in lignin peroxidase. In contrast, the dissociation constant (K_d) of the S167W variant mutant for the aromatic donor BHA was hardly affected, whilst that of the S167Y variant increased two-fold relative to the WT, implying a significant perturbation of the aromatic donor binding site and / or the associated haem-linked hydrogen bonding network.

After peroxide treatment the haem group of the S167Y variant could not be extracted into acid butanone in contrast to the WT. Only a proportion of the haem could be extracted even from the untreated S167Y variant, implying that a substantial fraction of the protein had formed the haem-protein linkage during folding and purification. These results were confirmed during reverse phase HPLC and MALDI-TOF / ESI mass spectroscopy measurements. The haem and protein completely co-eluted in the case of peroxide treated S167Y, while only ~50% of the haem was linked to the protein in the untreated as isolated enzyme. The MALDI-TOF and ESI mass spectrum showed that there was a large increase (614 Da) in the mass of the linked S167Y protein, compared to that of the unlinked enzyme. Unlike the sulfonium linkage obtained earlier, treatment with hydrogen peroxide was unnecessary to observe this increase. Interestingly, the 100% unlinked S167Y protein could only be isolated if enzyme was prepared in the presence of an efficient peroxidase substrate as an antioxidant scavenger. It appears that a Tyr residue at position 167 is highly reactive with respect of the haem vinyl side chain forming a spontaneous covalent link not otherwise seen in nature.

Pre steady-state comparison of the intermediates has shown that Compound I was formed essentially normally at near WT rates, however its stability was greatly affected in the S167Y variant (linked or unlinked), the life time being decreased to ~0.04 s, compared to of the WT enzyme, where it was ~80 s. The substrate preference of the cross-linked S167Y variant was also altered. Stopped-flow measurements of the individual rate constants for the partial reactions of the catalytic cycle with luminol as reducing substrate revealed an increase in the rate of reduction of Compound I to Compound II (k_2).

The X-ray crystal structure of S167Y variant was solved to 1.7 Å resolution and the structure has been modelled and determined by x-ray crystallography. The x-ray structure reveals an unanticipated linkage containing an additional ring structure bonded to the engineered Tyr. ESI mass measurements supported this structure.

Table of Contents

List of Figures

Chapter 1:

Chapter 2:

Chapter 3:

Chapter 4:

Chapter 6:

Chapter 7:

List of Tables

List of Schemes

Abbreviation

5C-HS	Five-coordinate high spin
6C-LS	Six-coordinate low spin
ABTS	2,2´-azino-di-(3-ethyl-benzthiazoline-6sulphonic acid)
BHA	Benzhydroxamic acid
BSA	Bovine serum albumin
DEAE	Diethylaminoethyl
DHB	2,5-dihydroxybenzoic acid
EDTA	Ethylenediaminetetraacetic acid
EPO	Eosinophil peroxidase
ESI	Electrospray ionization
FA	Ferulic acid
FPLC	Fast Protein Liquid Chromatography
H_2O_2	Hydrogen peroxide
HPLC	High performance liquid chromatography
HRP	Horseradish peroxidase
HRP-C	Horseradish peroxidase isoenzyme C
IAA	Indole-3-acetic acid
IPTG	Isopropyl-β-D-thiogalactopyranoside
LPO	Lactoperoxidase
MALDI	Matrix-Assisted Laser Desorption Ionization
MeCN	Acetonitrile
MPO	Myeloperoxidase
MS	Mass spectrometry
PCR	Polymerase chain reaction
PNK	Polynucleotide kinase
rpAPX	Recombinant pea ascorbate peroxidase
RZ	Reinheitszahl number
SA	Sinapic acid
TBE	Tris-borate-EDTA
TPO	Thyroid peroxidase
WPAM	Whole Plasmid Amplification Method
α-CHCA	α-cyano-4-hydroxycinnamic acid

Chapter One:

Introduction

1.1 Peroxidases:

Peroxidases are a group of enzymes that catalyze oxidation-reduction reactions. They were among the first enzymes to be discovered, more than a century and a half ago (Dunford, 1991). In 1855 Schonbein observed the ability of the compound hydrogen peroxide (H_2O_2) to oxidise certain organic compounds such as guaiacol, which was explained later by the presence of the enzyme peroxidase. The term peroxidase was used for the first time in 1898, when Linossier used this term for the enzyme that he was isolating from pus (Azevedo *et al.*, 2003). Peroxidases are classified as oxido-reductases and are given the official [EC number 1.11.1.]. Simply, the overall reaction catalysed by peroxidases can be expressed by the following equation:

$$\text{Donor} + H_2O_2 \xrightarrow{\text{Peroxidase}} \text{oxidised donor} + 2\,H_2O$$

Peroxidases are widely distributed throughout the biological world. They are found in many plants, in many animal tissues and in micro-organisms. These enzymes carry out a variety of biosynthetic and degradative functions with the concomitant consumption of peroxide compounds as oxidant, especially H_2O_2. In addition, they are responsible for protecting cells against the accumulation of these dangerously reactive peroxide compounds, that form as side-products of oxygen metabolism (Poulos and Kraut, 1980; Arnhold *et al.*, 2006).

Toxic molecules such as superoxide radicals, hydrogen peroxide and hydroxide radicals can be found in cells as side-products of metabolic reactions that involve the reduction of O_2 (Fridovich, 1998). Oxidative phosphorylation by mitochondria is one of the major sources of these metabolic reactions, and results in the production of superoxide free radicals (Loschen *et al.*, 1974). Several enzymes are also known to produce superoxide as a side-product, including aldehyde oxidase (Rajagopalan *et al.*, 1962), cytochrome P450 reductase (Bosterling and Trudell, 1981) and xanthine oxidase (McCord and Fridovich, 1968). Therefore, the primary radical produced in biological systems is the superoxide radical. This undergoes conversion into many other radicals, including the extremely reactive hydroxyl radical. It is thus important for organisms to get rid of the superoxide toxic molecule quickly, so that other more dangerous oxidants (e.g. hydroxyl radicals) do not accumulate. This reduces the risk of cell damage that occurs due to oxygen radicals, such as lipid peroxidation of membrane walls (Bus *et al.*, 1974), DNA damage (Halliwell and Gutteridge, 1989) and protein damage (Davies, 1987; Davies *et al.*, 1987).

The major defence system against superoxide involves a family of metalloenzymes, called superoxide dismutases, by which superoxide is converted to oxygen and H_2O_2 (Fridovich, 1986). So the degradation of superoxide produces hydrogen peroxide, but while hydrogen peroxide is not as potent an oxidising agent as superoxide, it is still dangerous to the cell. Hydrogen peroxide is therefore removed by two peroxidatic types of enzyme, catalase and peroxidase (Fridovich, 1998). Catalases decompose hydrogen peroxide into water and oxygen, whereas peroxidases reduce hydrogen peroxide to water. Peroxidases act as electron acceptors when they have reacted with hydrogen peroxide, they then dissipate their oxidative potential via reaction with a variety of

substrates (Smith and Veitch, 1998). Thus, peroxidases are oxido-reductases, which use H_2O_2 as an electron acceptor for catalyzing a wide variety of oxidative reactions. The pathways of formation and decay of reactive oxygen species is shown in Scheme 1.1.

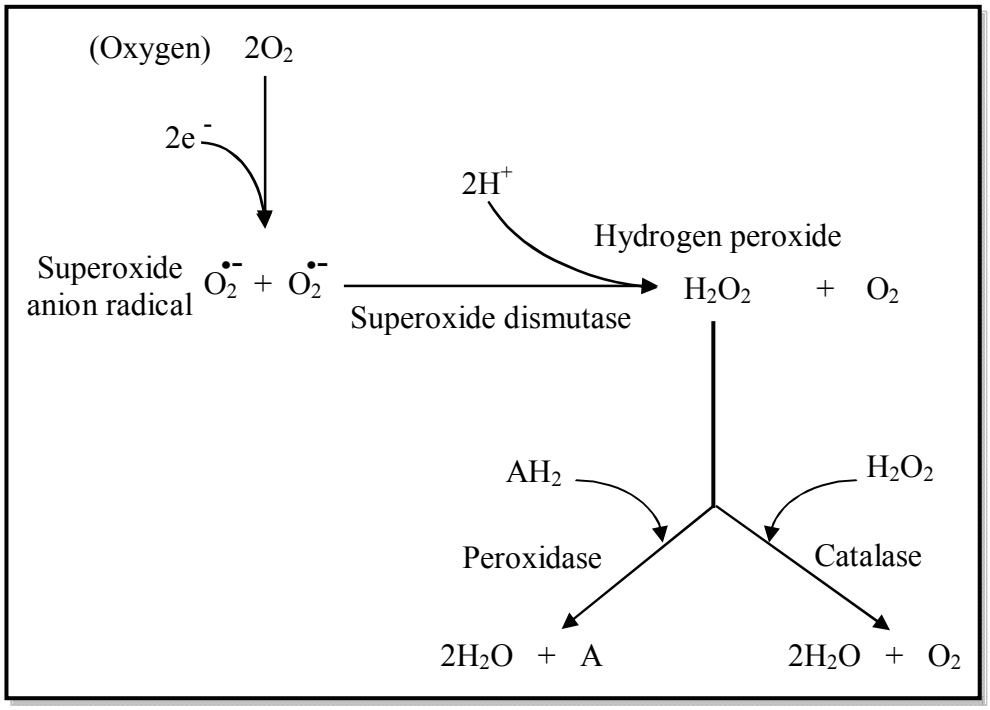

Scheme 1.1: Pathways of formation and decay of reactive oxygen species.

1.2 Classification of Peroxidases:

Peroxidases are found in animals, plant and microorganisms, and they are classified as metalloenzymes. The greater proportion of them contains the ferri-protoporphyrin IX (haem) as a prosthetic group in their active site (Smith and Veitch, 1998). On the basis of their structural and catalytic properties, haem-containing peroxidases can be divided into two main superfamilies, the mammalian peroxidase superfamily and the plant peroxidase superfamily (Figure 1.1) (Welinder, 1991; Dunford, 1999a; Dunford, 1999b). In addition, there are two further, rather indistinct groups of haem peroxidases, chloroperoxidases (Sundaramoorthy *et al.*, 1995) and the di-haem cytochrome *c* peroxidases (Fulop *et al.*, 1995).

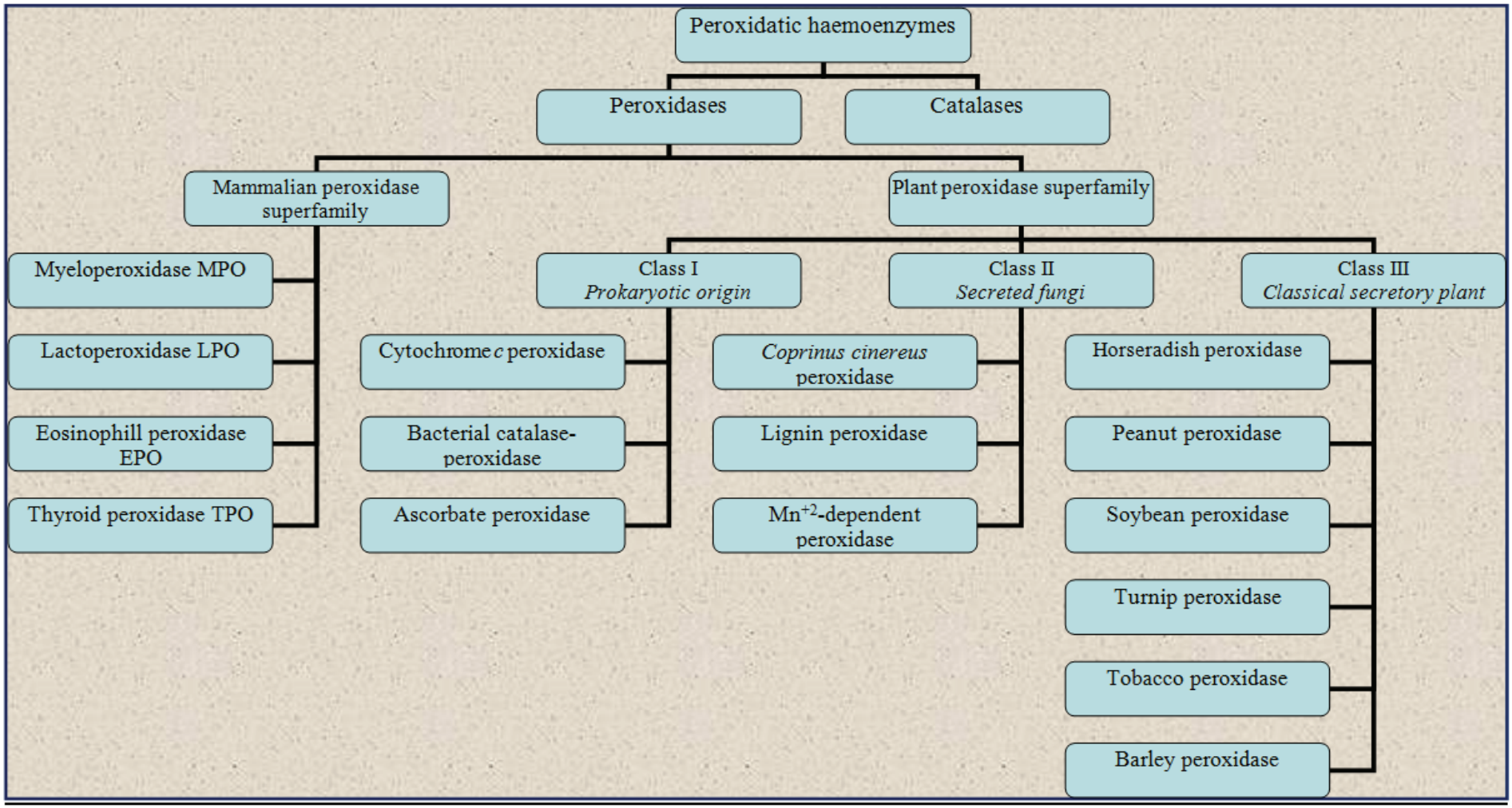

Figure 1.1: Classification of haem-peroxidases. There are two main haem peroxidase superfamilies, the plant and mammalian peroxidases.

The primary sequences and three dimensional structures of the plant and mammalian peroxidase superfamilies are quite different and distinct. The most important chemical difference between them is in the nature of the interactions that bind the apo-protein to the haem prosthetic group.

1.3 Mammalian peroxidase superfamily:

This superfamily includes enzymes such as myeloperoxidase, MPO, (EC 1.11.1.7), thyroid peroxidase, TPO, (EC 1.11.1.7), eosinophil peroxidase, EPO, (EC 1.11.1.7), lactoperoxidase, LPO, (EC1.11.1.7) and a partial region of prostaglandin endoperoxide synthase (EC 1.14.99.1) (Figure 1.1). The naming of the mammalian peroxidase superfamily derived from the fact that its members were originally identified only in mammals (Hiraga *et al.*, 2001; Zederbauer *et al.*, 2007b). Note that, although glutathione peroxidase is categorized as an animal peroxidase (Churin *et al.*, 1999), it is not a member of this superfamily and does not contain a haem group.

1.3.1 Functional importance:

The main functions of mammalian peroxidases are in host defence against infections, pathogenesis of microorganisms and hormone synthesis (Furtmuller *et al.*, 2006). MPO, EPO and LPO play a prominent role in the immune system by exerting antimicrobial effects indirectly through catalyzing the hydrogen peroxide mediated peroxidation of halide ions, particularly chloride and the pseudo-halide thiocyanate (Harrison and Schultz, 1976; Klebanoff, 1991; Thomas *et al.*, 1991; Van Dalen *et al.*, 1997), to form the powerful antimicrobial agents hypohalous and hypothiocyanous acids, respectively, as described by the following equation where X^- represents the halide or thiocyanate:

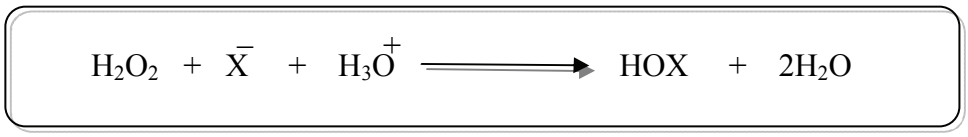

$$H_2O_2 + X^- + H_3O^+ \longrightarrow HOX + 2H_2O$$

The products of this equation are responsible for the killing of invading pathogens and viruses (Belding *et al.*, 1970; Klebanoff, 1970; Zederbauer *et al.*, 2007b). MPO is the most abundant protein present in the azurophilic granules of neutrophils and in the lysosomes of monocytes. It represents the cornerstone of cell-mediated antimicrobial activity in the innate immune system of humans (Zederbauer *et al.*, 2007b). LPO is found in human exocrine secretions, such as milk, tears and saliva, that represent the first line of protection against harmful microorganisms entering the human body (Thomas *et al.*, 1991). EPO is released from activated eosinophils and plays an important role in eliminating tissue-invasive parasites (Gleich *et al.*, 1989). In contrast, TPO has a key role in the biosynthesis of the thyroid gland hormones, thyroxin and triiodothyronine (Taurog, 1970).

1.3.2 Structures of mammalian peroxidases:

For the mammalian peroxidases, the crystal structures of MPO and LPO have been solved, while the structures of EPO and TPO are not yet known. The crystal structure of MPO became available in 1992, when Zeng and Fenna were able to determine the overall enzyme structure at 3 Å resolution by X-ray crystallography of the canine enzyme (Zeng and Fenna, 1992). After that, the X-ray crystal structure of human MPO at 2.8 Å and 2.3 Å resolution was obtained, and this structure has since been extended to 1.9 and 1.8 Å resolution using data recorded at -180 ^{o}C (Fiedler *et al.*, 2000; Blair-Johnson *et al.*, 2001; Capena *et al.*, 2009). Recently, the crystal structure of caprine (goat) LPO at 2.4 Å resolution has been determined (Singh *et al.*, 2008).

Figure (1.2) shows the overall protein fold for human MPO (Fiedler et al., 2000). Human mature MPO is a glycosylated, cationic, dimeric molecule with a single disulfide bridge between the two monomers. Each symmetry related monomer (73 kDa), contains two polypeptide chains of 14.5 and 58.5 kDa respectively, known as heavy and light chains. The heavy chain is composed of 467 amino acids and contains five intra-chain disulfide bridges, while there are 106 amino acids in the light chain with one intra-chain disulfide bridge. The secondary structure is largely α-helical, with very little β-sheet, with a total of 22 helices ranging in length from 4-29 residues (Zeng and Fenna, 1992; Fiedler *et al.*, 2000).

Human mature EPO (69.8 kDa) is a highly cationic, monomeric glycoprotein consisting of 715 amino acids. The molecule has two polypeptide chains, a 57.9 kDa heavy chain and a 11.9 kDa light chain, similar to the arrangement of the MPO monomer (Carlson *et al.*, 1985; Olsson *et al.*, 1985; Furtmuller *et al.*, 2006).

Human LPO is a predominantly α-helical single-chain polypeptide glycoprotein with molecular weight of 80 kDa. The DNA sequence of human LPO codes for a protein of 712 amino acids with an observed 51 % similarity on basis of sequence alignment with both human MPO and EPO (Langbakk and Flatmark, 1989; Ueda *et al.*, 1997). The complete amino acid sequence determination of caprine LPO shows that it is a single-chain polypeptide of 595 amino acid residues including 15 cysteine residues that form seven disulfide bridges. From X-ray data the monomeric structure is largely α-helical with only two small anti-parallel β-sheets (Singh *et al.*, 2008). Figure 1.3 depicts a schematic diagram of the caprine LPO molecule.

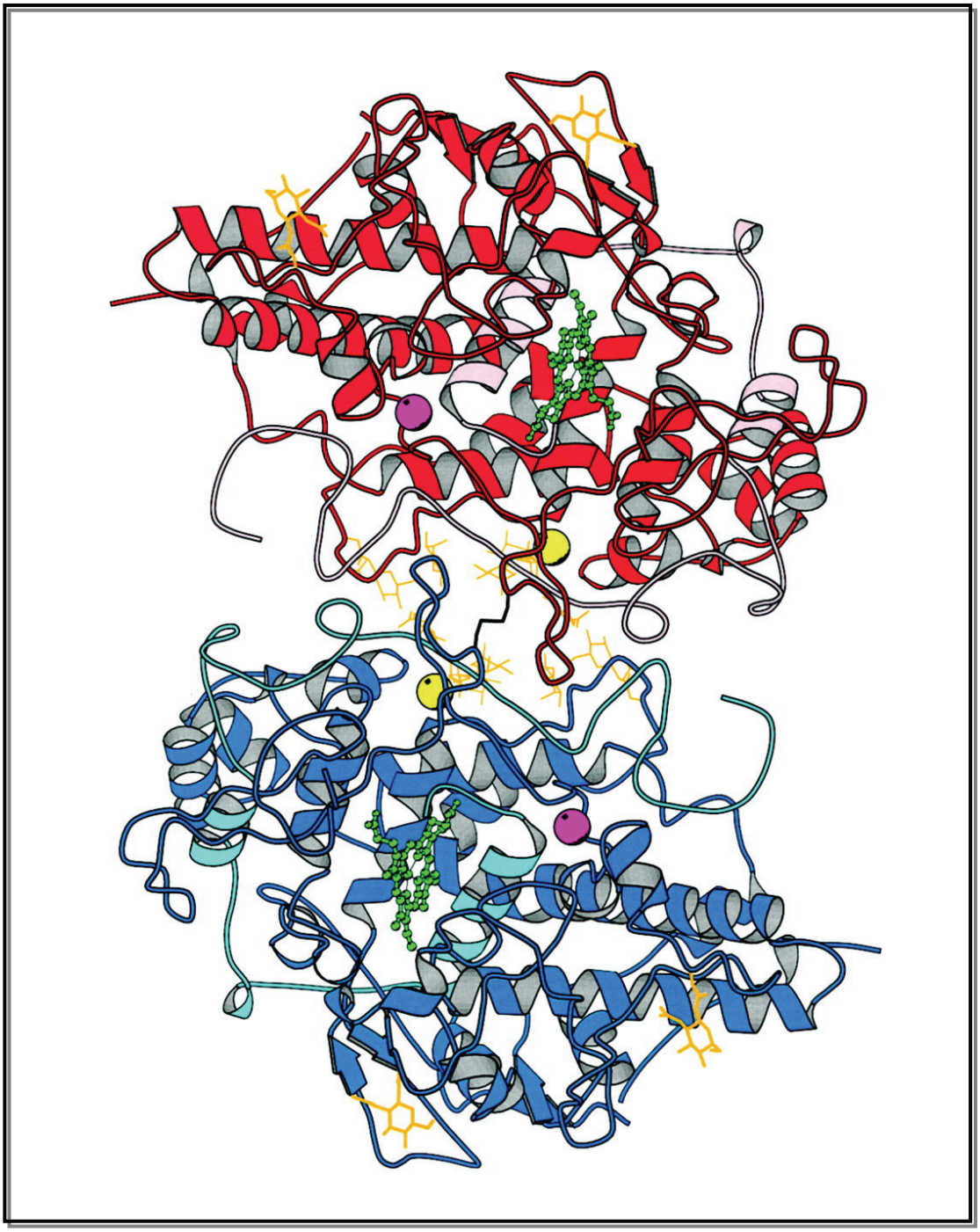

Figure 1.2: The overall protein fold for human MPO dimer. The heavy polypeptides of the two halves are coloured red and blue, whereas the light polypeptides are in a lighter shade of the same colour. Other colour coded features include: haems (green), carbohydrate (orange), calcium (pink), and chloride (yellow). At the centre of the molecule the disulfide linking the two monomers is shown in black. This figure is reproduced from Fiedler *et al.,* 2000.

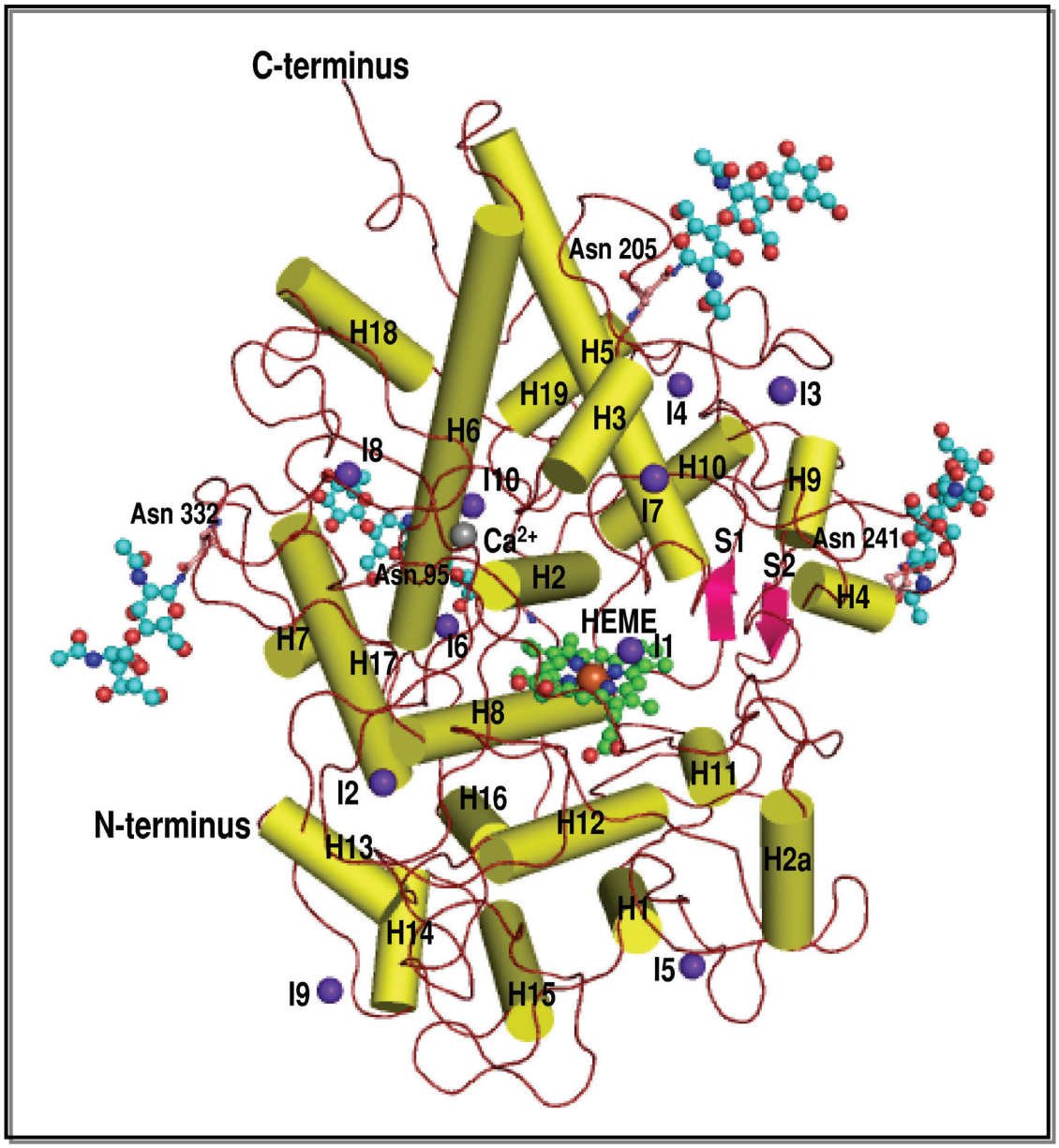

Figure 1.3: Schematic diagram of the caprine LPO monomer. α-helices are represented as cylinders, and β-sheets are indicated by arrows. The iron atom is shown as a brown-coloured sphere, iodine ions are shown as purple-coloured spheres, and the calcium ion is shown as a grey-coloured sphere. The haem moiety is indicated in CPK representation (green), and the four carbohydrate chains attached to Asn95, Asn205, Asn241, and Asn332 are shown in ball-and-stick representation. The helices have been numbered. This figure is reproduced from Singh *et al.,* 2008.

The gene for human TPO encodes a single-chain polypeptide consisting of 933 residues which has a molecular weight of approximately 100 kDa. Compared to the other mammalian peroxidases TPO has a C-terminal extension and is a type-1 glycosylated transmembrane protein (Kimura *et al.*, 1987; Baker *et al.*, 1994; Nishikawa *et al.*, 1994). In general therefore, the overall structures of the four mammalian peroxidases seem to have a similar core. Each monomer, or catalytic domain, of these peroxidases also contains one iron atom, present as a covalently bound ferri-protoporphyrin IX derivative, in addition to one calcium ion (Zederbauer *et al.*, 2007b).

1.3.3 Active site architecture of mammalian peroxidases:

The haem group is essential to the active site of all peroxidase enzymes. This group consists of a ring structure, called a tetrapyrrole ring system, complexed to a central iron atom. The pyrrole rings are linked together by methene bridges (-CH=) to create a conjugated double bond system where electrons can be shared across the whole ring. The carbon atoms of the methene bridges are located at positions α, β, γ and δ. Each pyrrole ring bears a number of different side chains; four methyl groups are located at positions 1, 3, 5 and 8, two vinyl groups at positions 2 and 4 and two propionate groups are present at positions 6 and 7 (Figure 1.4) (Dunford, 1999e).

One of the most important structural features of mammalian peroxidases is the nature of the binding of the haem group to the protein molecule. In MPO the methyl groups on pyrrole rings A and C of the protoporphyrin IX are modified to allow the formation of ester linkages with the carboxyl groups of Glu242 of the heavy polypeptide chain and Asp94 of the light polypeptide chain (human enzyme). In addition, the β-carbon of the vinyl group on pyrrole ring A forms a covalent bond with the sulfur atom of Met243 of

the heavy chain (human enzyme), giving rise to a sulfonium ion linkage (Figure 1.5). By these interactions the haem porphyrin ring is considerably distorted from planarity and takes on a bow-shaped structure (Fiedler *et al.*, 2000).

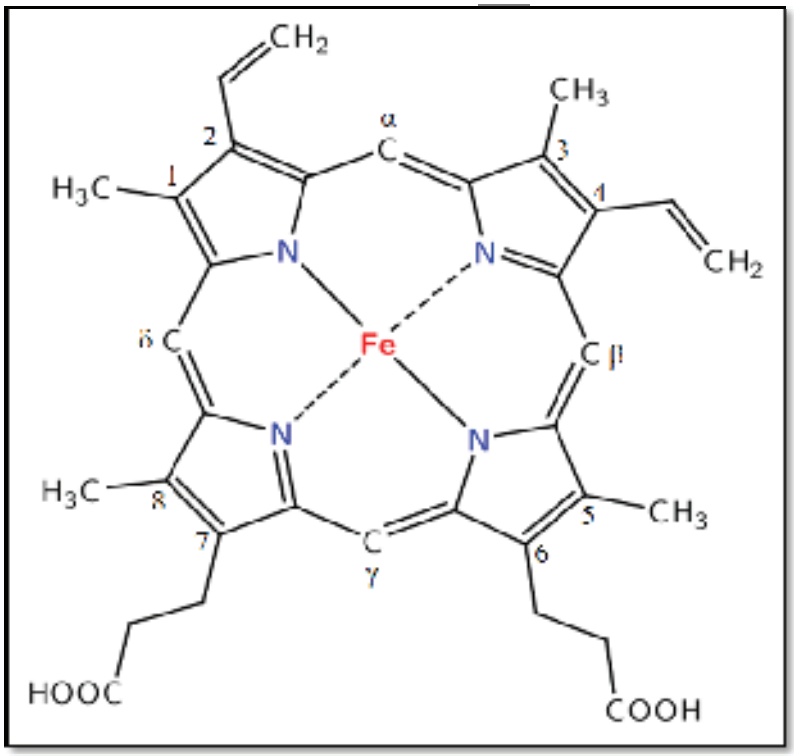

Figure 1.4: Structure of ferri-protoporphyrin IX (haem). The modified Fisher numbering system is used to describe the overall structure (Dunford, 1999e).

The full mode of haem binding revealed by Fiedler and co-workers (Fiedler *et al.*, 2000) is so far unique to MPO. Although all other members of the mammalian peroxidase superfamily contain equivalents to Asp94 and Glu242 in their sequences, they lack a methionine at positions equivalent to 243. There is a lot of biochemical and biophysical evidence which confirms the presence of haem-protein ester linkages, analogous to those of MPO, in human LPO using Asp225 and Glu375 (Andersson *et al.*, 1996; Rae and Goff, 1996; DePillis *et al.*, 1997; Suriano *et al.*, 2001; Colas *et al.*, 2002), in human EPO through Asp93 and Glu241 (Oxvig *et al.*, 1999), and in human TPO using Asp238 and Glu399 (Taurog, 1999). However, the methionine at position 243 in human MPO is

substituted by threonine in human EPO (Sakamaki *et al.*, 1989), whereas in human TPO a valine is found at this position (Kimura *et al.*, 1987); also human LPO has been shown to contain a histidine at this position (Ueda *et al.*, 1997), and in bovine LPO a glutamine is present (Cals *et al.*, 1991). Thus, the sulfonium linkage from the protein to the ring A vinyl group is a unique feature of MPO, and the presence of this positively charged sulfur atom covalently attached to a pyrrole ring vinyl group may be responsible for the unusual spectral properties that distinguish this protein from other mammalian peroxidases (Fenna *et al.*, 1995). It is important to note here that all covalent links between the haem and the protein lie on the distal side of the haem group.

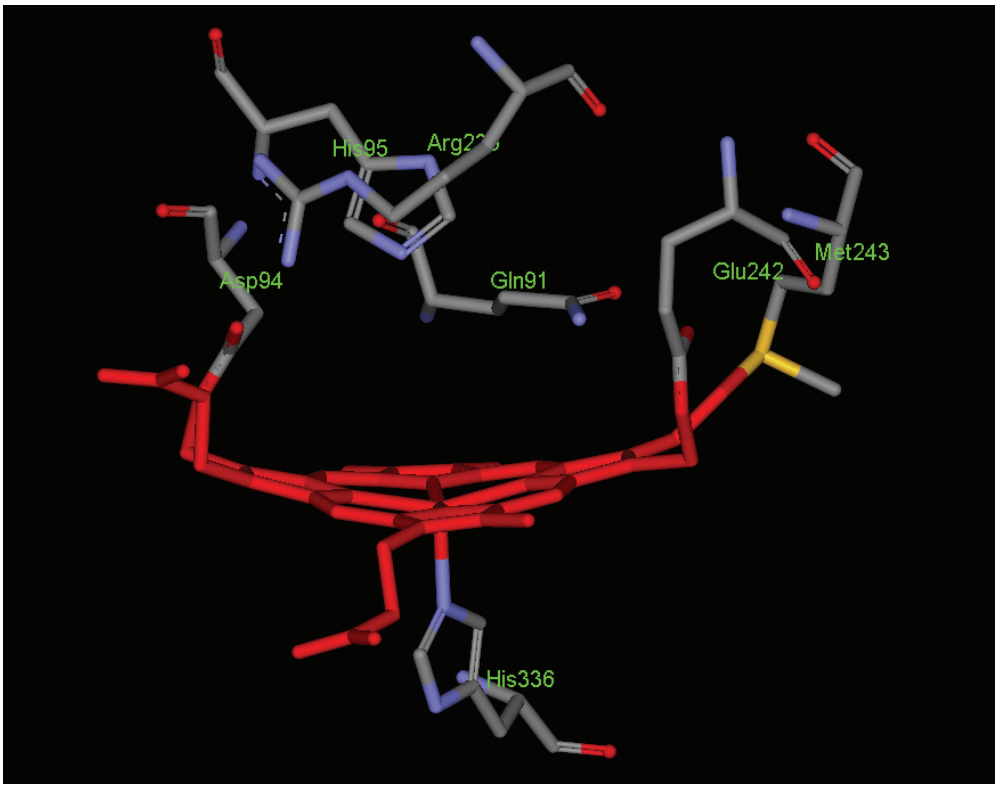

Figure 1.5: The non-planar porphyrin ring in human MPO and its covalent attachments to the protein via two ester bonds [Asp94 and Glu242] and one sulfonium linkage [Met243]. In addition the catalytic residues His95, Arg239, and Gln91 are shown, the latter being important in halide binding. The figure was constructed by Accelrys DS visualizer using the coordinates deposited in the PDB (accession code 1CXP).

1.3.4 Spectral features of mammalian peroxidases:

In the haem of haemoproteins, there are four coordination positions in a plane around the iron atom which are occupied by nitrogen atoms of the porphyrin, and the fifth coordination position at least, and possibly the sixth position also, is occupied by a donor group from the protein. In peroxidases, the fifth position is occupied generally by a nitrogen atom of the imidazole group of a histidine residue (referred to as the proximal histidine). Two main spin states are found for the ferri-protoporphyrin of peroxidases. The first has the spin moment of five unpaired electrons (spin 5/2) and is called the high spin state, while the second has only one unpaired electron (spin 1/2) and is called the low spin state (Brill and Williams, 1961).

The electronic absorption spectra of haem proteins are characterised by the presence of two groups of intense bands. The first group, which includes Soret, α and β bands, is due to transitions of the π-electrons of the haem porphyrin group, while the second group consisting of two bands, one at about 600-650 nm (CTI) and the other at 450-500 nm (CTII), is due to charge transfer to the high spin Fe^{3+} ion. The analysis of absorption spectra therefore allows one to establish the coordination and spin-state(s) of the haem iron atom, on the basis of correlation with structurally characterised proteins and model compounds. Both high and low spin states show typical Soret, α and β bands. The intensity of the α and β bands is low in the high spin state, and they are often obscured by the charge transfer bands, while the charge transfer bands are absent in the low spin state. The intensity of the α band in the low spin state is very dependent on the character of the fifth and sixth ligands, but the β band intensity is almost independent of the fifth and sixth ligands (Brill and Williams, 1961).

The unusual, additional, haem-protein covalent binding in mammalian peroxidases is responsible for their peculiar spectroscopic properties. The Soret bands of the visible absorption spectra of mammalian peroxidases are characteristically red-shifted with respect to those seen for other haem proteins, and this spectral shift has generally been ascribed to the influence of the protein environment on the spectral properties of the haem. LPO, TPO and EPO have two ester bonds in their structures between the haem and protein. MPO is distinctive from other mammalian peroxidases in that it forms an extra covalent sulfonium ion linkage between the haem and protein. This difference in the number of linkages that bind the protein with the haem has been interpreted as the major factor that contributes to the variation in optical properties between MPO and other mammalian peroxidases (Fiedler *et al.*, 2000; Zederbauer *et al.*, 2007b).

Spectral analysis of LPO shows that the Soret band is fairly sharp with a maximum at 412 nm, and the visible spectrum also exhibits maxima at 501, 542, 595, and 631 nm. The width and wavelength of the Soret band, as well as the wavelength of CT1 at 631 nm are characteristic of a six-coordinate (6C) high-spin (HS) ferric haem (Eaton and Hochstrasser, 1967; Sievers, 1980; Zederbauer *et al.*, 2007b). The spectral features of both EPO and TPO are very similar to that of LPO (Table 1.1). The absorption maxima of MPO are red shifted compared to other mammalian peroxidases, and are responsible for the characteristic green colour of the enzyme. The visible spectrum displays a Soret band at 428 nm, with additional maxima at 498, 570, 622 and 690 nm (Andrews and Krinsky, 1981; Wever and Plat, 1981). Important in this regard, it is noteworthy that replacement of Met243 (the residue responsible for the sulfonium linkage) in MPO produces an enzyme that exhibits a Soret band at 410–412 nm, considerably blue-shifted from the 428 nm band of the native enzyme and similar to those of the other

mammalian peroxidases (Jacquet *et al.*, 1994; Kooter *et al.*, 1997a; Kooter *et al.*, 1999b). Similarly, the E242Q mutant of MPO, presumably lacking one of the haem-protein ester bonds, exhibits a blue-shifted Soret band at 416–418 nm, and the mutants D94N and D94V, presumed to lack the other ester bond, also have a blue-shifted Soret band at 413-414 nm (Jacquet *et al.*, 1994; Floris *et al.*, 1995; Kooter *et al.*, 1999a). These studies strongly suggest that the presence of one more linkage from the haem to the protein in MPO is responsible for its unusual spectral properties.

Table 1.1: Electronic absorption spectra data of native mammalian peroxidases and some mutants of MPO.

Enzyme	Soret peak (nm)	CTI (nm)	CTII (nm)	α band (nm)	β band (nm)
LPO[a]	412	631	501	595	542
EPO[b]	413	638	500	580	542
TPO[c]	412	638	496	582	547
MPO[d,e]	428	690	498	622	570
M243T MPO[f]	413	690	502	590	548
D94V MPO[g]	413, 428	682	596	620	568
E242Q MPO[h]	418	665	508	647	554

[a](Sievers, 1980), [b](Furtmuller *et al.,* 2006), [c](Dunford, 1999c), [d](Zederbauer *et al.,* 2007b), [e](Wever and Plat, 1981), [f](Kooter *et al.*, 1999c), [g](Kooter *et al.,* 1999a), [h](Kooter *et al.,* 1999b).

It is also clearly evident that the extra haem-protein covalent linkages are important in maintaining the catalytic activities of mammalian peroxidases. The catalytic properties

of mutants of human MPO, in which residues involved in the covalent ester or sulfonium haem attachments were replaced, were found to be markedly different from those of the native enzyme. Mutation of Met243 had a huge effect on the activity of the enzyme, neither the M243Q nor the E242Q mutants showed chlorination activity and both mutants had reduced catalytic activities when substrates for single electron oxidation reactions were used. In addition, the D94N mutant had about 30% peroxidase activity while the D94V mutant had activity at even lower levels (a small percentage activity was observed) (Floris *et al.*, 1995; Kooter *et al.*, 1997a; Kooter *et al.*, 1999a; Kooter *et al.*, 1999b).

1.3.5 Mechanism of action of mammalian peroxidases:

Mammalian peroxidases efficiently catalyze both oxidation and halogenation cycles, producing oxidizing and halogenating agents. The first step of these cycles is the reaction of the ferric haem [Fe(III)] form of the peroxidase with hydrogen peroxide to form a redox intermediate called Compound I (Step 1). Compound I, which has a porphyrin π-cation radical and an oxygen atom coupled by a double bond to Fe (IV), contains two oxidizing equivalents more than the resting enzyme (Dolphin and Felton, 1974; Marquez *et al.*, 1994).

$$\underset{\text{Native enzyme}}{PorFe(III) + H_2O_2} \longrightarrow \underset{\text{Compound I}}{{}^{\bullet+}PorFe(IV)=O + H_2O} \qquad \text{Step 1}$$

Under physiological conditions, mammalian peroxidases are characterised by their ability to oxidise halides and thiocyanate into hypohalous and hypothiocyanous acids, respectively, with concomitant reduction of Compound I in a two-electron step back to

the ferric enzyme form (Step 2, where: X^- represents the halide or thiocyanate and HOX the corresponding acid).

$$^{\bullet+}\text{PorFe(IV)=O} + X^- + H^+ \longrightarrow \text{PorFe(III)} + \text{HOX} \qquad \text{Step 2}$$

This step along with step 1 above is the fall halogenation cycle (Figure 1.6). The electron donors can be arranged by the ease of oxidation as follows: $SCN^- > I^- > Br^- > Cl^-$ (Arnhold *et al.*, 2006). All haem peroxidases, including plant superfamily peroxidases without extra covalent haem links, can oxidise iodide and thiocyanate. The more difficult oxidation of bromide is catalyzed by mammalian peroxidases, but with less efficiency also by the plant peroxidases (Munir and Dordick, 2000). However, MPO Compound I is the only one that is capable of oxidizing chloride at pH 7.0 (Marquez *et al.*, 1994; Furtmuller *et al.*, 1998), by a mechanism that includes a Compound I-chloride intermediate. At low chloride concentration, the formation of Compound I-chloride is rate limiting, while at high chloride concentration the transition back to native enzyme and the formation of the hypochlorous acid is rate controlling (Furtmuller *et al.*, 2000). It has been observed that the presence of the sulfonium linkage in human MPO has a significant role to play in chloride oxidation. Mutation of Met243 into Thr, Gln or Val (the corresponding residues in EPO, LPO and TPO) all had a dramatic effect on the overall chlorination activity. With the exception of M243T, all variants completely lost their chlorination activity (Kooter *et al.*, 1999b). In addition, it was found that replacement of the ester residue Glu242 by Gln lead to a decrease in the overall chlorination and bromination activity to 20% and 24%, respectively, compared to wild-type recombinant MPO. The variants D94N and D94V have also been shown to have a chlorination activity substantially lower than that of wild-type MPO (Kooter *et*

al., 1999a; Zederbauer *et al.*, 2005; Zederbauer *et al.*, 2007a). Also, the peroxidative activity of recombinant LPO was shown to be highly dependent on the number of esters to the haem in the enzyme (DePillis *et al.*, 1997).

Compound I of mammalian peroxidases can also react with numerous other substrates, including tyrosine, tryptophan, nitrite, phenol and indole derivatives, by two consecutive one-electron steps to produce the ferric enzyme again. This process involves the formation of a second intermediate called Compound II [PorFe(IV)=O], and leads to the formation of substrate free radicals as shown in the following, Steps 3 and 4.

$$^{\bullet+}\text{PorFe(IV)=O} + AH_2 \longrightarrow \underset{\text{Compound II}}{\text{PorFe(IV)=O}} + {}^{\bullet}AH + H^+ \quad \text{Step 3}$$

$$\text{PorFe(IV)=O} + AH_2 + H^+ \longrightarrow \text{PorFe(III)} + {}^{\bullet}AH + H_2O \quad \text{Step 4}$$

These two steps, in addition to the oxidation of the ferric enzyme by hydrogen peroxide (Step 1), are combined to form the peroxidase cycle (Figure 1.6) (Marquez and Dunford, 1995; Burner *et al.*, 1999; Jantschko *et al.*, 2002; Zederbauer *et al.*, 2007b).

Finally, in the absence of one-electron donors, a third enzyme state named Compound III is formed slowly. This can occur either by reaction of Compound II with hydrogen peroxide (Step 5) or by the fast reaction of superoxide with native enzyme (Step 6) (Dunford, 1999d).

$$\text{PorFe(IV)=O} + H_2O_2 \longrightarrow \underset{\text{Compound III}}{\text{PorFe(II)}O_2} + H_2O \quad \text{Step 5}$$

$$\text{PorFe(III)} + O_2^{\bullet-} \longrightarrow \text{PorFe(II)}O_2 \quad \text{Step 6}$$

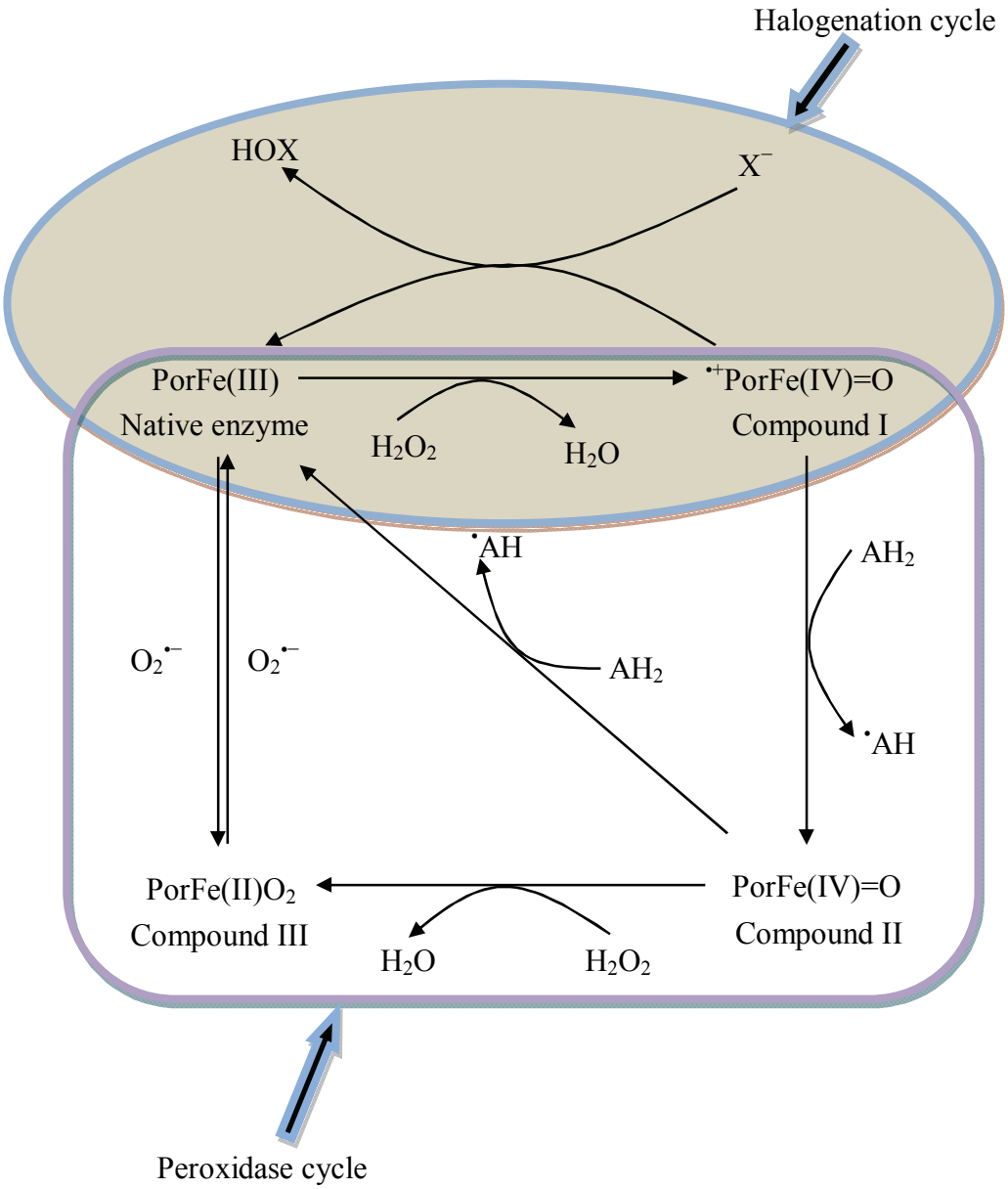

Figure 1.6: The overall reaction mechanisms of mammalian peroxidases. Both halogenation and peroxidase cycles utilize hydrogen peroxide to oxidise the native ferric peroxidase to Compound I. AH_2 and $^{\bullet}AH$ represent substrate being oxidised and the formed radical product, respectively. X^- represents halide or thiocyanate and HOX the corresponding acid.

1.4. Plant peroxidase superfamily:

The second superfamily of peroxidases, the plant peroxidase superfamily, consists of peroxidases from plants, fungi, bacteria and yeast. This superfamily has been further subdivided on the basis of sequence and structural homology into three classes (Figure 1.1) (Welinder *et al.*, 1992).

1.4.1. Class I. Peroxidases of prokaryotic origin: These include the intracellular enzymes in plants, bacteria and yeast, such as microbial cytochrome *c* peroxidase (EC 1.11.1.5), bacterial catalase-peroxidase (EC 1.11.1.6) and ascorbate peroxidase (EC 1.11.1.11). In fact, ascorbate peroxidase is not plant-specific, it has also been isolated and purified successfully from the bovine eye with the N-terminal sequence of the purified enzyme showing a very high homology to plant enzymes (Wada *et al.*, 1998). Class I peroxidases are characterised by the fact that they do not have glycosylation, cysteine disulphide bridges, calcium ions or N-terminal signal sequences for secretion. It was observed that the Trp191 residue of the yeast cytochrome *c* peroxidase appears to be conserved in other Class I peroxidases (Welinder, 1992; Dunford, 1999b).

1.4.2 Class II. Secreted fungal peroxidases: These are extracellular peroxidases from fungi, including *Coprinus cinereus* peroxidase, CiP, (EC 1.11.1.7), lignin peroxidase, LiP, (EC 1.11.1.14) and Mn^{+2}-dependent peroxidase, MnP, (EC 1.11.1.13). Unlike the Class I peroxidases, the fungi secretory peroxidases are characterised by having an N-terminal signal sequence for secretion. Also, they have about 5% carbohydrate, two calcium ions and four conserved disulfide bridges in their structure (Welinder, 1992). Tyrosine residues are rare in Class II peroxidases, appearing once

only in lignin peroxidases, and absent from other class members. Class II peroxidases have an additional 40 to 60 amino acid residues at their C-termini, compared to the peroxidases in other classes (Welinder, 1992).

1.4.3 Class III. Classical secretory plant peroxidases: The most intensively studied and well known enzyme in this class is horseradish peroxidase (HRP, EC 1.11.1.7). Besides the structure of horseradish peroxidase, HRP, other known Class III structures are those for peanut peroxidase, PNP, (Schuller *et al.*, 1996), soybean peroxidase, SoP, (Puppo *et al.*, 1980), turnip peroxidase, TuP, (Hosoya, 1960), tobacco peroxidase, TobP, (Mader and Fussl, 1982) and barley peroxidase, BaP, (Henriksen *et al.*, 1998b). Similarly to Class II peroxidases, the Class III peroxidases contain two ions of calcium, an amino-terminal signal sequence for secretion and four conserved disulfide bridges. In addition, they have extra helices that play a role in restricting access to the haem edge and binding aromatic electron donor molecules. The carbohydrate content in their structures ranges between 0-25% (Welinder *et al.*, 1992).

A comparison of the structures of plant peroxidase superfamily enzymes shows that all members contain 10 common α-helices, which can be considered as two five-helical structures, one the distal domain, and the other the proximal domain. Members of Classes I and II have one extra helix unique to their Class, whilst there are three extra helices found in Class III peroxidases, two of these three helices, F and F" are involved in the substrate access channel leading to the edge of the haem (Schuller *et al.*, 1996; Gajhede *et al.*, 1997).

1.5 Horseradish Peroxidase:

1.5.1 Horseradish:

The horseradish (*Armoracia rusticana*) belongs to the family Brassicaceae (*Crusiferae*). Horseradish is a hardy perennial herb cultivated in temperate regions of the world, particularly, South-Eastern Europe, Western Asia and North America. Principal production areas are located in the USA and, to a lesser extent, Europe. The plant grows up to 1.5 metres tall and is mainly cultivated for its large white root, which grows entirely underground to about 1 metre. The root contains a pungent, acrid and vesicating volatile oil. It also contains useful minerals including calcium, sodium, magnesium and vitamin C; the fresh root contains an average of 302 mg per 100 g vitamin C (Peter, 2004).

Horseradish is the only natural source of horseradish peroxidase. Production of the enzyme from horseradish roots occurs on a relatively large scale due to its commercial uses; it is used in diagnostic, analytical, biochemical and biotechnological applications, for example as a component of clinical diagnostic kits, and for immunoassays (Tijssen and Kurstak, 1984; Maidan and Heller, 1992; Garguilo *et al.*, 1993; Veitch, 2004).

1.5.2 General introduction to the enzyme:

Horseradish peroxidase (HRP, EC 1.11.1.7), is one of the most important haem-containing enzymes obtained from a plant source and has been studied for more than a century. The first observation of a reaction catalysed by horseradish peroxidase was by Lois Antonie Planche when he mentioned it in his note of 1810 (Veitch and Smith, 2001; Veitch, 2004).

Horseradish peroxidase is not one enzyme, but a group of isoenzymes. As long ago as 1958, five isoenzymes had been isolated from horseradish root using carboxymethylcellulose chromatography, called HRP A, B, C, D and E (Paul, 1958). In 1966 seven isoenzymes were isolated and purified using DEAE-cellulose chromatography, where HRP-A could be further resolved into three fractions called A1, A2 and A3 (Shannon *et al.*, 1966). Since then, more than 40 isoenzymes have been identified and they are divided into groups according to their isoelectric points. The acidic group contains A1, A2 and A3 isoenzymes, the neutral group contains B and C isoenzymes and the basic group contains D and E isoenzymes (Kay *et al.*, 1967; Shin *et al.*, 1971; Veitch and Smith, 2001). HRP-C is the most abundant isoenzyme isolated from horseradish root. Significant progress has been made on HRP-C structure and function since 1990, after a recombinant form of the enzyme, HRP-C*, was expressed successfully in *E. coli* and refolded *in vitro* (Smith *et al.*, 1990). Native HRP-C enzyme has 18-22% carbohydrate, attached to the enzyme through eight asparagine residues Asn13, Asn57, Asn158, Asn186, Asn198, Asn214, Asn255 and Asn268, evenly distributed over the surface of protein but with some heterogeneity (Chance and Maehly, 1955; Welinder and Mazza, 1975; Welinder, 1976; Welinder, 1979).

1.5.3 Structure of horseradish peroxidase:

1.5.3.1 General features:

HRP-C was completely sequenced in 1976 (Welinder, 1976), although the first solution of its three dimensional structure using X-ray crystallography was not achieved until 1997 on the recombinant enzyme HRP-C* (Figure 1.7) (Gajhede *et al.*, 1997). The enzyme has been characterised as a single polypeptide chain with 308 amino acid

Figure 1.7: Ribbon representation of HRP-C* structure. Helices are shown in red colour while the small region of β structure is shown as a light blue arrow. The haem group is shown in red. The structure also has two calcium ions in green. The figure was constructed by Accelrys DS visualizer using the coordinates deposited in the PDB (accession code 2ATJ).

residues, folded into the 10 core α helices plus 3 extra helices and molecular weight of 33,890 Da (Welinder, 1979). It has four disulfide bridges Cys11–Cys91, Cys44–Cys49, Cys97–Cys301 and Cys177–Cys209 (Welinder, 1976). Two different types of metal centre are found in HRP-C, which play essential roles in the structural and functional integrity of the enzyme; these are iron (III) protoporphyrin IX and two calcium ions (Haschke and Friedhoff, 1978; Shiro *et al.*, 1986; Gajhede *et al.*, 1997).

1.5.3.2 Haem prosthetic group:

HRP-C contains iron (III) protoporphyrin IX (ferri-protoporphyrin IX), i.e. a haem group, as a prosthetic group in its active site. In addition to the four coordination positions with the nitrogen atoms of the porphyrin pyrrole rings, the haem iron has two axial coordination sites (the fifth and sixth positions) where binding can also occur. The haem group is attached to the protein at the fifth position through a covalent bond between the iron atom and the Nε2 atom of His170 (proximal histidine). The sixth coordination site is essentially unoccupied in the resting state of the enzyme (Veitch and Smith, 2001; Veitch, 2004). Indeed, this is the only covalent link between the haem prosthetic group and the protein; there are no additional covalent linkages observed similar to those in mammalian peroxidases between the protein and porphyrin (Kooter *et al.*, 1997b). Nevertheless, between the haem group and the protein there is a hydrogen bonding network, between the propionate groups and the amino acid side chains of Glu176, Ser73, Ser35 and Arg31 (Gajhede *et al.*, 1997).

The spin state of the Fe (III) in the haem group depends greatly on the orbital occupancy of its ***d***-orbital electrons. The nature of this occupancy is influenced by the ligand bond electrons at the fifth and sixth iron atom positions (Dunford, 1999f). In HRP, the ferric

iron has five unpaired electrons in the ***d***-orbital (spin 5/2) and is referred to as high spin. Indeed, it is reasonable to state that the dominant species of the resting state of HRP-C is five-coordinate high spin (5C-HS), although a small amount of six-coordinate high spin haem (6C-HS) can be detected. In the presence of a ligand in the sixth coordination site of the ferric iron, the spin state is affected due to the impact of the ligand field on the distribution of electrons in the ***d***-orbital (paired or unpaired). If the ligand field is 'weak', such as with a fluoride ligand, the electrons in the ***d***-orbital are not affected too much and remain unpaired, and as a result the state is described as 6C-HS. However, in the presence of a 'strong' ligand like cyanide, the ligand field will force the electrons to be paired in the ***d***-orbital, and therefore only one electron remains unpaired (spin 1/2), this state is described as 6C-LS (Dunford, 1999f; Veitch and Smith, 2001).

1.5.3.3 The active site structure of HRP-C:

The distal (the region of the enzyme lying above the plane of the haem when viewed in the usual orientation) and proximal (the region lying below the plane of the haem) domains of HRP-C contain residues crucial to the function of the active site of the enzyme (Figure 1.8) and are described in detail below.

1.5.3.3.1 Proximal region:

In the proximal domain, the His170 residue is considered the most important residue for catalysis which, as noted previously, is covalently bonded to the haem iron. In addition, there is the Asp247 residue, which forms a hydrogen bond via its carboxylate side chain with the His170 Nδ1. The strength of this interaction controls the basicity of the proximal histidine and also maintains the resting state haem in its five-coordinated state.

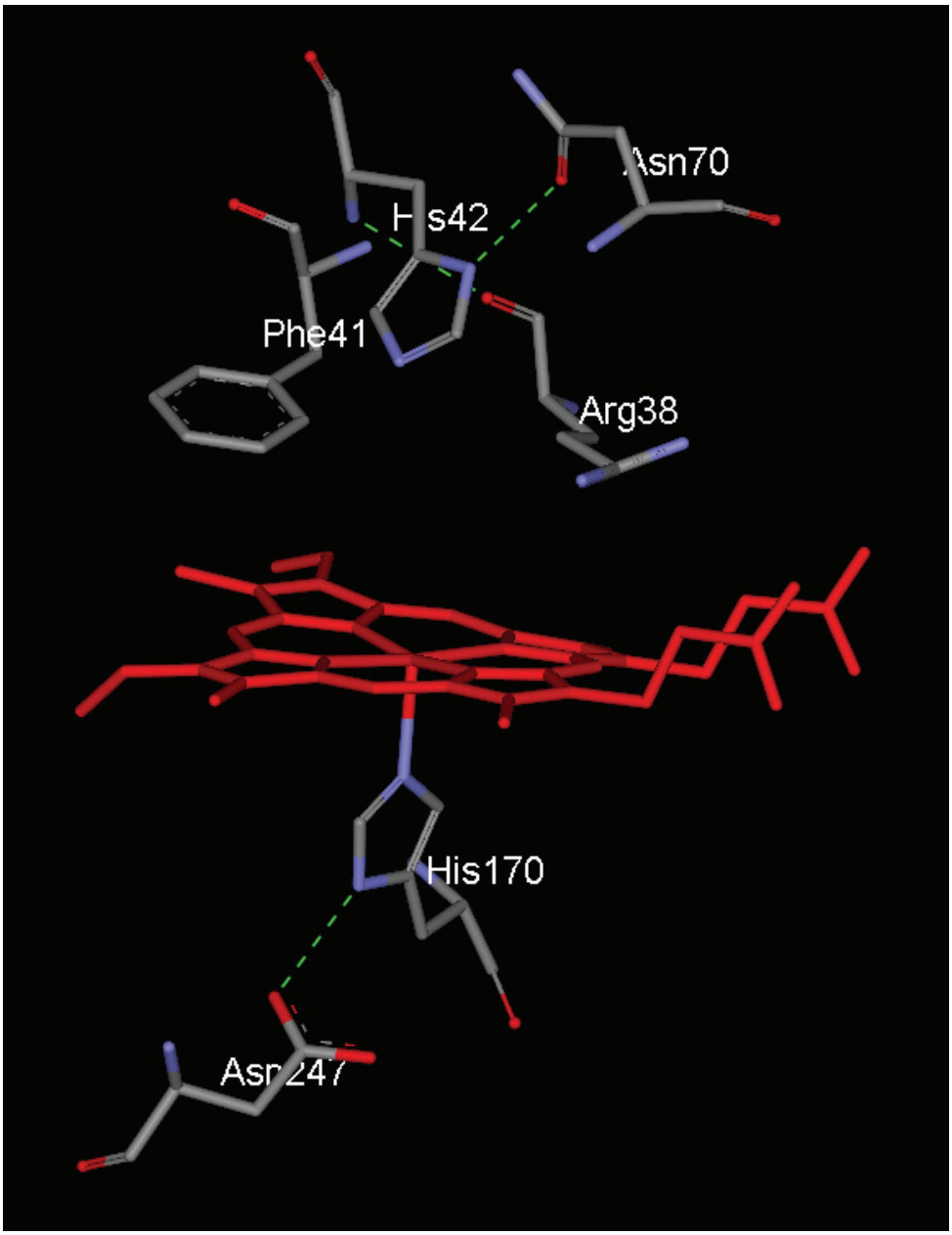

Figure 1.8: Haem and catalytic residues in the active site of HRP-C. The haem group (shown in red colour) is coordinated to the proximal histidine His170. The sixth coordination site distal to the haem group is vacant. The figure shows the location of important distal site residues Arg38, Phe41, His42 and Asn70. The figure was constructed by Accelrys DS visualizer using the coordinates deposited in the PDB (accession code 2ATJ).

It was found that the imidazole ring of His170 is tightly stacked against the side chain of Phe221 (Gajhede *et al.*, 1997), and the loss of this π–π interaction leads to a perturbation of the haem pocket in the enzyme (Howes *et al.*, 2001c). The role of the proximal histidine ligand in peroxidase function has been studied by replacing His170 with alanine. It was observed that the reaction of H170A variant with H_2O_2 did not give any spectroscopically detectable Compound I or Compound II but resulted in the gradual degradation of the haem group. The activity of the mutant could be partially rescued by the addition of exogenous imidazole (Newmyer *et al.*, 1996b). This has also been shown for other peroxidases of the plant peroxidase superfamily (Goodin and McRee, 1993).

1.5.3.3.2 Distal region:

The distal region of HRP-C contains a number of amino acid residues that have an essential role in catalysis; these include Arg38, Phe41, His42 and Asp70 (Figure 1.8). Two of these residues Arg38 and His42 are conserved in all plant peroxidases and are known to play a role in the acid-base catalytic cleavage of the O-O bond of peroxide during the process of Compound I formation. The catalytic role of the histidine residue in the formation of the Compound I intermediate was first proposed in 1980 by Poulos and Kraut (Poulos and Kraut, 1980), and then confirmed in 1993 by Erman and co-workers when they found that the replacement of histidine by leucine caused a reduction of 10^5 fold in the rate of Compound I formation (Erman *et al.*, 1993).

It has since been shown that the rate of Compound I formation is drastically decreased by more than five orders of magnitude when His42 is replaced by other non-polar residues, such as Ala or Val (Newmyer and Ortiz de Montellano, 1995; Newmyer and

Ortiz de Montellano, 1995; Rodriguez-Lopez *et al.*, 1996a). The addition of exogenous imidazole (2-substituted imidazoles) partially rescues both the rate of Compound I formation and the peroxidase activity of the H42A mutant (Newmyer and Ortiz de Montellano, 1996a). The catalytic activity can also be partially rescued by the introduction of another histidine residue in a different position as with the double mutant [H42A:F41H] HRP (Savenkova *et al.*, 1996) and [H42V:R38H] HRP (Savenkova *et al.*, 1998). In Chloroperoxidase, a versatile but unusual haem-containing peroxidase, the catalytic base used to assist in the process of O-O bond cleavage during Compound I formation is a glutamic acid residue rather than histidine (Sundaramoorthy *et al.*, 1995). Thus, the effect of replacing His42 with glutamic acid, to give an enzyme that mimics in part the distal pocket of chloroperoxidase, has been investigated (Tanaka *et al.*, 1996; Jennings, 1998). An intermediate rate of Compound I formation can be achieved with H42E, suggesting that this residue can act as an alternative proton acceptor, although it is only weakly basic (Veitch and Smith, 2001).

The catalytic role of Arg38 in HRP-C has also been investigated through site directed mutagenesis. The importance of Arg38 comes from its ability to stabilise the transition state intermediate Compound 0 (hydroperoxide complex) during the formation of Compound I (Rodriguez-Lopez *et al.*, 1996a; Rodriguez-Lopez *et al.*, 1996b). In the case of the R38L mutant, the absence of the Arg residue at position 38 leads to a decrease in the rate of Compound I formation, but not as drastically as in the His42 mutants (Rodriguez-Lopez *et al.*, 1996a). Similar results were reported for the R38L mutant, where it was found that there was a 500-fold decrease in Compound I formation compared to the wild type enzyme (Smith *et al.*, 1993). The double mutant H42E:R38S

proved the importance of these two residues in the catalytic reduction of H_2O_2, as it shows one of the slowest rates of Compound I formation known (Meno *et al.*, 2002).

It has been observed that the presence of the hydrogen bond between the His42 Nδ1 hydrogen and Asn70 Oδ1 oxygen plays an important role in maintaining the basicity and alignment of the catalytic His42 residue, and fixes it in the correct position for participation in the acid-base catalytic reduction of H_2O_2 (Nagano *et al.*, 1995; Nagano *et al.*, 1996; Tanaka *et al.*, 1997). Disruption of this hydrogen bond, as in N70D and N70V variants, leads to a presumed decrease in the basicity of His42 and decreases the rate of Compound I formation (Nagano *et al.*, 1996).

1.5.3.4 Calcium binding sites:

Calcium ions are the most abundant metal ions found in proteins. They have the ability to bind to oxygen containing ligands, with a coordination number of 6 or 7. All plant peroxidases in Classes II and III contain two calcium binding sites, one proximal and the other distal to the haem plane. In HRP-C, the coordination number of each calcium ion is seven. The distal calcium is coordinated with oxygen-donor ligands provided from the side chain carboxylates of Asp43 and Asp50, the side chain hydroxyl of Ser52, the backbone carbonyls of Asp43, Val46 and Gly48 and the structural water molecule W15 (Figure 1.9). The proximal calcium is coordinated with oxygen-donor ligands provided from the side chain carboxylates of Asp222 and Asp230, the side chain hydroxyls of Thr171 and Thr225, and the backbone carbonyls of Thr171, Thr225 and Ile228 (Veitch and Smith, 2001; Azevedo *et al.*, 2003). In addition, there is a hydrogen bond connection between the distal calcium binding site and the distal haem pocket, as besides coordination with calcium, W15 is also hydrogen bonded to the Oε1 of Glu64

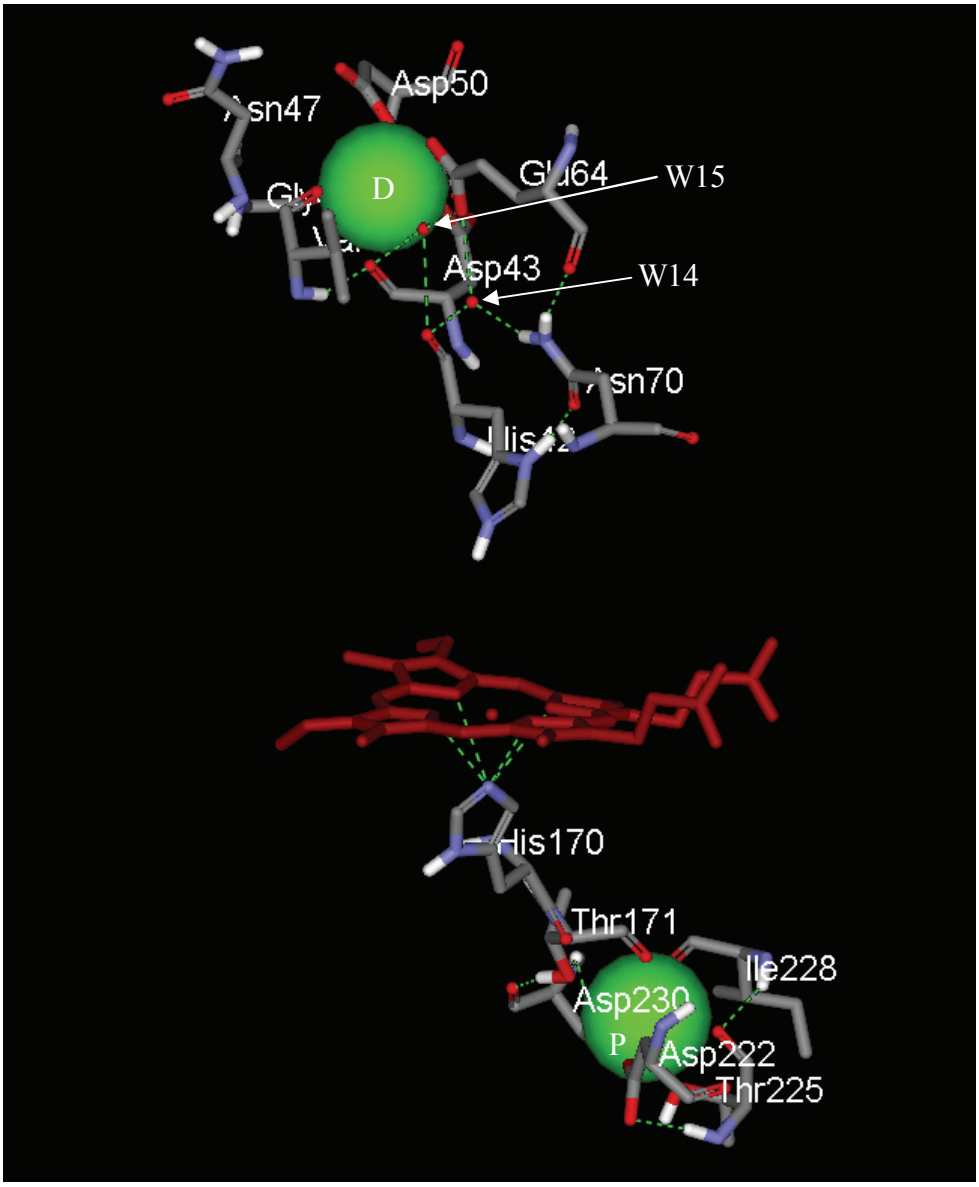

Figure 1.9: Calcium binding sites in HRP-C*. The haem group is shown in red with distal (D) and proximal (P) calcium ions shown in green. The hydrogen bonding linkages are shown in green colour also. The figure was constructed by Accelrys DS visualizer using the coordinates deposited in the PDB (accession code 2ATJ).

which in turn is hydrogen bonded to another water molecule W14. This water molecule and the backbone carbonyl of Glu64 are then hydrogen bonded to Asp70 Nδ2, and Asp70 is hydrogen bonded to the Nδ1 of the distal His42 (Figure 1.9) (Gajhede *et al.*, 1997).

The importance of the calcium ions to the activity of the HRP enzyme is thought to be due to their ability to maintain the haem pocket structure and hence catalytic activity. It was reported that the loss of calcium from the structure of HRP-C leads to a decrease in both enzyme activity (about 40% reduced) and thermal stability (Haschke and Friedhoff, 1978), and subtle changes in the environment of the haem can be detected spectroscopically (Howes *et al.*, 2001a). The importance of Glu64 to the calcium stabilisation of HRP-C and enzyme activity has been studied by site directed mutagenesis. Three mutants E64G, E64P and E64S were constructed and all exhibited substantially decreased enzyme activities, implying that this Glu residue is a key residue for the stable binding of the distal calcium, maintaining the structural integrity of the distal cavity (Tanaka *et al.*, 1998).

1.5.4 Horseradish peroxidase reaction cycle:

HRP-C is an enzyme that catalyses the oxidation of a wide variety of organic and inorganic substances, with H_2O_2 as electron accepter (Yamazaki, 1974; Dunford and Stillman, 1976; Dunford, 1991; Zhu *et al.*, 2001). The general catalytic cycle proceeds via a sequence of reactions which can be described by the following equations (Smith and Veitch, 1998; Veitch and Smith, 2001):-

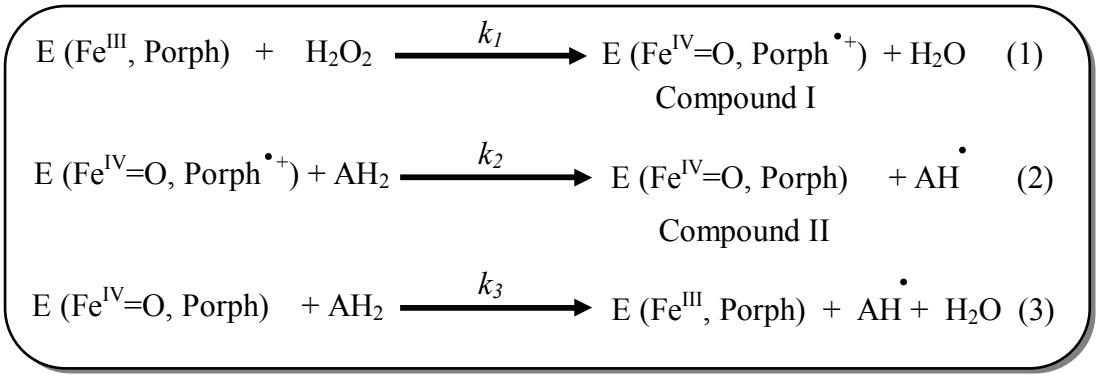

E: HRP-C enzyme, Porph: the haem porphyrin ring

AH_2: reducing substrate, $\dot{A}H$: oxidation product of AH_2

In the first step of this cycle (equation 1) the HRP-C resting state reacts with hydrogen peroxide and is oxidised to a high oxidation state intermediate known as Compound I, in which one electron is removed from the ferric iron to give the Fe^{IV} oxyferryl centre and a second electron is removed from the porphyrin to give a porphyrin π-cation radical (Dunford and Stillman, 1976). The second step in the cycle involves a single electron oxidation of the substrate by Compound I. The porphyrin π-cation radical is reduced to give a second high oxidation state intermediate known as Compound II; the rate of this step of reaction is dependent on the substrate (Hasinoff and Dunford, 1970). Finally, in the third step, Compound II reacts with another substrate molecule from which an electron is extracted by the Fe^{IV} oxoferryl to regenerate the resting enzyme. The overall reaction of this cycle can be described in the net equation 4 (below).

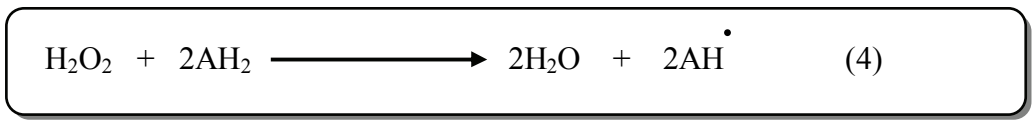

The HRP-C reactions cycle can also be described as a modified ping-pong mechanism (Scheme 1.2) (Dunford, 1999e).

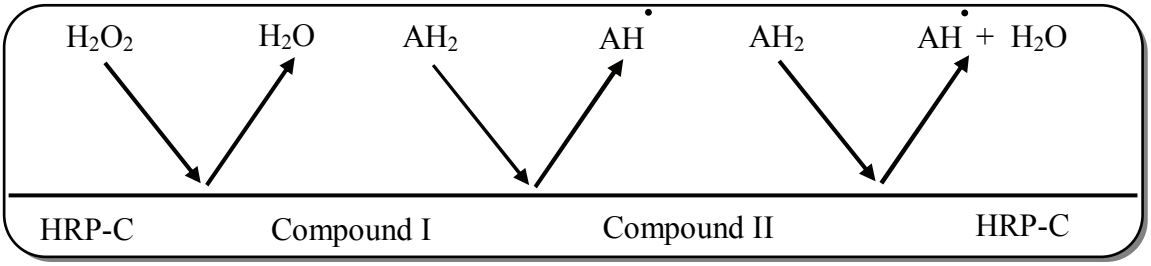

Scheme 1.2: The HRP-C ping-pong mechanism. Hydrogen peroxide reacts with the resting enzyme to produce an intermediate named Compound I, after which the substrate AH_2 reacts with Compound I to yield Compound II, and finally a second molecule of the substrate AH_2 reacts with Compound II to regenerate the resting enzyme.

1.5.4.1 Mechanism of Compound I formation:

The catalytic mechanism for the formation of Compound I was initially proposed by Poulos and Kraut from analysis of the crystal structure of yeast cytochrome *c* peroxidase. It involves two crucial residues in the distal region, the distal His and the distal Arg (Poulos and Kraut, 1980). It is supposed that a similar mechanism operates in HRP-C, given that these His and Asp residues are conserved in all members of the plant peroxidase superfamily (Dunford, 1991).

The mechanism of Compound I formation is considered to be a two-step process, shown for HRP-C in Scheme 1.3. Step 1 starts with the entry of the hydrogen peroxide molecule (H_α-O_α-O_β-H_β) into the peroxidase distal haem cavity which leads to the formation of a hydroperoxide complex, referred to as Compound 0; this step is a reversible reaction. During this step, the α-proton of the hydrogen peroxide is abstracted

by His42 and a covalent bond is formed between the haem iron and the O_α of the hydroperoxyl anion (^-OOH), generating an iron-oxygen bond. This leads to a hydrogen bond between the newly protonated His42 and the β-oxygen atom of the hydroperoxide complex (Baek and Van Wart, 1992).

In the second step of Compound I formation, the hydroperoxide complex moves through a transition state, where the positively charged side chain of Arg38 assists in stabilising the charged transition state intermediate via hydrogen bonding and electrostatic interaction. Heterolytic cleavage of the O_α-O_β covalent bond occurs as one electron is transferred from the haem iron and another one from the porphyrin. Therefore, the resulting high oxidation state intermediate, Compound I, has an oxyferryl haem ($Fe^{(IV)}$=O) and a porphyrin π-cation radical. In addition, a departing water molecule is formed from the remaining O_β-H_β leaving group of hydrogen peroxide and the H_α previously donated to His42 (Everse, 1998).

1.5.4.2 Reduction of Compound I and II:

The mechanism of Compounds I and II reduction has not been as intensively studied as the mechanism of Compound I formation. Site-directed mutagenesis studies have clearly demonstrated that the HRP-C distal residues His42 and Arg38 are also important in the reduction of Compounds I and II (Rodriguez-Lopez *et al.*, 1996a; Rodriguez-Lopez *et al.*, 1996b).

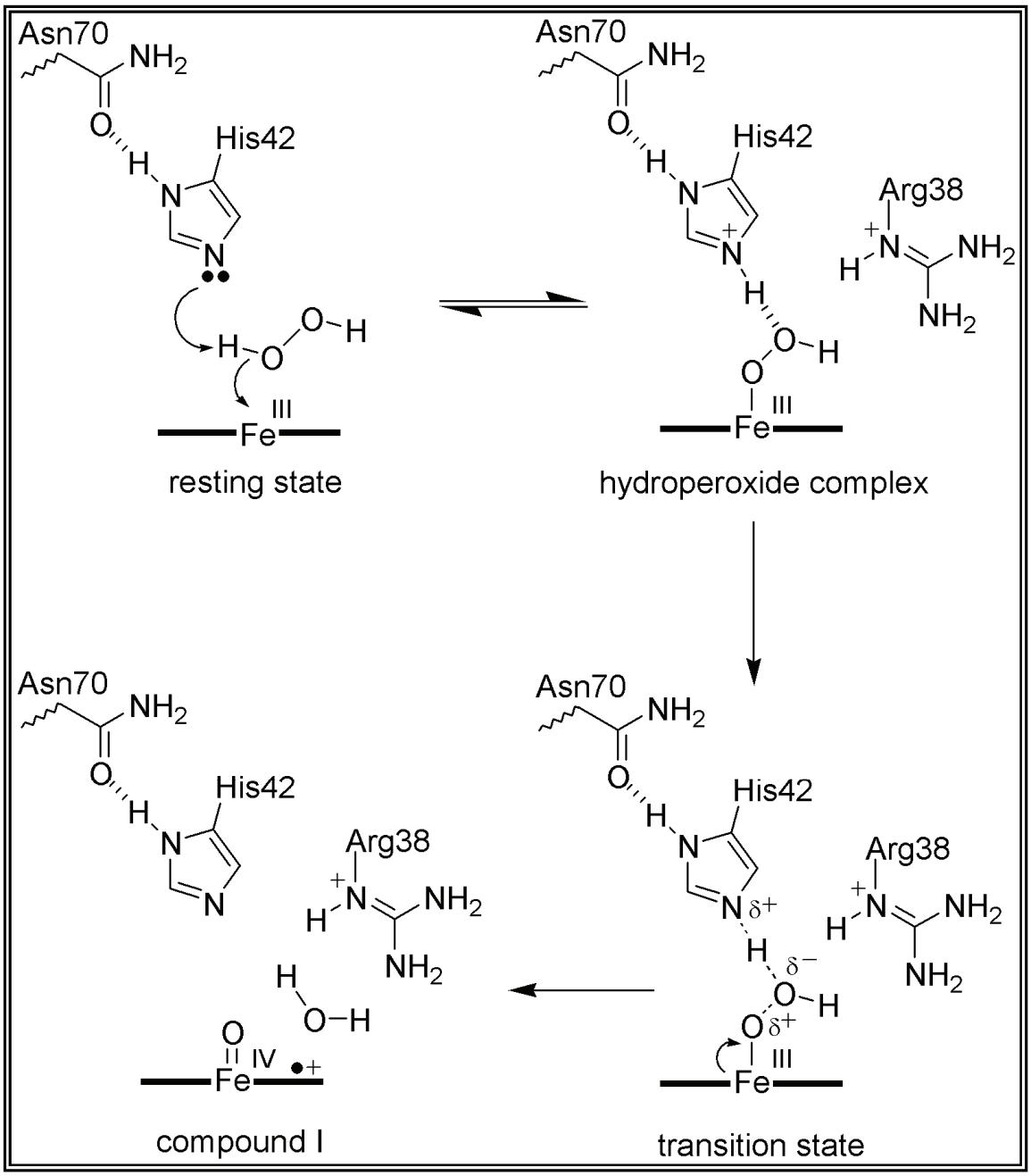

Scheme 1.3: Proposed mechanism for the formation of Compound I in HRP-C. The α-proton of H_2O_2 is abstracted by His42, and the positively charged side chain of Arg38 assists in stabilising the transition state. The scheme also includes Asn70 that forms a hydrogen bond with His42, a critical function affecting the rate of Compound I formation, reproduced from Veitch and Smith, 2001.

Nearly 20 years after the proposed mechanism for Compound I formation by Poulos and Kraut (Poulos and Kraut, 1980), a detailed mechanism for the reduction of Compounds I and II by a small phenolic substrate has been proposed, based on data from the 1.45 Å crystal structure of a ternary complex of cyanide-ligated HRP-C and ferulic acid (Henriksen *et al.*, 1999). Two assumptions have been made in this mechanism: firstly that the orientation of ferulic acid in the pre-electron transfer complexes formed transiently with Compounds I and II is likely that in the ternary complex with cyanide-ligated HRP-C, secondly, that the position of Arg38 remains undisturbed by the binding of any exogenous compounds during the reduction of enzyme intermediates; this is supported by several substrate-bound crystal structures (Henriksen *et al.*, 1998a; Henriksen *et al.*, 1999).

It is generally accepted that when a substrate molecule binds to Compound I, an electron is transferred to the porphyrin ring via the exposed haem edge, and the π-cation radical disappears. In the case of ferulic acid, the proposed mechanism for Compounds I and II reduction is illustrated in Scheme 1.4. The carbonyl group of a proline residue (Pro139), which is conserved throughout the plant peroxidase superfamily (Veitch and Smith, 2001), acts as a hydrogen bond accepter for a structurally conserved water molecule, which also acts as a conduit for a proton from the hydroxyl group of ferulic acid to the Nε2 atom of His42. This process of proton transfer is coupled to the electron transfer from ferulate to the exposed haem edge. The hydrogen bond between Arg38 and the ferulate oxygen is thought to assist the proton transfer from the ferulic acid to His42. As Compound II is formed the ferulic acid radical leaves the enzyme and is substituted by a fresh substrate molecule.

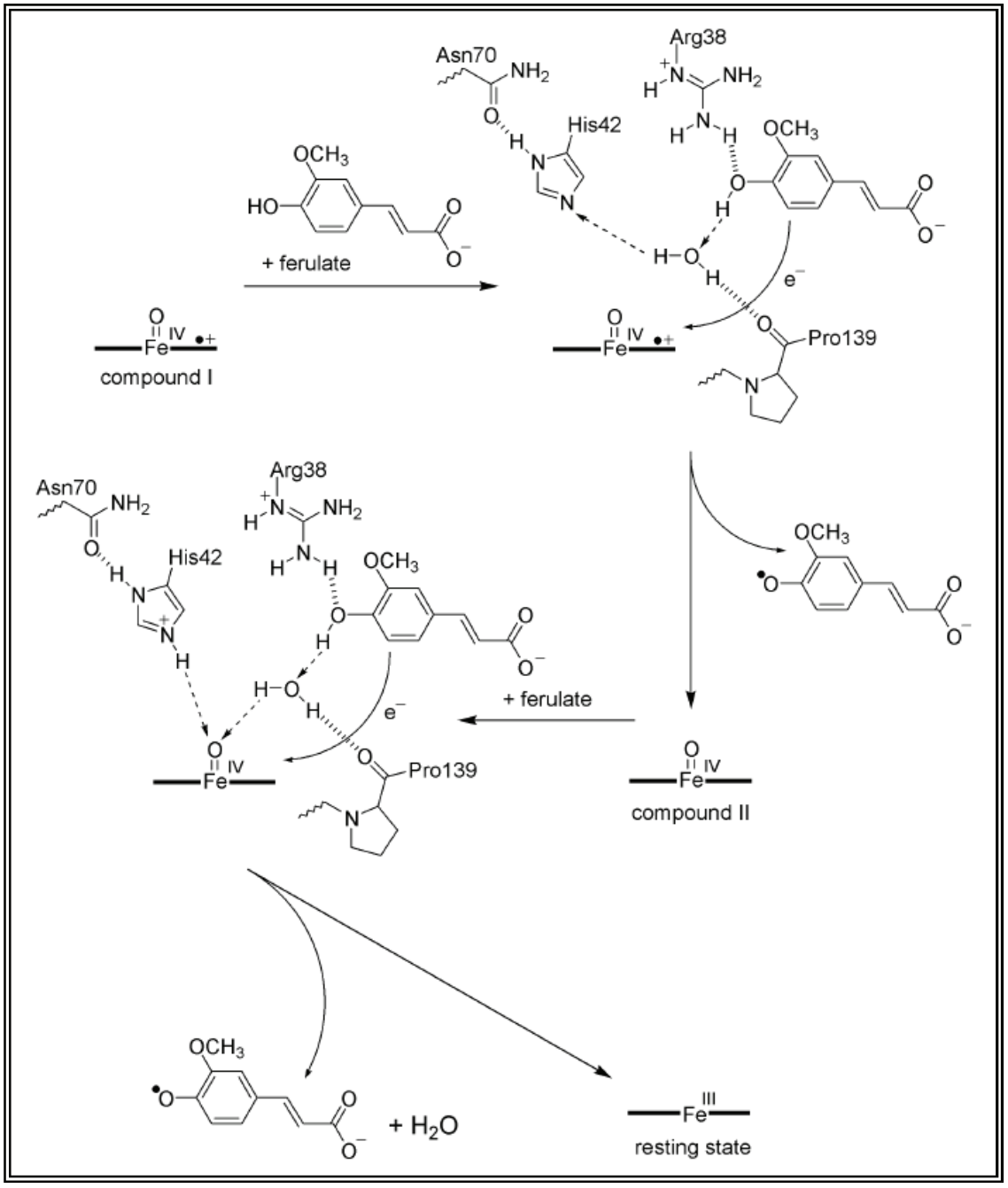

Scheme 1.4: Mechanism of Compounds I and II reduction in HRP-C by ferulic acid. The scheme is based on a 1.45 Å resolution crystal structure of the ternary complex of ferulic acid and cyanide-ligated HRP-C (Henriksen *et al.*, 1999). The direction of proton transfer is indicated by the dotted arrows. The mechanism also shows the participation of Pro139 in the formation of an important hydrogen bond with the water molecule via its carbonyl group, reproduced from Veitch and Smith, 2001.

The reduction of Compound II occurs by a similar mechanism, but this time the final destination of both proton and electron is the ferryl-oxygen which is reduced to the resting ferric state. The ferryl oxygen accepts two protons, one from the substrate molecule and the other from the distal His42, to form a water molecule that is released from the haem iron (Azevedo *et al.*, 2003).

1.5.5 Aromatic substrate binding site:

There is agreement that the minimal distance between the haem iron atom in HRP-C and the aromatic substrate is 8−11 Å, therefore excluding the metal as the binding site. It has been suggested that aromatic donors bind at a hydrophobic site in the vicinity of the exposed haem edge, a region comprising the haem methyl C8 and haem *meso* Cδ protons (Dunford, 1991; Veitch and Smith, 2001). Inactivation experiments of HRP-C by alkyl- and phenylhydrazines, sodium azide, cyclopropanone hydrate and nitroalkanes provide strong support that substrate oxidation occurs at the exposed haem edge. When different alkylhydrazine reagents are incubated with HRP-C and hydrogen peroxide the addition of the alkyl moieties is exclusively to the *meso* carbon of the haem edge. Cyclopropanone hydrate, nitromethane, and sodium azide similarly add to the *meso* carbon after being oxidised by the enzyme to radical intermediates (Ortiz de Montellano, 1992).

In fact, substrate access to the oxoferryl centre of HRP-C Compounds I and II appears to be hindered by the local protein environment, an example of ‘closed’ haem architecture. Attempts to alter this aspect of the chemistry of HRP-C have been made by site-directed mutagenesis. Substituting the distal residue Phe41 by smaller amino acid residues such as Ala, Leu and Thr, as well as replacement of His42 with Ala and Val,

all resulted in an increase in substrate access to the oxoferryl centre of Compound I (Newmyer and Ortiz de Montellano, 1995; Ozaki and Ortiz de Montellano, 1995).

On the basis of optical difference spectroscopy, hyperfine shifted NMR spectroscopy, and nuclear magnetic relaxation studies, it has been shown that HRP-C can bind with a variety of aromatic donor molecules (Figure 1.10) reversibly to form 1:1 enzyme-donor complexes (Critchlow and Dunford, 1972; Burns *et al.*, 1975; Schejter *et al.*, 1976; Morishima, 1978). The complexes are formed with either the resting state of the enzyme or with ligand bound forms, most commonly the cyanide ligated state. Spectroscopic and crystallographic studies have revealed a wealth of information on the site where these aromatic substrates are located.

The X-ray structures of ferulic acid (FA) complexed with resting state HRP-C* or the cyanide-ligated enzyme have been solved to 2.0 Å and 1.45 Å, respectively (Henriksen *et al.*, 1999). It was found that the aromatic ring of FA is almost coplanar with the haem group and that there are hydrogen bonding interactions between Arg38 $N\eta H_2$ and the phenolic and methoxy oxygen atoms of FA, as well as between the phenolic oxygen and an active site water molecule. This active site water molecule is also hydrogen bonded both to the backbone oxygen of Pro139 and to the cyanide ligand nitrogen. The other interactions between the FA molecule and HRP-C can be defined as hydrophobic interactions with amino acid side chains of Phe68, Gly69, Pro139, Ala140, Phe142, Phe179, as well as with the C8 methyl and Cδ of the haem group (Henriksen *et al.*, 1999).

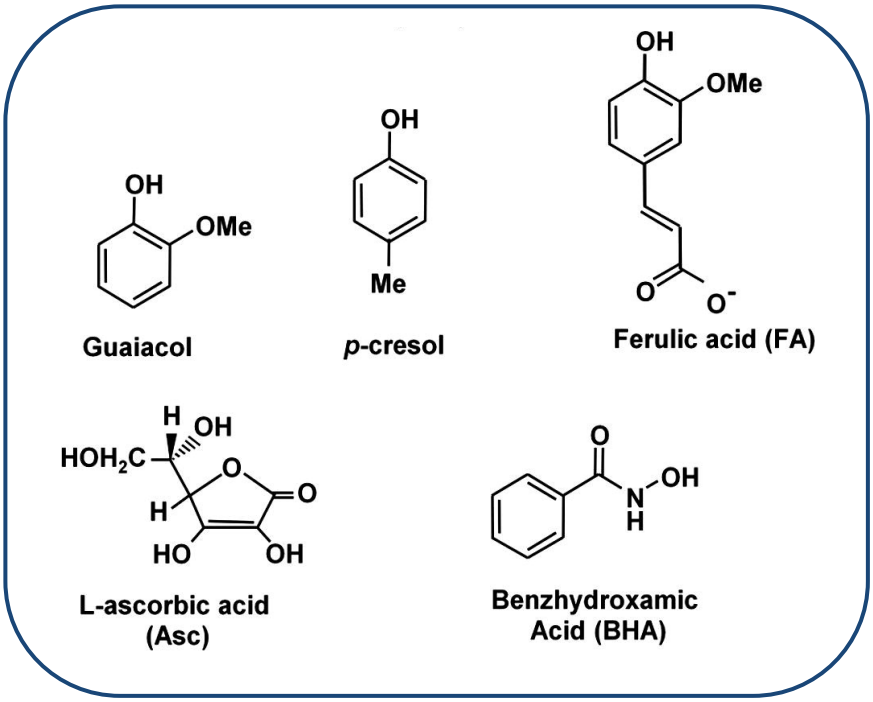

Figure 1.10: Aromatic donor molecules that can form complexes with HRP-C.

1.5.6 Biological roles of horseradish peroxidase:

In general, plant peroxidases are constitutive enzymes mainly found in the cell wall, vacuoles and transport organelles and rough endoplasmetic reticulum. They play an important role in plant physiological actions including auxin catabolism, modification of the cell wall, lignification, pathogen defence and wound healing (Azevedo *et al.*, 2003).

Auxins are plant hormones that have an important role in plant growth and development, including the control of the elongation, division and differentiation of cells. One of the most important auxins produced by plants is indole-3-acetic acid (IAA). HRP-C is considered to be the main enzyme responsible for the catabolism of IAA (Campa, 1991). The ability of HRP-C to degrade the plant hormone IAA has been

reviewed as early as 1955 (Kenten, 1955). In contrast to most peroxidase-catalysed reactions, the oxidation of IAA by HRP-C has been shown to occur in the absence of hydrogen peroxide; for this reason authors used to refer to peroxidases in the older literature by the term indole acetic acid oxidases (Veitch and Smith, 2001). The mechanism of this oxidation is complex and has been studied experimentally in great detail by several groups (Campa, 1991; Dunford, 1999g). The major products of IAA oxidation include indole-3-methanol, indole-3-aldehyde and 3-methylene-2-oxindole, the latter most probably as a result of the non-enzymatic conversion of indole-3-methylhydroperoxide.

The cell wall is sometimes considered the primary site of action of plant peroxidases, as they play an integral role in cell wall biosynthesis. The oxidative coupling of phenolic monomers such as *p*-coumaryl, coniferyl and sinapyl alcohols can be catalyzed by HRP (Campa, 1991). These reactions are also essential in the biosynthesis of lignin, a complex and highly branched phenylpropanoid polymer that constitutes 20-30% of a plant cell wall. The cell wall peroxidase-catalyzed reactions are, however, not restricted to lignification. The synthesis of suberin, a wax that reduces water loss from cells, involves a peroxidase in a manner similar to that proposed for lignin biosynthesis (Campa, 1991; Azevedo *et al.*, 2003).

It has been reported in several plant systems, that the level of peroxidase expression and the isoenzyme pattern is altered by stress conditions. Peroxidases are part of the first line of plant defence, and increases in activity were observed upon plant exposure to ozone, pollution, radiation, nutritional disorders, wounding, infections, salinity and

aging. One of the clearest examples of this induction of HRP-C activity is the rapid response on wounding of horseradish leaves (Campa, 1991).

1.5.7 Applications of horseradish peroxidase:

HRP is one of the most widely used enzymes *in vitro*, as a reagent for organic synthesis and bio-transformation, as well as in coupled enzyme assays, chemiluminscent assays and immunoassays. The enzyme meets many requirements for successful use in these systems, such as flexibility in assay, stability, sensitivity in range of analyte detection, as well as availability of pure form at reasonable cost (Azevedo *et al.*, 2003; Veitch, 2004).

One of the major applications of HRP in preparative organic synthesis is using it as a mild catalyst; it has the ability to catalyze a number of useful oxidative *N*- and *O*-dealkylation reactions that are relatively difficult to carry out synthetically (Meunier, 1991). In addition, HRP has been used in the organic synthesis of optically active compounds such as (*S*)-hydroperoxides and (*R*)-alcohols (Adam *et al.*, 1995). Epoxidation of styrene in the presence of a mediator such as 4-methylphenol (Ortiz de Montellano and Grab, 1987) and selective hydroxylation of some aromatic compounds in the presence of oxygen and dihydroxyfumaric acid (Klibanov *et al.*, 1981) can also be achieved using HRP.

One of the most commercial uses of HRP is in immunoassays. The term immunoassay describes a wide range of assays used to detect and quantify antigens using antibodies. HRP-antibody conjugates have been extensively used in enzyme-linked immunosorbent assays (ELISA), Western blotting and immunohistochemistry assays (IHC). These are

the basis for many diagnostic kits, such as pregnancy testing kits. In these systems, it is convenient to be able to detect peroxide activity colorimetrically (Veitch and Smith, 2001; Azevedo *et al.*, 2003).

Another commercial use of peroxidases is to detect and quantify molecules of clinical interest, such as glucose, uric acid and cholesterol in biological fluids (blood, plasma and urine). In the case of glucose, for example, it is oxidised by glucose oxidase to yield stoichiometric amounts of hydrogen peroxide, which are then used by HRP to oxidise selected substrates to give products that can be monitored easily by colorimetric, fluorometric or chemiluminescent methods (Veitch and Smith, 2001). One of the advantages of using HRP in clinical assays is that few inhibitors of the enzyme are found in biological fluids, thus reducing the possibility of errors. Chemiluminescent assays are particularly sensitive and widely used. These assays involve the oxidation of luminol, or a derivative, to yield 3-aminophthalate and light, with sensitivity up to 1000 times more than when using a chromagenic substrate (Coulet and Blum, 1992; Nakayama and Amachi, 1999).

1.6 Introduction of haem-protein covalent linkages into plant peroxidases:

As discussed before (sections 1.2 and 1.3.3) mammalian peroxidases share a feature not found in the enzymes of the plant peroxidase superfamily, in that the haem prosthetic group is covalently attached to the protein via at least two ester linkages from the porphyrin. In addition, MPO has an additional sulfonium linkage between a methionine residue and the β-carbon of the 2-vinyl group of the porphyrin. Early studies on the ester linkages have indicated that they are formed autocatalytically, by reaction with

H_2O_2 (DePillis *et al.*, 1997). Incubation of recombinant LPO, which as expressed in the baculovirus system has only part of the haem bound, with hydrogen peroxide led to an increase both in covalent haem binding and catalytic activity (DePillis *et al.*, 1997). In addition, the haem group in the E375D mutant of LPO is initially only partially covalently bound, but exposure to H_2O_2 again results in complete covalent binding and a fully active protein (Colas *et al.*, 2002). This provides further evidence that the mammalian peroxidases haem-protein ester linkages are formed by an autocatalytic process. Furthermore, it has been demonstrated unambiguously that the protein-haem ester linkages in EPO are also formed by an autocatalytic process (Oxvig *et al.*, 1999), and that for TPO, exposure to H_2O_2 is very important for the formation of mature and active enzyme (Fayadat *et al.*, 1999).

More recently, efforts have been made to mimic the haem-protein covalent linkages of mammalian peroxidases in plant peroxidases. A glutamic acid residue has been introduced into the distal cavity of HRP (Colas and Ortiz de Montellano, 2004) near to the haem. The HRP-C* mutant F41E was found to be isolated with no covalently bound haem, but the haem was completely covalently bound upon incubation with H_2O_2. These results clearly show that the presence of an appropriately situated carboxylic acid group is sufficient for ester bond formation with the haem porphyrin (Colas and Ortiz de Montellano, 2004). The first information about the mechanism of formation of the sulfonium linkage in MPO was revealed in 2004, when a methionine residue was engineered close to the 2-vinyl haem group in recombinant pea cytosolic ascorbate peroxidase (rpAPX) (Metcalfe *et al.*, 2004). The S160M mutant was isolated, and upon incubation with H_2O_2 a covalent sulfonium ion linkage was seen to be formed. These results provide the first evidence that covalent linkage formation between a methionine

residue and the haem vinyl group occurs as an H_2O_2–dependent process. They also identified a transient Compound I-like species as a reaction intermediate (Metcalfe *et al.*, 2004). Recently, the same group have reported the introduction of a tyrosine residue at the same position in rpAPX (S160Y). This lead, on treatment with H_2O_2, to the formation of a haem-tyrosine covalent link (Pipirou *et al.*, 2007b), and in addition, a second covalent link from the haem to Trp41, previously also seen on treatment of wild-type rpAPX with excess of H_2O_2 for a long time (Pipirou *et al.*, 2007a). Although no Compound I-like species was seen for the S160Y mutant, a tyrosine radical was seen by EPR experiments and the haem-Trp41 linkage was assumed to occur via a tryptophan radical. However, the importance of an, at least transient, π-cation radical to the linkage process was identified by experiments with cytochrome *c* peroxidase (C*c*P). Only for the mutant W191F was a tryptophan-haem linkage observed between the distal tryptophan (Trp51) and porphyrin, on treatment with excess H_2O_2 for a long time; the wild-type enzyme, which uses a Trp191 radical instead of a porphyrin π-cation radical showed no such tryptophan linkage under similar conditions (Pipirou *et al.*, 2009).

Recent work by another member of author's group, Dr. Kasim Cali, has successfully created a covalent sulfonium linkage between the [S167M] HRP-C* mutant protein and the prosthetic haem group, through an H_2O_2-dependent activation process (Cali, 2008). Previously, to determine which residue in HRP-C might be in a suitable position for the introduction of a sulfur side chain, the X-ray structure of HRP-C* (Gajhede *et al.*, 1997) was superimposed on that of MPO using the coordinations of the haem. The superposition revealed that the position of the methionine residue (Met243), responsible for the formation of the sulfonium linkage in MPO, was close to the serine residue Ser167 in HRP-C and close to the 2-vinyl group of the haem. This work was the first to

generate a haem-protein sulfonium bond in the commercially valuable HRP-C enzyme, but the linkage was not found to be stable indefinitely (Cali, 2008).

1.7 The aim of the present work:

Commercially important horseradish peroxidase (HRP: EC 1.11.1.7) is the most intensively studied member of the plant peroxidase superfamily. This project was designed to build on previous work to introduce novel haem-protein covalent linkages into HRP, to try to increase the stability, and possibly the activity, of the enzyme, and also to attempt to understand more about the mechanism of formation and the advantage of these linkages in mammalian peroxidases in which they naturally occur. The previous work involved the introduction of a sulfonium linkage into HRP-C* (Cali, 2008). Here, by comparison with work on rpAPX (Pipirou *et al.*, 2007b), the current work aimed to introduce other covalent linkages between the haem porphyrin and protein in HRP-C, i.e. tyrosine and tryptophan linkages. To this end, two site-directed HRP-C* mutants at position 167 have been constructed, in which Ser167 was substituted by tyrosine or tryptophan (S167Y and S167W). The new mutant genes were generated using a PCR-based Whole Plasmid Amplification Method of site-directed mutagenesis. The resulting mutant enzymes were characterised using UV/Visible spectroscopy and attempts were made to introduce the covalent linkage using incubation with H_2O_2. The presence of a linkage was determined using Electronic absorption spectroscopy, acid butanone haem extraction, MALDI-TOF and ESI mass spectrometry and HPLC methods. The results provide proof of the formation of a tyrosine-haem covalent linkage. The effect of this linkage on the activity of the enzyme was also characterised using steady-state and pre steady-state enzyme kinetics.

Chapter Two:

Materials and Methods

2.1 Materials:

All molecular biology methods used are those described in Sambrook *et al.,* 1989, unless otherwise stated. BDH, Fisher, and Sigma Aldrich supplied all chemicals used and all restriction enzymes and their appropriate buffers were supplied by NEB (UK) Ltd, unless otherwise stated. The synthesis of oligonucleotide primers and DNA sequencing were performed by MWG-biotech.com.

2.2 Generation of mutants:

2.2.1 Site-directed mutagenesis:

Site-directed mutagenesis of recombinant horseradish peroxidase (WT HRP-C*) at position 167 was carried out using the polymerase chain reaction (PCR) based Whole Plasmid Amplification Method (WPAM) mutagenesis technique in order to construct two new variants [S167Y] HRP-C* and [S167W] HRP-C*. This method has been described previously (Veitch *et al.*, 1997; Doyle *et al.*, 1998). The synthetic WT HRP-C gene (Smith *et al.*, 1990), cloned in the commercially available expression vector pFLAG1 (Doyle *et al.*, 1998), was used as the template; the length of the resulting plasmid (known as pFLAG1-HRP-C) is 6.3 kb. During the PCR process, a thermostable and proof-reading DNA polymerase (*Pfu* polymerase) was used. *Pfu* polymerase was

preferred to *Taq* polymerase, due to the higher fidelity that it has in comparison with *Taq* polymerase (Lundberg *et al.*, 1991; Cline *et al.*, 1996).

2.2.2 Primer design:

PCR oligonucleotide primers were designed to anneal exactly 'back to back' at their 5' termini on opposite template DNA strands. The designed primers included the necessary nucleotide mismatches required to generate the desired amino acid substitutions in the protein, in addition to silent mutations which generated a new restriction enzyme site in order to facilitate screening of the transformed clones. Two primers were designed for each mutant gene to be made and the software Webcutter[1] was used to assist in the design of the primers. This software permits the user to examine a given nucleotide sequence for the presence of both existing restriction enzyme sites and silent sites that can be introduced by exploiting natural codon degeneracy (see Figure 3.2). The first primer was the mutagenic primer which covered the area to be mutated and contained the intended base changes. The second primer was the reference primer which annealed to the other DNA strand.

High purity, salt free (HPSF) primers were synthesized and supplied by MWG-Biotech in a lyophilized form. These primers were dissolved in sterile, distilled deionised water (ddH_2O) to produce 100 μM stock primer solutions that were further diluted to produce 10 μM working stock primers.

[1] http://www.users.unimit.it/Camelot/tools/cut2.html

2.2.3 DNA Amplification Mutagenesis using PCR:

To generate each mutant gene, a 50 µl PCR was carried out containing 5 µl of 10x *Pfu* reaction buffer, 5 µl dNTPs (1 mM each), 1 µl template DNA (5 ng), 5 µl of 10 µM each of the two primers, 0.5 µl of *Pfu* polymerase (1.25U Promega, added after a Hot Start) and 28.5 µl of sterile ddH_2O. The PCR tubes containing the mixture above were placed in a thermocycler (Perkin-Elmer GeneAmp 2400) and subjected to twenty five cycles, each cycle was as follows:

Hot Start	95 ^oC for 10 minutes
Pause for 5 minutes to add the P*fu* polymerase followed by 25 cycles of	
Denaturation	95 ^oC for 45 seconds
Annealing	56 ^oC for 1 minute
Extension	72 ^oC for 17 minutes

At the end of the 25 cycles, the thermocycler was set to automatically reduce the temperature down to 4 ^oC until the next morning.

2.2.4 Identification of correctly sized PCR product:

On completion of the PCR, in order to check if a PCR product was made and of the correct size, agarose gel electrophoresis was carried out using a DNA size marker. PCR products of the correct length should be 6.3 kb. This was done by preparing a 70 ml agarose gel containing 1% (w/v) agarose in a 1x Tris-borate-EDTA (TBE) buffer (89 mM Tris base, 89 mM Boric acid and 2 mM EDTA, pH 8.0). 10 µl of each of the PCR solutions were taken and mixed with 2 µl of 6x Ficoll loading buffer (15% (w/v) Ficoll

400, 0.25% Bromophenol Blue and 0.25% xylene cyanol FF). The PCR samples and the marker were loaded on the gel. The gel was placed in a gel tank filled with 1x TBE buffer, and run under a constant potential difference of 60V until the blue dye approached the end of gel. Since the DNA is negatively charged due to the phosphate backbone, the samples will be separated according to their size, smallest moving quickest, towards the positive charged end. The gel was removed and placed into a staining box containing ddH_2O and 20 µl of 10mg/ml ethidium bromide. The box was rocked for about 30 minutes, and then DNA bands were visualized under UV light by using a transllluminator.

2.2.5 Purification of PCR product:

To remove the methylated template from the PCR samples, the next step was adding 1 µl of *Dpn*I. The mixture was incubated for two hours at 37 ^{o}C. The PCR solution was then made up to 150 µl with sterile ddH_2O, in an Eppendorf tube. 150 µl of Phenol: Chloroform: Isoamylalcohol mix (25:24:1) was added, and the tube inverted several times until an emulsion was formed. The emulsion was centrifuged for two minutes in a micro-centrifuge at 13,000 rpm. The aqueous DNA-containing top layer was carefully transferred to another tube. To remove traces of phenol, 150 µl of chloroform was then added, mixed well and then centrifuged at 13,000 rpm for one minute. The top aqueous layer was removed and transferred to the other tube, carefully as before.

2.2.6 Ethanol precipitation of the purified PCR product:

The DNA solution resulting from the phenol/chloroform extraction process was adjusted to a sodium concentration of 0.3 M by adding a volume of 3 M Na-acetate, pH 5.2, equal to $1/9^{th}$ volume of the DNA sample. 2.5 volumes of ice-cold 100% ethanol were added and the solution was again mixed well by shaking and then left at -20 ^{o}C for 30 minutes. The solution was centrifuged at 13,000 rpm in a micro-centrifuge for 10 minutes with the hinge of the tube outwards. The supernatant was carefully removed. 500 µl of 70% ethanol was added to the pellet and the tube centrifuged again at 13,000 rpm for 5 minutes, with hinge out as before. As far as possible the supernatant was carefully removed, and by leaving the lid of tube open in the filter hood the DNA was dried fully. 8 µl of sterile ddH_2O was then added to resuspend the purified DNA.

2.2.7 Circularization of the PCR products:

2.2.7.1 Phosphorylation of the PCR product:

In order to add 5' phosphate groups to the ends of the purified linear DNA fragments, the DNA solution was treated with 1 µl of 10x ligase buffer and 1 µl of T4 Polynucleotide kinase (10 units/µl) to give a total volume of 10 µl. The mixture was incubated at 37 ^{o}C for 2 hours.

2.2.7.2 Ligation of the phosphorylated PCR product:

In order to recircularize the phosphorylated linear DNA, 1 µl of 10x ligase buffer, 1 µl of T4 DNA Ligase (400 units/µl) and 8 µl of sterile ddH_2O were added to the mixture from the phosphorylation process to give a final volume of 20 µl. Then the solution was incubated overnight at 4 ^{o}C.

2.2.8 DNA Transformation into *E. coli* (DH5α):

The recircularized, mutant plasmid DNA was transformed into the *E. coli* DH5α strain (Invitrogen library efficient competent DH5α) using the heat-shock method (Sambrook *et al.*, 1989). The stored competent cells, which were frozen at -80 ^{o}C, were thawed on ice with no external heating. After this, 10 µl of the ligated plasmid DNA was added into 100 µl of the competent cells, gently mixed with pipette tip, and then left on ice for 20 minutes. The mixture was heat-shocked at 42 ^{o}C for 45 seconds in a water bath (as heat exchange is more efficient than in a hot-block). The sample was placed back on ice for five minutes for the cells to recover. 1 ml of sterile Luria-Bertani (LB) broth was added to the tube, and the cells were shaken at 37 ^{o}C for 1 hour to allow for the antibiotic resistance to be expressed. The sample was then centrifuged in a micro-centrifuge at 7,000 rpm for 2 minutes to produce a cell pellet. Most of the supernatant was poured off, leaving approximately 100 µl. The cells were resuspended gently by pipette tip and plated onto a Luria-Bertani (LB) agar plate containing 100 µg/ml ampicillin; the plate was left upside down and incubated overnight at 37 ^{o}C.

A transformation control was also carried out as follows: 100 µl of competent cells with 10 ng of WT pFLAG1-HRP-C plasmid DNA was plated onto an LB agar plate containing 100 µg/ml ampicillin. The aim of this was to check the efficiency of the competent cells and to discover any potential contamination.

2.2.9 Plasmid DNA miniprep:

Transformed DH5α colonies obtained on the ampicillin-containing LB agar plates were picked and inoculated into 5 ml LB broth containing 100 µg/ml ampicillin. The cultures

were shaken overnight in an incubator at 37 ^{o}C. 2 x 1.5 ml of each culture was centrifuged in a micro-centrifuge at 7,000 rpm for two minutes. The plasmid DNA miniprep was then carried out using the protocol of the QIAprep® MiniPrep Kit supplied by Qiagen. The final DNA solution was extracted into 50 µl of 10 mM Tris, pH 8.5.

2.2.10 Restriction enzymes analysis of miniprep plasmid DNA:

7 µl of each plasmid DNA miniprep was digested in a total volume of 10 µl that also included 1 µl of bovine serum albumin (BSA) to a final concentration 100 µg/ml, 1 µl of manufacturer recommended restriction endonuclease buffer and 1 µl of restriction endonuclease BssSI (4 units/µl). In all cases an undigested control was also performed where the restriction enzyme was substituted by sterile ddH_2O. The mixtures were incubated at 37 ^{o}C for one hour.

After incubation, 2 µl of 6x Ficoll loading buffer was added to both digested and undigested mixtures. The samples were analysed by electrophoresis, alongside a DNA size marker, on a 70 ml agarose gel (1% w/v agarose) at 60 V. The gel was stained with ddH_2O and 20 µl of 10 mg/ml ethidium bromide and shaken for 30 minutes. The stained gel was transluminated under UV light for DNA band identification.

2.2.11 Plasmid DNA midiprep:

The remaining 2 ml of a 5 ml LB broth culture, from which plasmid miniprep and digest showed a positive result, were used to inoculate a larger overnight culture. 250 µl of each positive culture was added to 50 ml LB broth containing 100 µg/ml ampicillin and

incubated overnight at 37 ^{o}C. Plasmid DNA midiprep was then carried out using a Wizard® DNA Purification System MidiPrep Kit supplied by Promega. The final DNA solution was extracted using 300 µl of 10 mM Tris, pH 8.5.

The purity and concentration of the midiprep plasmid DNA was determined using a spectrophotometer and the spectral range between 220-320 nm. The purity of DNA is given by the ratio of A_{260}/A_{280}; values between 1.8 and 2 indicate that DNA is pure. The concentration of the DNA was determined by the following equation, as a solution of DNA at 50 ng/µl has an absorbance at 260 nm of 1.0.

$$[DNA] = 50 * A_{260} * \text{dilution factor}$$

2.2.12 Submitting DNA for sequencing:

To confirm the presence of the desired mutations in the putative mutant plasmids, and to check for any PCR introduced error, two samples for each positive clone were prepared for sequencing by MWG-Biotech. The appropriate volume of midiprep DNA containing 1 µg DNA was made up to 10 µl with 10 mM Tris, pH 8.5. One sample was sent for sequencing with 10 µl of 10 µM in-house forward primer (lipseq1) and the other was sent with 10 µl of 10 µM in-house reverse primer (lipseq5). The sequencing results were checked using the Seqman section of DNASTAR software, by aligning the new HRP-C mutant sequences with wild-type HRP-C gene.

2.2.13 Glycerol Stocks:

The new HRP-C mutant plasmids in *E. coli* DH5α were stored as glycerol stocks for long-term use. A colony was inoculated into 5 ml LB broth containing 100 µg/ml

ampicillin and incubated overnight at 37 ^{o}C. 1 ml of the culture was pipetted into a Nunc cryovial using sterile technique. Then 0.5 ml of sterile 50% glycerol was added, the tube inverted to mix and the stock stored at -80 ^{o}C. When needed, the glycerol stock was thawed slightly and some of the cells plated onto an LB agar plate with ampicillin to generate single colonies.

2.3 Protein Expression and Purification:

Expression of protein from the synthetic HRP-C gene cloned in the pFLAG1 expression vector is regulated by *lac*I^{q} repression of the *tac* promoter, a strong promoter formed by the hybridisation of different regions of the *trp* and *lac* promoters (de Boer *et al.*, 1983). Repression is relieved in the presence of the lactose analogue isopropyl-β-D-thiogalactopyranoside (IPTG) and the protein is expressed in the form of misfolded aggregates or inclusion bodies, which require refolding to recover the active enzyme (Smith *et al.*, 1990).

2.3.1 Small-scale HRP-C* protein expression:

2.3.1.1 Transformation into *E. coli* protein expression strain W3110:

[S167Y] and [S167W] midiprep plasmid DNA (as confirmed by sequencing), as well as WT HRP-C DNA (used as a control), were transformed into *E. coli* W3110 cells. The -80 ^{o}C stored, chemically competent W3110 cells were thawed in ice with no external heating. 10 µl of the DNA was taken and added into 100 µl of the competent cells. The mixture was gently mixed with pipette tip, and then left on ice for 20 minutes. After that, the mixture was heat-shocked at 42 ^{o}C for 2 minutes in a water bath, and placed back on ice for five minutes. 1 ml of sterile LB broth was added, and the cells were

shaken at 37 ^{o}C for 30 minutes to allow the antibiotic resistance to be expressed. Then the sample was centrifuged in a micro-centrifuge at 7,000 rpm for 2 minutes to produce a cell pellet. Most of the supernatant was poured off, leaving approximately 100 µl. The cells were resuspended gently by pipette tip, plated onto a LB agar plate containing 100 µg/ml ampicillin, and incubated upside down overnight at 37 ^{o}C.

2.3.1.2 Culture growth:

Two transformed W3110 colonies were selected for each mutant HRP-C plasmid, in addition to one colony of WT, and were inoculated overnight in 5 ml LB broth containing 100 µg/ml ampicillin at 37 ^{o}C. A glycerol stock was prepared for each culture (section 2.2.13) and stored for future use. 50 µl of each culture was then inoculated into a further 5 ml LB broth containing 100 µg/ml ampicillin. The cultures were grown at 37 ^{o}C with vigorous shaking for 1.5 hours, then induced by adding 1 mM IPTG (10 µl of 500 mM stock), and grown for a further three hours. An inoculated but un-induced culture was also grown at the same time.

Cells were harvested from 3 ml of each culture by centrifugation in a micro-centrifuge at 7,000 rpm for two minutes. The cells were resuspended in 500 µl of buffer solution containing 20 mM Tris, pH 8.0, 1 mM EDTA, 1 mM DTT and 2 M urea, by pipetting. The resuspended cells were sonicated for 30 seconds and then centrifuged for 15 minutes at 13,000 rpm, and the resulting supernatant discarded. The protein containing pellet was resuspended in a further 500 µl of the above buffer, and the sonication step repeated. 500 µl of the same buffer, but supplemented with 2% Triton X-100, was then added and the mixture was left to stand for 10 minutes at room temperature. The

mixture was then centrifuged at 13,000 rpm for 15 minutes and the supernatant was discarded. The pellet was resuspended in 30 µl of a buffer solution containing 50 mM Tris, pH 8.0, 1 mM EDTA, 30 mM DTT and 10 M urea, by pipetting. The samples were centrifuged at 13,000 rpm for 10 minutes to remove any remaining insoluble (membrane) proteins. The HRP-C protein containing supernatant was removed carefully and stored as a 10 M urea extract at -20 ^{o}C.

2.3.1.3 Sodium Dodecyl Sulphate Polyacrylamide Gel Electrophoresis (SDS-PAGE):

2.3.1.3.1 Gel Recipes

1) 12% Resolving Gel, 10 ml

3M Tris, pH 8.55	1.25 ml
28% acrylamide, 1.5% bis acrylamide	4.30 ml
20% SDS	0.05 ml
ddH_2O	1.90 ml
0.14% Ammonium persulphate	2.50 ml
Temed	5.00 µl

2) Stacking Gel, 6 ml

1M Tris/SDS	0.75 ml (of 4.8ml 1M Tris, pH 7.0 + 0.2ml SDS)
28% acrylamide, 1.5% bis acrylamide	0.75 ml
ddH_2O	1.50 ml
0.14% Ammonium persulphate	3.00 ml
Temed	7.50 µl

3) 1:1 sample buffer:

SDS	1 g
Glycerol	2 ml
bromophenol blue (0.1% w/v ddH_2O)	2 ml
1M Tris, pH 7.0	1.25 ml
2-mercaptoethanol	2 ml
ddH_2O	2.75 ml

4) Stain solution: 10% acetic acid, 10% ethanol + 0.1% Coomassie Blue in ddH_2O.

5) Destain solution: 10% acetic acid, 10% ethanol in ddH_2O.

2.3.1.3.2 SDS-PAGE Method:

SDS-PAGE electrophoresis was performed using 5 µl of each of the 10 M urea extracts mixed with an equal volume of 1:1 gel sample buffer. Then samples were subjected to electrophoresis using the discontinuous buffer system through the acrylamide stacking gel and 12% acrylamide resolving gel. The Rainbow wide-range protein molecular weight marker used was from BioRad Laboratories. Electrophoresis was run first at a constant 30 mA until the sample reached the stacking gel, when the current was increased to 60 mA until the dye reached the bottom of the resolving gel.

The gels were stained with stain solution for 30 minutes at room temperature with rocking. The gels were then washed with ddH_2O and destained with destain solution and rocking at room temperature until the protein bands could be visually resolved from the background.

2.3.2 Large Scale HRP-C* protein production:

2.3.2.1 Culture growth and protein expression:

Solution 1) Terrific Broth (TB): 6 g tryptone, 12 g yeast extract, 4 ml glycerol and 450 ml ddH_2O were mixed in a 2 l baffled conical flask. The flask was fitted with a bung and then autoclaved.

Solution 2) 10x TB phosphate: 6.27 g of anhydrous K_2HPO_4 and 1.17 g of KH_2PO_4 were dissolved in 50 ml ddH_2O using vigorous stirring, and then autoclaved.

50 µl of glycerol stock of either WT HRP-C or mutant HRP-C pFLAG1 plasmid in W3110 *E. coli* were inoculated into 50 ml of LB broth containing 100 µg/ml of ampicillin, and shaken overnight at 37 ^{o}C. Each 5 ml of this 50 ml culture were inoculated into 500 ml of TB (solution 1 plus solution 2) containing 100 µg/ml of ampicillin. The cultures were shaken at 37 ^{o}C, and the growth rate was monitored by measuring the increase in light scattering at 600 nm. When the O.D. reached 0.8-1.0, the cultures were induced with 0.5 mM IPTG. The $O.D._{600}$ was recorded until little or no change was observed (approximately 4 hours); at this point all the cultures were harvested and centrifuged at 4,000 rpm for 30 minutes at 4 ^{o}C in a Beckman J-6B centrifuge. The supernatant was decanted and the cell pellets were stored at -20 ^{o}C.

2.3.2.2 Lysis of Cells and Washing of Protein Pellets:

All harvested cell pellets were resuspended in 200 ml 50 mM Tris, pH 8.0, 10 mM EDTA, 1 mM DTT, to give approximately 250 ml solution. The solution was transferred to a 500 ml plastic beaker, and lysozyme powder was added to give a final concentration of 2 mg/ml, mixed well and the extract was left for one hour on a bench at

room temperature until it became very viscous and stringy. The extract was then divided into 5 x 50 ml fractions and sonicated in a 100 ml plastic beaker with a large probe (CV33 probe) attached to an ultrasonic disintegrator (MSE Mod MK2), each fraction for 2 x 1 minutes. When the extract became thinner it was decanted into centrifuge tubes and centrifuged in a Beckman J2-21 centrifuge, rotor JA20, at 15,000 rpm for 30 minutes at 4 ^{o}C; the supernatants were discarded.

In each individual tube, the protein pellet was resuspended in 20 ml of 2 M urea, 20 mM Tris pH 8.0, 1 mM EDTA and 1mM DDT by manual homogenisation. Then 10 ml of the same solution supplemented with 3% Triton X-100 was added. The solutions were mixed well and left at room temperature for 15 minutes, then centrifuged at 15,000 rpm for 30 minutes at 4 ^{o}C. The supernatant was again discarded. This last step was repeated once more. It was repeated again for a third time, but this time without using the Triton X-100 part of the wash, in order to remove traces of Triton detergent that might subsequently affect the efficiency of the folding procedure. The HRP-C* protein pellets were stored frozen at -20 ^{o}C.

2.3.2.3 Folding and purification of HRP-C* protein:

For each variant or WT, all HRP-C* protein pellets were resuspended in 30 ml of freshly prepared buffer containing 50 mM Tris, pH 8.0, 6 M urea, 1 mM EDTA and 1 mM DTT by using a homogeniser, and were left at room temperature for 15 minutes. They were then centrifuged at 15,000 rpm for 30 minutes at 4 ^{o}C. The concentration of the protein in the supernatant was determined using the Bio-Rad Bradford protein assay with bovine serum albumin (BSA) as a standard. The enzyme was then diluted to a final concentration of 2 mg/ml using more of the buffer mentioned above. The volume of the

protein solution was multiplied by a factor of 10 to give the final total fold volume. A folding solution was prepared so that after the protein solution was added, the concentrations would be 2.1 M urea, 50 mM Tris, pH 8.0, 8 mM $CaCl_2$ and 0.7 mM of oxidised L-glutathione. The folding solution was chilled in the cold room for 30 minutes, and then the enzyme solution was added (giving 0.1 mM DTT and 200 μg/ml protein), and the mixture left in the cold room (stirring) for 18 hours. At this point 6 μM of haemin was added, and the mixture again left in the cold room with stirring for a further 48 hours.

The folded enzyme solution was then centrifuged in the Beckman J-6B centrifuge at 4,000 rpm for 30 minutes to remove any misfolded protein aggregates formed. The solution was concentrated down to about 300 ml using a large spiral-wound Amicon concentrator of 30,000 Da, pre-washed with 2 M urea, and then concentrated down again to less than 50 ml using Millipore 30,000 Da ultrafiltration membranes in a stirred cell at 4 ^{o}C. The protein solution was dialysed overnight at 4 ^{o}C against 20 mM Na acetate solution, pH 4.3 containing 1 mM $CaCl_2$. The aggregates formed during the dialysis process were removed by centrifugation at 4,000 rpm in the Beckman J-6B centrifuge for 10 minutes at 4 ^{o}C, and then by passing the supernatant obtained through a Millipore 0.22 μm Millex-GS sterilizing filter unit.

Final purification of the dialysed protein solution was achieved by cation exchange chromatography using the Pharmacia Fast Protein Liquid Chromatography (FPLC) instrument. The protein was loaded onto a Mono S cation exchange column, pre-equilibrated with 20 mM Na-acetate, pH 4.3. The purified HRP-C* enzyme was eluted from the column by the application of a NaCl gradient to a final concentration of 1 M.

The purified protein fractions were gel-filtered into 5 mM MOPS buffer, pH 7.0 using a PD–10 desalting column (Pharmacia). The purified HRP-C* enzyme was then frozen in liquid nitrogen and stored at -80 ^{o}C.

2.4 UV/Vis Spectroscopic studies:

All standard UV/Visible spectroscopic studies of HRP-C* enzyme samples were performed on a Shimadzu UV- 2401 PC spectrophotometer. The measurements were taken at 25 ^{o}C using quartz cuvettes.

2.4.1 Spectral features of WT HRP-C* and the new variants:

The UV/Vis spectra of the resting states of WT HRP-C* and the new S167 variants were recorded by scanning their diluted solutions in 5 mM MOPS buffer, pH 7.0; from 250-750 nm.

2.4.2 Haem Soret peak extinction coefficient (ε) determination:

The pyridine haemochrome method was used to determined the molar absorption coefficient of WT HRP-C* and the new variants (Fuhrhop and Smith, 1975) at the haem Soret peak; this method measures the total haem content of the sample by forming pyridine-haem complexes, from extracted haem produced on treating enzyme samples with alkali. The difference spectrum of the reduced minus oxidised forms is used to calculate the concentration of the haem extracted from the enzyme and, using a known extinction coefficient, to determine the Soret extinction coefficient.

For WT and each variant, 40 µl of diluted enzyme solution was made up to 400 µl with 5 mM MOPS buffer, pH 7.0, and the resting state Soret peak absorption recorded. The enzyme solution was recovered from the cuvette, diluted further to 800 µl with the same buffer, and then 88 µl of 1 M NaOH and 175 µl pyridine were added. The mixture was divided equally between two quartz cuvettes and a baseline was taken. The mixture in the sample cuvette was then reduced with a few crystals of sodium dithionite and a 250-750 nm spectrum was taken. The value of A_{555}-A_{542}nm was recorded, and the extinction coefficient for each new HRP-C* variant was calculated using the published extinction coefficient for the reduced minus oxidised haem pyridine complex, $\varepsilon_{555} - \varepsilon_{542} = 20.7$ mM^{-1} cm^{-1} (Fuhrhop and Smith, 1975), and the known Soret absorbance.

2.5 Benzhydroxamic acid binding assays:

Benzhydroxamic acid (BHA) binding assays were carried out on WT HRP-C* and the new S167Y and S167W variants in order to estimate the dissociation constant (K_d) of the enzyme-BHA complex. Difference spectra of the enzyme with BHA added or not were recorded between 350-450 nm using the following procedure.

1 ml of 3 µM solution of each enzyme in 5 mM MOPS buffer, pH 7.0, was placed in both the sample cuvette and reference cuvette, and a baseline was taken. Then successive volumes (10 µl) of stock BHA solution (200 µM) were added to the sample cuvette and an equal volume of buffer added to the reference cuvette, and the different spectra were recorded. Successive volumes of stock BHA solution were added until saturation of the enzyme sample occurred. Addition of BHA causes an increase in the absorbance of the Soret peak of the HRP-C* enzyme, and when the absorbance does not

change with the addition of more BHA, then saturation of enzyme has occurred. All experiments were conducted at 25 ^{o}C. The absolute BHA concentrations in the sample cuvette were determined and the absorbance values were corrected accordingly to the dilution factor.

The dissociation constant (K_d), as well as the maximum absorbance (A_ω), were determined by fitting the data, using a weighted least-squares error minimization procedure, to the equation:

$$A = 2A\omega L/\{(L + K_d + P) + [(L + K_d + P)^2 - 4PL]^{0.5}\}$$

corresponding to reversible binding of a ligand to a single site, where A is the absorbance change at 409 nm (Soret) for a total BHA concentration L, A_ω is the maximum absorbance change and P is the total protein concentration (Smith *et al.*, 1992).

2.6 Reaction of enzyme with hydrogen peroxide:

In order to further characterise the new S167 HRP-C* variants, and also to attempt to create a new covalent linkage between the haem and the protein, enzyme samples were treated with differing amounts of freshly prepared hydrogen peroxide solution (DePillis *et al.*, 1997; Colas and Ortiz de Montellano, 2004).

Samples of the S167W and S167Y mutants were gel-filtered using a NAP–5 column (pre-packed disposable columns containing Sephadex^{TM} G–25 Medium, Promega) into 50 mM Na-phosphate buffer (pH 7.0 for S167W and pH 9.5 for S167Y), and were then

diluted to a final concentration of 5 μM in the same Na-phosphate buffer. 0.5 mM of freshly diluted H_2O_2 was then added, and the reaction solution was incubated for two hours at 25 ^oC. After that, the H_2O_2 treated samples of the variants were gel-filtered back into 5 mM MOPS buffer, pH 7.0.

The UV/Visible spectra 250-750 nm of the resting states of WT HRP-C*, treated and untreated variants were then taken. Pyridine haemochrome assays were performed on all the enzyme samples as described in section 2.4.2.

2.7 Enzyme intermediates on treatment with hydrogen peroxide:

Repeat scans of S167 HRP-C* variants at different times after treatment with H_2O_2 were taken in order to monitor the differences in rate of formation and reduction of the enzyme intermediates, Compounds I and II, under steady-state conditions. This experiment was carried out for HRP-C* variants, where 0.5 mM of H_2O_2 was added to 5 μM of each mutant in 50 mM sodium phosphate buffer (pH 7.0 for S167W and pH 9.5 for S167Y) at 25 ^oC and 250-750 nm scans were taken at different times (1, 5, 10, 15, 20, 30, 60, 90, 120, 150 and 180 minutes) after the addition of H_2O_2.

2.8 Acid butanone haem extraction:

The ability to extract the haem prosthetic group from the new S167 variants (both before and after treatment with H_2O_2) was tested using the acid butanone extraction technique (Fuhrhop and Smith, 1975). This experiment was to look for the formation of a cross-linkage between the haem and the protein as a result of the enzyme's reaction with H_2O_2. For each 100 μl enzyme sample of WT HRP-C*, S167W or S167Y variant,

either treated or untreated with hydrogen peroxide, 25 µl of 2 M HCl was added (to denature the protein) plus 500 µl of butanone to extract the organic haem group. The solution was shaken well and then left on the bench to allow the separation of the aqueous layer below and the organic layer above; then the organic layer was carefully extracted. In general for WT HRP-C*, under these conditions, the haem group is extracted directly into the organic layer, leaving the apo-protein in the aqueous layer. Pyridine haemochrome analyses (section 2.4.2) were performed on the organic layer extracted samples and the amount of haem extracted from each of the samples was calculated accordingly.

2.9 High Performance Liquid Chromatography (HPLC) analysis:

2.9.1 Principles of chromatography:

Chromatography is one of the most powerful analytical methods, and is used for separation, identification and determination of the substances in complex mixtures. This method is characterised by the existence of two phases, a stationary phase and a mobile phase. The components of the mixture (solutes or analytes) are distributed between these two phases, and move with the mobile phase through the stationary phase according to their relative affinities towards each phase. The separation is performed by the difference in the rate of getting each component out of the system, which is known as elution. A substance that is distributed preferentially in the mobile phase will elute from the system more rapidly than those preferentially distributed in the stationary phase (Done, 1978).

There are two types of chromatography, based on the stationary phase. The first one is known as planar chromatography, in which the stationary phase is supported on a flat

plate or in the pores of a paper; in this type of chromatography the mobile phase passes the stationary phase under the effect of gravity or by capillary action. The second type is known as column chromatography, in which the stationary phase is packed into a column and the mobile phase moves under the influence of gravity, or by the effect of pressure. Chromatographic techniques can also be subdivided into gas or liquid chromatography, based upon the nature of the mobile phase, as well as solid or liquid chromatography depending on the form of the stationary phase (Skoog *et al.*, 1998).

2.9.2 Distribution ratio and Retention time:

The relative affinity of a solute towards the stationary and mobile phases is known as a distribution ratio K, which is expressed as:

$$K = S_{st}/S_{mo}$$

where, S_{st} is the concentration of solute on the stationary phase, and S_{mo} the concentration of solute in the mobile phase (Skoog *et al.*, 1996).

The K value is the key to the analysis process in chromatography techniques, large values of K lead to slow elution for the solute, while small values lead to rapid elution. Therefore, the best separation occurs when the differences between the distribution ratios of the solutes in the mixture are large and significant. The time it takes for the solute to pass through the stationary phase is called the retention time t_R, or in other words, the time it takes after sample injection for the solute peak to reach the detector (Skoog *et al.*, 1996; Higson, 2004).

2.9.3 HPLC apparatus:

High Performance Liquid Chromatography (HPLC) represents one of the most widely used forms of chromatography. The term 'high performance' relates to the ability of HPLC to perform high quality and selective separation of compounds in minimum times. In the HPLC system, the separation process is achieved by forcing the mobile phase to penetrate through the column under high pressure (Higson, 2004). A typical schematic diagram of High Performance Liquid Chromatography is shown in Figure 2.1. In general, an HPLC apparatus consists of three main sections: solvent delivery system, column and detector.

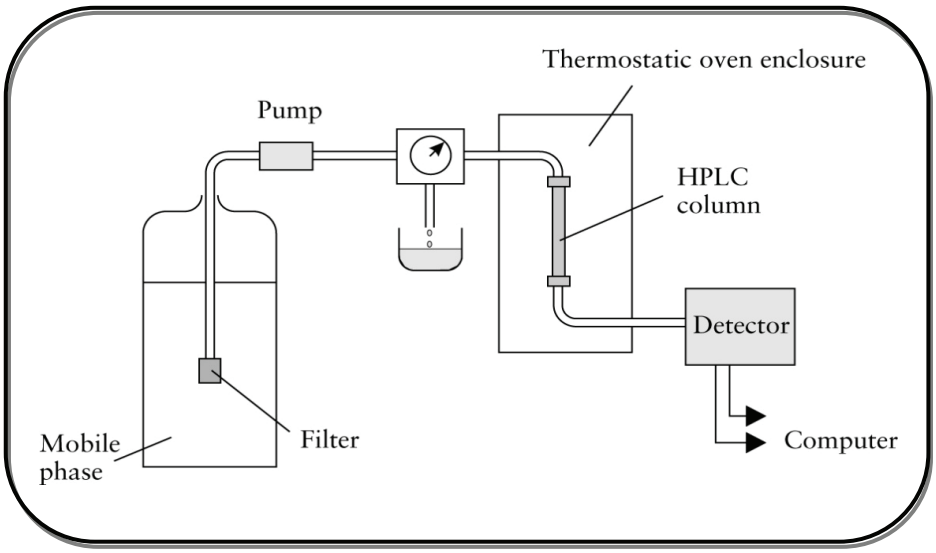

Figure 2.1: Simple scheme of an HPLC system, showing the main parts that make up the apparatus, reproduced from Higson, 2004.

2.9.3.1 Solvent Delivery System: This is the first section in the HPLC apparatus, and is responsible for providing an accurate, constant flow of mobile phase when required. This system consists of the following key parts.

a) Solvent reservoirs, which are usually equipped with inlet filters to remove dust and other particulate material; this facilitates the process of solvent pumping and protects the column from the possibility of blockage.

b) A solvent degassing unit, to remove dissolved air in the solvent; air can produce bubbles in the column, causing a reduction in the performance of detectors and disruption of elution peaks (Fifield and Kealey, 1995; Kealey and Haines, 2002).

c) Pumps, which are responsible for forcing the mobile phase through the column at a controlled flow rate; this is achieved by applying a constant pressure (Lindsay, 1992). Most pumping systems in HPLC include (1) a range of flow rates from 0.1-2 ml/min., (2) non pulse flow, to remove noise from the detector, (3) the generation of pressure up to 4500 psi, (4) the ability to resist corrosion from a wide range of solvents and (5) flow reproducibility of 0.5% or better, to ensure adequate analytical precision (Gilbert, 1987).

In the HPLC technique, liquid samples are injected directly into the flowing mobile phase, using highly controlled injection systems. Two types of injection system are available, syringe and valve. Syringe injection is more convenient than valve (Done, 1978). Up-to-date HPLC apparatus is generally equipped with automated injection systems, which have the ability to automatically inject up to 100 samples. A guard column is also sometimes used, positioned before the separation column. This serves to protect the column from aggregated particulate matter in the injected samples. It is a short column packed with the same stationary phase as the analytical column (Kealey and Haines, 2002).

2.9.3.2 Column: This holds the stationary phase. The columns in HPLC are usually constructed from stainless steel tubing, and most have lengths ranging from 10-30 cm with diameters ranging from 3-10 mm. These columns are packed typically with particle sizes of 5 or 10 μm. As a result of the need to improve and develop the efficiency of

HPLC, high performance micro-columns have been produced with smaller dimensions, ranging from 3-7.5 cm in length and 1-4.6 mm in diameter, with 3 or 5 μm particle size (Skoog *et al.*, 1996).

The main type of packing material for HPLC columns is micro porous particles with diameters from 3-10 μm. Silica is one of the most important materials that is used as a packing material as it can be made with highly uniform diameters. It is used to prepare chemically modified stationary phases with high quality separation properties. The particles are coated in most cases with thin organic films, which are bonded either chemically or physically to the surface. There are four major classes of modified silica: esterified silicas, Si-N functionalized silicas, Si-O-Si-C functionalized silicas and polysiloxane/silicone derivatized silicas. Other chemical materials that are used for column packing, include alumina particles, porous polymer particles, porous graphite carbon and ion-exchange resins (Higson, 2004).

Recently, a particle size of less than 3 microns has been used for HPLC. It produces improved peak shapes, and reduces the retention time by a factor of ten. This is named ultra performance liquid chromatography (UPLC) (de Villiers *et al.*, 2006).

2.9.3.3 Detector: The detector is essential to all types of chromatography techniques. It is responsible for detecting the elution positions of the separated components of a mixture that has been subjected to a chromatographic process. The results from the detectors are generally displayed in the form of a chromatogram with varying peaks, each one of these peaks representing one component of the mixture. The main characteristic of any detection system is the ability to give a recognizable signal, even

with a minimum concentration of solute, against the background noise of the instrument (Done, 1978).

A number of detectors are available for HPLC, and the most commonly used include UV-Visible absorption, fluorescence, electrochemical and refractive index detectors. By far the most widely used are UV-Visible detectors due to their high sensitivity and ability to monitor many different solutes as they elute from the column. Today, a variable wavelength detector (diode-array) is available for a range of 200-700 nm, which can display an entire spectrum as solutes exit the column (Pryde and Gilbert, 1979; Ardrey, 2003). A fraction collector may be added after the detector; this is useful for collecting pure fractions accurately for further spectroscopic analysis.

2.9.4 HPLC analysis of the new HRP-C* mutants:

HPLC analysis was used to examine the nature of any covalent linkage between the haem and the protein in WT HRP-C* and the S167 variants both before and after H_2O_2 treatment. All HPLC assays were conducted on the Agilent 1100 Series HPLC system with an analytical C_4, 4μm (100 × 4.5 mm) reverse phase column, under PC control. The mobile phase consisted of two buffer solutions, Buffer A: 0.1% (v/v) trifluroacetic acid (TFA) in water, and Buffer B: 0.1% (v/v) TFA in acetonitrile (MeCN). 20 μl of a 50 μM enzyme sample were mixed with an equal volume of 2% SDS (Metcalfe *et al.*, 2004) and boiled for 5 minutes at 95 ^{o}C, after which the sample was diluted to 100μl total volume with buffer A and injected (20 μl at a time) into the column pre-equilibrated with buffer A. The protein/haem elution was achieved by using the following elution profile with a flow rate of 1 ml/min.: 0 % buffer B for 5 minutes, after that 0-30 % buffer B for 5 minutes, followed by 30-40 % buffer B for 5 minutes, and

then 40-100 % buffer B for 45 minutes. The haem group was monitored at 400 nm while the protein was monitored at 280 nm.

2.10 Mass Spectrometry:

2.10.1 Introduction:

Mass spectrometry (MS) is a widely used analytical technique, in which the atoms or molecules of a sample are treated to form gaseous ions; these ions are then separated according to their mass-to-charge ratio *(m/z)* (Farmer, 1963). MS is characterised by high sensitivity, as very small amounts of analyte (picogram) are sufficient to provide information with high accuracy and precision (Ardrey, 2003). MS has been successfully applied to a wide range of research studies in organic chemistry, to determine the molecular weight and structure of organic compounds (Johnstone and Rose, 1996), and in inorganic and organometallic chemistry, to identify and determine complexes and compound components (Henderson and McIndoe, 2005). Furthermore, this technique has been used extensively in the field of biochemistry and biotechnology, to characterise a wide variety of bio-molecules such as sugars, oligonucleotides, peptides and protein molecules (Fountoulakis and Langen, 1997; Roepstorff, 1997; Mo and Karger, 2002). Currently, MS plays a significant role in determining the amino acid sequences of peptides and proteins, in addition to identifying the location of disulfide bridges in proteins (Hunt *et al.*, 1988; Carr *et al.*, 1991). MS has a lot of applications in the pharmaceutical industry, where it is invaluable for drug discovery and drug metabolism studies (Korfmacher, 2005; Ackermann *et al.*, 2008), and has important medical applications, in respiratory and blood gas analysis, lipid analysis and in studying the fate of pesticide and insecticide metabolism (Milne, 1991).

2.10.2 Main components of mass spectrometry:

MS consists of the following main parts: inlet system, ionization source, mass analyzer and detector, Figure 2.2. These fundamental parts are usually maintained under high vacuum in order to protect the system from the effects of air molecules, which would hinder and disrupt the mass spectra of samples by colliding with the gaseous ions, and also cause damage to some parts of the instrument such as the ionization source and detector (Kealey and Haines, 2002).

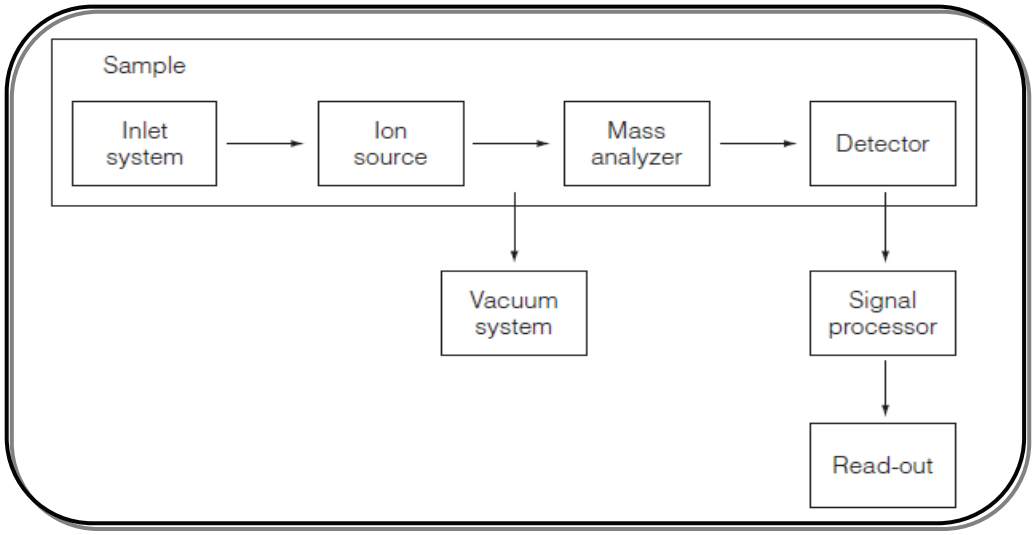

Figure 2.2: Block diagram showing the main parts of a mass spectrometer.

2.10.2.1 Sample Inlet System: The sample inlet represents the first part of the mass spectrometer instrument. It facilitates the controlled introduction of gaseous or vapourized liquid samples via a molecular leak, and solid samples via a heated probe. In fact, there are three inlet systems commonly used for introducing samples for ionization: these are batch, direct probe and chromatographic type inlet. Each one of these systems has high efficiency and are used for experiments depending on the nature of sample to be analyzed (Kealey and Haines, 2002; Higson, 2004).

2.10.2.2 Ionization Sources: The main function of this part is to produce as many ions as possible from the neutral particles of sample, and to form an ion beam that is suitable to enter into the analyzer. A variety of ionization sources are used for MS, the choice depending on the nature of the sample and the type of information desired. For example, electron ionization and chemical ionization sources are suitable for gas phase ionization, whilst fast atom bombardment, secondary ion mass spectrometry, electrospray and matrix assisted laser desorption ionization sources are used to ionize condensed phase samples. The principle of how most of these ionization sources work is the exciting of the neutral sample molecule which then ejects an electron to form a radical cation ($M^{+\cdot}$). Suitable ionization sources must also be characterised by possession of a stable ion beam that has sufficient intensity for accurate measurement. In addition, ionisation sources are designed to produce as low as possible an intensity of background ions which do not originate from the sample, and they should not exhibit mass discrimination (Elliot, 1963; Roboz, 1968).

2.10.2.3 Mass Analyzer: The sample ions, which are formed in the ionisation source, are then accelerated into the next part of the mass spectrometer, known as the mass analyzer, by applying an electric field. Within the mass analyzer, the ions are separated according to differences in their mass-to-charge (*m/z*) ratios. Ions formed from neutral sample molecules will have different masses, and therefore when accelerated towards the analyzer region, they will enter with a range of velocities; the greater the mass of the ions the slower they travel, hence ions with smaller mass will arrive and enter the analyzer first (Higson, 2004). Several forms of mass analyzers are available to achieve the separation process of the ions according to their *m/z* value. The selection of mass analyzer depends on the following properties: (1) resolution, (2) mass range, (3) scan

rate and (4) detection limits required. Commonly used mass analyzers include quadrupole filter, magnetic sector, time-of-flight, ion cyclotron resonance and quadrupole ion trap analyzers (Chapman, 1993; Bramer, 1998).

2.10.2.4 Detector and Data Processing: This is the last component of the mass spectrometer. Once the process of separation of the ions according to their *m/z* ratios in the analyzer region is completed, ion current of varying intensity reaches the detector. The detector monitors this ion current, amplifies it, and then transmits a signal into the data processing system, whereby the signal is processed and recorded in the form of a mass spectrum. The spectrum output is plotted as *m/z* values of the ions against their intensities. Important information can be obtained from this spectrum, such as the number of components, the molecular mass of each component and the relative abundance of the various components in the sample. The most common detectors include the photomultiplier, electron multiplier and micro-channel plate detectors, and are used to suit the type of analyzer (Bramer, 1998; Ashcroft, 2002; Polce and Wesdemiotis, 2002).

2.10.3 MALDI-TOF Mass Spectrometer:

Matrix-Assisted Laser Desorption Ionization (MALDI) is a soft ionization technique used in MS, which is characterised by high accuracy and sensitivity. The technique was developed in 1988 by Hillenkamp and Karas for protein analysis (Karas and Hillenkamp, 1988), and recently it has become one of the most widely used techniques for the analysis of bio-molecules. It is used mainly for rapid measurement of the molecular weights of peptides, proteins, lipids, oligonucleotides, oligosaccharides and

other bio-molecules, with an accuracy of up to 0.01% of the actual molecular weight of the sample (Johnstone and Rose, 1996).

MALDI-MS is based on exposing the sample to be analyzed, mixed with an excess of matrix compound, to a short period of bombardment by intense pulses of laser light, usually a pulsed nitrogen laser at a wavelength of 337 nm (Figure 2.3) (Polce and Wesdemiotis, 2002). The matrix is characterised by its high absorbance of laser light energy, which is transformed into excitation energy and leads to the ionization of the analyte. Experience has shown that the best and most reliable results can be obtained when the molar ratio of sample to matrix ranges from 1:100 to 1:50,000. Indeed, the matrix plays an essential role in the generation of intact ions from the analyte, as it assists in efficiently providing controllable energy to the sample, minimizing the possibility of decomposition (Hillenkamp *et al.*, 1991; Lewis *et al.*, 2000).

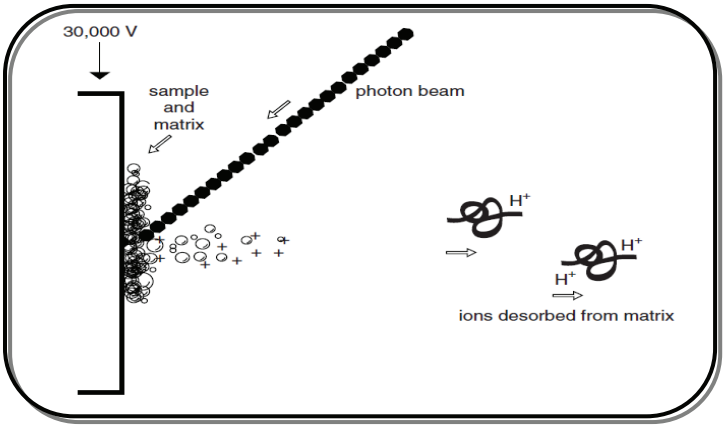

Figure 2.3: The process of the formation of sample ions by MALDI source, reproduced from Polce and Wesdemiotis, 2002.

2.10.3.1 MALDI Matrices:

Matrices that are used in MALDI-MS analysis should have the following properties: (1) high electronic absorption at the laser wavelength used, (2) good vacuum stability, (3) low vapour pressure and (4) good solubility in solvents that also dissolve the analyte

sample (Montaudo *et al.*, 2002). The most commonly used matrices are 2,5-dihydroxybenzoic acid (DHB) which is usually used for the analysis of glycopeptides, glycoproteins, small proteins and oligonucleotides, 3,5-dimethoxy-4-hydroxycinnamic acid (sinapic acid or SA) which is commonly used for peptides and proteins, and α-cyano-4-hydroxycinnamic acid (α-CHCA) which is mainly used for the analysis of peptides, glycopeptides and small proteins (Figure 2.4) (Lewis *et al.*, 2000).

2.10.3.2 Sample Preparation in MALDI:

The sample-matrix preparation is crucial to the quality of the spectrum obtained in MALDI-MS, as it strongly affects detection sensitivity, selectivity and mass resolution in the analysis of peptides and proteins. The most frequently used preparation method currently is the dried-droplet method. It is quite a simple and fast method, in which initially a saturated solution of a suitable matrix is prepared in water/organic solvent (usually either ethanol or acetonitrile). Appropriate amounts of this matrix solution are then mixed with the analyte dissolved in identical solvent(s) to give a mixture with a matrix to sample ratio of about 5000:1. After this, an aliquot of the mixture is transferred onto the MALDI target and allowed to dry at room temperature. The sample is then is ready to be loaded into the MALDI-MS instrument and analyzed (Hillenkamp *et al.*, 1991; Lewis *et al.*, 2000).

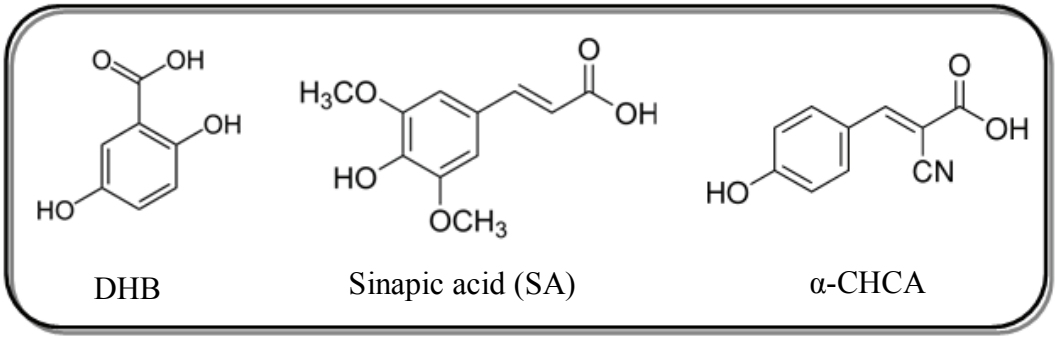

Figure 2.4: Chemical structures of the most common MALDI matrices.

2.10.3.3 Time-of-Flight analyzer in MALDI:

Time-of-Flight (TOF) analyzers are typically suited for use with MALDI-MS because of their theoretically unlimited mass range, high ion transmission and temporal separation of ions (Lewis *et al.*, 2000). TOF is characterised by its ability to produce high mass accuracy and high mass resolution. In MALDI TOF-MS, a packet of ions is produced by firing a laser onto the matrix-sample mixture, which is then accelerated by a fixed electric potential (V). The resulting velocity of the ions is characteristic of their *m/z* ratio. After the ions leave the acceleration region they then enter a field-free flight region known as a drift tube. They travel through the drift tube and reach the detector at different times depending on their initial velocity. The signal resulting from the detector is recorded as a function of time and displayed as a mass spectrum, on which the square of the flight time is proportional to the *m/z* ratio, as shown in the following equation:

$$m/z = 2\mathrm{V}t^2/l^2$$

where, *m* is the mass of the ion, *z* is the number of charges, V is the accelerating voltage, *t* is the ion flight time, *l* is the length of the flight tube. Since the V and *l* values are known, the *m/z* ratio can be calculated from the equation above (Chapman, 1993; Lewis *et al.*, 2000; Montaudo *et al.*, 2002).

There are two kinds of TOF analyzers which can be used to detect the ions through the drift tube; these are linear mode and reflectron mode (Figure 2.5). Higher sensitivity, particularly at high molecular mass, is achieved in linear mode, whilst higher resolution is obtained in reflectron mode, as the reflector (ion mirror) serves to increase the flight time of the ions and hence their separation. In linear mode, resolution is around (500–800) and only a short lifetime (1 μs) for the ion is required, even in the case of a metastable decay on the flight path. In reflectron mode, resolution is typically around 1000–2500 (Hillenkamp *et al.*, 1991; Montaudo *et al.*, 2002).

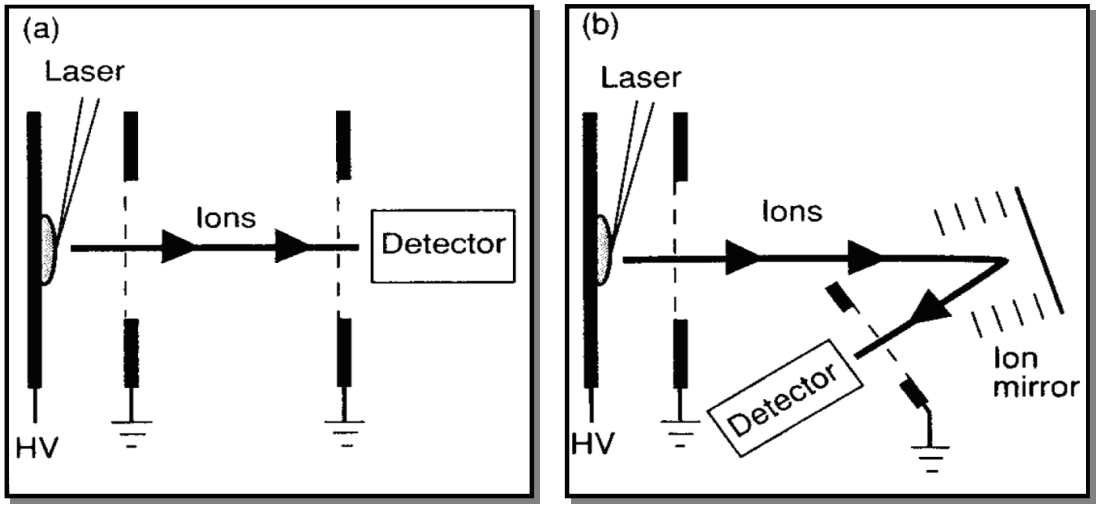

Figure 2.5: Diagram of a MALDI TOF-MS in (a) Linear mode and (b) Reflectron mode, reproduced from Hillenkamp *et al.,* 1991.

2.10.4 ESI Mass Spectrometer:

Electrospray ionization (ESI) has emerged as a powerful MS technique for the analysis of large and fragile polar molecules. Since it was first used by Yamashita and Fenn in 1984 (Yamashita and Fenn, 1984), this technique has become one of the common ways to measure the molecular weight of bio-molecules, particularly peptides and proteins. The principle of ESI is the formation of multiply charged ions from an analyte, with produced ions having one, two, three or more charges; therefore the corresponding *m/z* ratios will vary relative to the number of charges (*z*) carried by each ion. In this technique, large molecules such as proteins can be protonated or deprotonated at several sites, giving ions with an upper limit of *m/z* value not exceeding a few thousand. This is of significance as a mass spectrometer measures the *m/z* ratio of an ion, and the mass range of an instrument may therefore be effectively extended by a factor equivalent to the number of charges caused to reside on the sample molecule. Thus, massive molecules, even those with a molecular weight in excess of a hundred thousand, can be analyzed (Johnstone and Rose, 1996).

2.10.4.1 Mechanism of Electrospray Ionization:

Electrospray ionization occurs by three main steps: (1) formation of charged droplets, (2) desolvation of the droplets and (3) formation of gas-phase ions from the sample. During standard ESI (Figure 2.6), the sample is dissolved in a polar, volatile solvent and introduced into the instrument by a syringe pump in a region of atmospheric pressure (Ashcroft, 2002). The analyte solution is then passed through an electrospray capillary tube at a flow rate ranging between 1 μl/min to 1 ml/min, while a strong electric field is applied to the tip of the capillary. Typically, the potential difference between the capillary tip and a nearby counter-electrode is 3-4 kV. The sample emerging from the tip is charged by the field and hence dispersed into a mist of highly charged droplets, a process that is assisted by the co-axial flow of a nebulising gas, usually nitrogen, flowing around the outside of the capillary. The charged droplets then undergo a desolvation process during their passage across the front of the ionization source, assisted by a warm flow of nitrogen gas that is known as the drying gas. As a result of the removal of the solvent, the droplets decrease in size until they reach the Rayleigh instability limit; at this point a Coulombic explosion occurs and several even smaller droplets are formed. A series of solvent evaporation, droplet contraction and Coulombic explosions is repeated until gas-phase ions of the sample are produced (Figure 2.7), which are eventually transferred through a sampling cone under high vacuum towards the analyzer of the mass spectrometer (Fenn *et al.*, 1989; Ashcroft, 2002; Polce and Wesdemiotis, 2002; Prokai, 2002; Ardrey, 2003).

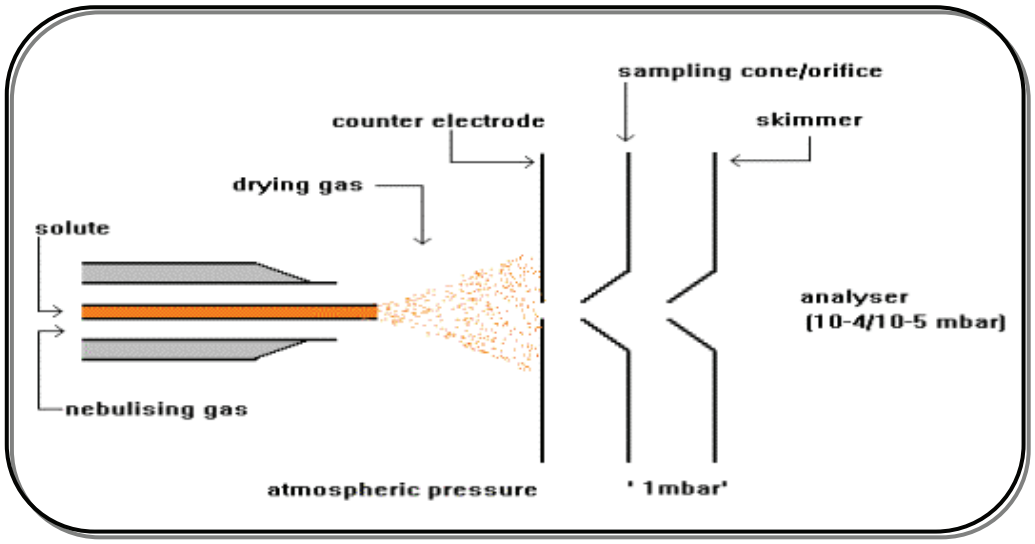

Figure 2.6: Standard Electrospray Ionization (ESI) spectrophotometer set up, reproduced from Ashcroft, 2002.

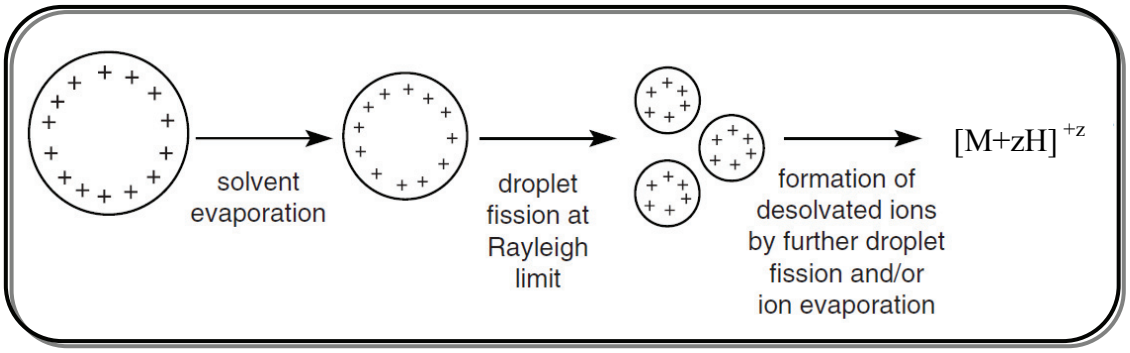

Figure 2.7: The formation of ions from droplets in ESI, reproduced from Polce and Wesdemiotis, 2002.

2.10.4.2 ESI spectrum appearance and Data processing:

As discussed before, ESI produces multiply charged ions, either by protonation in positive ionization mode, $[M+zH]^{+z}$, or deprotonation in negative ionization mode, $[M-zH]^{-z}$, from molecules that have multiple sites. The choice between negative or positive ionization modes would depend on the nature of the sample. Peptides and proteins are usually analyzed under positive ionization conditions, while saccharides and oligonucleotides are analyzed under negative ionization conditions. The analysis of

multiply charged (both protonated and deprotonated) ions has been accomplished using most types of analyzers, such as quadrupole, magnetic sector, ion taps and time-of-flight (Prokai, 2002). An ESI mass spectrum usually appears as a series of ion peaks of different *m/z* values, each of which represents a different charged state for the same analyte (Fenn *et al.*, 1989). The molecular weight of the sample can be determined from the spectrum, using the fact that adjacent peaks in the multiply charged series are different only by one charge. A typical ESI-MS spectrum, of horse heart myoglobin, is shown in Figure 2.8; in this spectrum, the *m/z* values recorded for multiply charged ions range from 616.35 to 1413.87 (Ardrey, 2003). Each peak observed in this spectrum represents the intact molecule of the analyte carrying an unknown number of charges, and the same number of protons. The value above each peak represents the molecular weight of the intact analyte divided by the charge number it carries (Ardrey, 2003).

The *m/z* value of an ion is related to the molecular weight of the analyte and can be expressed by the following equation:

$$m/z = (\mathrm{MW} + \mathrm{nH}^{+})/\mathrm{n}$$

where *m/z* = the mass-to-charge ratio, MW = the molecular mass of the analyte, n = the integer number of charges on the ion and H = the mass of a proton = 1.008 Da.

When the number of charges on an ion is known, then it is possible to calculate the molecular weight of the sample from one peak by using the equation. However, because the value of n is not known, this makes one peak insufficient to determine the molecular weight of the analyte. But if two adjacent peaks are examined, both unknown parameters (number of charges and molecular weight of analyte) can be solved from a pair of simultaneous equations (Johnstone and Rose, 1996; Ardrey, 2003). For example, if the ions appearing at *m/z* 848.62 in the horse heart myoglobin spectrum (Figure 2.8)

have "n" charges, then the ions at *m/z* 808.28 will have "n+1" charges, and the above equation can be written for these two ions as:

$848.62 = (\mathrm{MW} + \mathrm{nH}^+)/\mathrm{n}$ and $808.28 = [\mathrm{MW} + (\mathrm{n}+1)\mathrm{H}^+]/(\mathrm{n}+1)$

These simultaneous equations can be rearranged to exclude the MW term:

$\mathrm{n}(848.62) - \mathrm{nH}^+ = (\mathrm{n}+1)\,808.28 - (\mathrm{n}+1)\mathrm{H}^+$

$\mathrm{n}(848.62) = \mathrm{n}(808.28) + 808.28 - \mathrm{H}^+$

$\mathrm{n}(848.62 - 808.28) = 808.28 - \mathrm{H}^+$

$\mathrm{n} = (808.28 - \mathrm{H}^+) / (848.62 - 808.28)$

$\mathrm{n} = 807.272 / 40.34 = 20$

Putting the value of n back into the equation:

$848.62 = (\mathrm{MW} + \mathrm{nH}^+)/\mathrm{n}$

$848.62 \times 20 = \mathrm{MW} + (20 \times 1.008)$

$\mathrm{MW} = 16972.4 - 20.16$

MW = 16952.24 Da

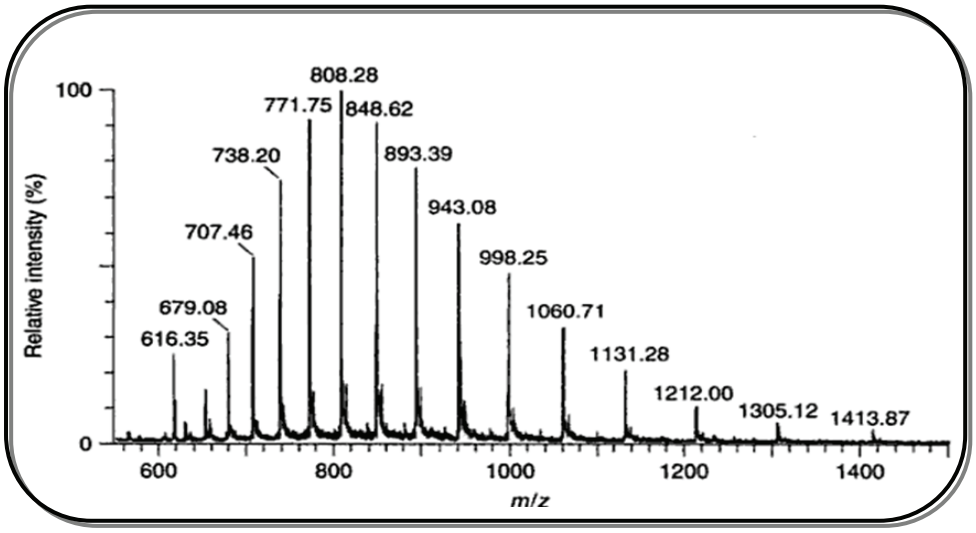

Figure 2.8: A positive ion ESI-MS spectrum of horse heart myoglobin, reproduced from Ardery, 2003.

2.10.5 MALDI-TOF analysis of HRP-C* mutants:

For MALDI–TOF MS analysis, 5 µl of a 50µM of WT HRP-C*, S167W or S167Y variant (either treated or untreated with hydrogen peroxide) were mixed with an equal volume of 25 mg/ml matrix solution (α-cyano-4-hydroxycinnamic acid dissolved in 1:1 MeCN and ddH_2O). 1 µl of the final solution with matrix was applied to the sample target plate and allowed to dry and crystallise at room temperature. The analysis of sample was performed by the MALDI-TOF machine (Waters Corporation), pre-calibrated with protein samples of high purity and known molecular weight. The sample was loaded under high vacuum, the laser fired (the energy of the laser was at 60% on medium range) and the detector placed in a linear mode. The data processing was achieved automatically using MassLynx V4.0 to calculate the mass of each enzyme sample.

2.10.6 Electrospray Ionization of HRP-C* mutants:

For ESI-MS analysis, HRP-C* proteins were analysed under positive ionisation conditions. 100 µl samples of WT-HRP-C*, S167W or S167Y variant (either treated or untreated with hydrogen peroxide) were dialysed overnight in the cold room (4 ^{o}C) against ddH_2O, then mixed with an equal volume of 0.1% (w/v) formic acid in 50:50 methanol and water. The final solution was directly injected at a rate of 15 µl/min into a Micromass Hybrid Q-TOF ultima machine (Waters Corporations), pre-calibrated with sodium iodide with *m/z* values range of 100-3000 Dalton. The dissolvation temperature was 400 ^{o}C and desolvation gas flow was 396 l/hr. Data processing and analysis of the resultant spectrum data was achieved automatically using MassLynx V4.1 to determine the mass of each protein sample.

2.11 Peroxidase activities under Steady-State Conditions:

2.11.1 Initial steady-state parameters for the oxidation of ABTS:

For WT HRP-C* as well as each of the S167 variants, initial steady-state parameters for peroxidase activity were determined using the substrate 2,2'-azino-bis (3-ethylbenzthiozoline-6-sulphonic acid) (ABTS), which is oxidised to a green radical product in the presence of peroxidase and hydrogen peroxide (H_2O_2).

Reactions were carried out in a citrate-phosphate buffer, pH 5.0, containing 51 mM disodium hydrogen orthophosphate and 24 mM citric acid. The assay reactions were initiated by the addition of substrate, hydrogen peroxide and then enzyme to a cuvette, giving final concentrations of 1 mM H_2O_2, 3 nM enzyme and 0.1-3 mM ABTS in 1 ml total final assay volume. All assay reagents were prepared in the assay buffer.

The formation of the green radical product, as a function of time, was measured at 25 ^{o}C by monitoring the change of absorbance at 414 nm for 60 seconds. Three independent measurements were made for each substrate concentration. The initial rates (μmol.min^{-1}.ml^{-1}) were determined using ε_{414} = 36.8 mM^{-1} cm^{-1} (Childs and Bardsley, 1975) and then converted to turnover number (s^{-1}) using enzyme concentration. The K_m and k_{cat} for ABTS were determined by fitting the data obtained to the Michaelis-Menten equation using the statistical analysis software SigmaPlot for Windows V4.01 (SPSS UK Ltd,). Hydrogen peroxide concentration was determined by measuring the absorbance of a dilution of the stock solution at 240 nm, and using the extinction coefficient ε_{240} = 39.4 M^{-1} cm^{-1} (Nelson and Kiesow, 1972).

2.11.2 Activity screening towards a panel of substrates:

WT HRP-C* enzyme and the S167 variants were also screened against a range of peroxidase substrates, in order to determine their specific activities. The assays were carried out in phosphate-citrate buffer, pH 5.0, containing 51 mM disodium hydrogen orthophosphate and 24 mM citric acid at 25 ^{o}C. The individual conditions for each substrate are given in Table 2.1. The reactions were initiated by the addition of enzyme, at suitable concentration, to the other reagents. The dilute stock enzyme solutions were prepared in 5 mM MOPS buffer, pH 7.0, containing 0.2 mM $CaCl_2$ and 0.2 mg/ml BSA, to promote enzyme stability.

2.11.3 Initial steady-state parameters with luminol as substrate:

Steady-state kinetic constants for luminol oxidation by WT HRP-C* and S167 variants were obtained by measuring the absorbance change at 400 nm for 60 seconds. The assays were carried out in a citrate-phosphate buffer, pH 5.0, as described in section 2.11.2 using 1 mM H_2O_2, 20 nM enzyme and 0.1−5 mM luminol in 1 ml total assay volume. The initial rates (μmol.min^{-1}.ml^{-1}) were determined using ε_{400} = 4.5 mM^{-1} cm^{-1} and then converted to turnover number (s^{-1}). Kinetic parameters K_m and k_{cat} for luminol were determined by fitting the data obtained to the Michaelis-Menten equation.

Table 2.2: Enzymatic reaction conditions for assays of WT HRP-C* and S167 variants with a range of substrates. The assays were carried out in phosphate-citrate buffer, pH 5.0, containing 51 mM disodium hydrogen orthophosphate and 24 mM citric acid at 25 ^{o}C using enzyme concentrations as shown below, 1 mM H_2O_2 (with the exception of point 2 below) and the different concentrations of substrates as shown below, in a final volume of 1 ml at 25 ^{o}C. The enzyme solutions were diluted in 5 mM MOPS buffer, pH 7.0, containing 0.2 mM $CaCl_2$ and 0.2 mg/ml BSA.

Substrate	[Substrate]	[Enzyme]	Extinction coefficient
ABTS	0.3 mM	0.5 nM	[a]ε_{414} = 36.8 mM^{-1} cm^{-1}
Ferulic acid	50 µM	0.25 – 0.5 nM	[b]ε_{310} = 8.68 mM^{-1} cm^{-1}
Caffeic acid	70 µM	0.2 – 0.25 nM	[c]ε_{320} = 10.4 mM^{-1} cm^{-1}
p-Cumaric acid	76 µM	0.1 – 0.25 nM	[d]ε_{308} = 12 mM^{-1} cm^{-1}
Potassium ferrocyanide	2 mM	2.5 – 5 nM	[e]ε_{420} = 1.06 mM^{-1} cm^{-1}
Guaiacol	5 mM	1 nM	[f]ε_{470} = 26.6 mM^{-1} cm^{-1}
Pyrogallol	20 mM	1 nM	[g]ε_{430} = 2.47 mM^{-1} cm^{-1}
o-Phenylenediamine	0.2 mM	0.5 nM	[h]ε_{450} = 11.1 mM^{-1} cm^{-1}
Chlorpromazine	2.2 mM	50 nM	[i]ε_{525} = 12.1 mM^{-1} cm^{-1}
Luminol[1]	0.5 mM	20 nM	[j]ε_{400} = 4.5 mM^{-1} cm^{-1}
Orange I[2]	50 µM	1 nM	[k]ε_{480} = 15.2 mM^{-1} cm^{-1}
Orange II[2]	50 µM	0.75 µM	[l]ε_{480} = 15.2 mM^{-1} cm^{-1}

[a](Childs and Bardsley, 1975), [b](Abelskov *et al.,* 1997), [c and d](Rasmussen *et al.,* 1995), [e](Hasinoff and Dunford, 1970), [f and h](Bovaird *et al.,* 1982), [g](Chance and Maehly, 1955), [i](Reilly and Aust, 1997), [j](Cali, 2008), [k and l](Coen, 2001).

[1] 0.01772 gm of luminol was dissolved in 1 ml DMSO solvent, then 9 ml of ddH_2O were added to this solution along with 200 µl of 1 M NaOH (to completely dissolve the luminol).

[2] The assay was carried out in 5 mM borate-phosphate buffer, pH 8.0, µ = 50 mM, using 0.1 mM of H_2O_2.

2.12 Pre steady-state kinetics measurements:

2.12.1 Introduction:

Stopped flow spectroscopy provides a way of monitoring fast reactions that have an accompanying spectral change. It was developed by Britton Chance in the 1950s and it is considered an efficient way of measuring the transient absorbance changes which occur when an enzyme reacts rapidly with substrate (Gutfreund, 1999). The method allows the measurement of pre steady-state rate constants for the formation of enzyme intermediates, which is impossible under normal steady-state kinetics. Pre steady-state kinetics describes the phase of an enzyme-catalysed reaction where enzymatic intermediates are accumulating, processes that may be completed typically within milliseconds. Therefore stopped flow spectroscopy is an extremely useful technique characterised by the ability to achieve a very rapid mixing of reagents and timely data collection (Cornish-Bowden, 2004).

The sampling handling unit (SHU) of the stopped flow system used (Applied Photo Physics SX18MV) (Figure 2.9) is composed of two syringes, one holds the enzyme sample and the other holds the substrate under investigation. Computer controlled pneumatic ram drivers load reactants from these syringes into a mixing chamber. Once the mixed solution has passed through the mixing chamber it forces back a ‘stopping’ syringe, which triggers a micro switch, stopping the rams and triggering the spectroscopic measurements of the reaction. This process takes approximately 2 ms and is known as the dead time; the dead time is thus essentially the age of the reaction as it enters the optical cell. The system is able to measure either rapid change in absorbance at a single wavelength or across a range of wavelengths (using a photodiode array, see

below). The changes in absorption are measured using a spectrophotometer equipped with a xenon light source and a photomultiplier.

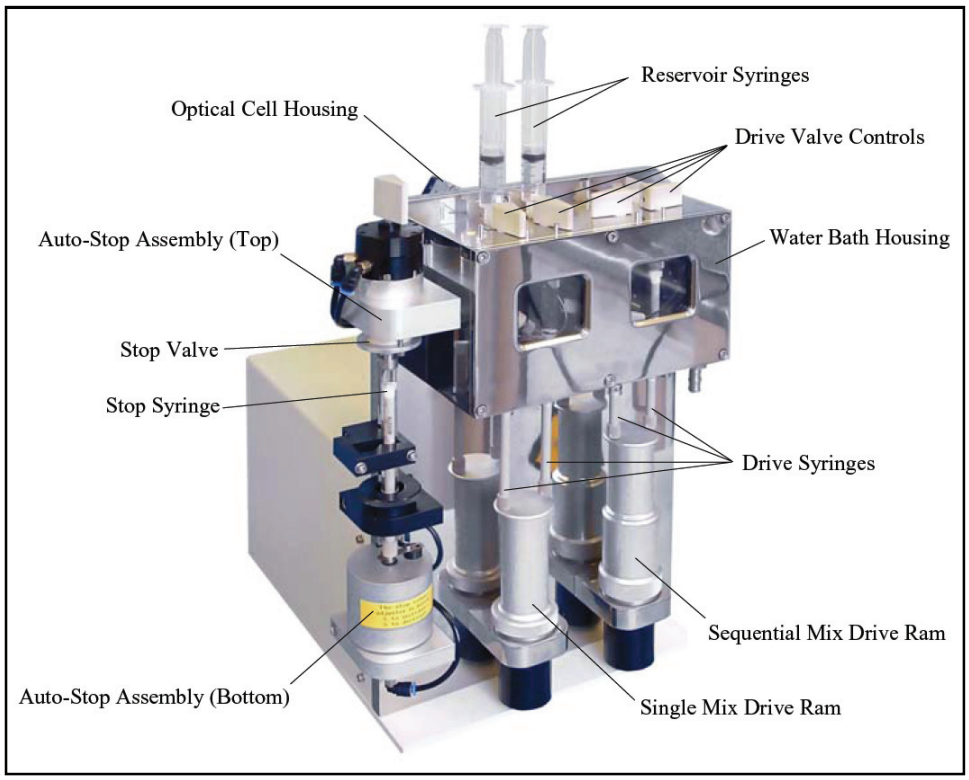

Figure 2.9: Sampling handling unit (SHU) of Stopped Flow spectrometer. The SHU is shown fitted with the sequential (double) mixing option. This option equips the SHU with 4 drive syringes and 2 pneumatic drives rams. The standard single-mix system is equipped with 2 drive syringes and 1 pneumatic drive ram[2].

2.12.2 Photodiode array experiments:

The photodiode array (PDA) of the Applied Photophysics stopped flow system used, uses a xenon light source to perform rapid UV-Visible spectral scans of the contents of the optical cell. The array has the ability to perform spectral measurements over the range of 300-735 nm, and enables repeat scans down to every 1.28 ms (this is known as the integration time). Repeat scans obtained were analysed using the global analysis

[2] The picture is adopted from Applied Photophysics, hardware user guide of the SX20 stopped flow system.

software, Pro-Kinetics V1.05, to model the presence of possible transient species in the enzymatic reaction.

Samples of WT HRP-C* and variants were exchanged from MOPS storage buffer, using a NAP-5 column (containing Sephadex G-25 Medium, Pharmacia) into 10 mM Na-phosphate buffer, pH 7.0, and then diluted to 4 μM with the same buffer. A 40 μM H_2O_2 solution was also prepared using the phosphate buffer. Enzyme and peroxide solutions were placed into the two driving syringes and mixed giving final concentrations of 2 μM enzyme and 20 μM H_2O_2. Rapid scan optical spectra were recorded in a logarithmic manner from 1.28 ms to 1000 ms.

2.12.3 Determination of k_1 value:

The Compound I formation rate constant k_1 for the reaction of WT HRP-C* or variant (both before and after treatment with hydrogen peroxide) with H_2O_2 was determined under pseudo first-order conditions using the stopped flow spectrophotometer. All measurements were conducted at 25 °C in 10 mM sodium phosphate buffer, pH 7.0.

Stock enzyme samples were exchanged from MOPS buffer, using a NAP-5 column (containing Sephadex G-25 Medium, Pharmacia) into 10 mM phosphate buffer, pH 7.0, and diluted to the desired concentration with more buffer. A constant concentration of enzyme ranging between 1-1.5 μM was used with variable concentrations of H_2O_2 ranging between 5-15 μM. Three independent determinations were made for each hydrogen peroxide concentration and the mean was taken. The changes in absorbance in the optical cell were monitored at 395 nm, the isosbestic wavelength for Compound I and Compound II (Smith *et al.*, 1992). By following the decrease in absorbance at 395

nm, the pseudo first-order rate constant (k_{obs}) at each H_2O_2 concentration was obtained by single exponential decay fit of the trace. The k_{obs} obtained were then plotted against H_2O_2 concentration and the resultant curve fitted by a weighted least square, linear regression analysis using SigmaPlot software. The gradient of the plot is the second-order rate constant k_1.

The auto-reduction of Compound I was also monitored, at 412 nm, by stopped flow spectroscopy. Upon stopped flow mixing of enzyme and H_2O_2, using final concentrations for H_2O_2 and enzyme of 2 μM and 20 μM, respectively, the traces obtained were biphasic in nature. The traces were recorded and fitted to a double exponential function and the pseudo first-order rate constant (k_{obs}) were obtained. The life time of the Compound I intermediate was determined as the reciprocal of the k_{obs} obtained.

2.12.4 Determination of k_2 and k_3 values:

The Compound I reduction, or Compound II formation, rate constant k_2 and Compound II reduction rate constant k_3 of the reaction of WT HRP-C* or variant with luminol as reducing substrate, were determined by monitoring the change in absorbance at 424 nm under pseudo first-order conditions using the stopped flow spectrophotometer. Pre-preparation of Compound I was by mixing 3 μM of enzyme sample with 2.7 μM of H_2O_2, which was then reacted with variable concentrations of luminol ranging from 10 – 50 μM. All measurements were carried out at 25 °C in 10 mM sodium phosphate buffer, pH 7.0. Stopped flow traces from these experiments were biphasic; an initial increase in absorbance was detected corresponding to the formation of Compound II, followed by a decrease in absorbance corresponding with the reduction of Compound II.

The traces were fitted to a double exponential function using the curve fitting application in the Pro-Data Viewer software (Applied Photo-Physics) to determine the pseudo first-order rate constants (k_{obs}) for the first and second phases at the same time. After that, the rate constants k_2 and k_3 were calculated, by a weighted least square regression analysis using SigmaPlot software, from the slope of a graph of the pseudo first-order rate constants (k_{obs}) against luminol concentration.

2.13 Crystallization of enzyme samples:

In order to determine X-ray crystal structures for the HRP-C* variants, the hanging drop vapour diffusion method (in which a drop of protein is brought gradually to super-saturation by loss of water from the droplet to the larger reservoir that contains a polyethylene glycol solution) was used to grow crystals as previously reported for WT HRP-C* (Henriksen *et al.*, 1999). Concentrated samples of HRP-C* variants were prepared by concentration to about 10 mg/ml using an Amicon YM-30 (30,000 Da) Centricon at 4 ^{o}C. A saturated solution of ferulic acid (FA) in isopropyl alcohol was also prepared, as well as 1 M calcium acetate, 1 M sodium cacodylate and 50% (w/v) polyethylene glycol 8000 (PEG 8000) solutions.

Crystals were grown in a mixture of equal amounts (2 µl) of enzyme variant and reservoir solution, plus 1 µl of saturated FA in isopropyl alcohol, in a hanging drop, by vapour diffusion in a 24 well VDX plate (Hampton Research). The drops were equilibrated against reservoir solution with different concentrations of polyethylene glycol 8000, calcium acetate and sodium cacodylate in a 1 ml final solution, as shown in Table 2.2. The VDX tray was left in the fridge at 4 ^{o}C.

Table 2.2: Layout of reservoir solutions for a 24 well VDX plate for HRP-C* variant crystallization. Each well contained a different concentration of polyethylene glycol 8000, Ca acetate, and Na cacodylate, in 1 ml final solution.

A1 **5% PEG 8000** **0.1M Ca acetate** **0.1M cacodylate**	**A2** **10% PEG 8000** **0.1M Ca acetate** **0.1M cacodylate**	**A3** **15% PEG 8000** **0.1M Ca acetate** **0.1M cacodylate**	**A4** **20% PEG 8000** **0.1M Ca acetate** **0.1M cacodylate**	**A5** **25% PEG 8000** **0.1M Ca acetate** **0.1M cacodylate**	**A6** **30% PEG 8000** **0.1M Ca acetate** **0.1M cacodylate**
B1 **5% PEG 8000** **0.2M Ca acetate** **0.1M cacodylate**	**B2** **10% PEG 8000** **0.2M Ca acetate** **0.1M cacodylate**	**B3** **15% PEG 8000** **0.2M Ca acetate** **0.1M cacodylate**	**B4** **20% PEG 8000** **0.2M Ca acetate** **0.1M cacodylate**	**B5** **25% PEG 8000** **0.2M Ca acetate** **0.1M cacodylate**	**B6** **30% PEG 8000** **0.2M Ca acetate** **0.1M cacodylate**
C1 **5% PEG 8000** **0.1M Ca acetate** **0.2M cacodylate**	**C2** **10% PEG 8000** **0.1M Ca acetate** **0.2M cacodylate**	**C3** **15% PEG 8000** **0.1M Ca acetate** **0.2M cacodylate**	**C4** **20% PEG 8000** **0.1M Ca acetate** **0.2M cacodylate**	**C5** **25% PEG 8000** **0.1M Ca acetate** **0.2M cacodylate**	**C6** **30% PEG 8000** **0.1M Ca acetate** **0.2M cacodylate**
D1 **5% PEG 8000** **0.2M Ca acetate** **0.2M cacodylate**	**D2** **10% PEG 8000** **0.2M Ca acetate** **0.2M cacodylate**	**D3** **15% PEG 8000** **0.2M Ca acetate** **0.2M cacodylate**	**D4** **20% PEG 8000** **0.2M Ca acetate** **0.2M cacodylate**	**D5** **25% PEG 8000** **0.2M Ca acetate** **0.2M cacodylate**	**D6** **30% PEG 8000** **0.2M Ca acetate** **0.2M cacodylate**

Chapter Three:

Generation of S167W and S167Y HRP-C* variants

3.1 Introduction:

The main aim of the described work was to introduce novel covalent linkages between the haem porphyrin and protein of HRP-C, similar to those found in myeloperoxidase and other mammalian peroxidases (Fiedler *et al.*, 2000). It has previously been reported that mutation of Ser160 to Met or Tyr (S160M or S160Y) in recombinant pea ascorbate peroxidase (rpAPX) results in a covalent linkage between the haem 2-vinyl and the protein on treatment with H_2O_2 (Metcalfe *et al.*, 2004; Pipirou *et al.*, 2007b). in addition, the distal tryptophan of APX (Trp41) can form a covalent bond to the haem if the protein is incubated for a long time with H_2O_2 (Pipirou *et al.*, 2007a); a result replicated for the W191F mutant of C*c*P where a link is formed between the distal tryptophan, Trp51, and the haem (Pipirou *et al.*, 2009).

Previously in this laboratory, the position 167 has been identified in HRP-C as the closet to the 2-vinyl of the haem (Cali, 2008). Work on the subsequently engineered [S167M] HRP-C* mutant showed that, upon incubation with H_2O_2, a sulfonium linkage was formed between the introduced methionine and the haem (Cali, 2008). Based on this work, and the work on rpAPX, it was decided to engineer two new mutants in HRP-C*: [S167Y] and [S167W] HRP-C*.

The process of replacement of an amino acid by another one in a protein requires the changing of the particular codon that codes for the original amino acid residue to the codon of the desired replacement amino acid in the expression vector used. This manipulation in the gene or cDNA of the protein of interest is known as site-directed mutagenesis, and is the basis for much of the protein structure/function studies performed today. Indeed, this technique has been, and is still being, used to investigate the structure/function of plant peroxidases, in particular HRP-C, and has led to the understanding of the critical role(s) played by the distal and proximal haem pocket amino acid residues Arg38, His42 and His170 in peroxide binding and catalysis (Newmyer and Ortiz de Montellano, 1995; Newmyer and Ortiz de Montellano, 1996a; Rodriguez-Lopez *et al.*, 1996a; Newmyer *et al.*, 1996b; Rodriguez-Lopez *et al.*, 1996b), as well as the functional importance and role(s) of other amino acid residues, such as Phe41, Glu64 and Asn70 in the substrate binding site, calcium binding sites etc. (Smith *et al.*, 1992; Smulevich *et al.*, 1994; Tanaka *et al.*, 1998; Heering *et al.*, 2002).

In this work, mutant genes encoding HRP-C variants S167W and S167Y were produced using a PCR-based Whole Plasmid Amplification Method (WPAM). This method (Figure 3.1) has already been successfully employed in the generation of a range of peroxidase mutants (Veitch *et al.*, 1997; Doyle *et al.*, 1998) and has proved to be efficacious, economical and specifically does not require the presence of a unique restriction enzyme site near the point of mutation. The template used in this work was the ampicillin resistant (Amp^R) expression vector pFLAG1-HRP-C, which contains a synthetic HRP-C gene (Smith *et al.*, 1990). This vector allows the expression of HRP-C recombinant enzyme in *E. coli* under the control of the *tac* promoter; it also contains a copy of the *lac*I^q repressor gene to ensure extra tight regulation of expression. The gene

is present in this vector between an *Nde* I site and a non-functional *Bam* HI/ *Bgl* II hybrid site (Figure 3.1).

3.2 Design of Primers:

Two oligonucleotide primers for the production of each mutant gene (Figure 3.2) were designed, to incorporate the necessary changed deoxynucleotide(s) required to generate the required amino acid substitution in the enzyme, as well as additional silent mutations to produce a new restriction enzyme site in order to facilitate transformant screening. These designed primers were synthesized by MWG-Biotech. For the S167Y mutant, the mutagenic primer contained a TAT codon, which encodes the amino acid tyrosine, instead of a TCC codon which encodes the amino acid serine. Also, correct ligation will lead to the formation of a new restriction site for the restriction enzyme BssSI, through the replacement of T at position 591 in the WT plasmid by C. It is important to mention here that the WT expression vector already has two restriction sites for BssSI at positions 1666 bp and 3049 bp, respectively. For the S167W mutant, the mutagenic primer contained the codon TGG, which encodes for the amino acid tryptophan, instead of the TCC codon (serine). The new introduced restriction site for the enzyme BssSI was the same as for the S167Y mutant. The reference primer used was the same for both S167Y and S167W.

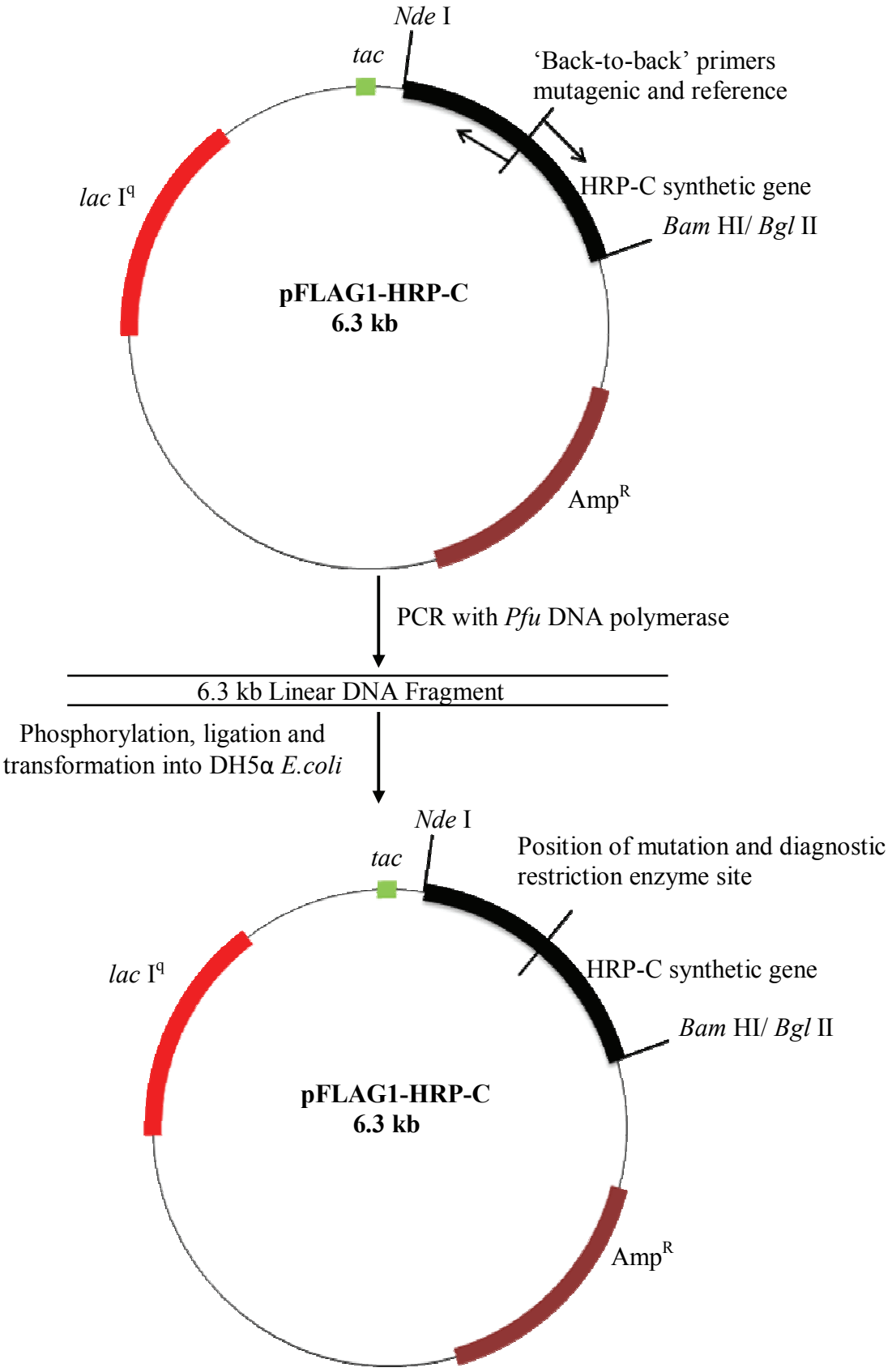

Figure 3.1: PCR-based Whole Plasmid Amplification Method of site-directed mutagenesis (Doyle *et al.*, 1998).

For [S167Y]HRP-C gene

Original WT sequence of the HRP-C gene:

S167

5'-AATCGCTCGAGTGAC***CTTGTG***GCTCTG**TCC**GGAGGACACACATTTG-3'

Engineered sequence to give [S167Y]HRP-C gene:

Y167

5'-AATCGCTCGAGTGAC***CTC*GTG***GCTCTG**TA*T***GGAGGACACACATTTG-3'

New restriction site for *Bss*SI

Mutagenic primer: 5'-**C*GTG**GCTCTG**TA*T***GGAGGACAC-3' Tm = 62 ^{o}C

Reference primer: 5'-**AG**GTCACTCGAGCGATTCAG-3' Tm = 62 ^{o}C

For [S167W]HRP-C gene

Original WT sequence of the HRP-C gene:

S167

5'-AATCGCTCGAGTGAC***CTTGTG***GCTCTG**TCC**GGAGGACACACATTTG-3'

Engineered sequence to give [S167W]HRP-C gene:

W167

5'-AATCGCTCGAGTGAC***CTC*GTG***GCTCTG**TG*G***GGAGGACACACATTTG-3'

New restriction site for *Bss*SI

Mutagenic primer: 5'-**C*GTG**GCTCTG**TG*G***GGAGGACAC-3' Tm = 62 ^{o}C

Reference primer: 5'-**AG**GTCACTCGAGCGATTCAG-3' Tm = 62 ^{o}C

Figure 3.2: Mutagenic and reference primers designed for the production of [S167Y]HRP-C and [S167W]HRP-C mutant genes, in the expression plasmid pFLAG1.

3.3 PCR Products:

PCRs were carried out for both HRP-C mutants, according to the conditions described in section 2.2.3, using an annealing temperature of 56 ^{o}C and *Pfu* polymerase. A proof reading polymerase was essential due to the large size of the DNA products expected, i.e. 6.3 kb. Agarose gel electrophoresis is the standard method used for separating DNA molecules of different lengths. Therefore, the PCR products obtained for both HRP-C mutants were checked by running a portion of the reaction mixture on a 1% agarose gel (Figure 3.3). It can be seen that only a linear DNA fragment of 6.3 kb was produced for both mutants, in quantities sufficient for the continuation of the WPAM site-directed mutagenesis method.

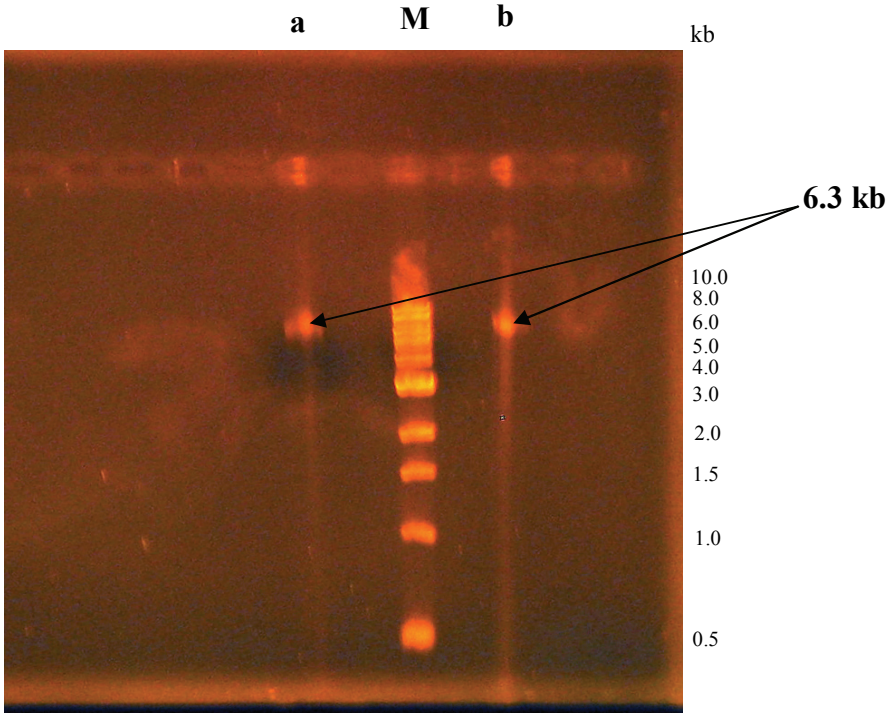

Figure 3.3: 1% Agarose gel electrophoresis of WPAM PCR products, where M: DNA size marker (Promega, 1 kb DNA Ladder), (a) [S167W]HRP-C DNA and (b) [S167Y]HRP-C DNA.

Next, the DNA template WT pFLAG1-HRP-C was removed from the PCR samples by using *Dpn*I, and the samples purified using phenol/chloroform extraction and ethanol precipitation (see sections 2.2.5 and 2.2.6). After that, the 5' termini of the linear, purified PCR products were phosphorylated using T4 polynucleotide kinase and the DNA re-circularized using T4 DNA ligase, to give circular pFLAG1-HRP-C mutated plasmids (section 2.2.7).

3.4 Restriction enzyme analysis of *E. coli* transformants:

The ligation mixtures for both mutants were transformed into DH5α *E. coli* cells and selected on ampicillin agar plates. The resulting colonies had DNA extracted which was then screened by restriction enzyme digest with BssSI (section 2.2.10), along with WT pFLAG1-HRP-C DNA as a control. This was to confirm the presence of the desired nucleotide changes and correct ligation as a new site for this enzyme should have been introduced. However, WT pFLAG1-HRP-C DNA already has two restriction sites at position 1666 bp and 3049 bp, which when digested will give two bands on a gel with sizes 1383 bp and 4812 bp, respectively. For the mutant plasmids the new restriction site has been inserted at position 591 bp, and so BssSI digestion should give three bands on a gel, of 1075 bp, 1383 bp and 3737 bp, respectively.

The results for DNA from [S167Y] and [S167W] putative mutant colonies, digested with BssSI, are shown in Figures 3.4 and 3.5. Seven colonies have the correct restriction pattern for the [S167Y] HRP-C mutant (Figure 3.4) and four colonies have the correct restriction pattern for the [S167W] HRP-C mutant (Figure 3.5). These results demonstrate the success of the site-directed mutagenesis method used at 58% and 44%, respectively. In Figure 3.4 there can be seen an unexpected extra DNA band for

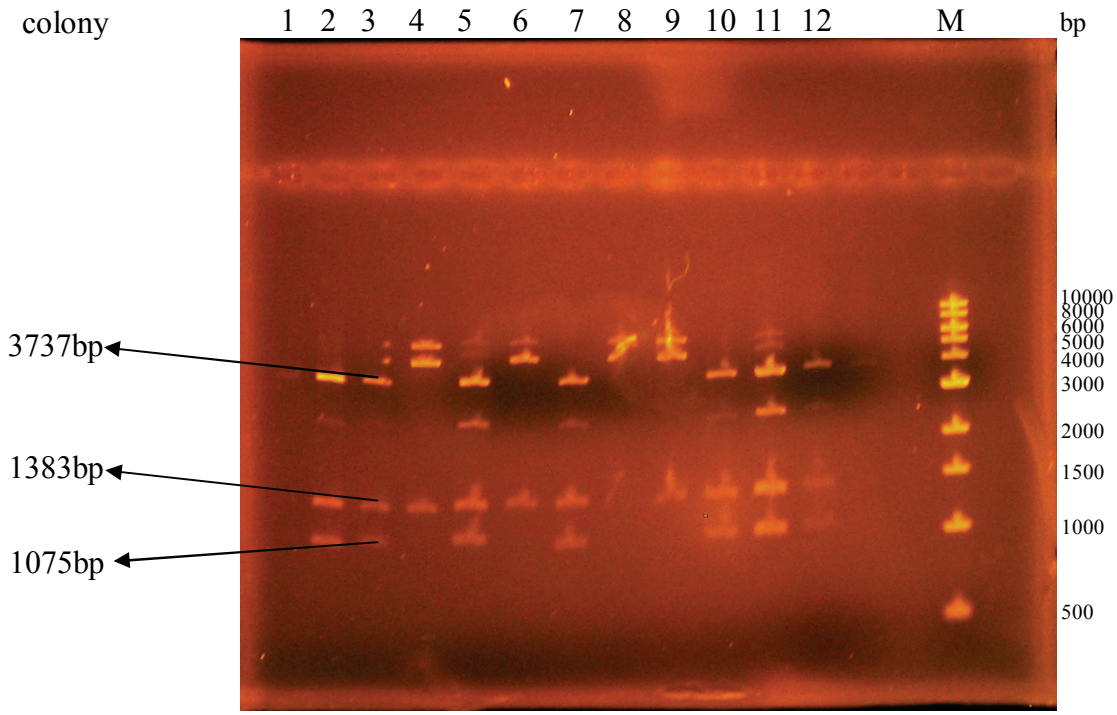

Figure 3.4: 1% agarose gel electrophoresis of BssSI digestion of DNA from transformed colonies for the putative pFLAG1-[S167Y]HRP-C mutant plasmid. M: DNA size marker (Promega, 1 kb DNA Ladder).

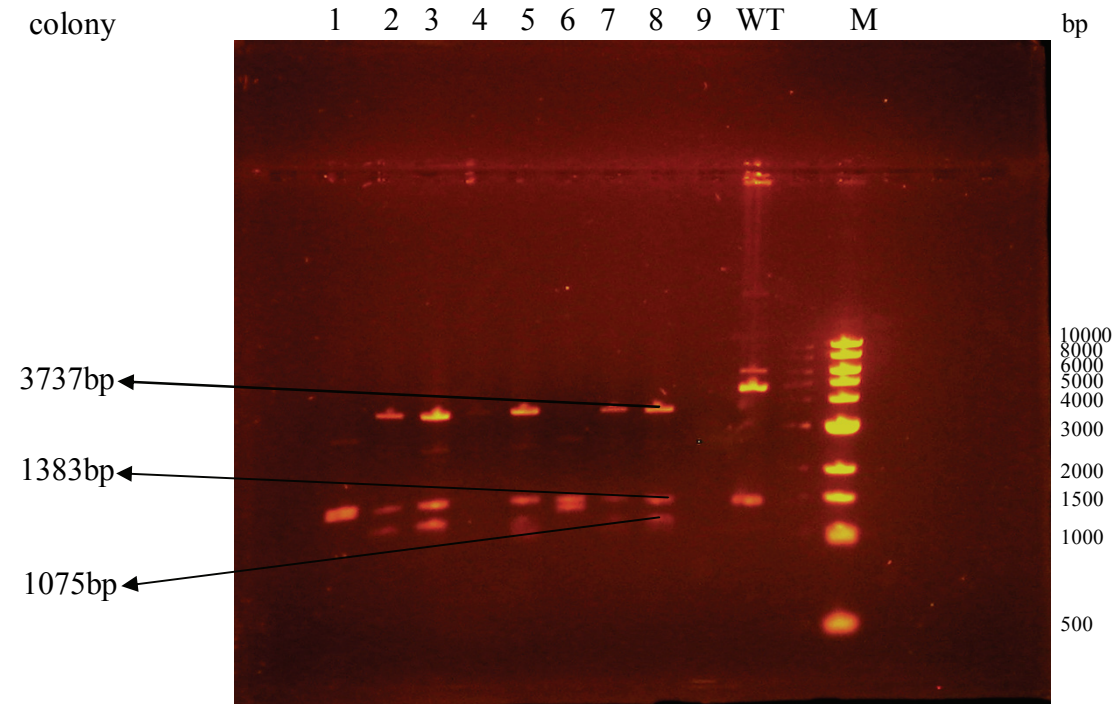

Figure 3.5: 1% agarose gel electrophoresis of BssSI digestion of DNA from transformed colonies for the putative pFLAG1-[S167W]HRP-C mutant plasmid. M: DNA size marker, WT: WT pFLAG1-HRP-C plasmid digested with BssSI.

colonies 2, 5, 7, 10, 11, and 12 at approximately 2.5 kb. This is assumed to be due to star activity.

3.5 Sequencing of [S167Y]HRP-C and [S167W]HRP-C mutant genes:

Plasmid DNA from two colonies of each mutant was submitted for DNA sequencing in order to confirm the expected mutations and the absence of any errors that may have occurred during the PCR procedure. The results obtained were analysed using the Seqman module of DNASTAR Lasergene software, by alignment with the sequence of WT pFLAG1-HRP-C. For both mutants, one sample contained the correct sequence without any error and the other sample had an error in the gene sequence. The colony containing the DNA that had the correct mutant gene sequence was selected for further work.

3.6 Protein expression of [S167Y]HRP-C and [S167W]HRP-C mutants:

Recombinant protein expression of HRP-C has been a major focus of researchers since the beginning of 1990s, and therefore a number of different expression systems have been developed (Veitch, 2004). Among these systems, expression in *E. coli* has proved to be the most valuable, as it is relatively low-cost and easy to obtain mutant proteins compared to other systems. In addition, the recombinant enzyme from *E. coli* expression is obtained in a non-glycosylated form, which helps in X-ray crystallization studies (Veitch and Smith, 2001; Veitch, 2004). However, the protein is expressed as non-active and in insoluble inclusion bodies and so *in vitro* refolding is needed.

3.6.1 Small-scale protein expression:

Both mutant plasmids were transformed into *E. coli* W3110 cells for high protein expression from the *tac* promoter after induction with 1 mM IPTG. Expression of protein and production of protein extracts were performed as in sections 2.3.1.1 and 2.3.1.2. The products of the expression were analyzed by SDS-PAGE on a 12% gel. This revealed that the size, 34 kDa, and expression levels of each new mutant were similar to those of the WT enzyme (Figure 3.6). In the absence of the inducer (IPTG), there was no detectable expression.

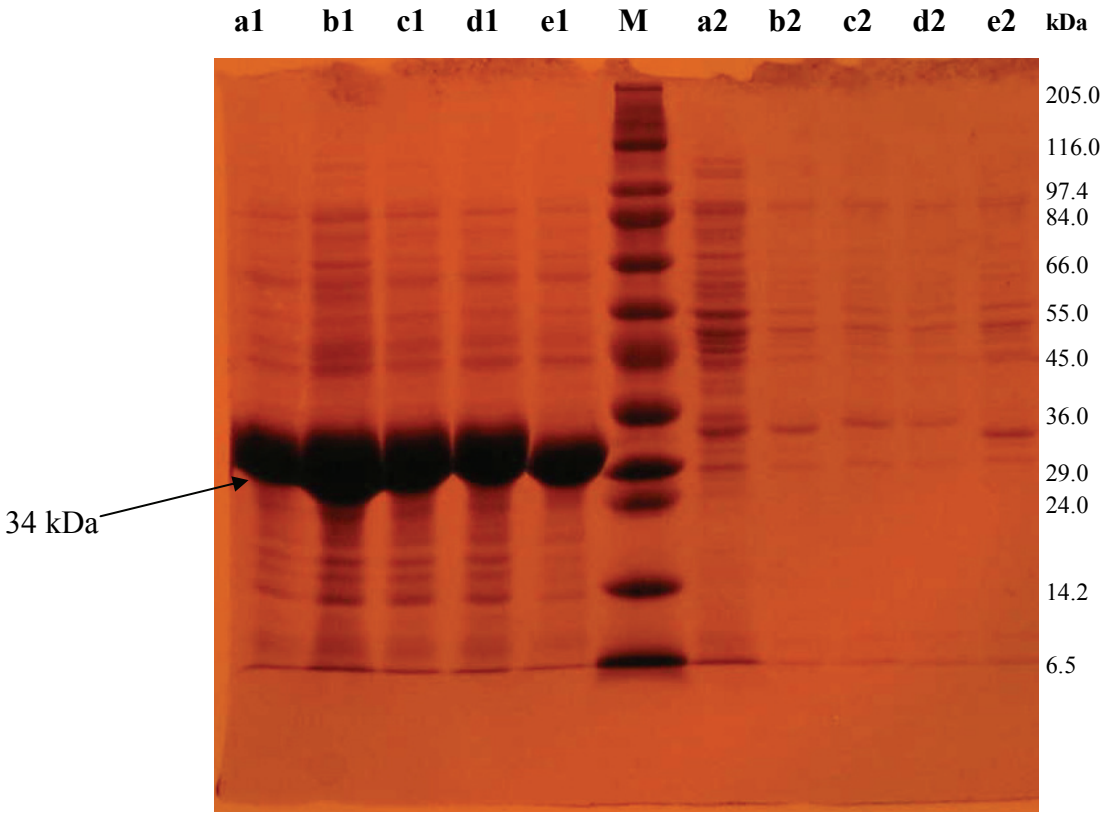

Figure 3.6: 12% SDS-PAGE of small-scale mutant HRP-C protein expression. The figure shows that both new mutants have size approximately 34 kDa, which is comparable to the size of WT HRP-C*. **a1** and **b1**: S167Y mutant induced with IPTG while **a2** and **b2** are without IPTG, **c1** and **d1**: S167W mutant induced with IPTG, **c2** and **d2** without IPTG, **e1** WT induced with IPTG and **e2** without IPTG. M: protein size marker (SigmaMarker^{TM}, Wide Range, 6.5-200 kDa).

3.6.2 Large-scale protein expression, *in vitro* refolding and active enzyme purification:

Large-scale protein expression, *in vitro* folding and purification were achieved for both new HRP-C variants, as well as for WT enzyme, using a slightly modified form of the method previously described by Smith and co-workers (Smith *et al.*, 1992); an alteration in the refolding procedure of the protocol (section 2.3.2.3) involved the addition of haem to the folding solution only after 18 hours of the process of refolding with the process then continuing for another 46 hours. This alteration has been shown to give a small, but significant, increase in enzyme yield (Cali, 2008).

The final active enzyme was purified after refolding and concentration using the Fast Protein Liquid Chromatography (FPLC) instrument and cation-exchange chromatography on a Mono S column (section 2.3.2.3). The FPLC elution profiles obtained for the variants [S167Y] and [S167W] HRP-C* were consistent with those obtained from the purification of WT HRP-C* (Figure 3.7), indicating that there was no significant variation in the folding of the new mutants, compared to the WT enzyme. Yields of the mutant enzymes were also similar to WT enzyme, at approximately 9 mg/L *E. coli*.

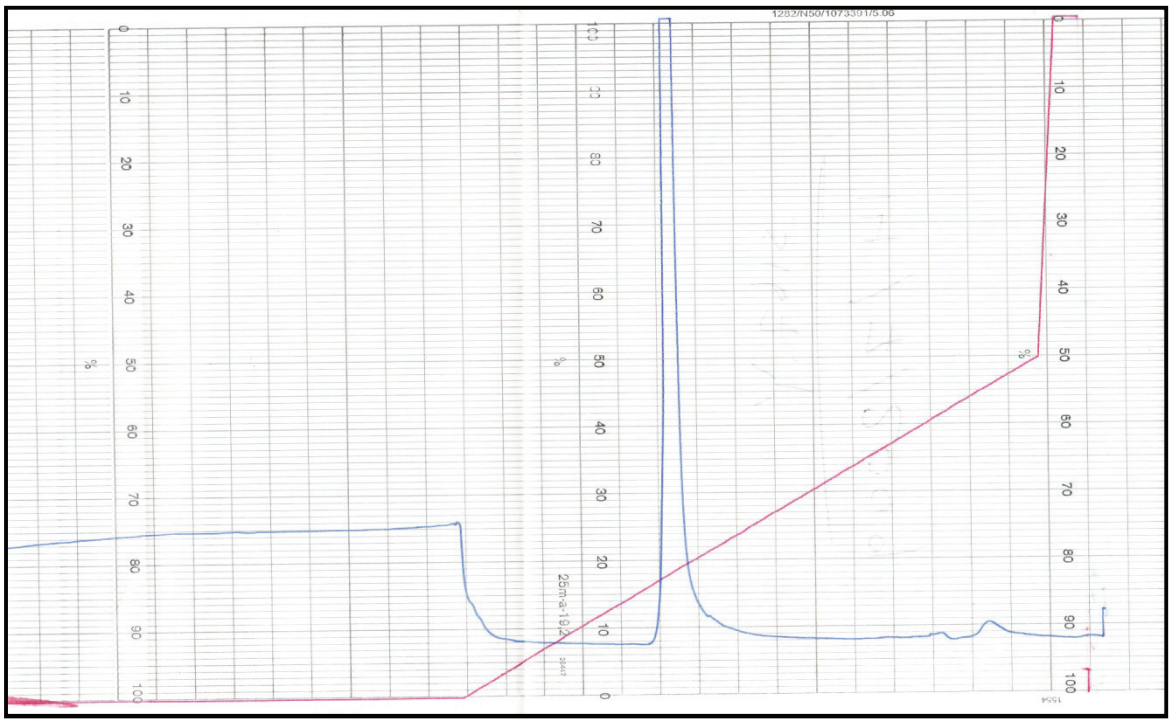

Figure 3.7: Cation exchange chromatography profile of [S167Y] HRP-C*. Active enzyme was purified using FPLC and cation exchange column Mono-S HR 10/10. Elution was achieved with a linear NaCl gradient of 0-1 M. The enzyme eluted as a single sharp peak at 160 mM NaCl, the same salt concentration as for the WT enzyme and S167W mutant.

3.7 Conclusion:

The PCR-based Whole Plasmid Amplification Mutagenesis method was successfully used to construct two HRP-C mutant genes, S167Y and S167W. The expected sequence changes in the HRP-C gene were confirmed by restriction enzyme screening as well as DNA sequence analysis, and no unexpected changes were detected. Both mutant proteins have been expressed in *E. coli* and SDS-PAGE analysis showed that the protein had the expected mass of 34 kDa. Finally, the purified variants [S167Y] and [S167W] HRP-C* were obtained in good yield after *in vitro* refolding and cation-exchange chromatography on an FPLC machine.

Chapter Four:

Characterisation of the new HRP-C S167 variants and evidence of covalent linkage

4.1 Introduction:

Despite considerable efforts made by a lot of researchers, the mechanism of formation of the haem-protein covalent linkages in mammalian peroxidases, and their functional advantage(s) remain unclear. In the last ten years, efforts have focused on introducing these bonds into plant peroxidases. Site directed mutagenesis of plant peroxidases, which lack these linkages and belong to a different peroxidase superfamily, has been used to study the effect of both the esters and sulfonium linkages of MPO in a simpler system, where fundamental parameters can be more easily measured and the effects, whether electronic or structural, determined. As mentioned before (section 1.6), new haem-protein covalent bonds have been successfully created in rpAPX and C*c*P, where it has been unambiguously demonstrated that creation of these linkages lead to a profound impact on the spectroscopic and functional properties of these enzymes (Metcalfe *et al.*, 2004; Pipirou *et al.*, 2007a; Pipirou *et al.*, 2007b; Pipirou *et al.*, 2009).

Recent work by another member of the group, Dr. Kasim Cali, highlighted position 167 in HRP-C as close enough to the haem to form a haem-protein bond in the site-directed HRP-C* mutant S167M. Dr. Cali concluded from UV/Visible spectroscopy studies and HPLC and MS analysis that a sulfonium linkage between the protein and the porphyrin of the haem prosthetic group was auto-catalytically generated in this mutant after

treatment with hydrogen peroxide. However, he also found that this linkage was unstable and that after a short time it broke to yield a modified haem species (Cali, 2008).

In this study, and building on the previous work, two new site-directed HRP-C* mutants S167W and S167Y have been constructed, and protein expressed, refolded and purified (Chapters 2 and 3). This chapter describes the initial characterisation of these new variants, the effect of treatment of these variants with hydrogen peroxide and the evidence for the creation of a new covalent linkage between the haem and the protein.

4.2 Spectroscopic characterisation of the new S167 variants:

Spectroscopic techniques are a particularly useful probe for understanding the electronic properties of the haem of the peroxidases. The UV/Vis spectrum of wild-type HRP-C is characterised by the presence of a Soret peak at 403 nm as a result of π-π* transitions, with a strong shoulder at about 380 nm. Charge-transfer bands (CTI and CTII) at 642 and 498 nm are also present and are due to partial transfer of electronic charge between the porphyrin and the iron (Dunford, 1999f). The iron in the resting state of HRP has six co-ordination sites: four positions are located in the plane of the haem iron atom and are occupied by the nitrogen atoms of a porphyrin group, the fifth co-ordination site is occupied by the proximal imidazole side chain of His170 residue, and the sixth position is vacant. Therefore, HRP-C is substantially a five coordinate high spin ferric haem iron. There are no additional cross-links between the side chains of the haem group and the protein.

The spectral features of the S167Y and S167W variants indicate small but significant electronic differences in the haem environment when compared to wild-type recombinant enzyme, Figure 4.1 and Table 4.1, the most obvious being the absence of the shoulder at 380 nm in the spectrum of the S167Y variant. This suggests a loss of 5-coordinate character of the haem iron and conversion to a 6-coordinate high spin form. The intensity of the shoulder at 380 nm is also much weaker in the S167W variant, suggesting that about 50% of the haem iron is converted from 5-coordinate high spin form to 6-coordinate high spin form. The Soret peak of S167W has also slightly red shifted to 404.

The spectra also show that the CTII band for both the S167W and S167Y variants is 496 nm, very slightly blue shifted when compared to the WT CTII band at 498 nm. However, there are more significant differences for the CTI band: being 636 nm for S167Y, 638 nm for S167W compared to 642 nm for WT. All these features are consistent with an increase in 6-coordinate character for the new variants. Also, consistent with this, there are significant increases in the molar extinction coefficients of both mutant variants, 180 mM^{-1} cm^{-1} for S167Y and 135 mM^{-1} cm^{-1} for S167W compared to 100 mM^{-1} cm^{-1} for the WT enzyme, implying a significant electronic effect especially for the S167Y variant. The large increase in molar extinction coefficient for the S167Y variant could be attributed to the resonance effect of the aromatic ring of the tyrosine residue as well as the auxochromic effect of the hydroxyl group.

The most convenient measurement of peroxidase purity is given by the Reinheitszahl number (RZ), which is the ratio of the absorbance of the enzyme at the Soret peak and 280 nm. RZ values between 3 and 3.4 are generally considered optimal for WT HRP-C

(Dunford, 1999f; Veitch and Smith, 2001). However, the reduction in the value of RZ for the S167W variant is reasonable as the addition of another tryptophan residue in the structure of enzyme will contribute to an increase in the absorbance at 280 nm, there is therefore no reason to suggest that the [S167W] HRP-C* sample is less pure.

Table 4.1: Spectrum parameters for resting state of WT HRP-C*, S167W and S167Y variants.

Enzyme	Shoulder (nm)	Soret peak (nm)	CTII (nm)	CTI (nm)	Extinction coefficient $mM^{-1}\,cm^{-1}$	RZ[1]
WT HRP-C*	380	403	498	642	100 ± 5	3.4
S167Y	very weak	403	496	636	180 ± 2	3.3
S167W	weak	404	496	638	135 ± 1	2.7

[1] Reinheitszahl number

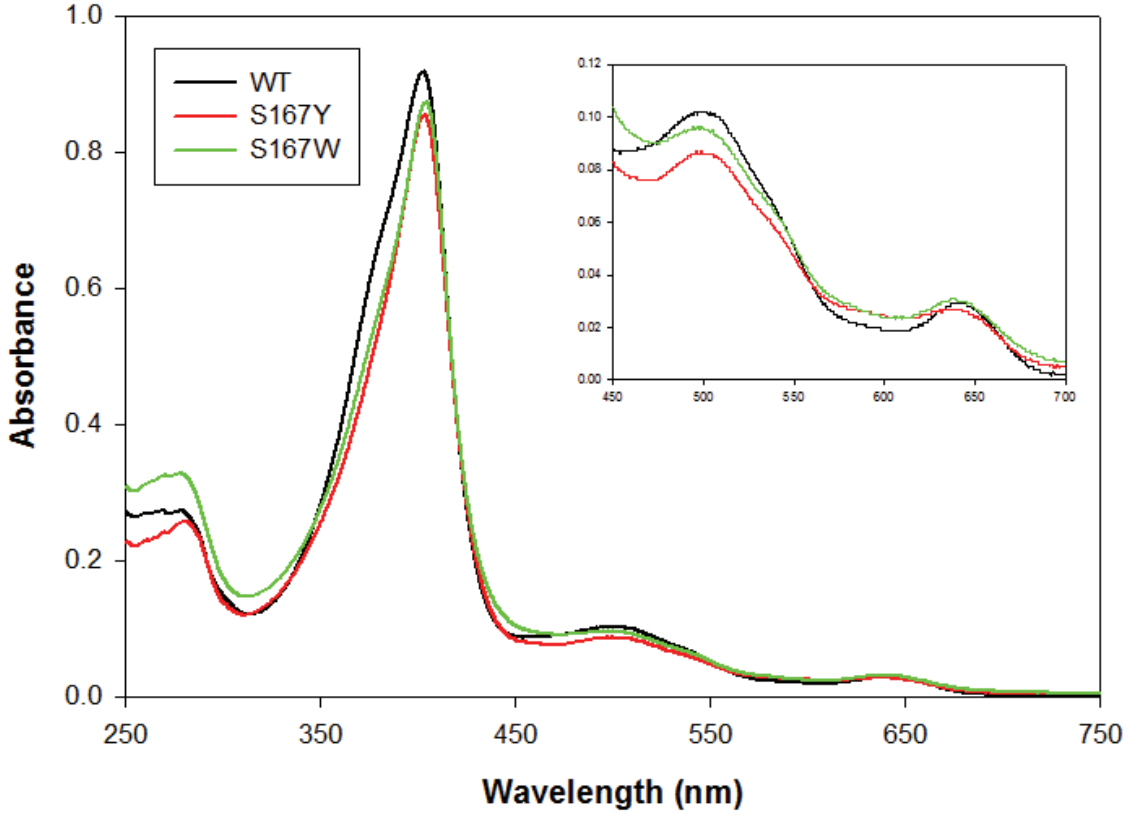

Figure 4.1: UV/Visible absorption spectra of WT HRP-C* and the new S167 variants. Spectra were recorded in 5 mM MOPS buffer, pH 7.0 at 25 ^{o}C using 9 μM WT HRP-C*, 5 μM S167Y variant and 6.5 μM S167W variant**.** The inset in the top right of the figure is a magnified view of the region between 450 nm and 700 nm, in order to highlight the CTI and CTII bands.

4.3 BHA binding to WT HRP-C* and the new S167 variants:

Benzhydroxamic acid (BHA) is capable of forming a spectroscopically distinct, reversible complex with both free and cyanide-ligated HRP-C (Schonbaum, 1973). In general, little selectivity is shown by HRP-C towards aromatic donors, however, BHA has become the donor molecule most favoured by researchers as a probe of the binding site due to its tight binding and strong spectroscopic effects (Veitch and Smith, 2001). The X-ray crystal structure of the BHA complex of the resting state of HRP-C* has been solved to 2.0 Å resolution (Henriksen *et al.*, 1998a). The results showed that a well-defined electron density for BHA is observed in the peroxidase active site, with a hydrophobic pocket surrounding the aromatic ring of the substrate. The aromatic ring of the BHA makes hydrophobic contacts with the side chains of His42, Phe68, Gly69, Ala140, Pro141 and Phe179 residues, as well as the haem methyl C8 and the haem *meso* proton Cδ, with the shortest distance (3.7 Å) found between the haem C8-methyl and BHA. In addition, the residues Arg38, His42 and Pro139, and the distal water molecule 2.6 Å above the haem iron, contribute to an extensive hydrogen bond network with the BHA side chain (Figure 4.2) (Henriksen *et al.*, 1998a).

The dissociation constant (K_d) is a specific type of equilibrium constant that is used to describe the affinity between an enzyme and a particular substrate or ligand. For HRP-C, it has been reported that BHA has a high affinity (K_d = 2.4 μM) for binding with the free enzyme (Schonbaum, 1973). Binding also causes a perturbation to the coordination state of the haem iron of the enzyme, changing it from a 5-coordinate high spin form to a 6-coordinate high spin form (Smulevich *et al.*, 1991). On the other hand, it has been found that BHA has a much weaker affinity for the cyanide-ligated form of the HRP-C

with a K_d value of 95 μM, 40-fold higher than for the free enzyme (Veitch and Williams, 1995).

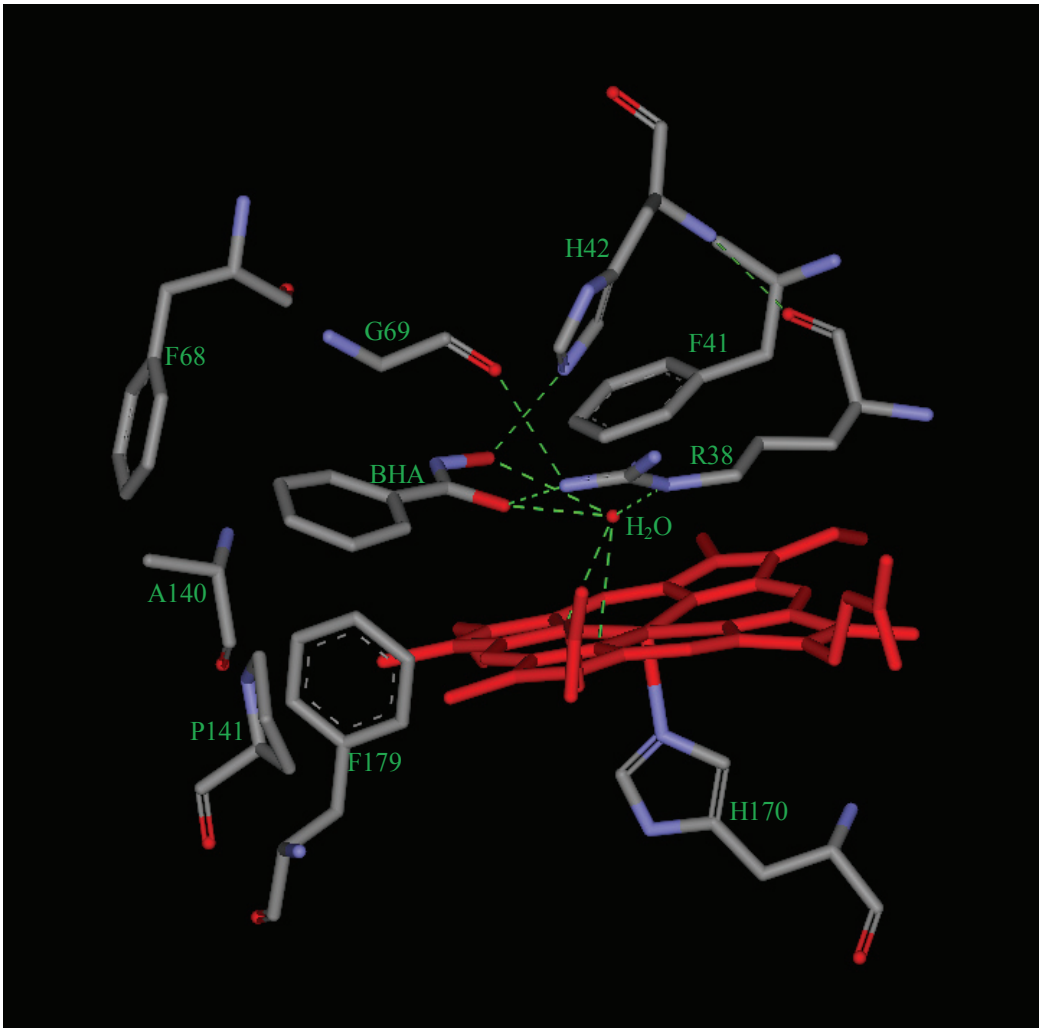

Figure 4.2: The binding mode of BHA to resting state HRP-C*. The donor molecule is located on the distal side of the haem plane and makes both hydrogen bond and hydrophobic interactions with the enzyme. The hydrogen bonds between the BHA side chain and distal residues, plus the structural water molecule above the haem group, are shown by dashed green lines. The figure was constructed by Accelrys DS visualizer using the coordinates deposited in the PDB (accession code 2ATJ).

Site-directed mutagenesis studies have been used to confirm the importance of the distal haem amino acid residues in the binding of the enzyme with the hydroxamate group of

BHA. It was found that the replacement of Arg38 by Lys or Leu, or His42 by Leu or Glu leads to a dramatic decrease in the affinity of the mutant enzyme towards BHA, as well as, a disruption of the coordination state of the haem iron in the enzyme-BHA complex. These findings have led to a clarification of the critical role(s) of His42 and Arg38 in the binding of BHA, via the hydrogen bonding network (Smith *et al.*, 1993; Rodriguez-Lopez *et al.*, 1996a; Howes *et al.*, 2001b). The significance of the amino acid residue Phe179 has also been investigated, by substitution of this residue by Ala, His or Ser. All three variants (F179A, F179H and F179S) exhibit a high K_d and therefore a significant decrease in affinity for BHA for both the free and cyanide-ligated enzymes, when compared to the wild-type enzyme (Veitch *et al.*, 1997; Howes *et al.*, 2001b). Furthermore, substitution of Phe68 by Ala (F68A) significantly increases the dissociation constant, indicating that this amino acid residue also plays a role in the binding site of aromatic substrates to the HRP-C (Veitch *et al.*, 1996).

In this section I explore whether the amino acid residue at position 167, chosen as the new potential haem-linkage site, has any affect on aromatic substrate binding in HRP-C. The effect of mutation of this residue on the affinity of the enzyme for BHA was determined. BHA binding assays were carried out for WT HRP-C*, as well as for the new S167 variants, by titrating an enzyme sample with successive amounts of BHA until there was no further obvious change in the absorbance spectra (Figure 4.3). The dissociation constant (K_d) for the BHA-enzyme complex, together with the maximum absorbance change of the Soret peak (A_{max}), was determined by fitting the change in the difference spectrum (bound minus unbound) of the Soret region to the quadratic binding equation given in section 2.5. The results obtained are shown in Figure 4.4 and Table 4.2.

The absorbance spectra of WT HRP-C* and the S167W variant complexes with BHA show the absence of the 380 nm shoulder of the resting enzyme spectra, which gives clear evidence of conversion from the 5-coordinate high spin form into the 6-coordinate high spin form, this phenomena is typical of formation of a BHA complex (Smith *et al.*, 1992). The K_d value obtained for WT HRP-C* was 2.4 μM, in excellent agreement with the published values: 2.4 μM (Schonbaum, 1973) and 2.5 μM (Smith *et al.*, 1992; Rodriguez-Lopez *et al.*, 1996a). The results obtained in Table 4.2 show that the dissociation constant of the S167W variant for BHA (2.89 μM) is hardly affected relative to that for the wild-type enzyme, whilst it slightly increased (4.36 μM) for the S167Y variant implying a small perturbation of the aromatic donor binding site in this enzyme. In fact, there was no reason to expect any structural or functional significance of the Ser167 residue to the BHA binding site of HRP-C, however the replacement of this amino acid residue with the bulkier Trp or Tyr residues may have had an indirect affect on the environment of the haem centre leading to disruption of the interaction of BHA with the enzyme.

Table 4.2: Dissociation constants (K_d) and the maximum absorbance change of the Soret peak (A_{max}) on the binding of BHA to HRP-C* and the new S167 variants. Results were determined by fitting the change in the difference spectrum (bound minus unbound) of the Soret region to the quadratic binding equation given in section 2.5.

Enzyme	K_d (μM)	A_{max}
WT HRP-C*	2.40 ± 0.25	0.165 ± 0.004
S167Y	4.36 ± 0.54	0.256 ± 0.009
S167W	2.89 ± 0.32	0.142 ± 0.004

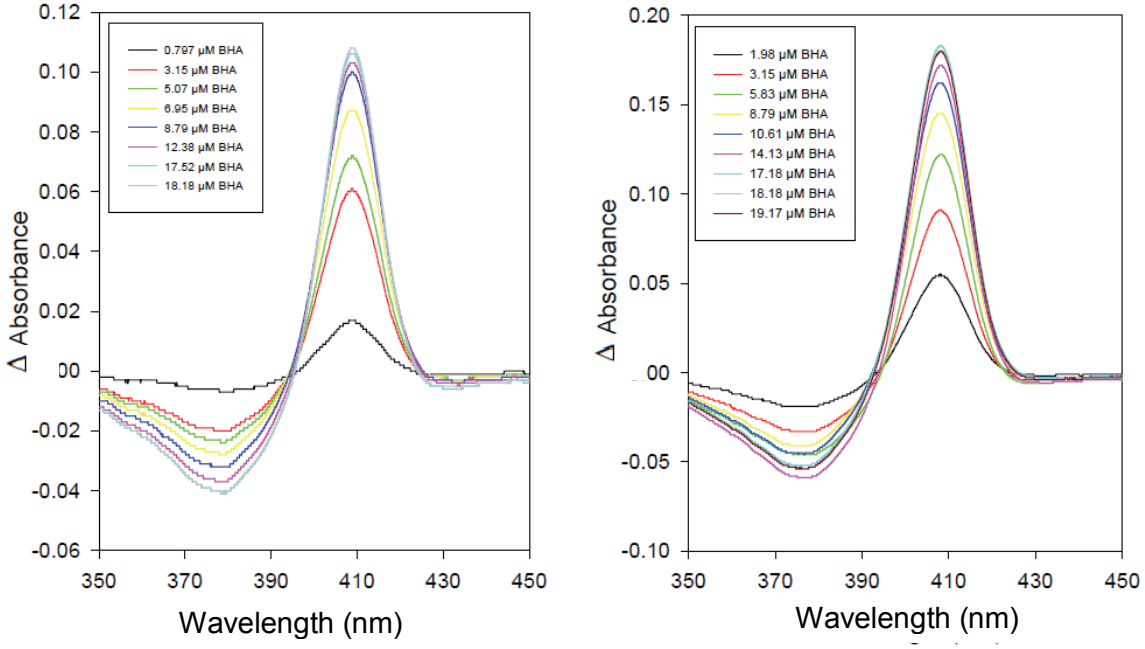

Figure 4.3: UV/Visible difference spectra resulting from titration of the S167Y (right) and S167W (left) HRP-C* variants with different concentrations of BHA. Spectra were recorded in 5 mM MOPS buffer, pH 7.0 at 25 ^{o}C.

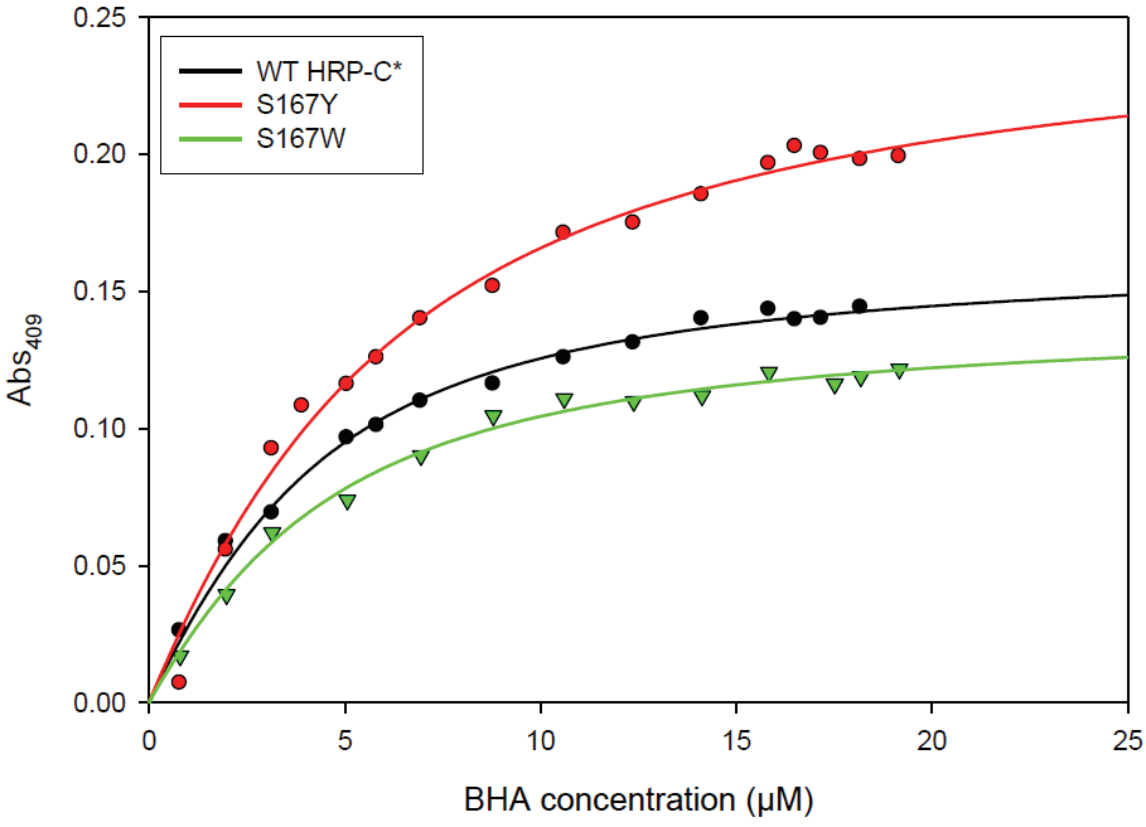

Figure 4.4: Change in absorption of the Soret peak obtained by titrating 3 µM of WT HRP-C*, S167Y and S167Y variants with different concentrations of BHA.

4.4 Treatment of [S167W] and [S167Y] HRP-C* variants with hydrogen peroxide:

As mentioned previously, exposure of recombinant LPO and EPO, [F41E] HRP-C*, [S167M] HRP-C* and the rpAPX variants S160M and S160Y to a stoichiometric excess of hydrogen peroxide results in covalent attachment of the haem to the protein through an autocatalytic process (DePillis *et al.*, 1997; Oxvig *et al.*, 1999; Colas *et al.*, 2002; Colas and Ortiz de Montellano, 2004; Metcalfe *et al.*, 2004; Pipirou *et al.*, 2007a; Pipirou *et al.*, 2007b; Cali, 2008). A similar approach has been used in this work in an attempt to introduce a novel new covalent linkage into HRP-C.

The new variants [S167W] and [S167Y] HRP-C* were incubated with hydrogen peroxide for two hours in sodium phosphate buffer at 25 ^{o}C (section 2.6) and in the absence of any reducing substrate. Observation by the naked eye noted the discolouration of the reaction solution to a pale green colour lasting for a few seconds, followed by a red colour. This observation was an indication of the rapid formation of the first high oxidation state intermediate Compound I (green) which is then quickly converted into the second high oxidation state intermediate Compound II. Repeated UV/Visible scans of the S167Y and S167W variants after treatment with H_2O_2 confirmed this initial observation (Figures 4.5 and 4.6). The first scan, taken one minute after the beginning of the reaction shows that the first intermediate Compound I, is less stable and undergoes a more rapid conversion to Compound II for each mutant, when compared to WT HRP-C*. The spectra of both variants show the more stable intermediate Compound II with spectral features at λ_{max} (nm) = 420, 555 and 523, which are consistent with those reported for Compound II of the wild-type enzyme (Dunford, 1999f). Further scans then show that Compound II decays over a further period of time

back to the resting state enzyme. However, it was found that in the case of the S167W variant, the return to the resting state was more rapid, after 15 minutes, compared to the S167Y variant, which needed 180 minutes to return to the resting state.

Treatment of the S167Y variant with H_2O_2 gave a final spectrum that was essentially identical to that of the pre H_2O_2 resting state (Figure 4.7); there are no changes in the position of the Soret peak or CTI band, which were 403 and 636 nm respectively. The only small difference between them appeared to be in the CTII band, where it was 496 nm for untreated S167Y variant and 499 nm for the treated sample. The results showed also that the treated S167Y variant has a molar extinction coefficient value equal to 178 mM^{-1} cm^{-1}, again essentially identical to that of untreated S167Y (180 mM^{-1} cm^{-1}). In the case of the S167W variant, the final spectrum after treatment with H_2O_2 is very different from the spectrum of the untreated variant and the wild-type enzyme (Figure 4.8). Although the Soret peak and CTI band are still at 404 and 638 nm, the CTII band appears very weak in the treated variant at 496 nm. Furthermore, the S167W variant has lost 40% of its total haem signal as a result of exposure to H_2O_2, with a lower extinction coefficient of 121 mM^{-1} cm^{-1} compared to 135 mM^{-1} cm^{-1} for the untreated S167W. These results give a strong indication that a change in the haem environment, i.e. a significant electronic effect, has occurred during exposure to H_2O_2.

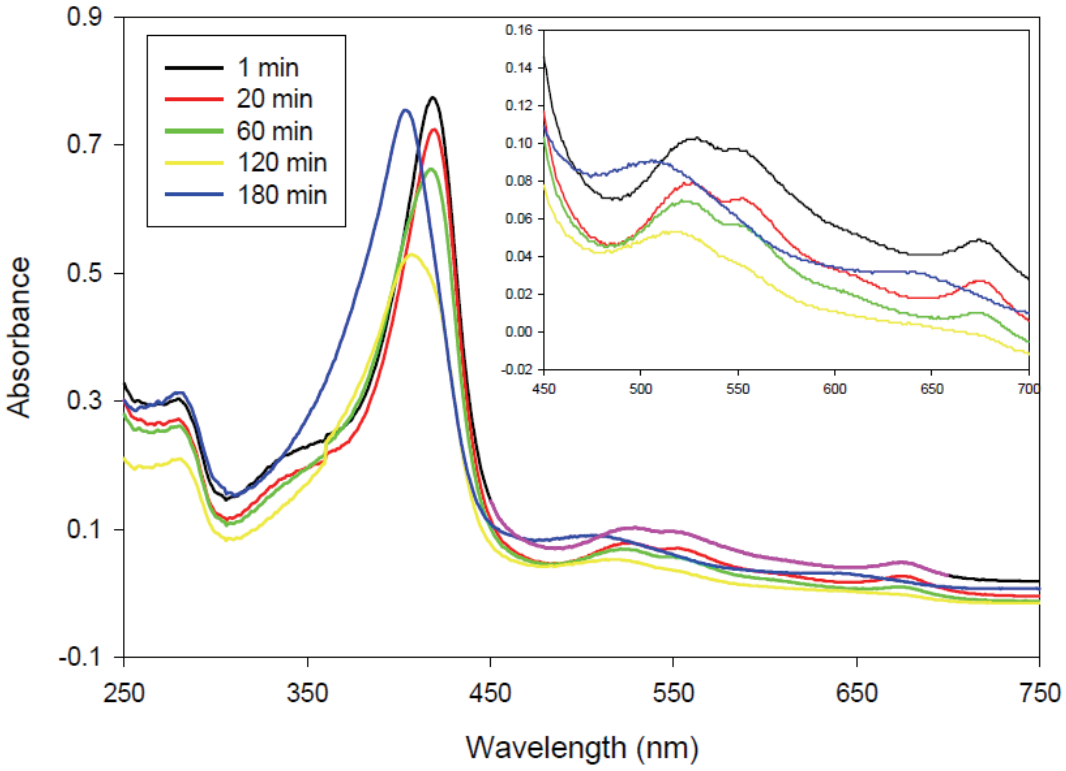

Figure 4.5: Repeat scan spectra collected during the reaction of [S167Y] HRP-C* with H_2O_2. The reaction was carried out in sodium phosphate buffer, pH 9.5 at 25 ^{o}C, where 0.5 mM of H_2O_2 was added to 5 µM of variant.

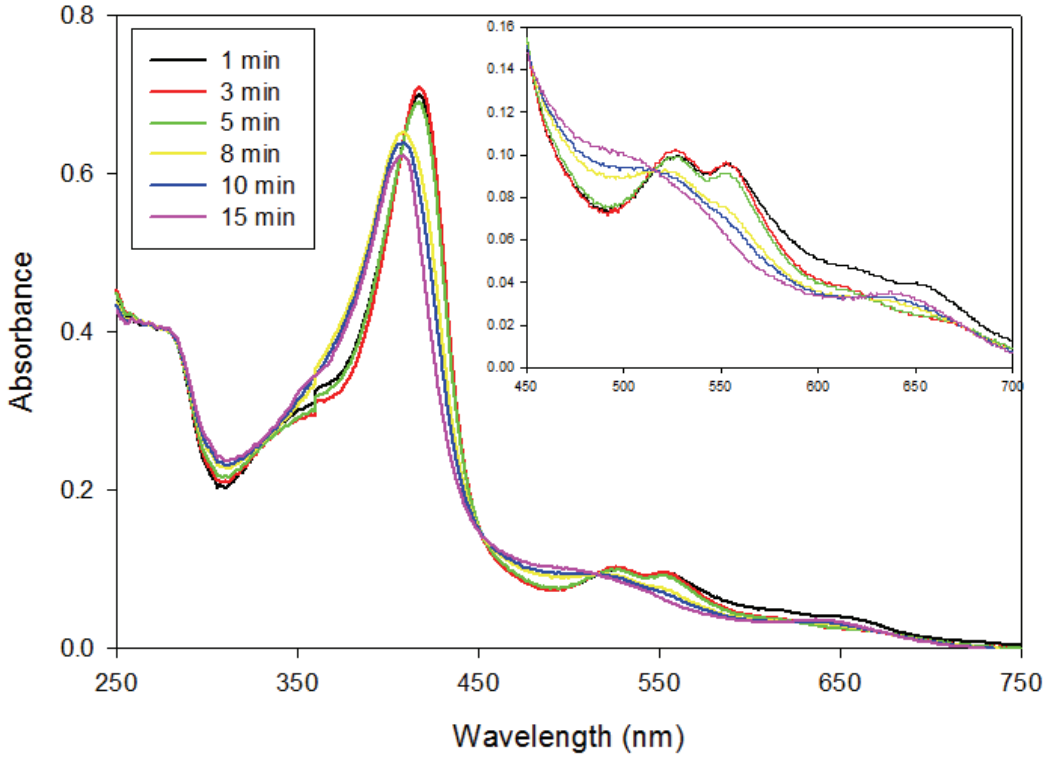

Figure 4.6: Repeat scan spectra collected during the reaction of [S167W] HRP-C* with H_2O_2. The reaction was carried out in sodium phosphate buffer, pH 7.0 at 25 ^{o}C, where 0.6 mM of H_2O_2 was added to 6 µM of the variant.

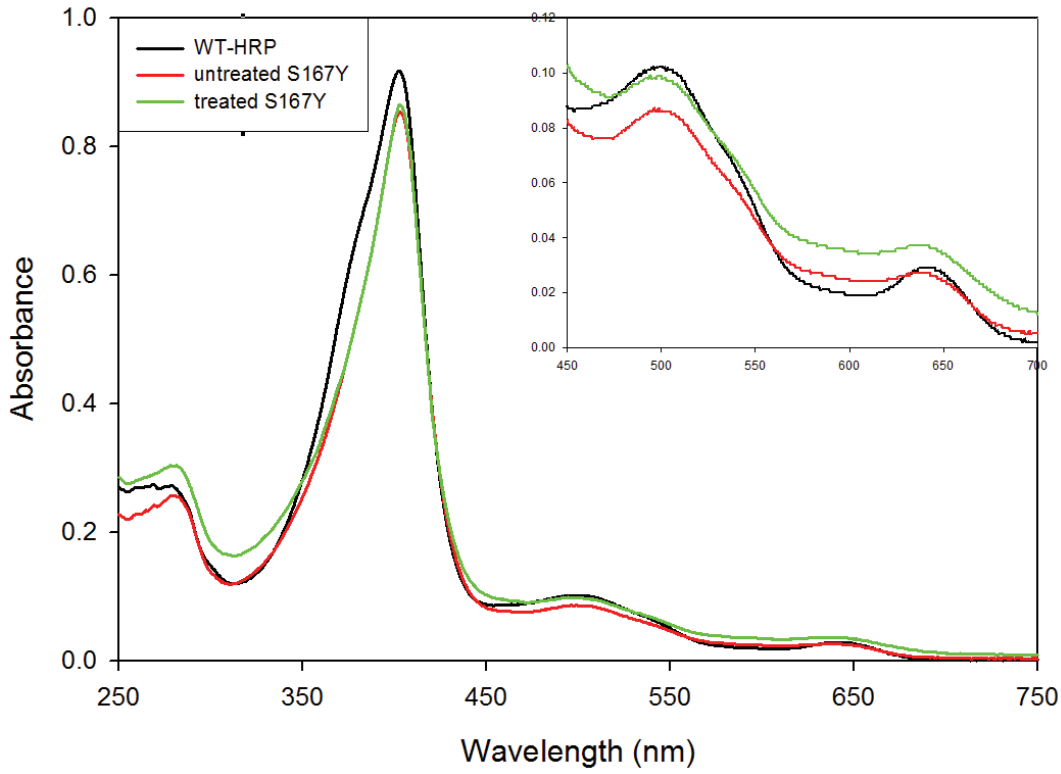

Figure 4.7: UV/Visible absorbance spectra of 9 µM WT HRP-C*, 5 µM S167Y variant treated and untreated with 5 mM H_2O_2.

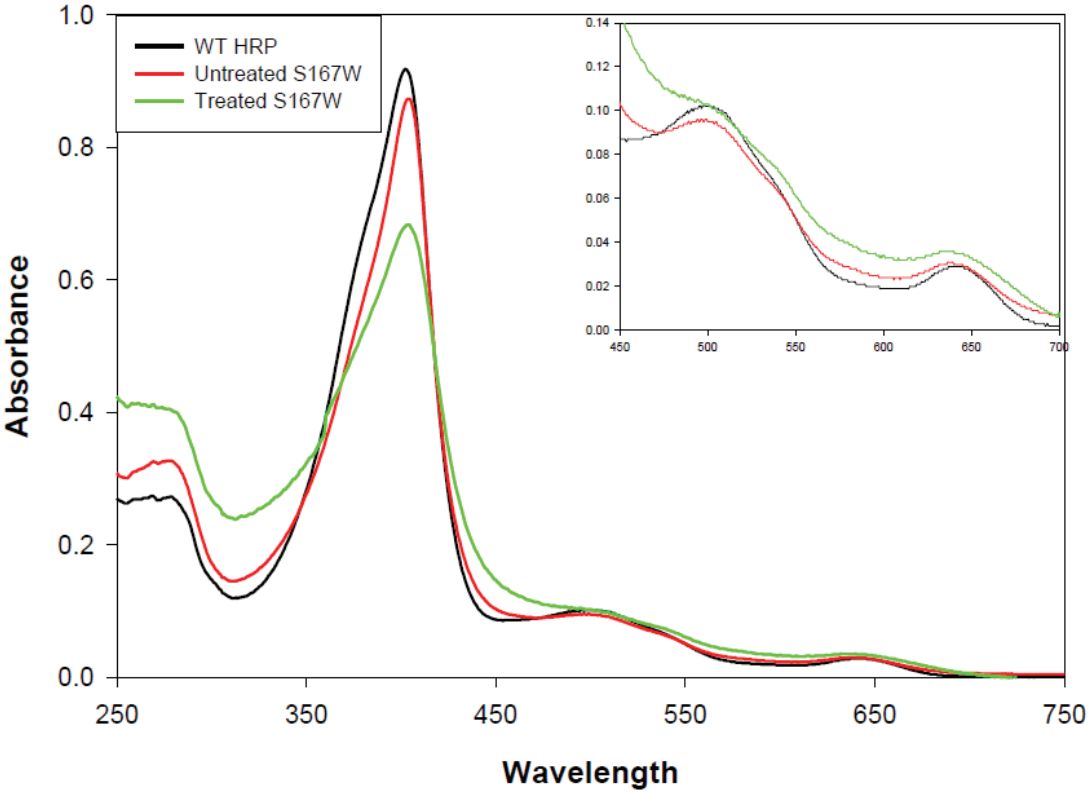

Figure 4.8: UV/Visible absorbance spectra of 9 µM WT HRP-C*, compared to 6.5 µM S167W treated and untreated with 6.5 mM H_2O_2.

4.5 Evidence for the generation of a covalent linkage between the haem and the protein:

4.5.1 Pyridine haemochrome assay:

Pyridine haemochrome spectra are often used to give an indication of the type of haem present. These spectra are measured in aqueous alkaline pyridine solutions after reduction with sodium dithionite. The high pH of the solution leads to the disruption of non-covalent interactions between the haem and the protein, and the haemochrome complexes are formed by the coordination of two molecules of a pyridine to the haem group. The sharp and characteristic α-bands of the pyridine haemochrome spectra are used for identification and determination of the molar absorption coefficient ε, as well as the concentration of the haemoproteins (Fuhrhop and Smith, 1975; Kooter *et al.*, 1997a; Kooter *et al.*, 1999a).

A pyridine haemochrome assay was carried out on WT HRP-C*, and the new S167 variants, both before and after treatment with hydrogen peroxide. The reduced-oxidized difference spectra obtained are presented in Figures 4.9 and 4.10, and the spectral features are summarised in Table 4.3. It was observed clearly that the pyridine haemochrome spectra of the S167W variant, either treated or untreated with H_2O_2, are identical to the spectra of WT HRP-C*; the maximum α-band appears at 555 nm and a Soret band at 419 nm. However, in the case of the S167Y variant, the pyridine haemochrome spectra showed a blue shifted maximum for the α-band, at 552 nm, beside a similarly shifted Soret band at 415.5 nm. These spectroscopic changes give a preliminary indication of the formation of a covalent linkage between the haem and the protein in the S167Y variant, since the electronic properties of the haem are modified, even before treatment of the enzyme with H_2O_2.

Similar results have been reported previously for rpAPX and HRP-C* mutants (Pipirou *et al.*, 2007a; Pipirou *et al.*, 2007b; Cali, 2008). A shift in the maximum α-band from 556 nm to 553 nm was observed for rpAPX spectrum, after treatment with H_2O_2, presumed to be due to the formation of a haem-tryptophan link in the enzyme (Pipirou et al., 2007a). Similarly, the pyridine haemochrome spectrum showed a maximum α-band at 556 nm for untreated [S160Y] rpAPX, but the peak blue shifted to 551 nm after reaction with H_2O_2 (Pipirou *et al.*, 2007b). Finally, the spectrum observed for the [S167M] HRP-C* variant after treatment with H_2O_2 showed a pronounced blue shift in its bands compared to untreated enzyme, indicating a possible sulfonium linkage between the haem and the protein (Cali, 2008).

The alkaline pyridine haemochrome spectrum of the MPO variant, [M243Q] MPO, is also greatly affected and showed blue shifted bands compared to that of WT MPO. This behaviour was attributed to the absence of the sulfonium linkage in the M243Q variant which is normally present in the native enzyme (Kooter *et al.*, 1997a; Kooter *et al.*, 1999a; Kooter *et al.*, 1999b).

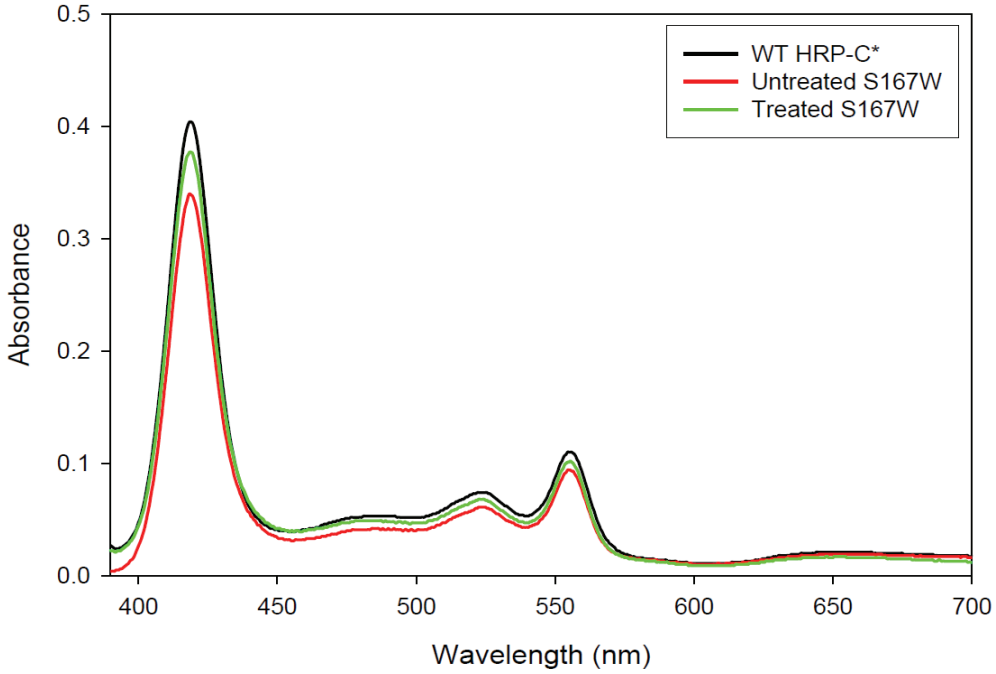

Figure 4.9: Comparison of the pyridine haemochrome difference spectra for WT HRP-C* and the S167W variant, before and after treatment with 100 equivalents of H_2O_2. Spectra were recorded in 5 mM MOPS buffer, pH 7.0, at 25 ^{o}C and the haem-protein species was reduced with disodium dithionite.

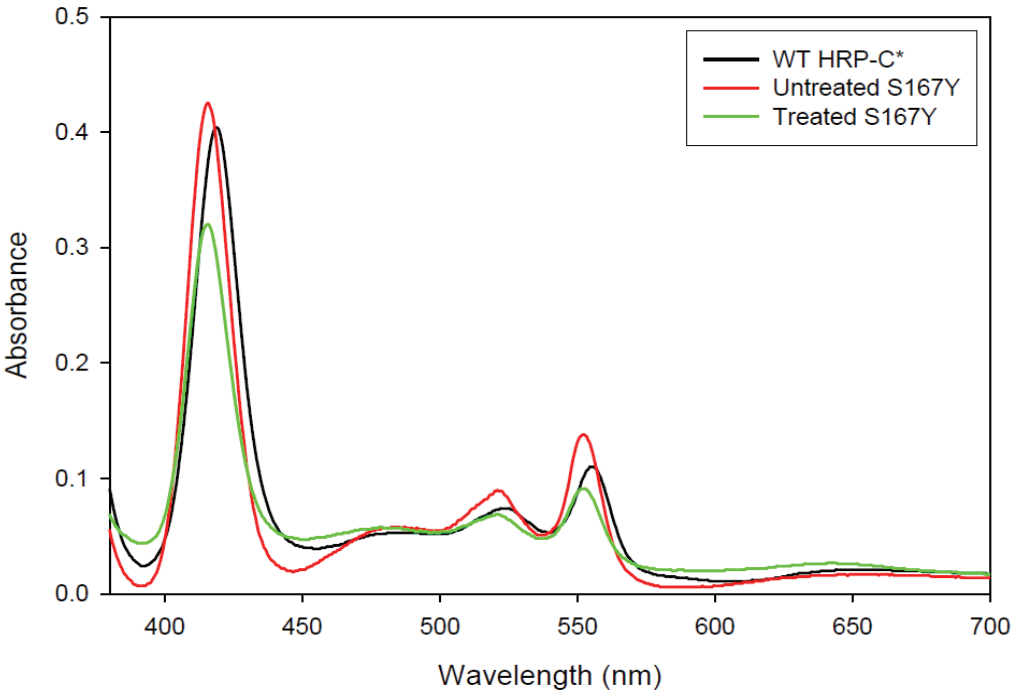

Figure 4.10: Comparison of the pyridine haemochrome difference spectra for WT HRP-C* and the S167Y variant, before and after treatment with 100 equivalents of H_2O_2. Spectra were recorded in 5 mM MOPS buffer, pH 7.0, at 25 ^{o}C and the haem-protein species was reduced with disodium dithionite.

Table 4.3: Spectral features of WT HRP-C* and the new S167 variants (both treated and untreated with 100 equivalents of H_2O_2) after treatment with alkaline pyridine. Spectra were recorded in 5 mM MOPS buffer, pH 7.0, at 25 ^oC and the haem-protein species was reduced with disodium dithionite.

Enzyme	Soret Peak (nm)	β max (nm)	β min (nm)	α max (nm)
WT HRP-C*	419	524	540	555
[a]Treated WT HRP-C*	418.5	524	540	555
Untreated S167W	418.5	524	540	555
Treated S167W	418.5	524	540	555
Untreated S167Y	415.5	521	536	552
Treated S167Y	415.5	521	536	552

[a](Cali, 2008)

4.5.2 Acid butanone haem extraction:

Acid butanone haem extraction is a simple and fast method used to separate the haem from a haemoprotein, by exploiting differences in their relative solubilities in two immiscible solvents. However, as a result of the inability of the acid extraction technique to remove the haem prosthetic group from MPO because of the covalent linkages between the haem and the protein (Wu and Schultz, 1975), acid butanone haem extraction (Fuhrhop and Smith, 1975) was carried out in a similar way in this work to examine the possibility of the presence of a covalent linkage between the haem and the protein in the new S167 variants. This test gives a preliminary indication of a haem-

protein covalent linkage. It did not remove the haem prosthetic group from the S160M and S160Y variants of rpAPX after treatment by H_2O_2 (Metcalfe *et al.*, 2004; Pipirou *et al.*, 2007b), or from [S167M] HRP-C* after H_2O_2 treatment (Cali, 2008).

Samples of WT HRP-C*, S167W and S167Y variants (before and after reaction with H_2O_2) were subjected to the acid butanone extraction method (section 2.8). In order to determine and calculate the haem content for each sample, a pyridine haemochrome assay was then carried out on the extracted organic layer and quantitation was achieved from the reduced-oxidized difference spectra. The results obtained are presented in Table 4.4.

For WT and both the S167W variant samples (before and after H_2O_2 treatment), essentially all the haem was recoverable from the butanone organic layer, which gives a strong indication that there is no haem covalently linked to the protein even after treatment with H_2O_2. However, very little or no haem was observed in the organic layer for the untreated and treated S167Y variant. These results clearly suggest that the haem group of the H_2O_2 treated S167Y variant is strongly and completely linked to the protein (0% recovery). In addition, 81% of the haem of the untreated S167Y variant was unrecoverable, suggesting that a haem-protein covalent bond occurs in this variant spontaneously. An acid butanone extraction and pyridine haemochrome was also applied to a sample of the S167Y variant that had been folded and purified in the presence of ferulic acid, a peroxidase substrate; almost all of the haem was then recovered in the organic layer, suggesting that the haem is unlinked to the protein when oxidation equivalents are scavenged.

A previous study from a member of this lab has concluded that the haem group from haem-protein cross-linked [S167M] HRP-C* was 100% unrecoverable on acid butanone extraction (Cali, 2008). He also reported that some 14% of the haem of the H_2O_2 untreated S167M variant was unrecoverable, indicating that a low level of haem-protein bonding might have occurred spontaneously (Cali, 2008).

Table 4.4: Acid butanone haem extraction of WT HRP-C*, [S167W] HRP-C*and [S167Y] HRP-C*. The acid butanone haem extraction technique was carried out for WT, S167W and S167Y samples, both before and after treatment with hydrogen peroxide. 100 µl of enzyme (using enzyme concentrations as shown below in nmoles) were treated with 25 µl of 2M HCl, and then 500 µl of butanone were added, the solution was mixed very well and then left on the bench to allow the separation of the aqueous layer below and the organic layer above. The pyridine haemochrome technique was then performed on the organic layer to measure the haem content.

Enzyme	Theoretical haem content (nmoles)	Practical haem content (nmoles)	Recovery percentage (%)
WT HRP-C*	1.65	1.61	97
Untreated S167Y	3.30	0.63	19
Treated S167Y	1.67	Nil	0
Untreated S167Y-Ferulic acid	3.00	2.80	93
Untreated S167W	2.70	2.60	96
Treated S167W	0.70	0.65	93

4.5.3 High Performance Liquid Chromatography (HPLC) Analysis:

High Performance Liquid Chromatography (HPLC) is a highly improved form of column chromatography used frequently in biochemistry to separate, identify and quantify biological compounds. It has been successfully applied and widely used for the separation of all classes of biochemical molecules such as lipids, steroids, carbohydrates, amino acids, proteins and vitamins from complex mixture (Pryde and Gilbert, 1979).

Compared to other chromatography systems, HPLC is preferred because it has high resolution, fast cycle times, high sensitivity, good accuracy, columns can be reused without repacking or regeneration and the system can be automated. The mobile phase is often varied during the analysis (gradient elution) to obtain the separation required.

Recently, reverse phase HPLC has been used to distinguish between covalently and non-covalently attached haem to protein links in haemoproteins (Reeder *et al.*, 2002; Limburg *et al.*, 2005). The term reverse phase refers to a non-polar stationary phase and polar mobile phase. Under these conditions, hydrophobic compounds stick to reverse phase HPLC columns from highly aqueous mobile phases (usually containing water) and are then eluted from the columns with a hydrophobic organic mobile phase (such as acetonitrile). Therefore, in reverse phase HPLC compounds are separated based on their hydrophobic character, polar solutes separate and elute quickly from the column, while less polar and non-polar (hydrophobic) solutes elute with a longer retention time.

This analytical technique was used in the present work in order to detect the formation of any new covalent linkages that might have occurred between the protein and the

haem prosthetic group for the new S167 HRP-C* variants. Enzyme samples for WT HRP-C*, [S167W] and [S167Y] HRP-C*, both before and after treatment with H_2O_2 were subjected to reverse phase HPLC analysis, under denaturing conditions, using an analytical C_4 column and a water/acetonitrile mobile phase under acidic conditions (0.1% v/v TFA). The haem group was monitored at 400 nm while protein was monitored at 280 nm during elution by an acetonitrile gradient (section 2.9.4). In a separate control experiment (data not shown) HPLC analysis was performed for free haem under the same conditions; the results showed that haem elution was 23 minutes. Representative chromatograms obtained for WT HRP-C*, [S167W] and [S167Y] HRP-C* variants are presented in Figures 4.11, 4.12, 4.13 and 4.14 respectively.

Chromatograms of WT HRP-C* and the S167W variant, both treated and untreated with H_2O_2, show two distinct peaks, one for the haem at 23 minutes and the other for the protein at 26 minutes, when monitored at 280 nm (Figures 4.11A, 4.11B, 4.12A and 4.12B). However, only one major peak at 23 minutes corresponding to elution of the haem group is observed at 400 nm for these same samples, suggesting that the haem is not linked covalently to the protein. In the case of the S167W variant after treatment with H_2O_2, a small peak at 17 minutes is observed along with the haem peak at 23 minutes and no absorbance is associated with the protein component, when monitored at 400 nm (Figure 4.12B). This indicates degradation of the haem group of [S167W] HRP-C* after exposure to H_2O_2.

Surprisingly, for the H_2O_2 untreated S167Y variant sample monitored at 400 nm, besides the previously described haem peak which elutes at 23 minutes, a significant and a clear fraction of the haem co-elutes with the protein peak at 26 minutes (Figure

4.13A), giving a clear indication that a haem-protein linkage had occurred spontaneously in this enzyme during preparation. On the other hand, for the S167Y variant after treatment with H_2O_2, it can be seen that the haem group is completely attached to the protein and therefore co-eluting at 26 minutes (Figure 4.13B). Another sample of the S167Y variant, which was expressed, refolded and purified in the presence of ferulic acid, was also subjected to analysis by reverse phase HPLC. The resultant chromatograms show only one peak observed at 23 minutes when monitored at 400 nm related to the free haem group. In addition, two peaks are observed at 23 and 26 minutes respectively when monitored at 280 nm (Figure 4.14). These results prove that this sample of the S167Y variant was completely unlinked. Presumably the presence of ferulic acid functioned as an antioxidant preventing cross-linking from occurring during preparation of the enzyme.

Previous work by a member of the group (Cali, 2008), showed similar cross-linking for [S167M]HRP-C* after incubating overnight with H_2O_2, when the haem group completely co-eluted with the protein, confirming the formation of a protein-haem covalent linkage. It has been confirmed that a covalent bond is formed between the haem and the protein as a result of an autocatalytic process in the CYP4A, CYP4F and CYP4B1 families of cytochrome P450 enzymes (Henne *et al.*, 2001; Hoch and Ortiz de Montellano, 2001; Lebrun *et al.*, 2002a; Lebrun *et al.*, 2002b; Baer *et al.*, 2007). Similarly, HPLC analysis provided clear evidence of an auto-catalytically haem-protein covalent linkage formation in LPO when exposed to H_2O_2 (DePillis *et al.*, 1997; Colas *et al.*, 2002; Colas and Ortiz de Montellano, 2003). Replacement of Ser 160 by Met (S160M) and Tyr (S160Y) in Ascorbate Peroxidase leads to the formation of a covalent haem-protein attachment after reaction with hydrogen peroxide, as judged by co-elution

of the haem and the protein when the product was subjected to the HPLC analysis (Metcalfe *et al.*, 2004; Pipirou *et al.*, 2007a; Pipirou *et al.*, 2007b). Furthermore, HPLC experiments provided clear evidence that the covalent attachment of the haem to an engineered cysteine residue can also occur in the S160C variant of APX (Metcalfe *et al.*, 2007). It has been reported that the haem group of F41E mutant in HRP-C* also co-elutes with the protein at the same retention time when the treated enzyme with H_2O_2 was examined by HPLC analysis (Colas and Ortiz de Montellano, 2004). The same process was used to confirm the formation of a covalent link between Trp51 and the haem in Cytochrome *c* Peroxidase (Pipirou *et al.*, 2009).

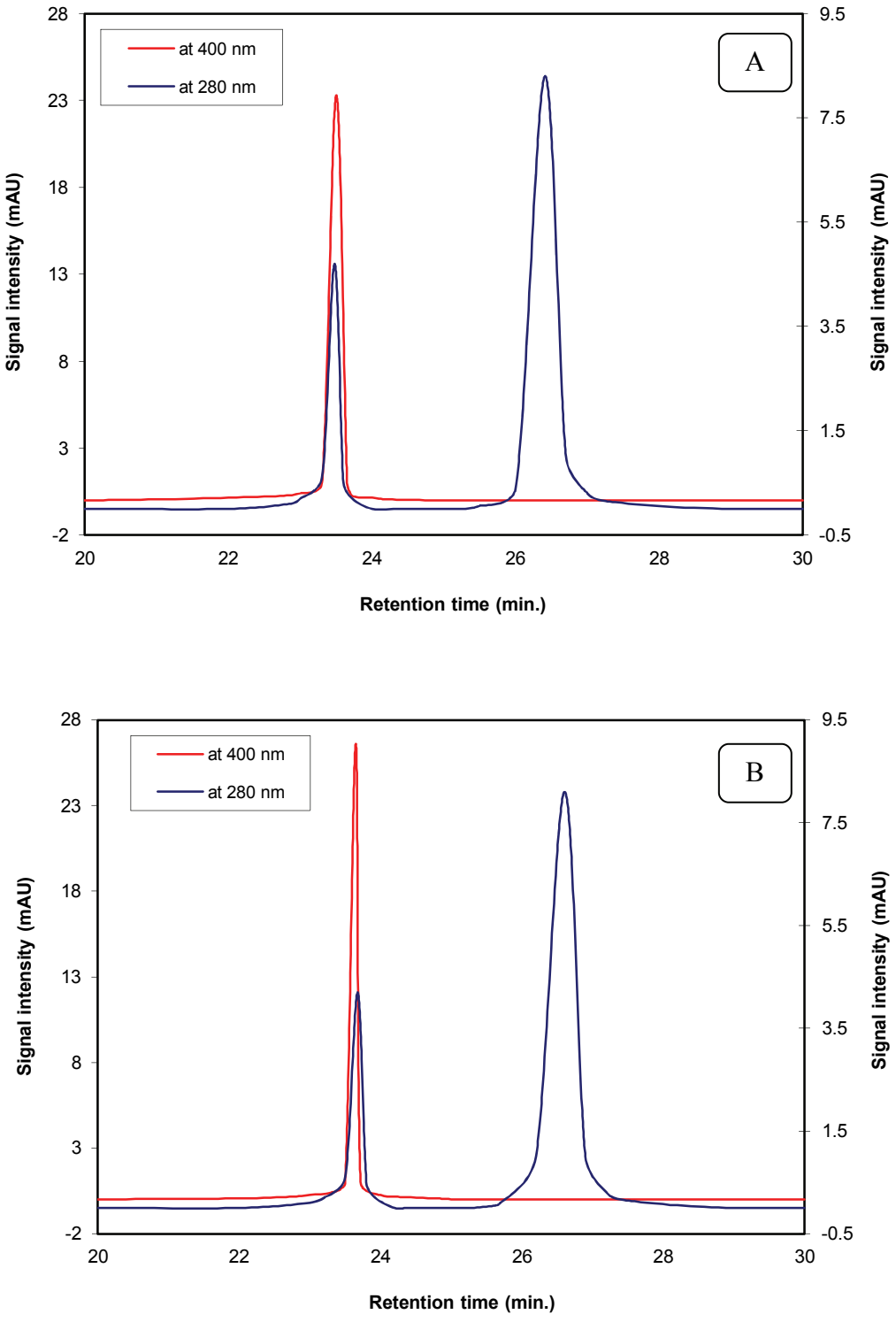

Figure 4.11: HPLC chromatograms of WT HRP-C* before and after treatment with H_2O_2. Left scale represents the absorbance at 400 nm while right scale represents at 280 nm, (A) WT HRP-C* before, and (B) WT HRP-C* after treatment with 100 equivalents of H_2O_2.

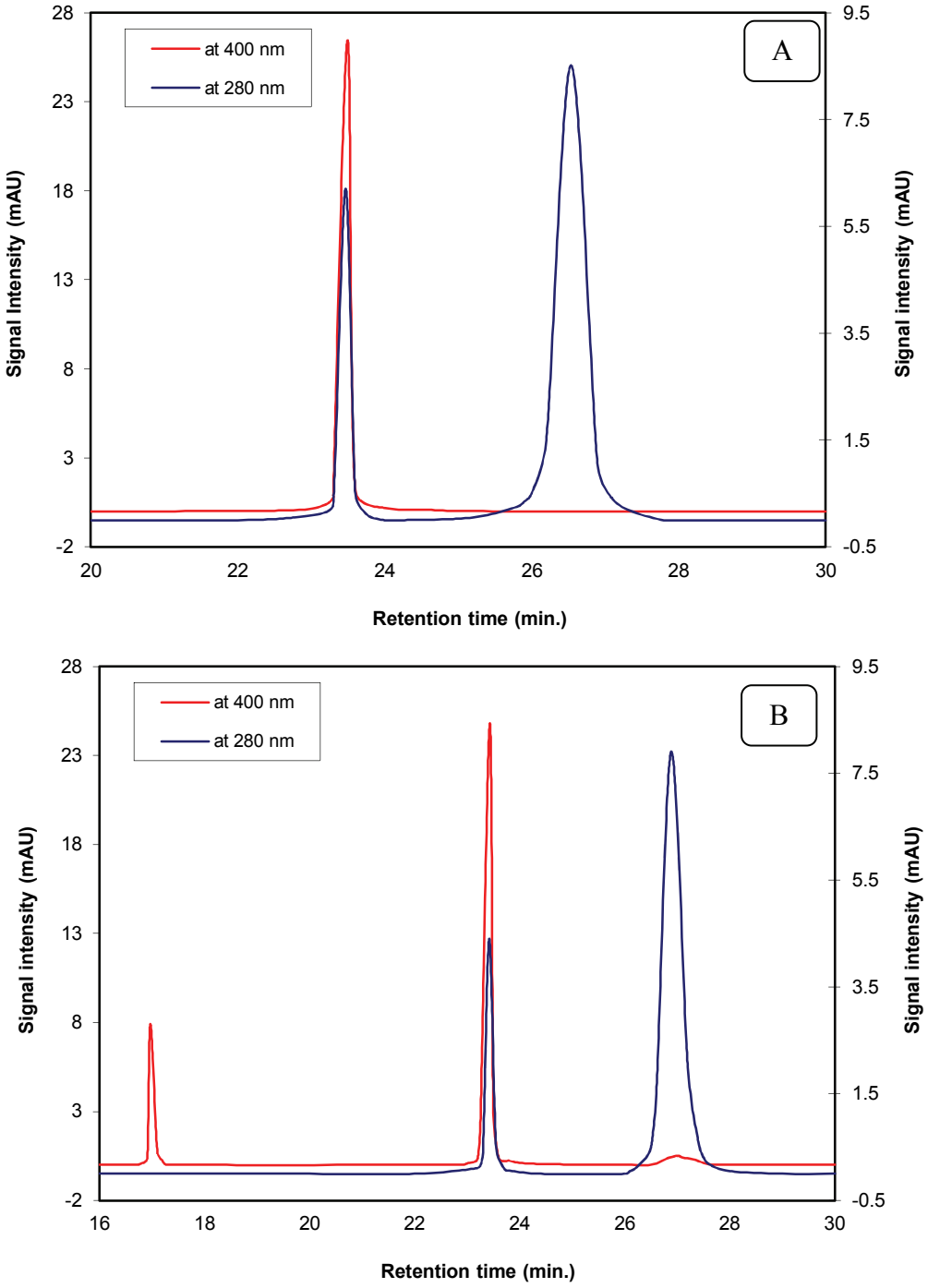

Figure 4.12: HPLC chromatograms of [S167W] HRP-C* before and after treatment with H_2O_2. Left scale represents the absorbance at 400 nm while right scale represents at 280 nm, (A) the S167W mutant before, and (B) the S167W mutant after treatment with 100 equivalents of H_2O_2. The unexpected elution peak at 17 minutes is due to degradation of the haem after exposure to H_2O_2.

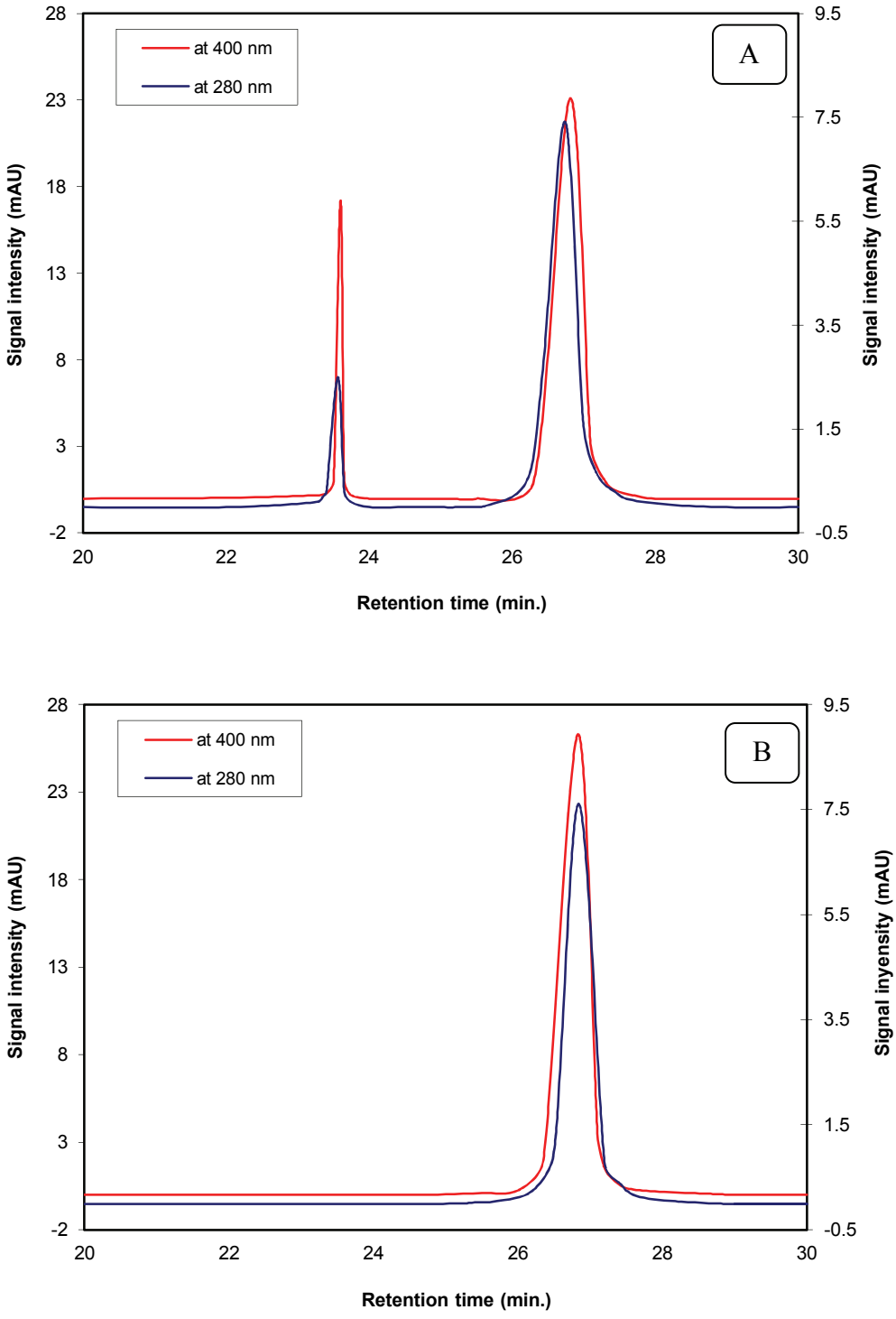

Figure 4.13: HPLC chromatograms of [S167Y] HRP-C* before and after treatment with H_2O_2. Left scale represents the absorbance at 400 nm while right scale represents at 280 nm, (A) Untreated S167Y mutant, and (B) Treated S167Y with 100 equivalents of H_2O_2.

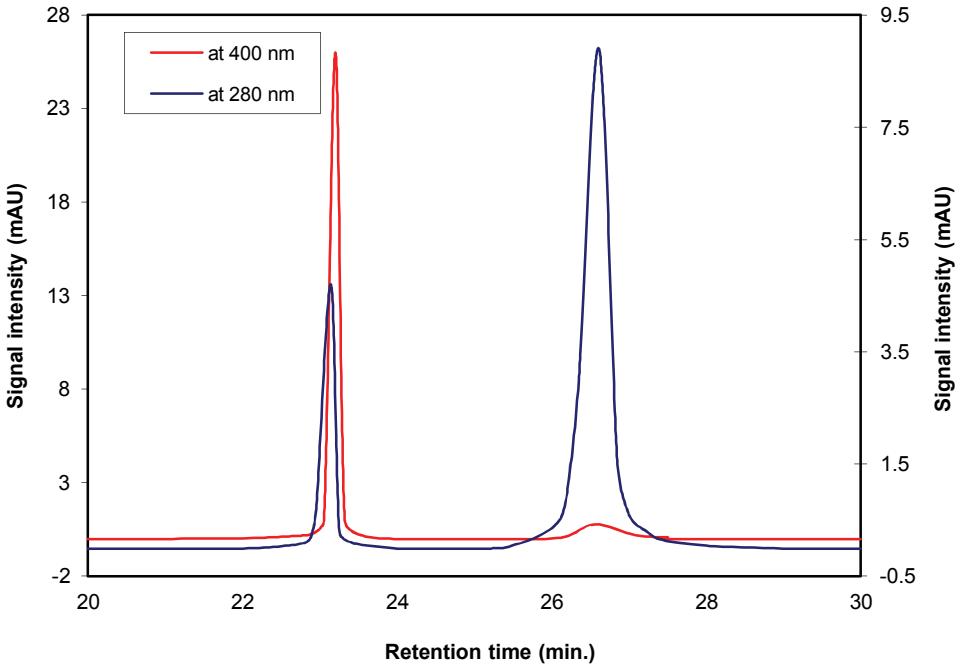

Figure 4.14: HPLC chromatogram of [S167Y] HRP-C* folded and purified in the presence of ferulic acid. Left scale represents the absorbance at 400 nm while right scale represents at 280 nm.

4.5.4 Protein analysis by Mass Spectrometry:

Mass spectrometry is an analytical technique which is used to determine the mass of a sample by measuring the mass-to-charge (*m/z*) ratio of the sample once ionized. In fact, it is generally considered one of the most powerful analytical techniques for both qualitative and quantitative analysis, because of its great power in identification by both molecular weight and structural information. The first stage of mass spectrometry is the introduction of a sample into an ionization source. The analyte is ionized and accelerated to pass into the analyzer region of the mass spectrometer instrument, where ions are separated according to their mass-to-charge (*m/z*) ratios. The separated ions are then detected and presented as a mass spectrum displayed with *m/z* values on the x-axis and ion abundances on the y-axis (Johnstone and Rose, 1996).

Among all types of mass spectrometry, soft ionization mass spectrometry, in particular matrix assistant laser desorption ionization (MALDI) and electrospray ionization (ESI), is ideal for the analysis of high molecular weight bio-molecules. Commercial availability of these MS instruments has made the analysis of bio-molecules such as peptides, proteins and many other compounds that were previously not accessible to mass spectrometric investigations, as routine. One of the greatest advantages of MALDI-TOF and ESI mass spectrometry is the sensitivity; the picomole to femtomole sensitivity range allows the investigation of bio-molecules even at very small quantities. Microgram quantities of sample are generally more than enough to do an analysis with a high accuracy up to ± 0.01 % (Daniel *et al.*, 2002). Indeed, the accuracy of MS analysis is quite sufficient to detect the mass changes that would occur in peptides and protein molecules as a result of the substitution of one amino acid by another.

ESI and MALDI-TOF mass spectrometry studies have been widely used to look for increases in protein molecular weights due to haem to protein covalent bonds. During previous work in this lab, these techniques clearly showed that formation of a sulfonium linkage in [S167M] HRP-C* can be achieved by incubation of the enzyme overnight with hydrogen peroxide (Cali, 2008). ESI-MS in conjunction with HPLC analysis was used to investigate the cross-linking process of the amino acid residues Asp225 and Gly375 with the prosthetic haem group of Lactoperoxidase (Colas *et al.*, 2002).

MS analysis results provided strong evidence that a thioether bond formation between haem and an engineered cysteine residue at position 160 can occur easily under reducing conditions in the S160C variant of ascorbate peroxidase (Metcalfe *et al.*, 2007). MALDI-TOF and ESI mass spectrometry analysis also confirmed that introduction of an engineered methionine residue at the position 160 (S160M variant) and tyrosine residue at the same position (S160Y variant), led to the autocatalytic formation of a haem-methionine sulfonium linkage (the mass recorded was 629 Da higher than the predicted value) and a haem-tyrosine covalent linkage (the mass was 632 Da higher than the predicted value) respectively in ascorbate peroxidase when treated with hydrogen peroxide (Metcalfe *et al.*, 2004; Pipirou *et al.*, 2007b). Mass spectrometry clearly showed that the exposure of ascorbate peroxidase to a sufficient quantity of hydrogen peroxide leads to the formation of a covalent linkage between the haem and the distal Trp 41 residue (Pipirou *et al.*, 2007a).

Recently, mass spectrometry studies indicated that the reaction of cytochrome *c* peroxidase with hydrogen peroxide leads to the formation of a covalent link with the distal tryptophan (Trp51) (Pipirou *et al.*, 2009). Furthermore, the presence of a covalent

linkage between the protein and the haem prosthetic group was confirmed for many members of cytochrome P450 enzymes particularly CYP4A, CYP101, CYP4B and CYP4F superfamilies, using mass spectrometry analysis (Henne *et al.*, 2001; Hoch and Ortiz de Montellano, 2001; Lebrun *et al.*, 2002a; Lebrun *et al.*, 2002b; Limburg *et al.*, 2005; Baer *et al.*, 2007). MS analysis was also used to detect the presence of a single Tyr-Trp cross-link in M255I mutant of Catalase peroxidase, which is postulated to be an intermediate generated during formation of the Met-Tyr-Trp cross-link (Ghiladi *et al.*, 2005a; Ghiladi *et al.*, 2005b). More recently, a combination of MALDI-TOF and ESI mass spectrometry analysis has been used in order to study the characteristics of the glycans of the glycopeptides from horseradish peroxidase (Chen *et al.*, 2010).

MALDI-TOF and ESI mass spectrometry were used in this work to investigate mass changes that may or may not occur in different HRP-C* samples after treatment with H_2O_2. The masses of WT, [S167Y] and [S167W] HRP-C* (treated and untreated with H_2O_2) were determined from MALDI-TOF mass spectra, and were also calculated from ESI-MS mass spectra shown in Figure 4.15, using the equation mentioned in section 2.10.4.2, as well as auto-calculated directly from the ESI-MS apparatus using MassLynx V4.1 (Figure 4.16). The collective results are presented in Table 4.5, where the theoretical masses were calculated from the gene sequences. ESI mass spectrometry gave an experimental mass for WT HRP-C* of 34,041 Da (Table 4.5) which corresponds closely to the theoretical calculated mass of 34,048 Da. The experimental mass for the untreated S167W variant is 34,142 Da, and this increase in mass over WT is consistent with the replacement of a serine residue with tryptophan; the molecular masses for these amino acids are 105 Da and 204 Da respectively. For peroxide treated [S167W] HRP-C* the mass spectrum gave a mass of 34,168 Da. which is 26 Da higher

than the mass of untreated S167W; the origin of this mass increase seems to be less clear. However, the results clearly indicate that there is no linkage formed between the haem and the protein in the S167W variant even after H_2O_2 treatment. The experimental masses for untreated and treated [S167Y] HRP-C* are both 34,730 Da, corresponding to an increase in mass of 614 Da over the predicted mass of 34,117 Da (the predicted mass is 76 Da higher than WT, consistent with the replacement of a serine residue with tyrosine, 105 Da and 181 Da, respectively). This increase in mass of 614 Da is consistent with the covalent attachment of haem (616 Da) to the protein. The MS data are therefore in agreement with the HPLC analysis, and provide further evidence of the formation of the covalent cross-link between the haem and the protein in the S167Y variant. However, the spontaneous cross-linking of untreated S167Y was unexpected. Therefore, protein folding and purification of [S167Y] HRP-C* was performed in the presence of ferulic acid as an antioxidant scavenger and examined by mass spectrometry. The MS results showed no difference in mass between the calculated and the expected values, at 34,117 Da, respectively.

Table 4.5: Comparison of the molecular masses of WT, [S167W] and [S167Y] HRP-C* treated and untreated with H_2O_2, as well as [S167Y] HRP-C* purified in the presence of ferulic acid. The molecular masses were calculated from the MALDI-TOF and ESI mass spectra.

Enzyme	Calculated mass (Da)	Experimental mass (Da)	Difference (Da)
WT HRP-C*	34,048	34,041	7
Untreated S167W	34,140	34,142	2
Treated S167W	34,140	34,168	28
Untreated S167Y	34,117	34,731	614
Treated S167Y	34,117	34,731	614
Untreated S167Y-Ferulic acid	34,117	34,117	0

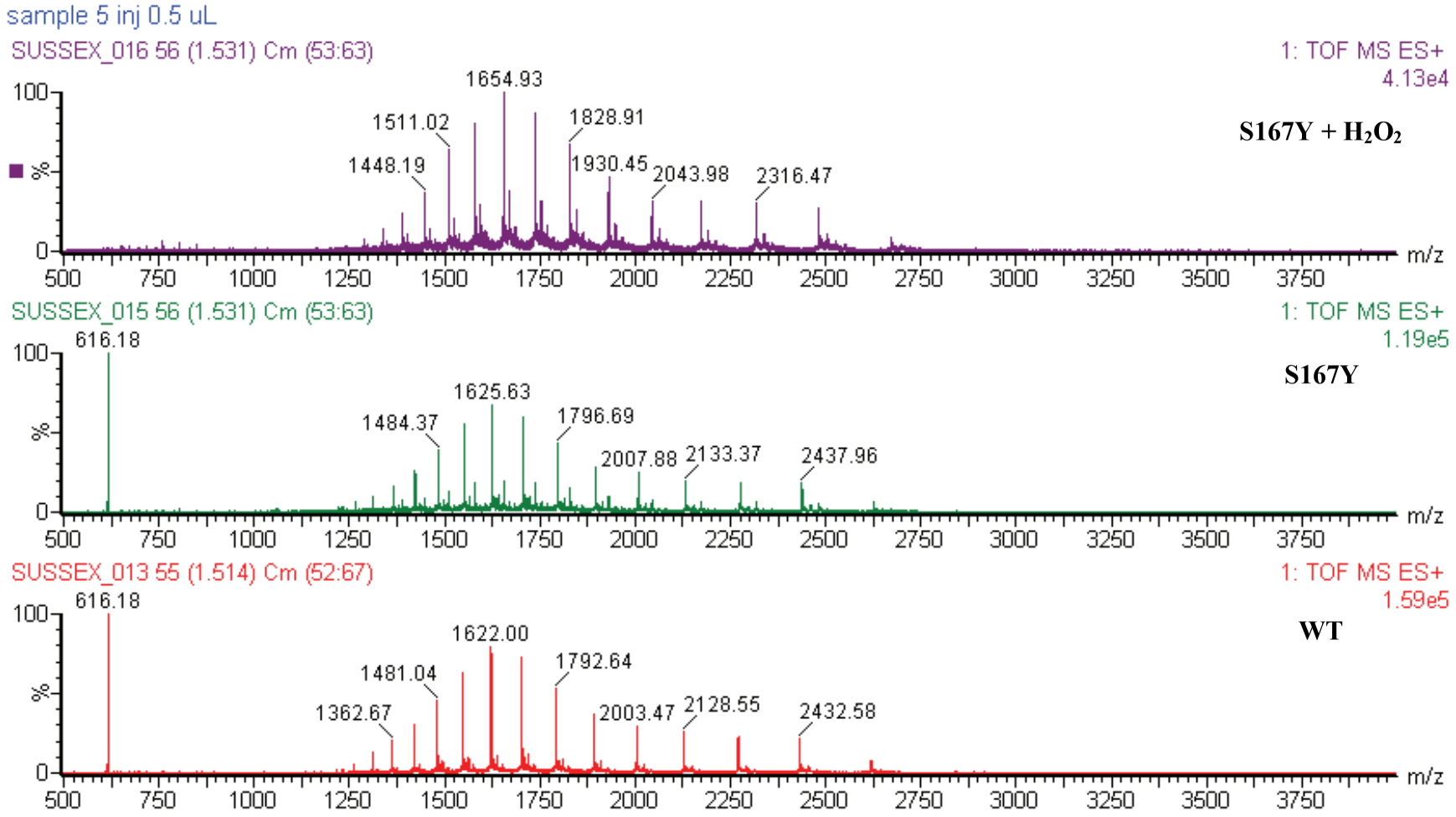

Figure 4.15: Electrospray mass spectra of WT HRP-C*, [S167Y] HRP-C* and [S167Y] HRP-C* treated with H_2O_2.

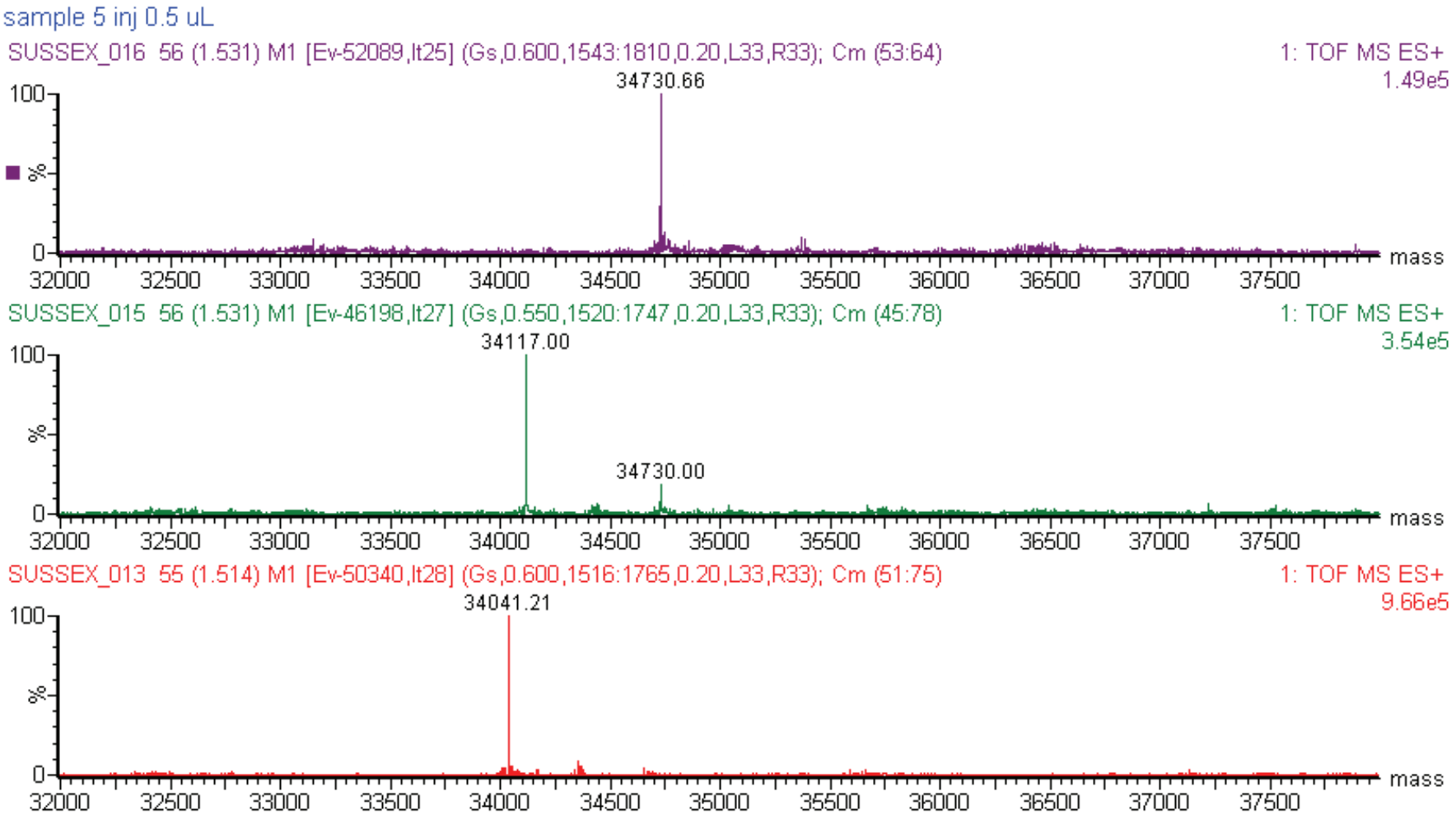

Figure 4.16: MassLynx auto-calculated mass from ESI-MS for HRP-C*, [S167Y] HRP-C* and [S167Y] HRP-C* treated with H_2O_2.

4.6 Crystal growth for [S167Y] HRP-C*:

The hanging drop method was used to grow crystals of the S167Y variant, as described in section 2.12. In this method, the concentration of protein in a drop is gradually increased as water is lost to a reservoir solution by vapour diffusion (Branden and Tooze, 1991). The crystals form and grow as the protein solution is brought to a supersaturated state as the protein concentration exceeds protein solubility. After one week, and in order to accelerate crystallization, the S167Y mutant protein solution was seeded with WT HRP-C* micro-crystals to serve as nucleation centres for rapid growth of larger crystals. The resultant S167Y crystals were visible to the naked eye and in about one third of the wells of the crystal tray used (Table 2.2). They were a few millimetres in length after 3-4 weeks, and are shown in Figure 4.17. The crystals were bathed in cryo-protective solution, i.e. reservoir solution containing 22% glycerol, and then frozen in liquid nitrogen prior to X-ray data collection. The same crystallization procedure was attempted for S167W mutant; unfortunately, unlike S167Y, all attempts to get S167W crystals were unsuccessful.

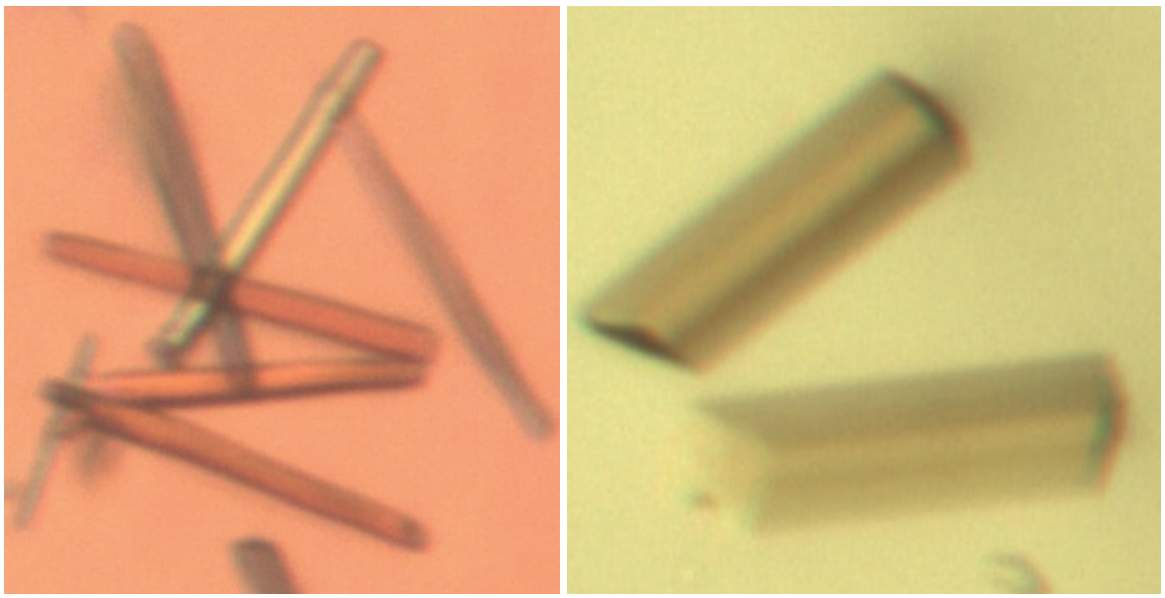

Figure 4.17: Selected crystals of the S167Y mutant of HRP-C*. The crystal were grown using hanging drop method and they were a few millimetres in length after 3-4 weeks.

4.7 Conclusions:

Spectroscopic characterisation of [S167W] and [S167Y] HRP-C* variants showed the absence of the shoulder at 380 nm on the Soret peak seen for WT HRP-C*, and a substantial increase in molar extinction coefficients. These changes can be attributed to an increase in the 6-coordinate high spin character of the haem at the expense of 5-coordinate high spin character. Studies on the effect of the mutations on the affinity of the HRP-C* enzyme for BHA, gave a dissociation constant (K_d) for the S167W variant that was only slightly higher than the WT. However, the K_d doubled for the S167Y variant, implying a small but significant perturbation of the aromatic donor binding site of the enzyme and / or the associated haem-linked hydrogen bonding network (Smith *et al.*, 1992; Veitch *et al.*, 1997).

Incubation of the new HRP-C* variants S167W and S167Y with hydrogen peroxide, in the absence of any reducing substrate, for two hours in sodium phosphate buffer at 25 ^{o}C showed changes in the individual catalytic reactivity of the enzymes compared to WT. Repeat UV/Visible scans demonstrated clearly that the first intermediate Compound I is less stable and undergoes a rapid conversion to the Compound II for both mutants, when compared to the WT enzyme. The spectroscopic properties of the more stable intermediate, Compound II (λ_{max} at 420, 555 and 523 nm) were consistent with those for WT HRP-C*. In the case of the S167W variant the return to the resting sate was more rapid, with complete loss of Compound II after 15 minutes, compared to the S167Y variant, which needed 180 minutes to return to the resting state.

The reduced, pyridine haemochrome spectrum of the S167Y variant only showed a blue shifted α-band at 552 nm in addition to a blue shifted Soret band at 415.5 nm, compared

to the 555 nm and 419 nm for WT HRP-C*. These spectroscopic changes, by analogy with MPO (Kooter *et al.*, 1997a), indicated the formation a covalent linkage between the haem and the protein in the [S167Y] HRP-C* enzyme even before treatment with H_2O_2.

The most important result from the reaction of the new variants with hydrogen peroxide, is the finding that the haem in [S167Y] HRP-C* is attached to the protein by covalent linkage. This was confirmed in three ways. Firstly, acid butanone haem extraction did not remove the haem from the protein, 100% of the haem of H_2O_2 treated S167Y variant was unrecoverable, compared with 97% of untreated WT and 96% of H_2O_2 treated S167W variant being recoverable. Interestingly, 81% of haem was also unrecovered from the non H_2O_2 treated [S167Y] HRP-C* sample.

Secondly, HPLC analysis of the S167Y variant after treatment with H_2O_2 clearly showed that the haem group was strongly attached to the protein as it co-eluted with the protein peak at 26 minutes in the HPLC elution profile. Again untreated S167Y samples were also substantially cross-linked, with a significant and a clear fraction of haem again co-eluting with the protein peak at 26 minute. Thirdly, ESI and MALDI-TOF analysis of both untreated and H_2O_2 treated [S167Y] HRP-C* showed a mass of 34,731 Da, corresponding to an increase in mass of 614 Da over the predicted mass of 34,117 Da. This increase is consistent with the covalent attachment of haem (616 Da) to the protein. Again this gives a clear indication that the majority of the haem is already covalently linked to the protein before [S167Y] HRP-C* is reacted with H_2O_2, suggesting that the haem-protein linkage is spontaneous. No clear evidence was found

for a haem-protein cross-link in the [S167W] HRP-C* variant even after treatment with H_2O_2.

The results obtained therefore show that a Tyr residue at position 167 close to the 2-vinyl of the porphyrin of the haem is sufficient to allow formation of the haem-protein covalent linkage in HRP-C, even before treatment with H_2O_2. One likely scenario is that the enzyme turns over during isolation, folding or purification with an oxidant, forming radicals (either Compound I or a radical on the haem 2-vinyl) that enable the reaction with tyrosine to occur. Therefore, protein folding and purification for a sample of S167Y variant was performed in the presence of ferulic acid, as an antioxidant scavenger. Acid butanone extraction, HPLC and MS analysis then showed no evidence of a spontaneous haem-protein cross-link in the variant. It is important to mention that from this time, the UmS167Y refers to the unlinked mutant while mS167Y refers to the haem-tyrosine covalent link mutant.

The S167Y variant has been successfully crystallised and data collected at the Diamond Light Source by Dr. Mark Roe (X-Ray Crystallography Collaborative Research Facility Manager, University of Sussex, UK). The structure was subsequently solved to 1.7 Å resolution. A more detailed account of the structural aspects of this mutant is given in chapter 7.

Chapter Five:

Steady-state enzyme kinetics

5.1 Introduction:

Enzyme kinetics is the study of the rates of enzyme-catalyzed reactions. The rate of catalysis is defined as the number of moles of product formed per second and this value rises linearly with increasing substrate concentration, then begins to level off and approach a maximum at higher substrate concentrations (Berg *et al.*, 2002). In 1913, Leonor Michaelis and Maud Menten proposed a classic model that describes an enzyme reaction (Michaelis and Menten, 1913). The model proposed is the simplest one that can be used to account for the kinetic properties of enzymes:

$$E + S \underset{k_{-1}}{\overset{k_1}{\rightleftharpoons}} ES \xrightarrow{k_2} E + P \qquad (1)$$

In this equation E is an enzyme that combines with the substrate S to form an ES complex, with a rate constant of k_1. The ES complex has two possible fates, it either dissociates back to E and S with a rate constant of k_{-1} or proceeds to form product P with a rate constant of k_2. Michaelis and Menten established from this model a basic equation (equation 5.1), called the Michaelis-Menten equation, to describe the kinetic data of this enzyme reaction:

$$V = \frac{V_{max}\,[S]}{K_m + [S]} \qquad (equation\ 5.1)$$

In this equation V is the rate of catalysis at any given substrate concentration and V_{max} is the maximum attainable rate of catalysis from the enzyme-catalyzed reaction (unit M s^{-1}). K_m is an important characteristic of enzyme kinetics and is called the Michaelis constant. K_m is expressed by the following equation:

$$K_m = \frac{k_{-1} + k_2}{k_1} \qquad (equaion\ 5.2)$$

K_m indicates the affinity between the enzyme and substrate, it is a measure of the strength of the ES complex (see model 1 above), where a high value of K_m indicates weak binding while a low value of K_m indicates strong binding. The maximum rate of catalysis V_{max} also leads to the turnover number of an enzyme (Berg *et al.*, 2002), which is the number of substrate molecules converted into product by an enzyme molecule in unit time, when the enzyme is fully saturated with substrate (unit s^{-1}). It is often called k_{cat}. When the total concentration of enzyme $[E]_o$ is known, the V_{max} is related to the turnover number k_{cat} by the following equations:

$$V_{max} = k_{cat}[E]_0 \qquad (equation\ 5.3)$$

$$and\ thus \quad k_{cat} = V_{max}/[E]_o \qquad (equation\ 5.4)$$

Under physiological conditions, the $[S]/K_m$ ratio is typically between 0.01 and 1.0 (Campbell and Farrell, 2009). However, when the substrate concentration is small compared to K_m, the enzymatic rate is much less than k_{cat} because not all the active sites of the enzyme molecules are filled with substrate. Under these conditions, the ratio value of k_{cat}/K_m behaves as the rate constant for the interaction between the substrate and the enzyme. The ratio k_{cat}/K_m is thus a measure of catalytic efficiency because it

takes into account both the rate of catalysis with a particular substrate (k_{cat}) and the strength of the enzyme-substrate interaction (K_m). Therefore, by using k_{cat}/K_m values, it is easy to compare an enzyme's preferences for different substrates. Enzymes that have k_{cat}/K_m values at the upper limits have attained kinetic perfection (Berg *et al.*, 2002).

Most enzymatic reactions in biological systems are more complicated than the classical Michaelis-Menten model and include two substrates (Berg *et al.*, 2002). Nevertheless, it is still possible to obtain data that conform to the Michaelis-Menten equation (equation 5.1), and determine the steady-state kinetic parameters for each substrate *in vitro*, by treating the catalysis as if it is a single substrate reaction. This is achieved by varying the first substrate concentration, at a constant concentration of the second substrate, and vice versa. The parameters obtained by this method are termed 'apparent' and may change if the concentration of the constant substrate is altered (Cornish-Bowden, 2004).

5.2 Initial steady-state kinetics of ABTS oxidation:

In order to study the effects of mutation at position 167 on the catalytic efficiency of HRP-C*, steady-state kinetic parameters for the reaction of WT HRP-C* and the new S167 variants were determined with hydrogen peroxide and using 2, 2′-azino-di-(3-ethyl-benzthiazoline-6sulphonic acid) (ABTS) as reducing substrate. ABTS is a relatively large molecule (Figure 5.1), with a sulphate oxygen to sulphate oxygen distance of 17.2 Å, and structurally is essentially a planar substrate (Mousty *et al.*, 1997). It is utilized as a convenient, low cost, commercially available substrate to assay peroxidase activity, as it is known as one of the most efficient electron donors for HRP (Childs and Bardsley, 1975; Smith *et al.*, 1990; Heering *et al.*, 2002). The chemical properties of ABTS and its oxidation by HRP-C have been extensively studied (Childs

and Bardsley, 1975; Wolfenden and Willson, 1982; Scott *et al.*, 1993; Campos and Lissi, 1997; Aliaga and Lissi, 1998). In the presence of HRP-C and hydrogen peroxide this substrate readily undergoes a single electron oxidation to produce a cation radical species with distinctive green colour (Figure 5.1). Accordingly, ABTS assays involve the measurement of the accumulation of this cation radical by following the colour production spectrophotometrically as a function of time (Childs and Bardsley, 1975).

The catalytic oxidation of ABTS by HRP-C is of course a two substrate reaction. The sequence of this reaction firstly involves interaction of the enzyme with hydrogen peroxide to produce the Compound I intermediate. This is followed by the oxidation of one molecule of ABTS concomitant with the reduction of Compound I to the second intermediate Compound II, and then, the oxidation of a second molecule of ABTS concomitant with the reduction of Compound II to the resting state of the enzyme (Childs and Bardsley, 1975).

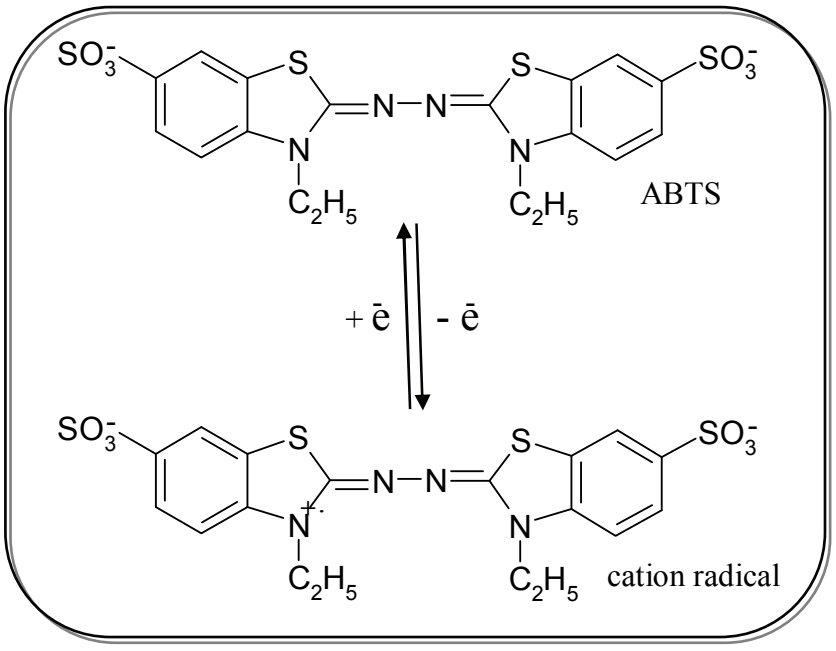

Figure 5.1: Chemical formula of ABTS and its oxidation product. Colourless, reduced ABTS undergoes a single electron oxidation in the presence of HRP-C and H_2O_2 to give a green, long-lived cation radical (Childs and Bardsley, 1975).

In this work, activity assays were carried out using varying concentrations of ABTS and a constant concentration of H_2O_2. The initial rates, expressed as turnover numbers, were measured by monitoring the increase in absorbance at 414 nm resulting from the oxidation of the ABTS. Figure 5.2 shows the calculated initial rates against ABTS concentration and the plots of the Michaelis-Menten equation (equation 5.1) to the experimental data (SigmaPlot). The apparent kinetic parameters K_m and k_{cat} determined from each fit are listed in Table 5.1. The values of k_{cat}/K_m, the catalytic efficiency constant for ABTS oxidation by HRP-C, or K_{ABTS}, are also included in this table as a measure of the specific enzymes effectiveness.

The kinetic parameters obtained show a number of important differences between the new mutants and the WT HRP-C*. The largest difference between the parameters for the S167W variant and WT HRP-C* is the higher apparent K_m for the former; 366 µM for [S167W] HRP-C* and 184 µM for WT, meaning there is a two-fold decrease in the affinity of the mutant towards ABTS compared with the wild-type enzyme. Moreover, the apparent k_{cat} of the mutant is also reduced, to approximately 75% of that of WT. These results indicate that replacement of the Ser167 residue by Trp has created an enzyme mutant with a somewhat reduced affinity towards ABTS and lower activity when compared to wild-type. Calculating the efficiency constant K_{ABTS} shows that the mutant has only 39% of the effectiveness of WT HRP-C* (Figure 5.3).

The UmS167Y variant, compared to the S167W variant, displayed different behaviour during the steady-state oxidation of ABTS (Table 5.1). This variant has a decreased apparent K_m value of 73 µM compared to 184 µM for WT (i.e. approximately 2.5-fold less) but also a reduction in the apparent k_{cat} value to 18% of the WT enzyme. These

results mean, in contrast to the S167W variant, that the replacement of Ser167 by Tyr has created an enzyme mutant with a higher affinity towards ABTS, but a much lower catalytic activity k_{cat}. As a result, the efficiency constant K_{ABTS} for Um[S167Y] HRP-C* is decreased to 45% of that of WT enzyme (Figure 5.3).

As with UmS167Y, the m[S167Y] HRP-C* also has decreased apparent K_m value to approximately half that of the wild-type enzyme (Table 5.1). However, the activity of mS167Y, as judged by the k_{cat} value, is almost 3-fold higher than that of UmS167Y but still nearly 2-fold lower than that of the wild-type enzyme. These results therefore give a value of K_{ABTS} for m[S167Y] HRP-C* over twice the value of UmS167Y and equal to that of WT HRP-C*. It can therefore be concluded that the creation of the haem-protein cross-linkage in the S167Y mutant, has led to an enzyme with a similar effectiveness to WT HRP-C* (Figure 5.3), presumably due to the linkage causing an adventitious perturbation of the structure.

In a previous study by a member of the group (Cali, 2008), it was observed that the K_m value for UmS167M HRP-C* with ABTS was similar to that of WT HRP-C*, but the k_{cat} value was 3-fold lower. Therefore, the S167M mutation decreased the enzyme's effectiveness (K_{ABTS}) by approximately 2.5-fold compared to WT. However, the formation of the sulfonium linkage in this mutant (mS167M) had a larger negative effect on efficiency, as it reduced the K_{ABTS} value of the enzyme towards ABTS by a factor of 15 (Cali, 2008).

From the present results, in conjunction with the findings of Cali (Cali, 2008), it seems clear that although Ser167 does not have any essential role in the catalytic function of

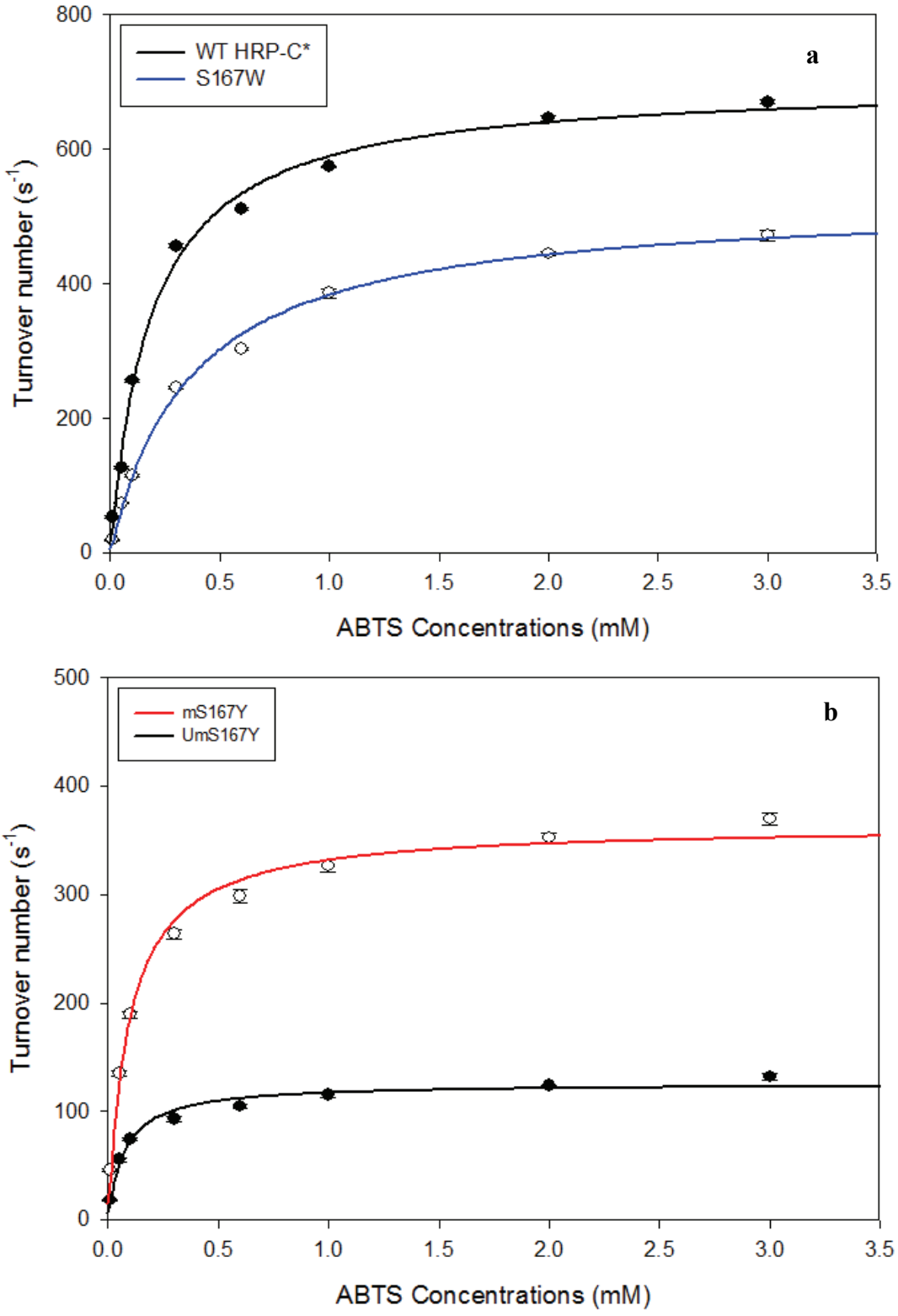

Figure 5.2: Plots depicting the initial rates (expressed as turnover numbers) against ABTS concentration. (a) WT HRP-C* and [S167W] HRP-C* and (b) Um[S167Y] and m[S167Y] HRP-C*. The assays were carried out in phosphate-citrate buffer, pH 5, using 0.5 nM of enzyme, 1 mM H_2O_2, in a final volume of 1 ml at 25 ^oC.

Table 5.1: Steady-state parameters of the oxidation of ABTS by WT HRP-C* and the new S167 variants. Data obtained from Figure 5.2.

Enzyme	K_m (μM)	k_{cat} (s^{-1})	K_{ABTS} ($M^{-1}s^{-1}$)
WT HRP-C*	184 ± 18	699 ± 16	3.8 x 10^6
S167W	366 ± 22	524 ± 13	1.4 x 10^6
UmS167Y	73 ± 12	126 ± 4	1.7 x 10^6
mS167Y	95 ± 11	363 ± 8	3.8 x 10^6

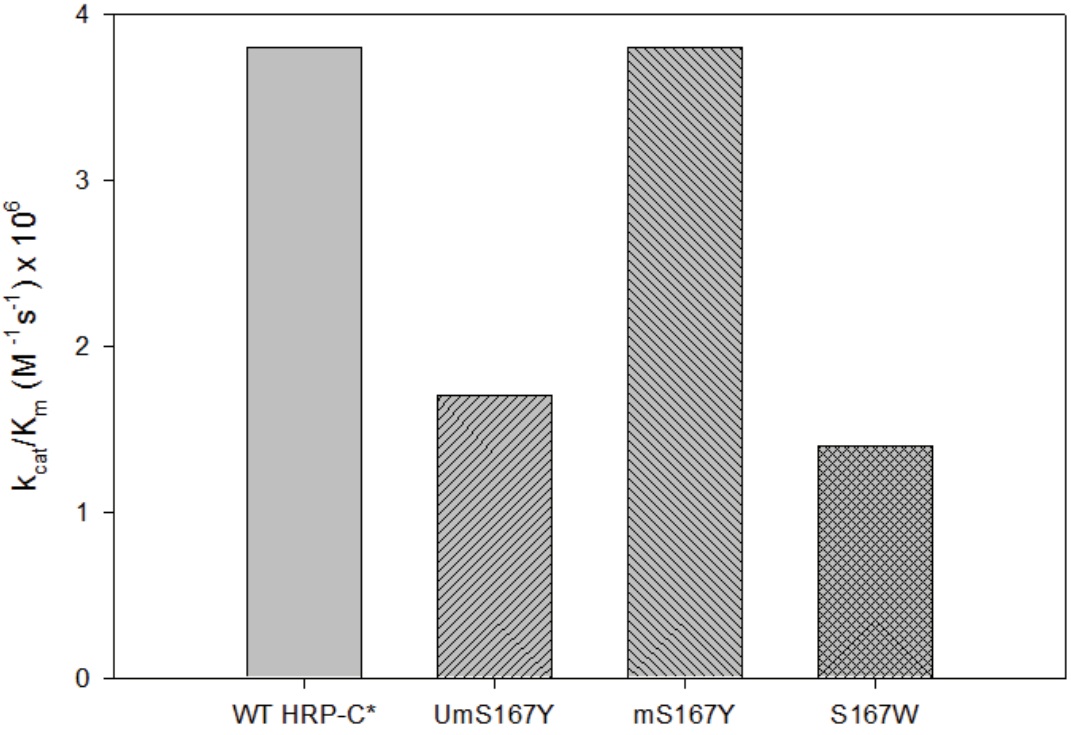

Figure 5.3: Histogram illustrating the effects of mutations at position 167 of HRP-C* on k_{cat}/K_m values for the oxidation of ABTS. Data obtained from Figure 5.2.

the enzyme, its mutation can affect indirectly either the substrate binding to the binding site or the rate of substrate turnover causing an alteration in the effectiveness of the enzyme towards ABTS. Interestingly, the only enzyme with the same effectiveness ratio as WT HRP-C* is the cross-linked S167Y variant.

5.3 Activity screening towards a panel of substrates:

HRP-C is characterized by having the capacity to oxidize a wide variety of substrates, albeit with varying efficiencies, e.g. aromatic amines, indoles, phenols and sulfonates (Veitch and Smith, 2001). In order to determine further the functional properties of the S167 enzyme mutants and whether the effects on the rate of ABTS oxidation already seen are replicated with other substrates, the new mutants were also studied against a panel of twelve further peroxidase substrates. Activity assays were carried out using varying concentrations of each substrate and a constant concentration of H_2O_2 (section 2.11.2). The results obtained are presented as specific activities in Table (5.2).

The S167W variant generally displays an impaired activity toward all substrates used compared to WT HRP-C*, although the degree of impairment varies considerably, ranging between 40-75% of the wild-type enzyme. While the specific activities for guaiacol and orange II oxidation are similar to those of the wild-type enzyme, most interestingly the S167W mutant exhibits an approximately 3-fold increase in luminol oxidation, under the conditions used.

The ability of the UmS167Y variant to oxidize substrates was also found to generally be decreased when compared to WT HRP-C*, with the exception of guaiacol and orange II. The specific activities measured were also more severely impaired than for S167W,

except for pyrogallol. This is consistent with the ABTS oxidation results reported in the last section. These results give an indication that the active site of the enzyme has been more modified when the Ser167 residue is replaced by Tyr, than when it is replaced by a Trp, perhaps surprisingly giving the amino acid structures involved.

Table 5.2: Substrate activity screening of WT HRP-C* and the new S167 variants. The assays were carried out in phosphate-citrate buffer, pH 5.0, at 25 ^{o}C. The results represent the specific activity of the enzyme in units (µmole. min^{-1}. mg^{-1}).

Substrate	WT	S167W	UmS167Y	mS167Y
ABTS	**824 ± 8**	**389 ± 3**	**264 ± 4**	**805 ± 8**
Ferulic acid	**3723 ± 33**	**1465 ± 12**	**1237 ± 38**	**3658 ± 141**
Caffeic acid	**3742 ± 101**	**2030 ± 66**	**1312 ± 22**	**3648 ± 66**
***p*-Coumaric acid**	**2216 ± 64**	**1626 ± 75**	**1063 ± 11**	**2244 ± 19**
Potassium ferrocyanide	**1247 ± 60**	**301 ± 2**	**260 ± 27**	**856 ± 42**
Guaiacol	**387 ± 4**	**433 ± 11**	**338 ± 22**	**969 ± 40**
Pyrogallol	**2931 ± 62**	**1055 ± 15**	**1172 ± 28**	**3853 ± 37**
***o*-Phenylenediamine**	**1672 ± 35**	**764 ± 10**	**598 ± 23**	**1655 ± 14**
Chlorpromazine	**12 ± 1**	**5 ± 1**	**4 ± 1**	**13 ± 1**
Luminol	**71 ± 2**	**201 ± 4**	**49 ± 1**	**163 ± 3**
Orange I	**442 ± 14**	**305 ± 9**	**266 ± 8**	**755 ± 6**
Orange II	**0.12 ± 0.01**	**0.12 ± 0.01**	**0.10 ± 0.01**	**0.17 ± 0.01**

The most interesting observations were found for m[S167Y] HRP-C*, which displays an overall increase in specific activity of 2-4 fold towards all the substrates used, when compared to the unlinked enzyme. This increase in activity also leads to equivalent or higher activities compared to the WT enzyme (Figure 5.4), except for the potassium ferrocyanide. Of particular note is the approximately 2.5-fold increase in activity compared to WT for guaiacol and luminol. Again this is generally consistent with the previous results for ABTS. Presumably the perturbation of the structure brought about by the initial S167Y mutation is again altered by the production of the linkage so that the active site and substrate binding site are once more like the wild-type arrangement, although for a few substrates a small change must still be present that allows for the increased activities. It is interesting that the linked S167Y mutant has higher activities against all substrates tested than the linked S167M mutant (Cali, 2008), which were all lower than the unlinked S167M mutant. Presumably in this mutant the formation of the sulfonium linkage increases the perturbation of either, or both, the active and substrate binding sites. On the other hand, it has been reported that the specific activity of F41E HRP-C* towards guaiacol was significantly increased 10-fold after treatment with H_2O_2 and creation of a haem-protein covalent bond (Colas and Ortiz de Montellano, 2004).

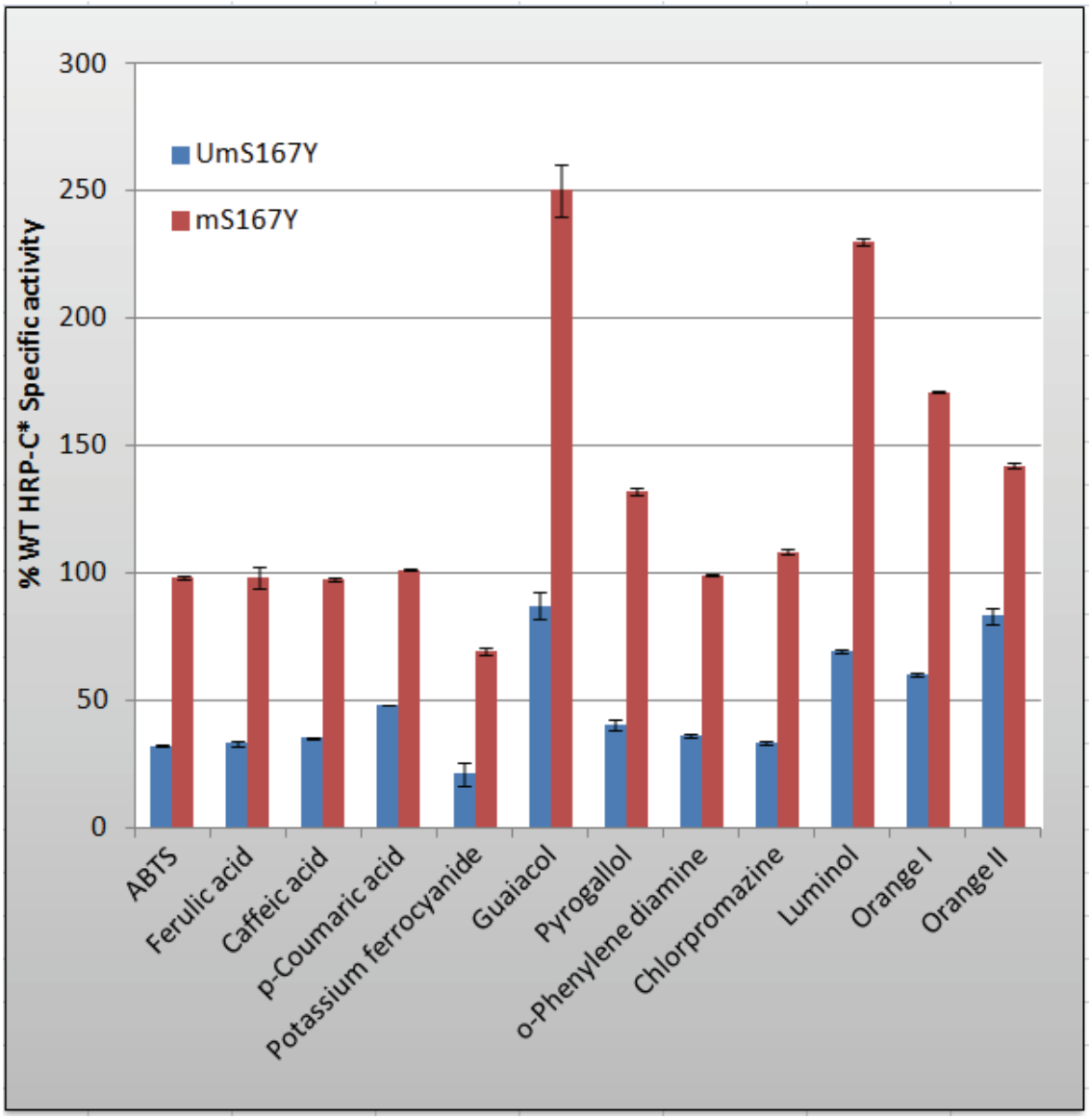

Figure 5.4: Histogram of specific activities for the oxidation of a panel of peroxidase substrates by Um[S167Y] and m[S167Y] HRP-C* expressed as a percentage of the values obtained for WT HRP-C*. Data obtained from Table 5.2.

5.5 Steady-state kinetics of Luminol oxidation:

The oxidation reaction of 5-amino-2,3-dyhydrophthalazine-1,4-dione (Luminol), mediated by HRP-C, to yield 3-aminophthalate and light is called chemiluminescence and is considered one of the many important applications of HRP (Thorpe and Kricka, 1986; Veitch and Smith, 2001). This reaction produces light and has been used frequently in clinical applications, for immunoassays, metabolic pathway monitoring, detection of inorganic and organic compounds, determination of enzymatic reaction and detection of blood at crime scenes (Briheim *et al.*, 1984; Radi *et al.*, 1993; Lundqvist and Dahlgren, 1996).

The chemiluminescence assay involves the normal catalytic cycle of HRP-C with both its intermediary complexes, Compound I and Compound II, being able to rapidly remove an electron from luminol to form a luminol cation radical. Then, the luminol radicals enter a complex chemical pathway to produce diazoquinione, luminol endoperoxide and finally, the light emitting excited state of a 3-aminophthalate ion and nitrogen gas. In the final step of the reaction the excited 3-aminophthalate ion yields a 3-aminophthalate dianion and light (Bhandari *et al.*, 2010).

One disadvantage of the conventional chemiluminescence assay with HRP-C is the inefficiency of the luminescence reaction due to its low quantum yield (Tanaka *et al.*, 1999). Therefore, and in order to detect and measure smaller amounts of analytes in clinical assays, many efforts have been made to enhance the luminol activity of HRP-C. It has been found that the sensitivity of the luminol assay can be increased by addition of enhancers, such as 4-Iodophenol and 4-Iodophenylboronic acid but this can be costly (Kricka *et al.*, 1988; Kricka *et al.*, 1996). An attempt has been made to enhance the

direct luminol oxidation activity of HRP, by mimicking in HRP-C a possible binding site for luminol from *Arthromyces ramosus* peroxidase (ARP); the results showed a significant increase in enzyme activity towards luminol, with some HRP variants prepared having 500-fold higher activity for luminol than the wild-type enzyme (Tanaka *et al.*, 1999).

As mentioned before, from the specific activity screening against a panel of substrates, the luminol oxidation results showed that there was an interesting increase in activity of the S167W and mS167Y mutants relative to the wild-type enzyme. Therefore, apparent steady-state parameters were determined for these two mutants this time using luminol as reducing substrate, instead of ABTS, and conditions as described in section 2.6.3.

The initial rates obtained, expressed as turnover numbers, were plotted against luminol concentration and were fitted to the Michaelis-Menten equation using SigmaPlot software (Figure 5.5). Apparent kinetics parameters obtained (K_m and k_{cat}) for WT HRP-C*, S167W, UmS167Y and mS167Y are compiled in Table 5.3. The efficiency constant (k_{cat}/K_m) for each enzyme was calculated and is also included in this table. In order to facilitate visual comparison between WT HRP-C*, and the S167W, UmS167Y and mS167Y mutants, the efficiency constants are illustrated graphically in Figure 5.6.

The results obtained for the S167W mutant show a significantly decreased apparent K_m value by a factor of 7-fold and a k_{cat} value decreased by a factor of 1.5-fold compared to the wild-type enzyme. These results lead to a clear increase in the efficiency of this enzyme variant towards luminol, with the k_{cat}/K_m for luminol being 5-fold higher than that of WT HRP-C* (Figure 5.6).

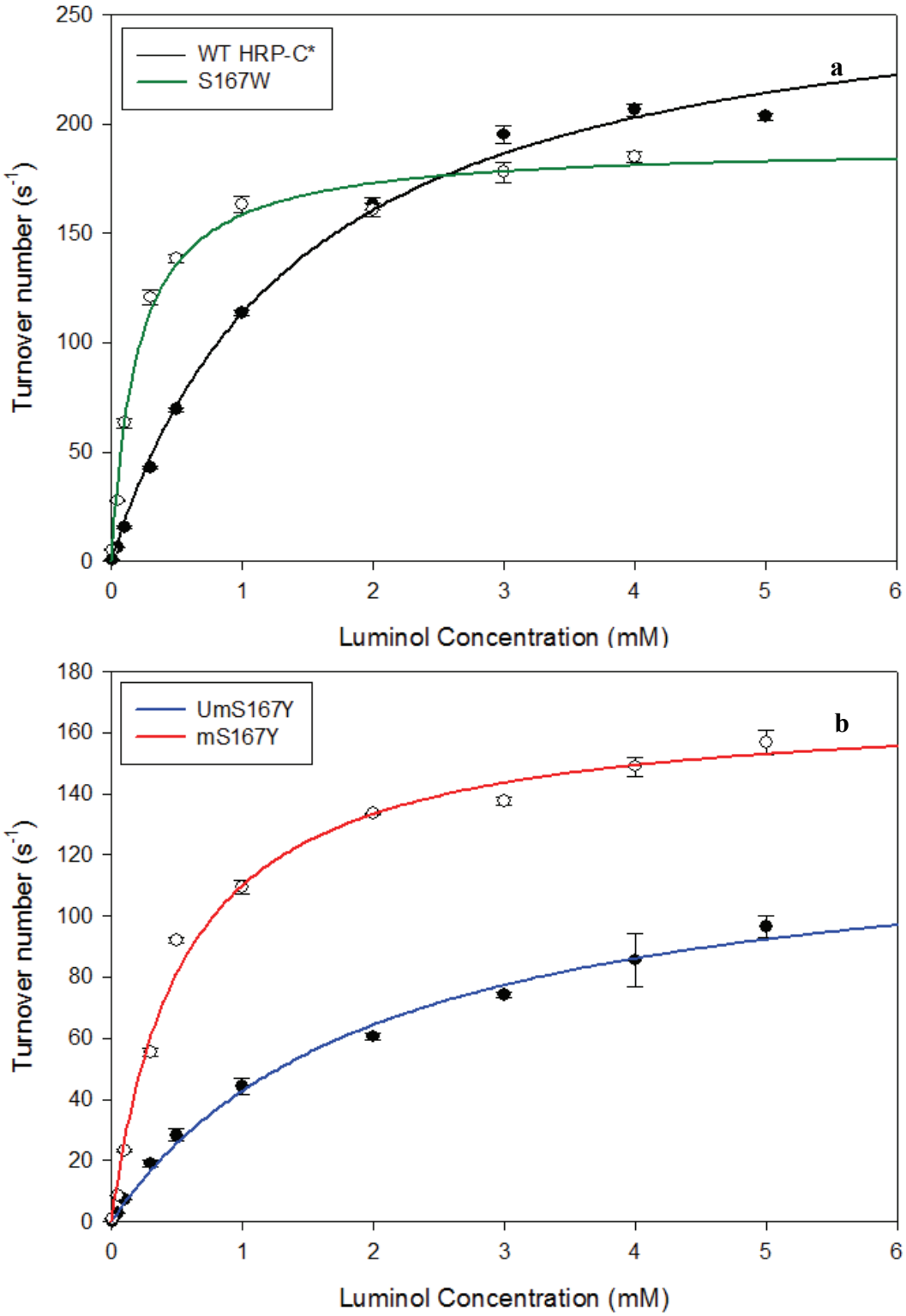

Figure 5.5: Plots depicting the dependence of initial rates of luminol oxidation on luminol concentration during steady-state HRP-C assays. The data were fitted to the Michaelis-Menten equation and the values determined are given in Table 5.3. (a) WT HRP-C* and S167W mutant, and (b) Um[S167Y] and m[S167Y] HRP-C*. The assays were carried out in phosphate-citrate buffer, pH 5.0, using 20 nM of enzyme, 1 mM H_2O_2 and varying concentrations of luminol in a final volume of 1 ml at 25 ^{o}C.

Table 5.3: Steady-state parameters of the oxidation of luminol by WT HRP-C* and the new S167 mutants. Data obtained from Figure 5.5.

Enzyme	K_m (μM)	k_{cat} (s^{-1})	k_{cat}/K_m ($M^{-1}s^{-1}$)
WT HRP-C*	1425 ± 93	275 ± 10	1.93 x 10^5
S167W	199 ± 24	190 ± 9	9.56 x 10^5
UmS167Y	2030 ± 163	130 ± 7	0.65 x 10^5
mS167Y	541 ± 49	170 ± 5	3.14 x 10^5

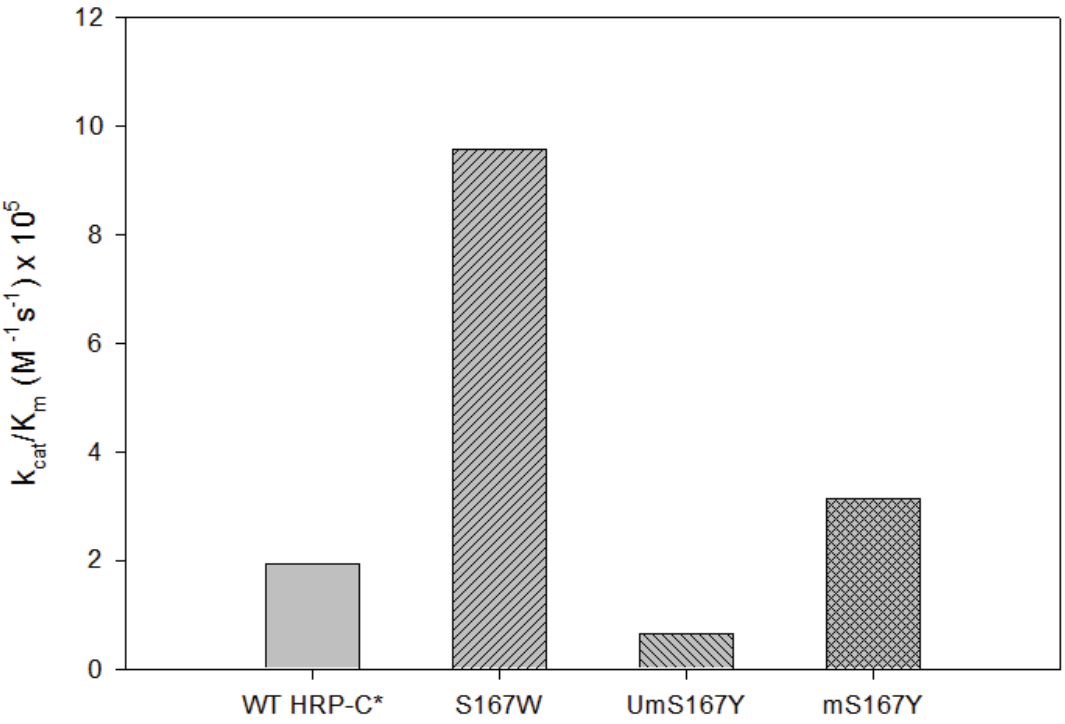

Figure 5.6: Histogram illustrating the effects of mutations at position 167 of HRP-C* on k_{cat}/K_m values for the oxidation of luminol. Data obtained from Figure 5.5.

The UmS167Y variant displays very different behaviour to that of the S167W variant. It has an increased apparent K_m value of 2030 μM compared to 1425 μM for WT HRP-C*, accompanied by a 2-fold decrease in apparent k_{cat} value. The efficiency constant for this mutant is therefore decreased by a factor of 3-fold compared to that of wild-type enzyme. However, the results for the mS167Y enzyme are again different to those of Um[S167Y] HRP-C*. For this linked mutant the decrease is 2.5-fold in K_m and 1.6-fold in k_{cat} compared to values for WT HRP-C*, leading to an overall 1.6-fold higher catalytic efficiency (k_{cat}/K_m) than the wild-type enzyme and 5-fold higher than the Um[S167Y] HRP-C*. The increase in catalytic effectiveness for both S167W and mS167Y enzymes is achieved by a decrease in the apparent K_m value, which reflects a higher binding affinity for luminol.

5.6 Conclusion:

The changes in the kinetic parameters of the S167Y and S167W variants, relative to WT HRP-C*, are interesting. It can be concluded that the replacement of Ser167 by either a Tyr or Trp, leads to an indirect effect on the active and substrate binding sites of HRP-C and as a result modulates the activity of the enzyme towards certain substrates. The nature of this modulation seems to be substrate specific to some extent. In general, the introduction of a Tyr or Trp in position 167, leads to an enzyme with lower activity towards most substrates. However, surprisingly, and in contrast to other substrates, there is a significant enhancement in the oxidation activity of the S167W variant towards luminol leading to an enzyme efficiency approximately 5-fold that of WT HRP-C*. For the S167Y mutant formation of the haem-protein covalent linkage leads to an enzyme that has much more WT-like levels of activity against all substrates tested. This is very different to that previously found for the S167M mutant (Cali, 2008), where the

formation of the sulfonium linkage between the heam and protein leads to a further decrease in enzyme activity by approximately 12-16 fold. This is presumably due to an increase in the perturbation to the HRP-C* active site for m[S167M] HRP-C* but for m[S167Y] HRP-C* the linkage in some way compensates for the perturbations already caused by the mutation itself. A further discussion of the steady-state kinetic results and the functional changes accompanying the mutations of the HRP-C will be presented in chapter 7.

Chapter Six:

Pre steady-state kinetic characterisation of HRP S167 variants and effect(s) of haem-protein covalent linkage

6.1 Introduction:

The term pre steady-state kinetics is usually applied to the observation of rates of reaction that occur in very short time intervals (usually fractions of a second) and at very low product concentrations. In enzyme kinetics, this period covers the time from the enzyme encountering its target substrate, up to the point that the system reaches an equilibrium state. Figure 6.1 illustrates the changes in concentration observed for the reaction participants, with time, during the pre steady-state and steady-state (Berg *et al.*, 2002).

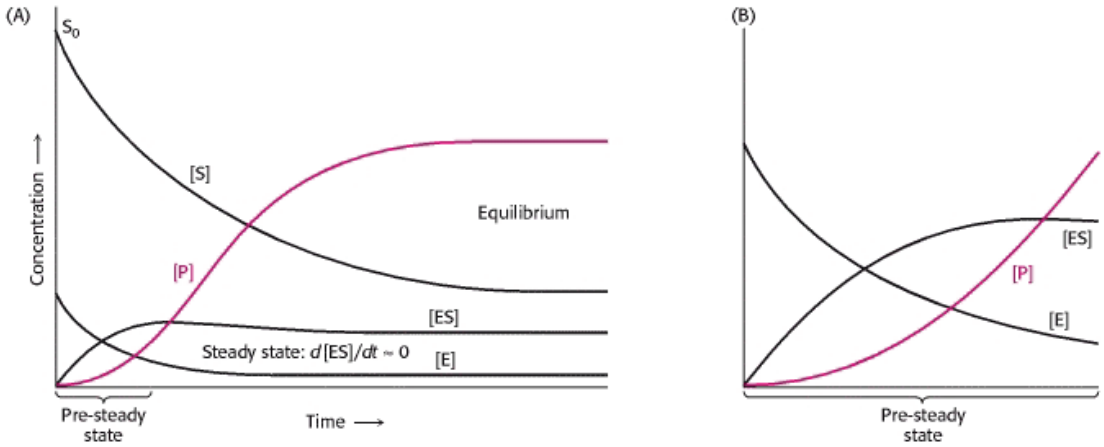

Figure 6.1: The concentration changes in reaction participants in an enzyme-catalyzed reaction with time. Concentration changes under (A) steady-state conditions, and (B) pre steady-state conditions. This figure is adopted from Berg *et al.,* 2002.

The figure demonstrates that, from the beginning of the reaction, the concentration of Enzyme-Substrate complex (ES) rises from zero to its steady-state value. The steady-state approximation is therefore not valid during this early stage and for this reason it is called the pre steady-state or transient-phase. The pre steady-state of an enzyme-catalyzed reaction usually occupies a very brief period of time (milliseconds), therefore special rapid techniques have to be used for investigation. One of the most frequently used techniques is stopped-flow, in which a spectroscopic signal is observed during the pre steady-state stage (Wang, 2007). Pre steady-state kinetic experiments with peroxidases are often carried out using the stopped-flow apparatus, as it permits the direct monitoring of the kinetic behaviour of the resting enzyme and intermediates Compounds I and II (Dunford, 1999h). Stopped-flow spectroscopy was developed by Britton Chance in the 1950's (Chance, 1952) and allows the measurement of pre steady-state rate constants for the formation of enzyme intermediates, which is not possible using steady-state methods.

As mentioned in Chapter 5, the rate of an enzyme reaction is the quantity of reactants that disappear, or quantity of products that appear, in a specified unit of time. It is directly related to the concentration of reactants by a proportionality constant, called the rate constant (k). The number of reactant concentration terms which need to be considered when determining the rate of reaction is called the order of reaction (Berg *et al.*, 2002). The pre steady-state reactions between the catalytic species of HRP and substrates are first-order with respect to each reactant, and second-order overall. Therefore, the rate of these reactions is dependent on the concentration of both the enzyme species and the substrate used. In general, the rate of such a second-order reaction is described by the following equation.

$$V = k[E][S] \qquad (equation\ 6.1)$$

where k is the second-order rate constant governing the reaction, [E] the concentration of enzyme and [S] the concentration of the substrate (Atkins and Paula, 2009). The rate constant (k) has the unit $M^{1-n}\ s^{-1}$, where n is the order of the reaction. A first-order rate constant has unit s^{-1} and second-order rate constant has the unit $M^{-1}\ s^{-1}$ (Berg *et al.*, 2002).

Direct kinetic measurement of second-order reactions with two reactants can be problematic and less precise if the concentrations of the two reactants are followed simultaneously, or if one is measured and the other calculated as a difference. Therefore, in order to minimise the complexities arising from dealing with two reactants, the reactions are forced to operate under pseudo first-order conditions (Job and Dunford, 1976). Maintaining a small concentration of the enzyme, reacting with a large excess of substrate (at least 5-fold greater than enzyme concentration), will allow the rate of the reaction to be first-order, because the relatively small changes in substrate concentration during the reaction will not contribute to the total order, as it is in excess and can be viewed as a constant (Berg *et al.*, 2002). These reaction conditions are called pseudo first-order and can be described by the following equation:

$$V = k_{obs}[E] \qquad (equation\ 6.2)$$

where: k_{obs} is the pseudo first-order rate constant, that has the unit s^{-1} (Job and Dunford, 1976).

Valuable information can be obtained when the pseudo first-order rate constant is measured directly as a function of substrate concentration (Dunford, 1999h), including an apparent second-order rate constant (k_{app}) for a given reaction. A plot of k_{obs} against substrate concentration gives a linear relationship, and from equation 6.3 the slope of the plot gives the most accurate determination of k_{app} in units of M^{-1} s^{-1} (Dunford, 1993). A linear plot passing through the origin indicates that, in practical terms, the reaction is irreversible (Dunford, 1999h).

$$k_{app} = \frac{k_{obs}}{[S]} \qquad (equation\ 6.3)$$

In the previous chapter, steady-state data showed that the kinetics of luminol oxidation were different for cross-linked [S167Y] HRP-C* compared to unlinked. Therefore, in order to determine the rate constants k_1, k_2 and k_3 directly (see section 1.5.4) for the reaction of HRP-C with luminol, the pre steady-state kinetic experiments described in this chapter were carried out under pseudo first-order conditions, maintaining the substrate concentrations at 5-10 times greater than the enzyme. Linear plots obtained from the observed pseudo first-order rate constants against corresponding substrate concentration confirmed that the respective partial reactions were really second-order overall with respect to the substrate used and the enzyme.

6.2 Stopped-flow rapid scan photodiode array:

As mentioned before in section 4.2, the main feature of the resting state spectrum of HRP-C is the presence of a Soret band at 403 nm, with two other bands at 642 nm (CTI) and 498 nm (CTII) related to charge transitions (Dunford, 1999f). Upon exposure to

H_2O_2, the resting enzyme is rapidly converted to the Compound I intermediate, concomitant with a decrease in the molar absorptivity of the Soret peak by a factor of approximately two (Dunford, 1982; Dunford, 1999i). After this, over a period of time, the spectrum of the second intermediate Compound II is observed as the result of a slow auto-reduction of Compound I. A comparison of the resting enzyme spectrum with the typical spectrum of Compound II shows that the maximum peak in the Soret region is red shifted from 403 nm to 420 nm and the peak intensity is increased slightly. A double peak in the visible region of the spectrum, with maxima at 527 nm and 554 nm, is also considered a characteristic feature of Compound II (Dunford, 1999i). In fact, Compound II is more stable than Compound I, and hence is easier to characterize.

In order to have an overview on the nature of the changes that occur in the UV/Vis spectrum during the first part of the catalytic cycle of the S167W and S167Y HRP-C* variants upon reaction with hydrogen peroxide, rapid scan photodiode array absorption spectrometry was used, in the presence of 10 equivalents of H_2O_2 and the absence of reducing substrate, using a stopped-flow spectrophotometer equipped with an attached diode-array detector (section 2.12.2). 500 data points were collected on a logarithmic scale over a total time of 1000 s. The results are presented in Figures 6.2a, 6.3a, 6.4a and 6.5a. These figures show selected spectra obtained from 64 milliseconds to 992 seconds for WT HRP-C*, and S167W, UmS167Y (unlinked enzyme) and mS167Y (linked enzyme) variants, respectively. In addition, data analysis was performed using the Pro-K Global Analysis Program (Applied Photo-Physics), to fit the time-dependent spectra collected and obtain computer modelled enzymatic species. Figures 6.2b, 6.3b, 6.4b and 6.5b show the obtained intermediate species spectra from computer modelling

of the original data, and there is an inset in each figure indicating the relative abundance of each species as a function of time.

The predominant species of WT HRP-C* (Figure 6.2b) agree well with those reported previously (Dunford, 1982), with the only slight difference being that the Compound II Soret peak appears less intense than that of the resting state; this is attributed to not fully converting the enzyme to Compound II. For all four enzyme samples studied, it was found that the initial decrease in the Soret absorption of the resting state on conversion to Compound I was almost the same, i.e. approximately a factor of two. The original spectra of Um[S167Y] and m[S167Y] HRP-C* (Figures 6.4a and 6.5a) show clearly that the formation of Compound I occurs more rapidly than for WT HRP-C* (Figure 6.2a). However, and at the same time, the relative abundance of the enzyme species shows that the Compound I is of UmS167Y and mS167Y are also unstable compared to WT Compound I and quickly convert to Compound II. Computer modelling simulation of the raw data confirms this rapid formation and reduction of Compound I, where a three species model (A $\longrightarrow$ B $\longrightarrow$ C) for both UmS167Y and mS167Y (Figures 6.4b and 6.5b) could not detect the resting state of the enzyme that is clearly indicated for wild-type enzyme (Figure 6.2b). The first species found (A) is approximately 90% Compound I, the second species (B) seem to be a 50/50 mixture of Compounds I and II, and the third species (C) represents Compound II.

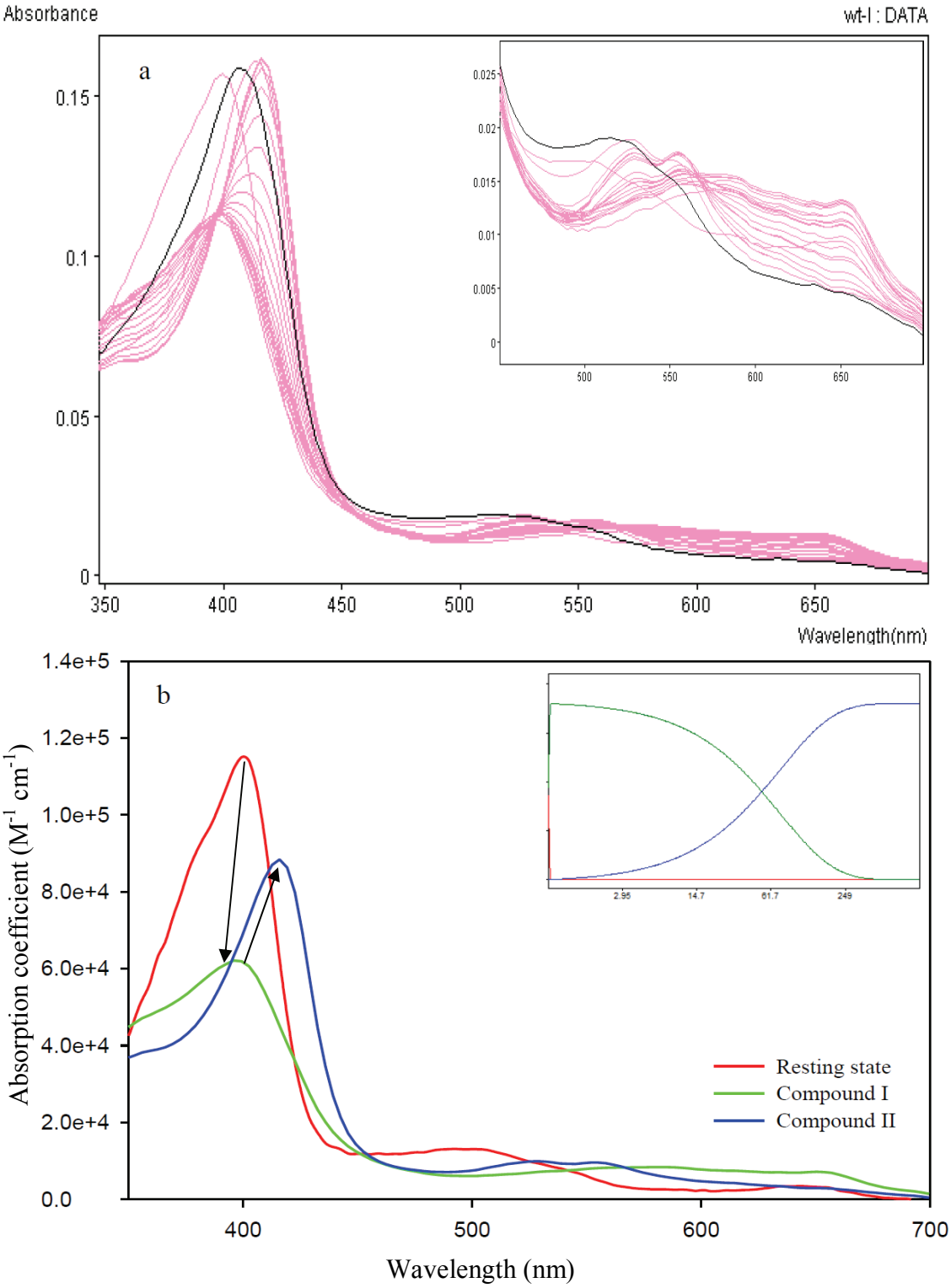

Figure 6.2: Rapid scan absorption spectra of WT HRP-C* reaction with H_2O_2. 3.6 µM of enzyme were treated with 40 µM of H_2O_2 in 10 mM sodium phosphate buffer, pH 7.0, at 25 ^{o}C. (a) Rapid scan absorption spectra from 64 ms to 992 s. (b) Enzyme intermediate species spectra obtained from computer simulation of the raw data by global analysis (APP Pro-K) software, the figure in the top right represents the relative abundance of each one of the enzyme intermediates as a function of time.

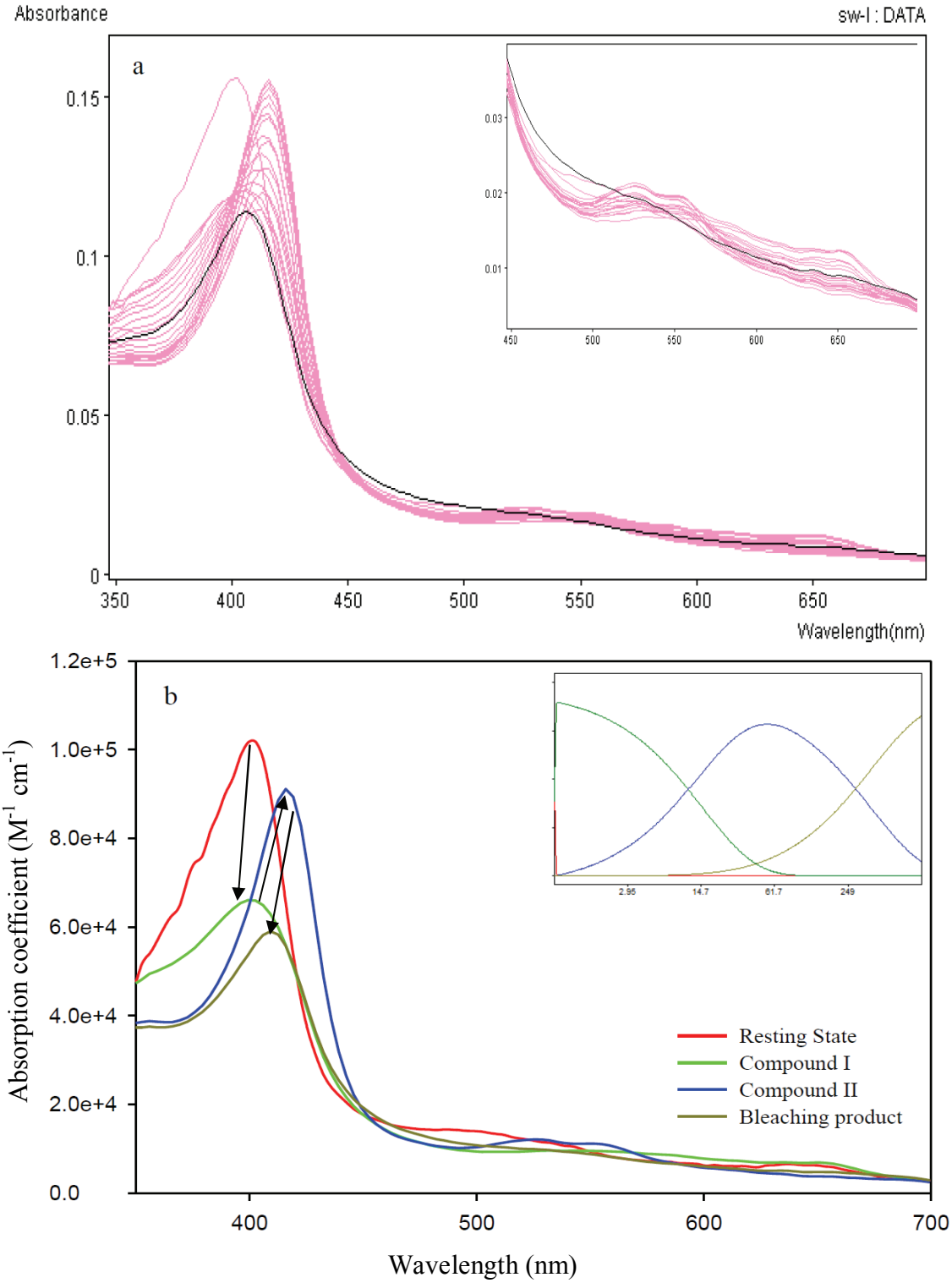

Figure 6.3: Rapid scan absorption spectra of [S167W] HRP-C* reaction with H_2O_2. 4 µM of enzyme were treated with 40 µM of H_2O_2 in 10 mM sodium phosphate buffer, pH 7.0, at 25 °C. (a) Rapid scan absorption spectra from 64 ms to 992 s. (b) Enzyme intermediate species spectra obtained from computer simulation of the raw data by global analysis (APP Pro-K) software, the figure in the top right represents the relative abundance of each one of the enzyme intermediates as a function of time.

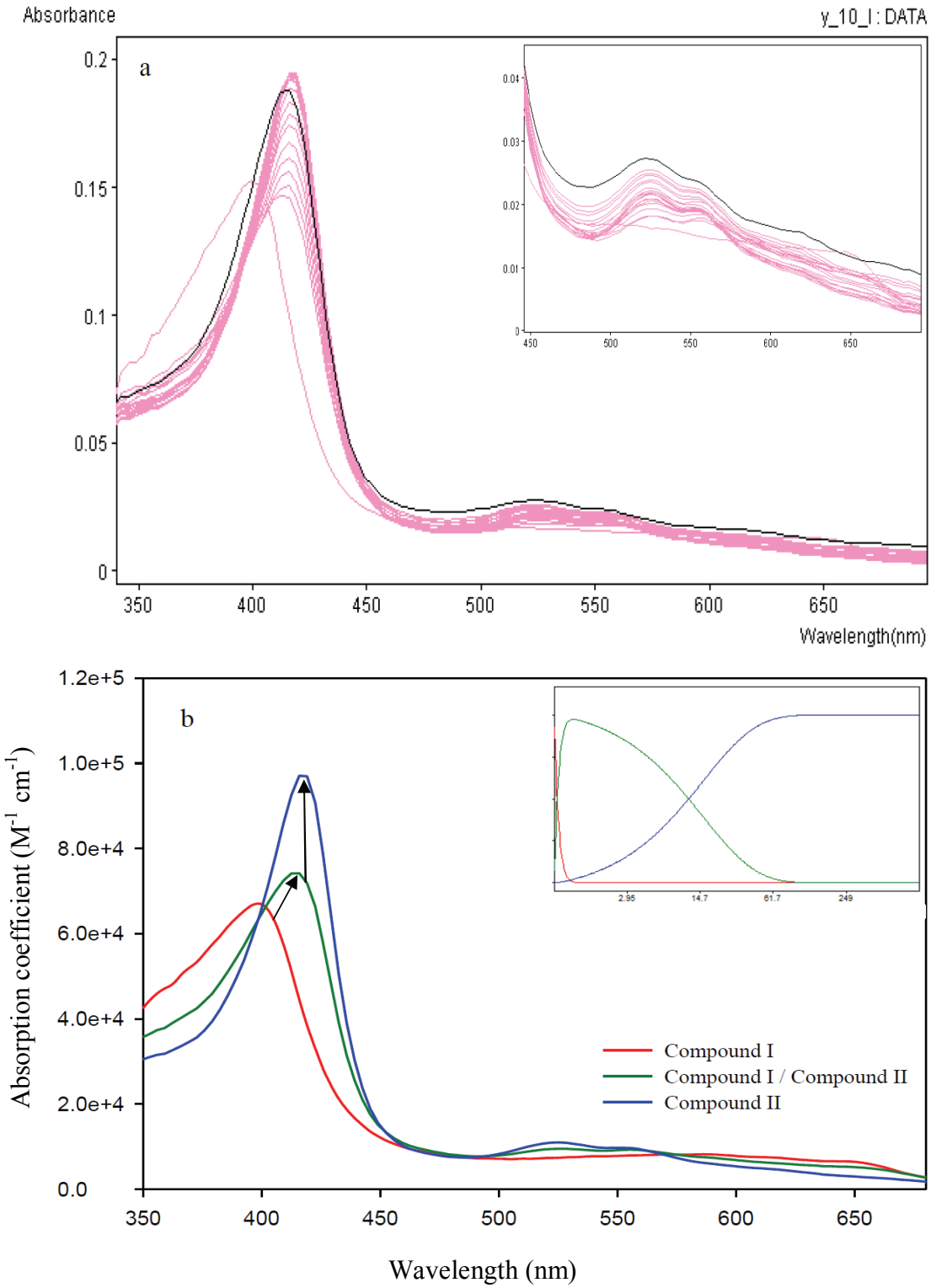

Figure 6.4: Rapid scan absorption spectra of Um[S167Y] HRP-C* reaction with H_2O_2. 4 µM of enzyme were treated with 40 µM of H_2O_2 in 10 mM sodium phosphate buffer, pH 7.0, at 25 ^{o}C. (a) Rapid scan absorption spectra from 64 ms to 992 s. (b) Enzyme intermediate species spectra obtained from computer simulation of the raw data by global analysis (APP Pro-K) software, the figure in the top right represents the relative abundance of each one of the enzyme intermediates as a function of time.

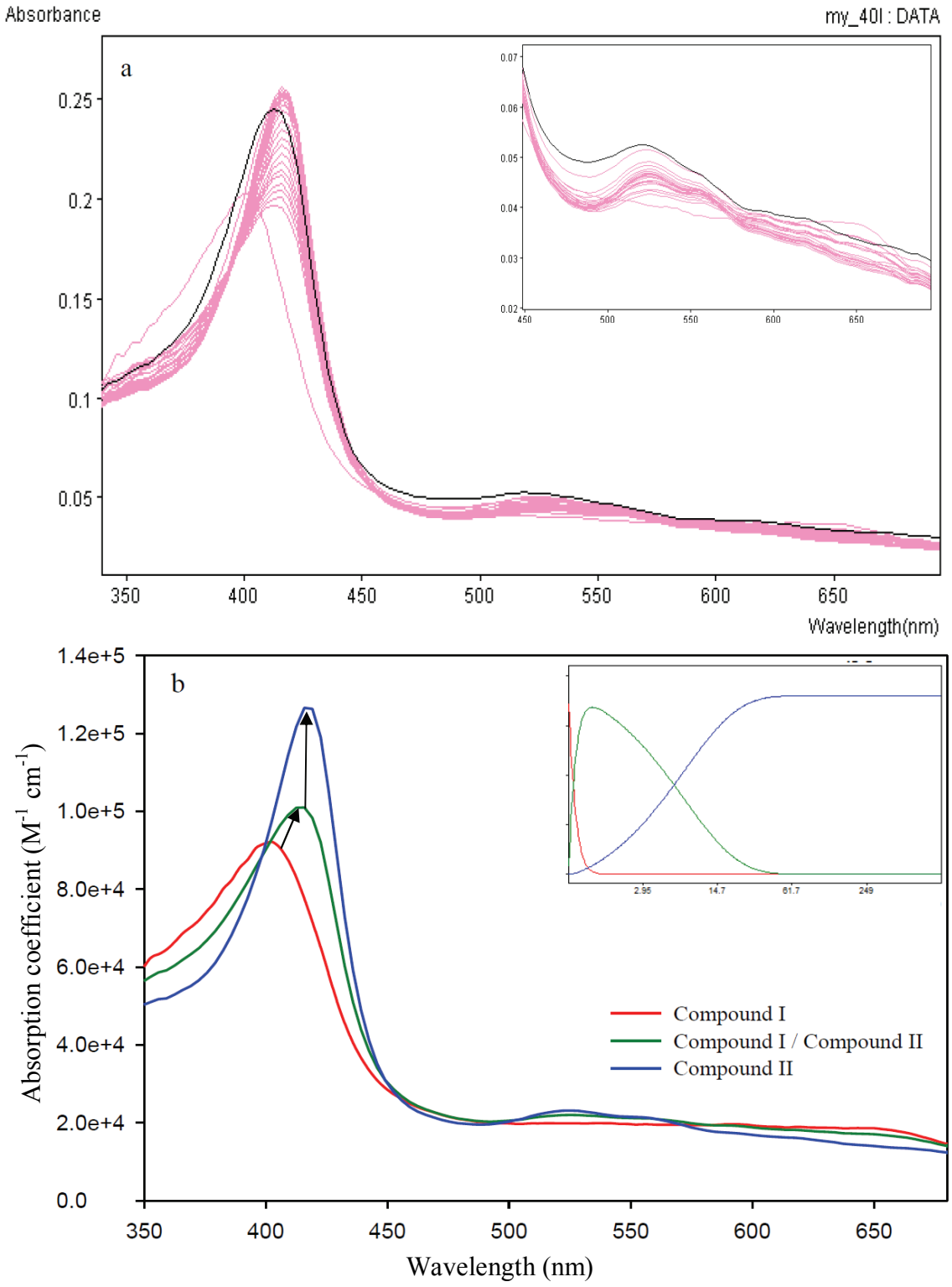

Figure 6.5: Rapid scan absorption spectra of m[S167Y] HRP-C* reaction with H_2O_2. 4 µM of enzyme were treated with 40 µM of H_2O_2 in 10 mM sodium phosphate buffer, pH 7.0, at 25 °C. (a) Rapid scan absorption spectra from 64 ms to 992 s. (b) Enzyme intermediate species spectra obtained for computer simulation of the raw data by global analysis (APP Pro-K) software, the figure in the top right represents the relative abundance of each one of the enzyme intermediates as a function of time.

Analysis of the rapid scan absorption spectra of the S167W mutant shows only a good fit to the experimental data when using a model of four species (A ⟶ B ⟶ C ⟶ D) instead of the three species model of the WT enzyme, where A represents the resting state, B Compound I, C Compound II and D a new form of the enzyme. The rapid scan spectra show clearly another decrease in the Soret peak intensity (Figure 6.3), beginning 150 s after the start of the reaction, where instead of reduction of Compound II back to the resting state enzyme (the normal process that occurs in the wild-type enzyme) it appears to suffer from a bleaching process. This phenomenon gives an indication that destruction, i.e. methylene breakage, may occur to the haem because of increased sensitivity of this mutant to H_2O_2 in the absence of reducing substrate. More chemical analyses, such as NMR analysis, need to take place in order to prove this, although a similar possibility was seen in chapter 4 results from HPLC analysis.

6.3 Pre steady-state enzyme kinetics:

6.3.1 Determination of the rate constant (k_1) for the reaction of resting enzyme with H_2O_2:

The reaction cycle of HRP-C starts with the formation of the first intermediate, Compound I, by reaction of resting enzyme with H_2O_2 (equation 6.4). In this reaction the ferric haem group undergoes a two equivalent oxidation to an oxyferryl, Fe^{IV}, porphyrin π-cation radical state (Hasinoff and Dunford, 1970), with a second-order rate constant (k_1) equal to 1.6×10^7 M^{-1} s^{-1} for the wild-type enzyme (Shiro *et al.*, 1986).

$$E + H_2O_2 \xrightarrow{k_1} \text{Compound I} + H_2O \qquad \text{(equation 6.4)}$$

In order to examine the effects which may be caused by the mutations introduced into HRP-C* at position 167, on the rate of formation of Compound I, the second-order rate

constant (k_1) for the reaction of WT enzyme and the new variants with H_2O_2 was determined under pseudo first-order conditions at pH 7.0 (section 2.12.3). Upon mixing of the enzyme sample and a known concentration of H_2O_2 in the stopped-flow system, a decrease in absorption due to the formation of Compound I was monitored at 395 nm. When measuring k_1 for HRP-C, the wavelength of 395 nm is generally used as this is the isosbestic wavelength between Compound I and Compound II (Smith *et al.*, 1992). As the Compound I species is forming it is also unstable and will be auto-reduced slowly to Compound II even without the addition of any reductants (Dunford and Stillman, 1976). However, interference to the data caused by this reduction can be avoided, as there is no change in the A_{395} during the reduction of Compound I to Compound II.

The pseudo first-order rate constants (k_{obs}) at a number of H_2O_2 concentrations were determined by fitting the traces obtained, i.e. a decrease in A_{395} as a function of time, to a single exponential decay function (Figures 6.6 - 6.9). In order to then calculate the value of the second-order rate constant for each enzyme sample used, the obtained values for k_{obs} were plotted against the corresponding hydrogen peroxide concentrations using a weighted least square linear regression analysis (Figures 6.10 and 6.11). The slope of the resultant graph in each case represents the k_1 value (see equation 6.3) for the relevant enzyme, values obtained presented in Table 6.1.

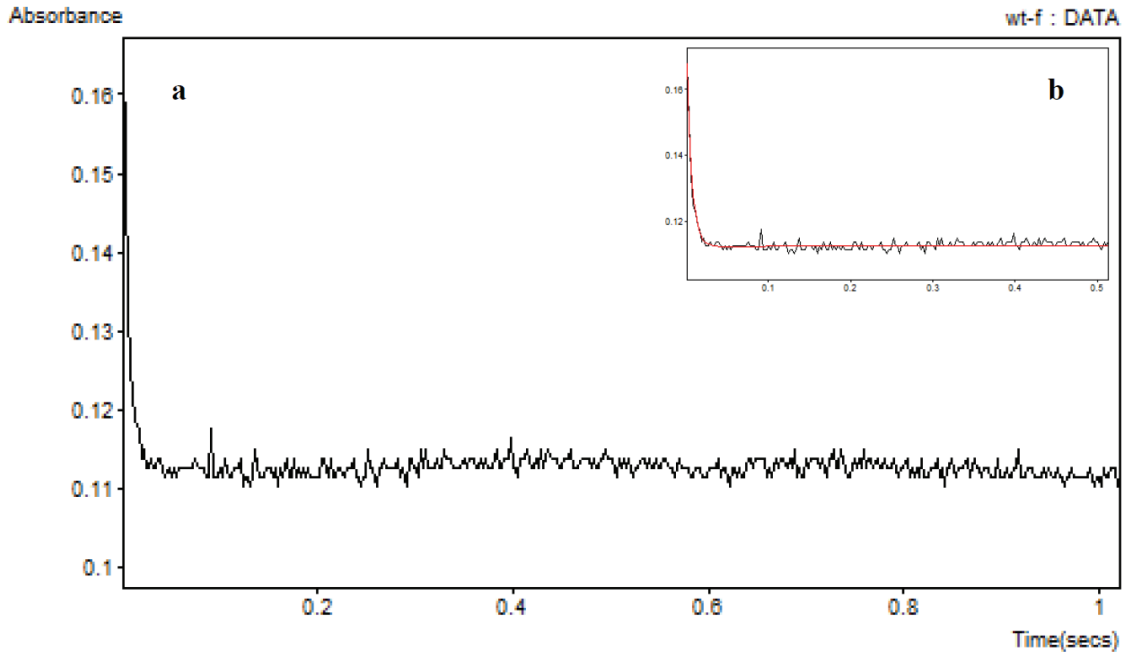

Figure 6.6: Stopped-flow trace of Compound I formation of WT HRP-C*. The trace shows the change in A_{395} for one second after 3.6 µM of enzyme was mixed with 40 µM of H_2O_2 in 10 mM sodium phosphate buffer, pH 7.0, at 25 ^{o}C. (a) original trace, (b) single exponential fit (in red) of the A_{395} versus time progress curve.

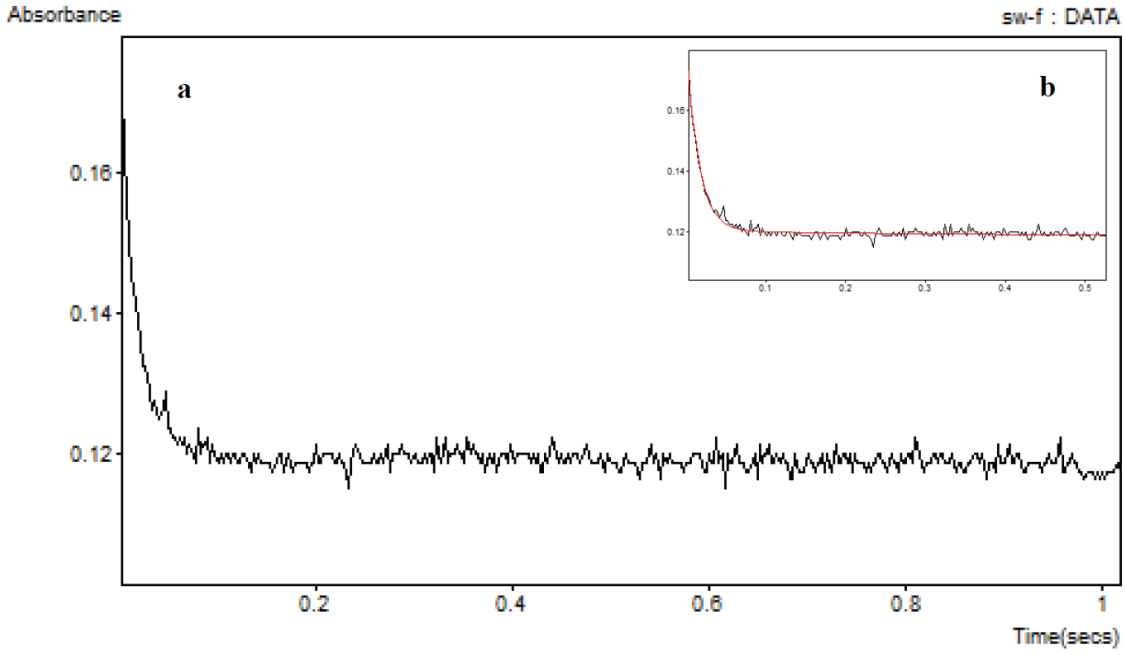

Figure 6.7: Stopped-flow trace of Compound I formation of [S167W] HRP-C*. The trace shows the change in A_{395} for one second after 4 µM of enzyme was mixed with 40 µM of H_2O_2 in 10 mM sodium phosphate buffer, pH 7.0, at 25 ^{o}C. (a) original trace, (b) single exponential fit (in red) of the A_{395} versus time progress curve.

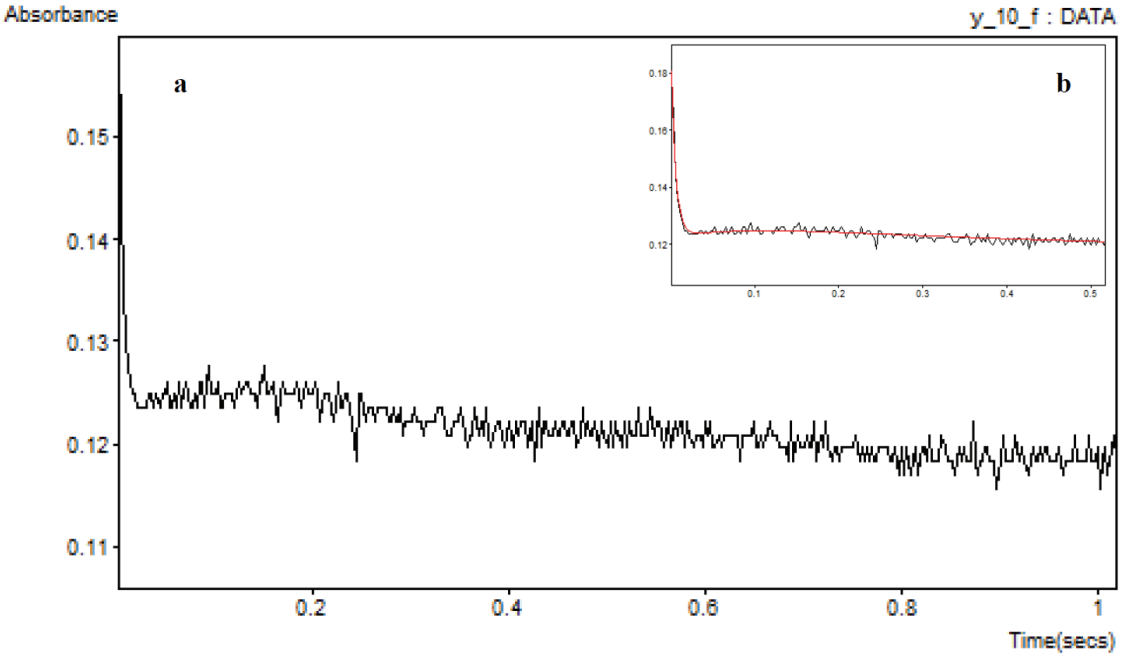

Figure 6.8: Stopped-flow trace of Compound I formation of Um[S167Y] HRP-C*. The trace shows the change in A_{395} for one second after 4 µM of enzyme was mixed with 40 µM of H_2O_2 in 10 mM sodium phosphate buffer, pH 7.0, at 25 ^{o}C. (a) original trace, (b) triple exponential fit of the trace, but that this likely reflected non-specific absorption drift over the longer timescale, the values used in Figures 6.11 come from a single exponential fit of the data over the first 0.2 seconds of the reaction.

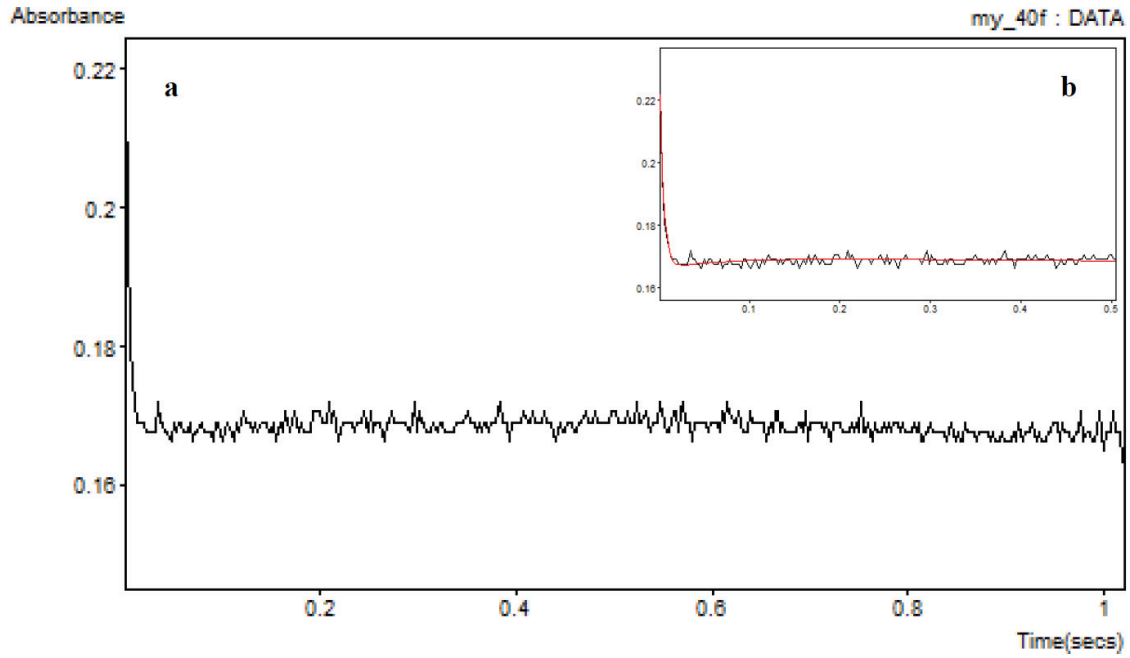

Figure 6.9: Stopped-flow trace of Compound I formation of m[S167Y] HRP-C*. The trace shows the change in A_{395} for one second after 4 µM of enzyme was mixed with 40 µM of H_2O_2 in 10 mM sodium phosphate buffer, pH 7.0, at 25 ^{o}C. (a) original trace, (b) single exponential fit (in red) of the A_{395} versus time progress curve.

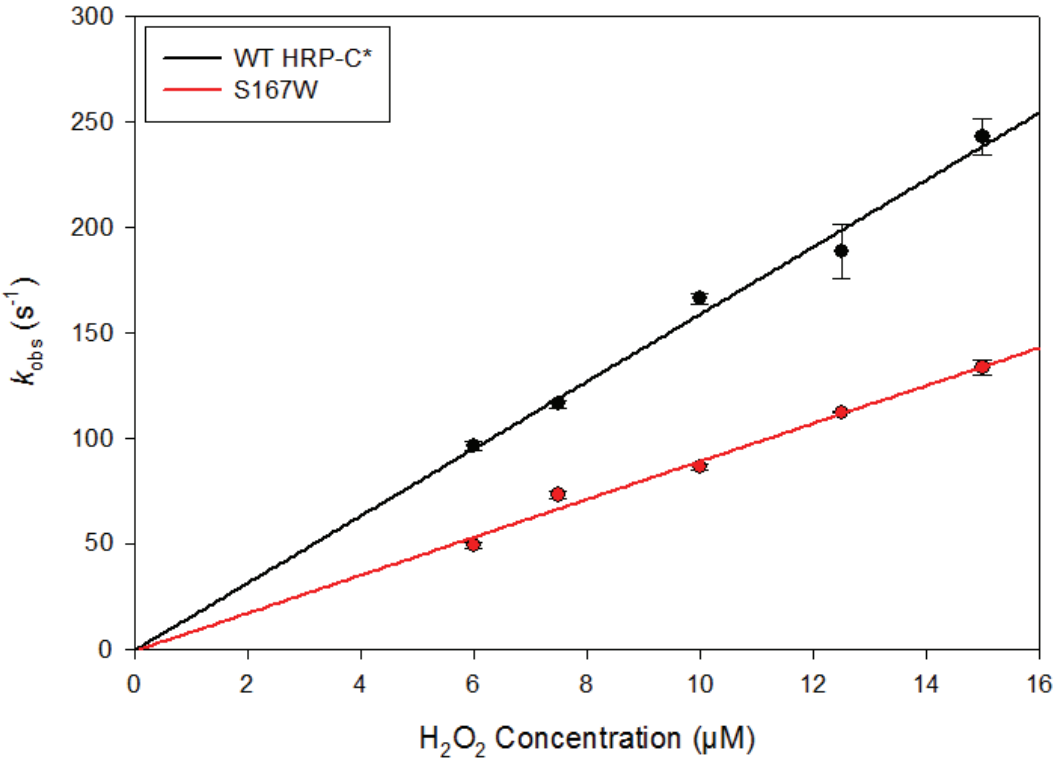

Figure 6.10: Pseudo first-order rate constant plots for Compound I formation for WT HRP-C* and [S167W] HRP-C*.

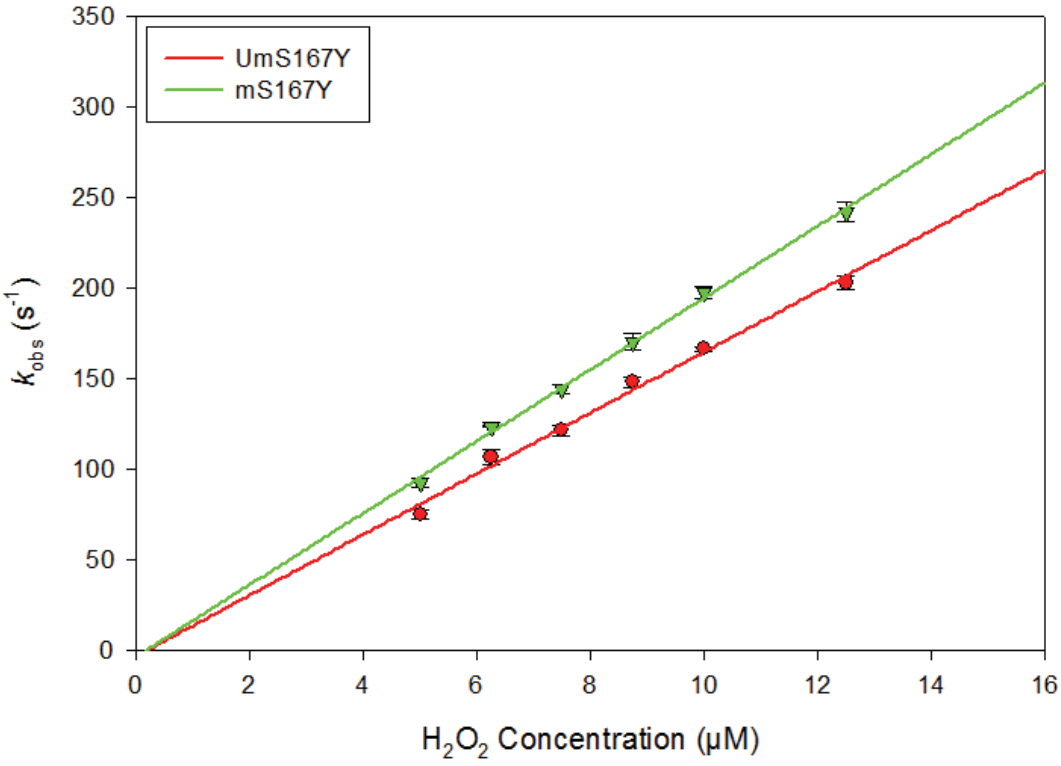

Figure 6.11: Pseudo first-order rate constant plots for compound I formation for m[S167Y] and Um[S167Y] HRP-C*.

As mentioned before, the linear nature of the pseudo first-order rate constants versus H_2O_2 concentration plot passing through the origin (Figure 6.10), indicates that the formation of Compound I is an essentially irreversible process for wild type HRP-C* (Dunford, 1999h). The similar linear behaviour, and going through the origin, of the plots for the mutants, Figures 6.10 and 6.11, shows that the introduction of a tryptophan or tyrosine residue at position 167, instead of serine, also does not affect the mechanism of Compound I formation, i.e. the formation of Compound I has remained much faster than the rate of dissociation of the hydroperoxide complex (see scheme 1.3).

Table 6.1: Second-order rate constants (k_1) for Compound I formation by WT, Um[S167Y], m[S167Y] and [S167W] HRP-C*. All assays were carried out in 10 mM Na-Phosphate buffer, pH 7.0, at 25 ^{o}C. The k_1 values were determined from the slopes of regression line plots of the pseudo first-order rate constants against hydrogen peroxide concentration. Data analysis and processing were carried out using Sigmaplot software.

Enzyme	k_1 ($M^{-1} s^{-1}$)
WT HRP-C*	$1.59 \pm 0.10 \times 10^7$
S167W	$9.0 \pm 0.07 \times 10^6$
UmS167Y	$1.84 \pm 0.20 \times 10^7$
mS167Y	$2.12 \pm 0.10 \times 10^7$

The k_1 value obtained for WT HRP-C* is $1.59 \pm 0.10 \times 10^7$ M^{-1} s^{-1} and is in very good agreement with the published value, which is 1.64×10^7 M^{-1} s^{-1} (Smith *et al.*, 1992). The results show a small but significant decrease in the k_1 value of the S167W mutant compared to wild type enzyme, its value is reduced to almost half the value of WT HRP-C*. In the case of the UmS167Y mutant, a small but significant increase by a factor of 1.2-1.3 fold in the second-order rate constant for the formation of Compound I is observed relative to the wild-type enzyme. The production of the haem-protein covalent bond in this mutant (mS167Y) can be seen to have little effect on this value.

Examination of the influence of haem pocket residues on the mechanism of Compound I formation in HRP-C, and their relative contribution to the k_1 rate constant, has been a major focus of site directed mutagenesis studies. A study has been presented by Veitch and Smith that summarizes the haem pocket mutations of HRP-C on the rate of formation of Compound I (Veitch and Smith, 2001); this study shows the relative contributions of the distal and proximal haem pocket residues Arg38, Phe41, His42, Glu64, Asn70 and His170 of HRP-C.

For enzymes engineered to be able to introduce a haem-protein covalent linkage, the k_1 rate constant of Compound I formation for the unlinked [F41E] HRP-C* variant showed a value 100 times lower than that of the wild-type enzyme, presumably a result of either an ionic or steric interaction between His42 and Glu41. However, interestingly, after treatment with hydrogen peroxide and formation of the covalent bond between the glutamic acid and the 3-methyl group of the haem, this mutant exhibited a rate of Compound I formation, equivalent to that of wild-type enzyme (Colas and Ortiz de Montellano, 2004). It has also been reported that, neither the S167M mutation alone,

nor the covalent modification of this enzyme, has any drastic affect on the basic mechanism for Compound I formation. The k_1 value obtained of Compound I formation for the Um[S167M] HRP-C* was 1.32×10^7 M^{-1} s^{-1}, while for m[S167M] HRP-C* it was 1.64×10^7 M^{-1} s^{-1} (Cali, 2008).

6.3.2 Auto-reduction and life time of Compound I:

Compounds I of the S167W and S167Y variants, formed by the addition of hydrogen peroxide to the enzyme at pH 7.0, were found to be unstable, and in a manner similar to Compound I of WT HRP-C* reverted to the resting state of the enzyme even in the absence of reducing agents (Figures 6.2-6.5). Therefore, in order to determine the life-time of the Compound I species for each enzyme, the auto-reduction was monitored at 412 nm in the stopped-flow system over a total time of 1000 s. This wavelength was chosen as it is the isosbestic point between Compound II and resting enzyme and therefore interference from the reduction of Compound II is avoided. The time traces obtained at 412 nm were found to be biphasic for all enzymes (Figure 6.12). The first phase is more rapid compared to a second slower phase. The traces were fitting to a double exponential equation using the curve fitting application in the Pro-Data Viewer software (Applied Photo-Physics), and two life times were determined using the reciprocal of the rate constants associated with both exponential rise phases of the traces (Table 6.2).

The stopped-flow traces show that the amplitude changes associated with the two phases differ for each enzyme, Figure 6.12 and Table 6.2. The trace for WT HRP-C* has a fast phase with a small amplitude change of 15% and a slow phase with a much

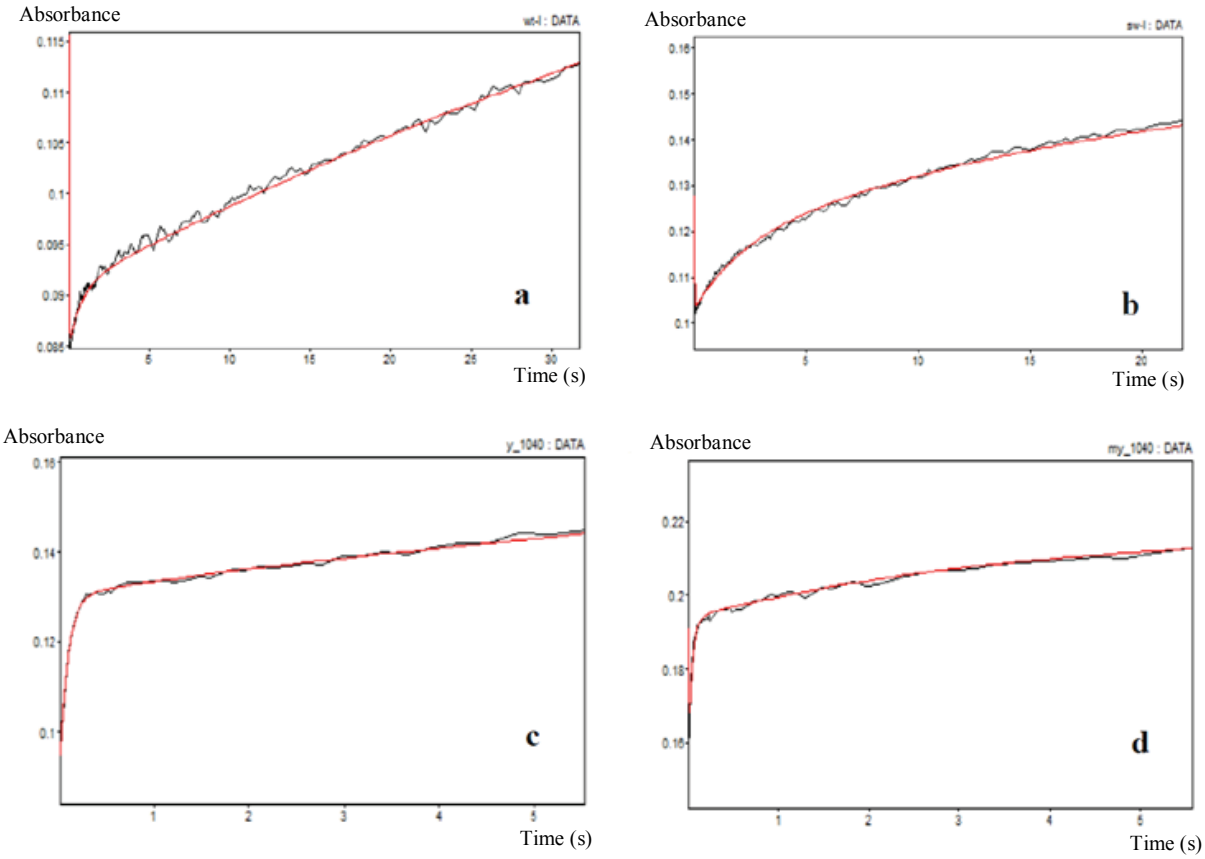

Figure 6.12: Stopped-flow traces of Compound I auto-reduction followed at 412 nm. The double exponential fits of the traces show a biphasic change in absorbance. A 4 µM of enzyme sample was mixed with 10 equivalent of H_2O_2 in 10 mM sodium phosphate buffer, pH 7.0, at 25 ^{o}C. (a) WT HRP-C*, (b) [S167W] HRP-C*, (c) Um[S167Y] HRP-C* and (d) m[S167Y] HRP-C*.

Table 6.2: Life times for Compound I of WT HRP-C*, [S167W] HRP-C*, Um[S167Y] HRP-C* and m[S167Y] HRP-C*. Values were calculated from the reciprocal of the rate constants obtained for the two phases of the traces in Figure 6.12.

Enzyme	Life Time of Compound I Intermediate	
	Fast phase	Slow phase
WT HRP-C*	850 ± 17 ms (15%)	89 ± 13 s (85%)
S167W	2.4 ± 0.2 s (37%)	22.6 ± 4.3 s (63%)
UmS167Y	135 ± 8 ms (72%)	9.3 ± 0.2 s (28%)
mS167Y	40 ± 3 ms (76%)	3.7 ± 0.2 s (24%)

larger amplitude change of 85%. In the case of the S167W variant, the trace shows an increase in the amplitude change of the fast phase (37%) at the expense of the slow phase, when compared to the wild-type enzyme. The traces of Um[S167Y] and m[S167Y] HRP-C* both show a dramatic change in the amplitude changes, with the early fast phase associated with a large amplitude change, of 72% and 76% respectively.

The life times obtained show that the Compound I auto-reduction for the S167W mutant was 3-4 times faster overall than for wild-type enzyme; this result is in good agreement with the rapid scan diode array observations (Figures 6.2 and 6.3). The most interesting results are for the S167Y mutant, where over 70% of Compound I of both Um[S167Y] and m[S167Y] HRP-C* is auto-reduced in the fast phase within only 135 ms and 40 ms, respectively (Table 6.2) and then only another 4 or 10 seconds is needed to completely reduce Compound I to Compound II. The overall reduction is therefore 10 times and 25 times, respectively, faster than for WT HRP-C* Compound I reduction. However, the majority of the effect is from the mutation itself and only a small further instability is introduced by the presence of the cross-link. A previous study in this laboratory showed that the Compound I of Um[S167M] HRP-C* has an overall life time 1.5 times shorter than the wild-type enzyme, while m[S167M] HRP-C* is 2.5 times shorter (Cali, 2008), i.e. there is clearly less effect on the stability of Compound I from the S167M mutation than the S167Y mutation.

6.3.2 Determination of the second-order rate constants (k_2 and k_3) for the HRP-C catalysed oxidation of luminol:

The normal HRP-C reaction cycle is via the sequence: resting enzyme ⟶ Compound I ⟶ Compound II ⟶ resting enzyme (see section 1.5.4), so that after the

formation of Compound I, two sequential single electron reductions of Compound I by the reducing substrate occur and the resting enzyme is regenerated via Compound II; the rate constants k_2 and k_3, respectively, describe the reductions of Compounds I and II. Compound I and Compound II usually react with the same reducing substrate, i.e. once the reaction between Compound I and reducing substrate is initiated and some Compound II is formed, the Compound II begins to react with the substrate as well (Dunford, 1999h). It has been found that wild-type Compound I reacts more rapidly with reducing substrates than does Compound II, i.e. Compound II reduction is the rate limiting step.

In this study, in order to determine the rate constant (k_2) for reduction of Compound I, or formation of Compound II, and the rate constant (k_3) for reduction of Compound II by luminol at the same time, approximately 3 μM of WT HRP-C* and the S167 variants were treated with 2.7 μM of H_2O_2. Then, directly, the reaction mixture was reacted under pseudo first-order conditions with a range of luminol concentrations. The kinetic measurements were performed in 10 mM sodium phosphate buffer, pH 7.0, at 25 ^{o}C and were monitored by a change in absorbance at 424 nm (at this wavelength both k_2 and k_3 can be measured) using the stopped-flow instrument. This wavelength is the isosbestic point between Compound I and resting enzyme (Smith *et al.*, 1992). It has been found that any excess of hydrogen peroxide in the reaction mixture would recycle some of the enzyme and cause interference with accurate measurement (Dunford, 1999h). For this reason, a slightly less than stoichiometric amount of hydrogen peroxide was used.

The traces obtained of change in absorbance at 424 nm as a function of time were biphasic (Figure 6.13), where the rise in absorbance represents the Compound I

reduction stage (Compound II production), and the decay in absorbance represents Compound II reduction. The pseudo first-order rate constants (k_{obs}) for Compounds I and II reduction were determined by fitting the traces obtained to a double exponential function. The slope of a plot of k_{obs} from the rise phase against luminol concentration was used to calculate the second-order rate constant k_2 for Compound I reduction (Figure 6.14), while the slope of a plot of k_{obs} from the decay phase against luminol concentration was used to calculate the second-order rate constant k_3 for Compound II reduction (Figure 6.15). The calculated k_2 and k_3 values are presented in Table 6.3.

For the k_3 determination, the plots of k_{obs} against luminol concentration all show the presence of a small positive intercept on the x-axis (Figure 6.15). This intercept is due to a reduction of the concentration of luminol by one equivalent of enzyme through its initial reaction with the Compound I intermediate.

In general, the results show that the rates of Compound I reduction are much faster (50-360 times greater) than the rates of Compound II reduction, for all enzymes, and that the rates of Compound II reduction vary only over a two-fold range. However, the results do reveal that the rate of Compound I reduction (k_2) for [S167W] HRP-C* is increased to approximately 4 times that of WT HRP-C*. This suggests that the substitution of the Ser residue for Trp at position 167 has a substantial effect on the way that the luminol molecule is able to interact with the Compound I intermediate, resulting in an enhancement in the reaction rate. However, as the rate limiting step for the overall reaction with luminol is the reduction of Compound II this will not result in an increase in steady-state activity.

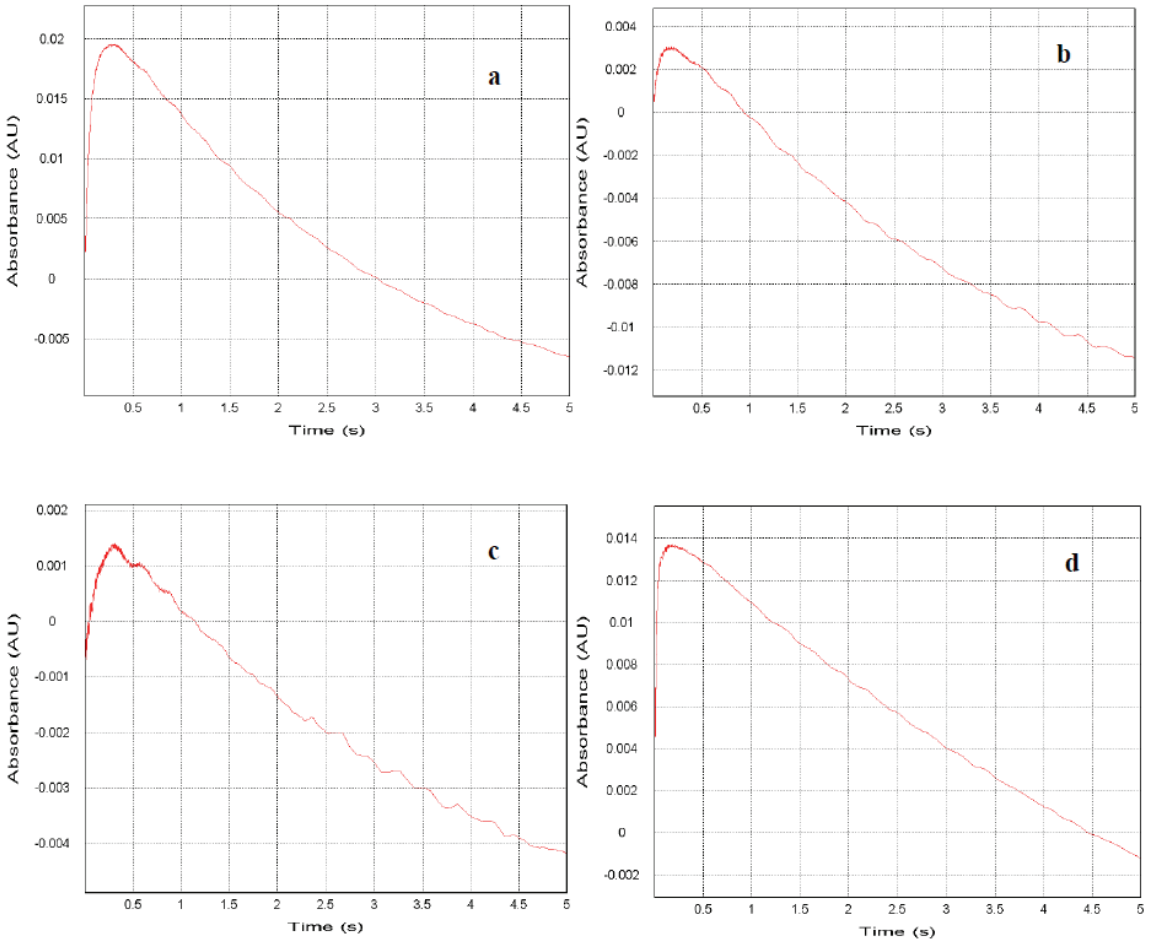

Figure 6.13: Stopped-flow traces of Compound II formation and reduction with luminol as reducing substrate. The traces show the change in absorbance at 424 nm for five seconds after reaction of Compound I (mixture of 3 μM enzyme and 2.7 μM H_2O_2) with 10 μM of luminol in 10 mM sodium phosphate buffer, pH 7.0, at 25 ^{o}C for each of (a) WT HRP-C*, (b) [S167W] HRP-C*, (c) Um[S167Y] HRP-C* and (d) m[S167Y] HRP-C*. The rise in absorbance represents the Compound I reduction stage, while the decay in absorbance represents the Compound II reduction stage.

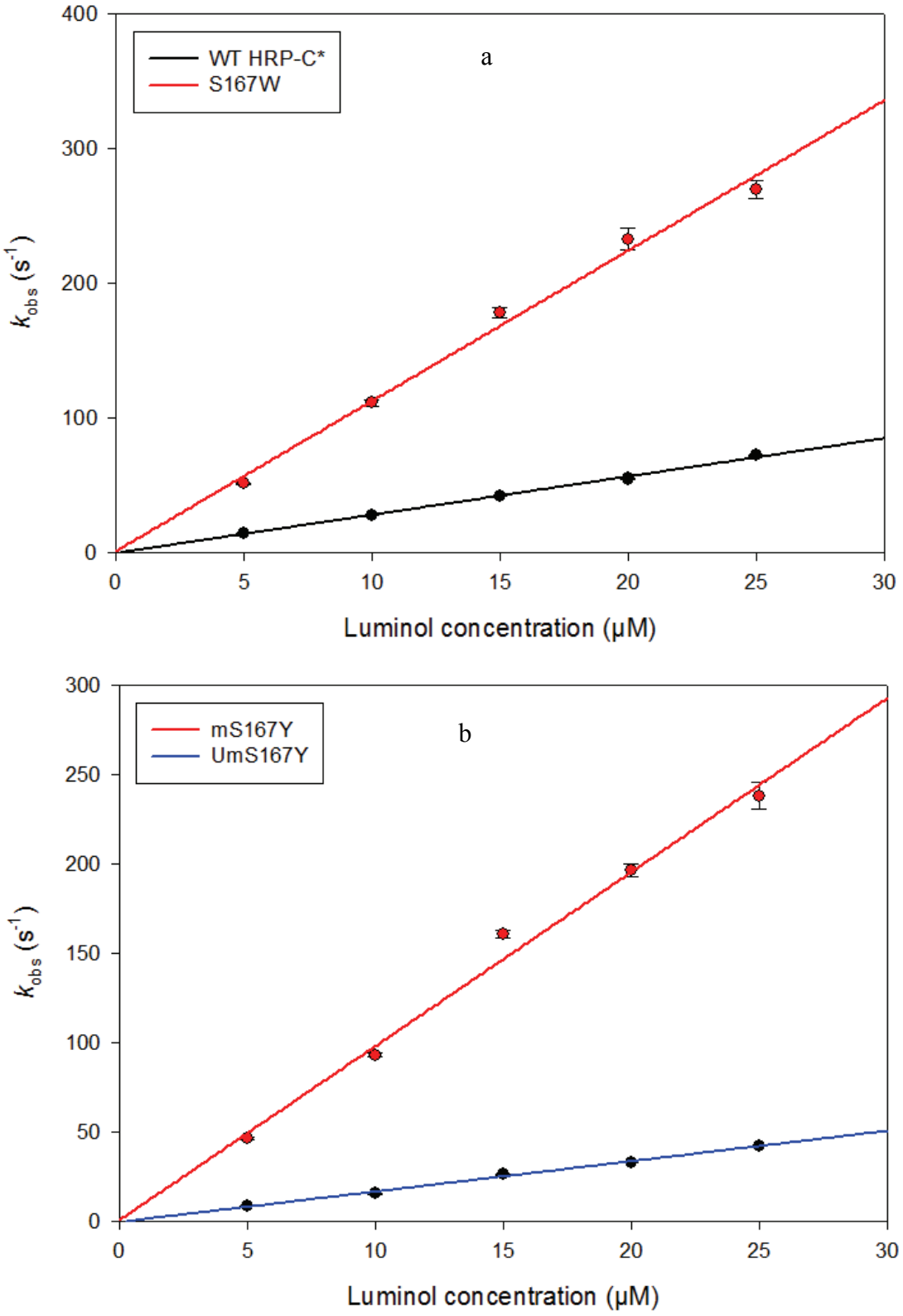

Figure 6.14: Plots of the pseudo first-order rate constants for Compound I reduction by luminol. (a) WT HRP-C* and [S167W] HRP-C*, and (b) Um[S167Y] and m[S167Y] HRP-C*.

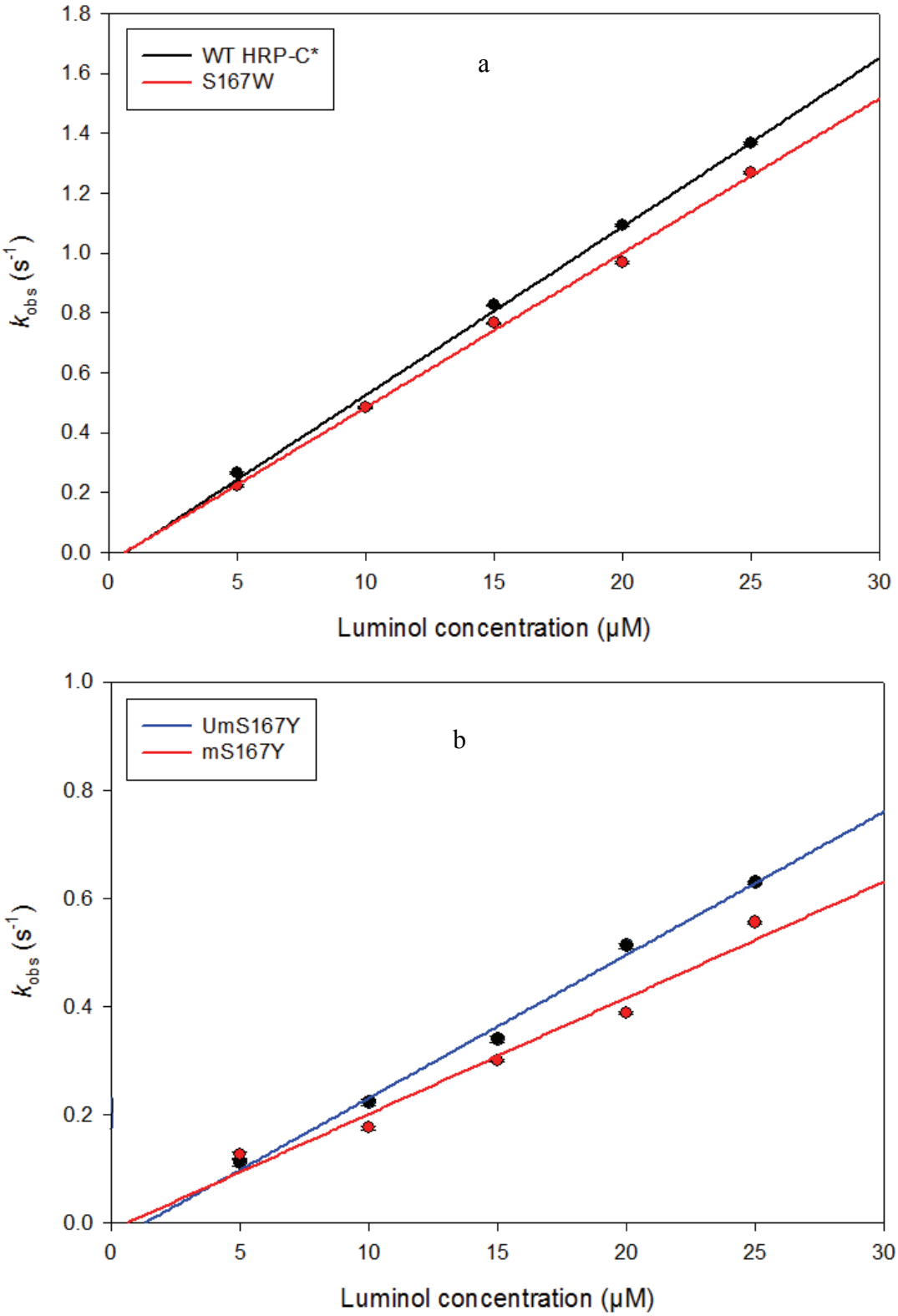

Figure 6.15: Plots of the pseudo first-order rate constants for Compound II reduction by luminol. (a) WT HRP-C* and [S167W] HRP-C*, and (b) Um[S167Y] and m[S167Y] HRP-C*.

Table 6.3: The pre steady-state kinetic parameters k_2 and k_3 obtained for WT HRP-C* and S167 variants, using luminol as reducing substrate. Rate constants k_2 and k_3 were calculated by weighted least square regression analysis using SigmaPlot software, from the slopes of plots of the pseudo first-order rate constants (k_{obs}) against luminol concentration (Figures 6.14 and 6.15).

Enzyme	k_2 (M^{-1} s^{-1})	k_3 (M^{-1} s^{-1})
WT HRP-C*	2.8×10^6	5.6×10^4
S167W	1.07×10^7	5.2×10^4
UmS167Y	1.7×10^6	2.2×10^4
mS167Y	9.7×10^6	2.7×10^4

The results obtained for Um[S167Y] HRP-C* show that there is a small decrease in the k_2 value by a factor of 0.6 fold when compared with wild-type enzyme. However, after incubation with hydrogen peroxide and creation of the haem-protein covalent linkage, m[S167Y] HRP-C* shows an enhancement in the rate of reduction of Compound I with a value 3.5 times faster than that of WT HRP-C*. These results indicate that while the replacement of the Ser residue by Tyr at position 167 initially causes a slight weakening of the interaction between the Compound I intermediate and luminol, formation of the haem-protein covalent linkage by treatment with H_2O_2, leads to a conformation where Compound I is able to oxidize luminol more rapidly. However, as k_3 is still the rate limiting step for the overall HRP-C* reaction in this mutant the slight decrease in k_3 will lead to an approximately 2-fold slower steady-state rate for both the cross-linked and unlinked S167Y mutant.

6.4 Conclusion:

The use of pre steady-state kinetic methods has revealed that the mutation of HRP-C at position 167 causes some modulation in the rate of Compound I formation, compared to WT. It has been observed that there is a small decrease in the rate of Compound I formation for [S167W] HRP-C* and a small increase for [S167Y] HRP-C*, with no significant difference between linked and unlinked enzyme. Additionally, it was shown that the auto-reduction of Compound I occur in two phases, fast and then slow. The amplitude changes of the slow and fast phases reveal that the majority of WT Compound I auto-reduction is in the slow phase (85%), while the majority of UmS167Y and mS167Y Compound I auto-reduction is in the fast phase (72-76%). The S167W mutation has an intermediate effect. Interestingly therefore the S167Y mutation leads to a 10-fold greater overall instability of Compound I. this instability is enhanced further by 2.5-fold if the haem-protein covalent linkage is formed.

Despite of the small negative effect on both the k_2 and k_3 rate constants for Um[S167Y] HRP-C* with luminol as reducing substrate compared to wild-type, m[S167Y] HRP-C* shows a 3.5-fold increase in the rate of Compound I reduction when compared with the wild-type enzyme, suggesting that the formation of the haem-protein covalent linkage has resulted in more favourable conditions for the electron transfer step between luminol and the porphyrin π-cation radical of Compound I. Approximately the same enhancement in the rate of reduction of Compound I has also been observed for the S167W variant. However, although both S167W and mS167Y variants have increased Compound I reduction by luminol, neither shows an increase in Compound II reduction, which is the rate limiting step of the reaction, under the pre steady-state conditions.

Chapter Seven:

Final discussion

The mammalian peroxidases are distinguished, in contrast to plant peroxidases, by the presence of two or three covalent bonds between the haem porphyrin and the protein. The available information about these linkages, such as how they are formed and what their functional advantages, is limited. Therefore, efforts have been made recently to attempt to understand the mechanism of linkage formation and the effects on the enzyme containing them, by introducing equivalent bonds into plant peroxidases, e.g. HRP or APX, using site-directed mutagenesis (Colas and Ortiz de Montellano, 2004; Metcalfe *et al.*, 2004; Pipirou *et al.*, 2007a; Pipirou *et al.*, 2009). Previous work in this laboratory involved the identification of a residue, Ser167, in HRP-C in a similar position relative to the haem as Met243 in the mammalian peroxidase MPO, which is involved in a sulfonium linkage to the haem porphyrin. The mutant [S167M] HRP-C* was therefore produced and was found to contain a sulfonium bond between the protein and haem after treatment with hydrogen peroxide (Cali, 2008). However, the linkage was found to be unstable and broke down after a few days.

In this work, the same residue, Ser167 of HRP-C, has been replaced by both Tyr and Trp using a PCR-based site-directed mutagenesis. Both enzyme variants have been successfully expressed in *E. coli* as inclusion bodies, refolded and characterized. Resting state spectra of both enzyme variants suggest that, in contrast to WT HRP-C*, the haem iron exists predominantly in a six-coordinate high spin form, similar to that found in Lip and MnP (Blodig *et al.*, 2001). Consistent with this, the Soret peak

extinction coefficient of the variants is much more than that of the wild-type enzyme. These results indicate that replacement of Ser167 residue by a bulky residue leads to a perturbation in the environment of the haem, so that the sixth coordination position of the iron is occupied by a weak ligand, probably a water molecule. Binding studies have also revealed that the affinity of the enzyme towards BHA has been impaired as a result of the mutagenesis. This effect is most likely caused indirectly by a perturbation in the aromatic donor binding site and / or the associated haem-linked hydrogen bonding network of the enzyme, rather than suggesting a direct role of Ser167 in substrate binding.

The most important conclusion of the current work is the finding that on exposure of the S167Y mutant to an adequate amount of hydrogen peroxide, a covalent attachment of the haem to the protein is formed autocatalytically. Different analytical techniques have been used to confirm the formation of the covalent cross-linkage. The inability to remove the haem prosthetic group by the acid butanone haem extraction technique, the coelution of the protein and the haem together during HPLC analysis and the increase in mass of 614 Da over the predicted mass of the protein by MS analysis, all provide strong evidence for the formation of the haem-protein covalent bond in the S167Y variant. In addition, the results indicate that the positioning of a Tyr residue at position 167 near to the haem 2-vinyl side chain is sufficient to form the haem-protein covalent linkage, even in the absence of H_2O_2, this requires formation of radical species on the iron (e.g. compound I) and/or on the 2-vinyl group to initiate reaction with the tyrosine. Again, this likely happens as a consequence of turnover of the HRP-C during its isolation, folding or purification. In contrast to the sulfonium linkage formed in the [S167M] HRP-C* mutant (Cali, 2008), which was found to be unstable and broke down

after few days, the haem-protein cross linking in [S167Y] HRP-C* was found to be very stable. The linkage was followed up after a period of 14 days at 4 ^{o}C and room temperature, and using MS and HPLC analysis the results were the same as immediately after formation of haem-protein covalent bond. Opposite to the results for the [S167Y] HRP-C* variant, no protein-haem linkage could ever be detected for the [S167W] HRP-C* variant.

Results from kinetic studies on the two new S167 variants indicate that, even though there is no major functional role of Ser167 in the catalytic activity of HRP-C, the catalytic properties of the mutants somewhat altered. Generally, the reactivity of both mutants is significantly reduced against reducing substrates, with the exception of luminol and guaiacol, for the S167W variant. However, after treatment with hydrogen peroxide and formation of the covalent linkage, the S167Y mutant has a higher reactivity towards all enzyme substrates, equivalent to or higher than WT HRP-C*. This suggests that, as a result of covalent linkage formation, a favourable conformational change has occurred in either the haem environment and / or substrate binding site.

The two new S167 variants were also examined by pre steady-state kinetics. Measurement of Compound I formation showed a 2-fold reduction for S167W and a small increase for either unlinked or linked S167Y. In addition, Compound I was found to be much more unstable for both unlinked and linked [S167Y] HRP-C*. However, unlike the increased activity towards luminol shown by the S167W and linked S167Y variants under steady-state conditions, only Compound I reduction showed an increased rate constant for these two mutants under pre steady-state conditions; the rate determining step of Compound II reduction is not increased. This apparent contradiction

is explained by the different pH's used for the two different experiments, pH 5.0 for steady-state and pH 7.0 for pre steady-state assays.

Indeed, unlike Compound I reduction, the rate of reduction of Compound II to resting enzyme is highly dependent on the pH. It has been reported that Compound II is easiest to reduce at low pH, while at high pH it becomes less and less reactive (Dunford, 1999h). It was also found that the k_{cat} value for the oxidation of ABTS by HRP-C* is drastically affected and decreased by changes in the pH value form pH 5.0 to pH 7.0 (Rodriguez-Lopez *et al.*, 1996b). An attempt has been made to do a comparison between steady-state and pre steady-state enzyme kinetics results, but unfortunately this was not possible due to the differences in the pH used in each case which has led to a change in the activity of enzyme Compound II.

7.1 X-ray crystal structure:

X-ray data collection, generation of electron density maps and structure refinement for the S167Y variant were all carried out in collaboration with Dr. Mark Roe (X-Ray Crystallography Collaborative Research Facility Manager, University of Sussex). The data were collected at the Diamond Light Source, beamline I03, and refined to 1.7 Å resolution using the PHENIX software suite. [S167Y]HRP-C* structural coordinates have been deposited in the protein data bank under the accession code 2YLJ. Superposition of the crystal structure of the S167Y mutant on that of the wild-type enzyme showed that the overall folds of the two enzymes are very similar. The structure also indicates that the new Tyr167 residue occupies a position similar to that of Met243 in MPO, i.e. in a potential position to form a covalent linkage with the haem vinyl group.

In fact, the crystal structure obtained was found to be a mixture of both linked and unlinked S167Y mutant (Figure 7.1). The linked structure reveals a highly unusual five member ring linkage from Tyr167 to the haem that has never been seen before, supported by the increase of 614 Da seen from ESI mass measurements of the linked S167Y protein, compared to the unlinked enzyme. In addition, it was observed that the haem porphyrin ring is considerably distorted from its planarity in the linked structure. This distortion in the haem planarity has been reported previously in the MPO structure as a result of the sulfoinum linkage, giving a bow-shaped structure of the haem (Fiedler *et al.*, 2000). The X-ray crystal structure of the unlinked S167Y mutant shows that the distance between the engineered Tyr167 hydroxyl and the haem vinyl β carbon is 2.43 Å, while the distance between the *O*-carbon of the phenyl ring and the haem vinyl β carbon is 1.64 Å (Figure 7.2), while there is 3.82 Å between the Ser167 hydroxyl and the haem vinyl β carbon in the wild-type enzyme. Therefore, for a cross-linked S167Y protein to be formed it is easier to initially form a C-C bond between the haem vinyl β carbon and the phenyl ring; then the five member ring linkage is constructed as described in the following proposed mechanism (Scheme 7.1).

The mechanism involves the following steps: (1) Initial reaction of the S167Y mutant with H_2O_2 to form Compound I, (2) oxidation of Tyr167 by Compound I associated with removal of its hydroxyl proton to form a Tyr radical. The phenoxy radical of Tyr (i) readily rearranges to the benzyl radical (ii), (3) the benzyl radical of Tyr167 is then added to the C_β of the 2-vinyl group of the haem leading to breakage of the double bond and resulting in a radical on C_α, (4) the ferryl haem is reduced by the radical on C_α leading to release of a water molecule and formation of a carbocation on the C_α and (5) finally, elimination of the proton occurs in concert with resonance arrangement and

attack on the electrophilic carbocation, resulting in the creation of a five member ring linkage giving a haem structure consistent with the mass spectrometry results. The mechanism for the formation of a covalent linkage between an engineered methionine at position 160 (S160M) and the haem in ascorbate peroxidase has been proposed (Metcalfe *et al.*, 2004). This mechanism includes in the final step addition of a hydroxyl group to the C_α of the vinyl group of the haem resulting in the loss of the double bond. On the other hand, a proposed mechanism for the formation of the vinyl-sulfonium linkage in MPO suggests the loss of a proton from the C_β of the vinyl group and retention of the double bond (Colas and Ortiz de Montellano, 2003). The typical MPO spectroscopic characteristics, especially the red shift in the Soret peak, have been attributed to the conjugation of the sulfonium ion with the haem group via this double bond (Kooter *et al.*, 1999b). Metcalfe and co-workers therefore suggest that the loss of the double bond in [S160M] APX is the reason of why the UV/Visible spectrum does not show the significant red shift in the Soret peak as in MPO (Metcalfe *et al.*, 2004). The results in this work, where no significant change in the Soret peak position of linked [S167Y] HRP-C* is seen to strongly support this reasoning.

7.2 Finally to summarise the main results of this thesis:

Although the [S167W] HRP-C* variant does not form a covalent linkage between the haem and protein on treatment with H_2O_2, it exhibits an enhanced luminol turnover which might be interesting commercially, as an alternative to the WT enzyme in chemiluminescence assays. However, the reason(s) for haem degradation in this mutant after exposure to H_2O_2 should be further investigated; analytical techniques such as LC-MS and Fourier Transform Infrared Spectroscopy (FTIR) analysis would be useful. FTIR is an analysis technique that provides information about the molecular structure

and chemical bonding of materials. It can be utilized to study the chemical changes that might occur in the haem structure after exposure to H_2O_2.

Most interestingly, this work has shown that a haem-protein covalent linkage can be formed either autocatalytically on the addition of hydrogen peroxide, or indeed spontaneously in the absence of H_2O_2, in the [S167Y] HRP-C* mutant. The X-ray crystal structure reveals an unanticipated linkage structure, containing an additional ring, between the engineered Tyr and the haem; a structure not seen before. This linkage seems to be much more stable than the sulfonium linkage previously investigated in [S167M] HRP-C*. In contrast to the S167M variant, however, in which formation of the linkage significantly lowers the activity of the enzyme against all substrates tested, the activity of [S167Y] HRP-C* is enhanced by linkage formation, even to levels greater than WT enzyme for some substrates. This retention of good levels of activity after the covalent bond formation shows that it should be possible to use this mutant as an alternative to WT in commercial and clinical applications of HRP-C. If, as it is hoped, the linked mutant displays increased stability over the WT enzyme, e.g. at high temperature, then it's use in diagnostic kits would be a great advantage, particularly in areas of the world where there is less access to refrigeration.

The results obtained in this work show that the presence of a haem-protein covalent bond significantly alters the electronic and catalytic properties of a haem enzyme. This suggests that the reason for the existence of the haem-protein covalent linkages in mammalian peroxidases, in addition to possible contributions to the stability of the enzymes, might well be related to the catalytic properties required.

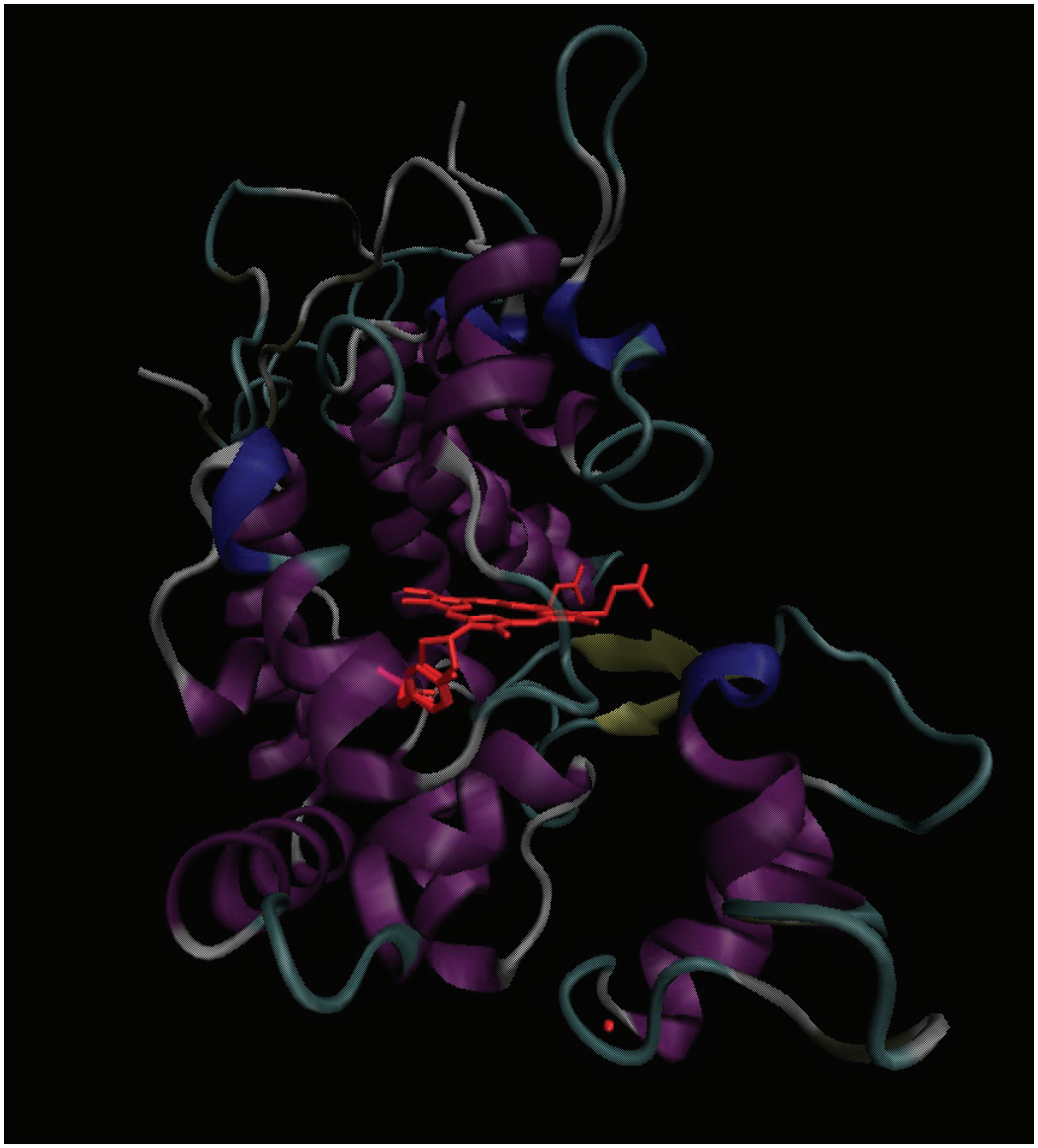

Figure 7.1: Ribbon representation for the structure of [S167Y] HRP-C* mutant. The figure was constructed by the **VMD** molecular visualization programme using the molecular coordinates of the X-ray crystal structure of [S167Y] HRP-C* mutant, accession code 2YLJ.

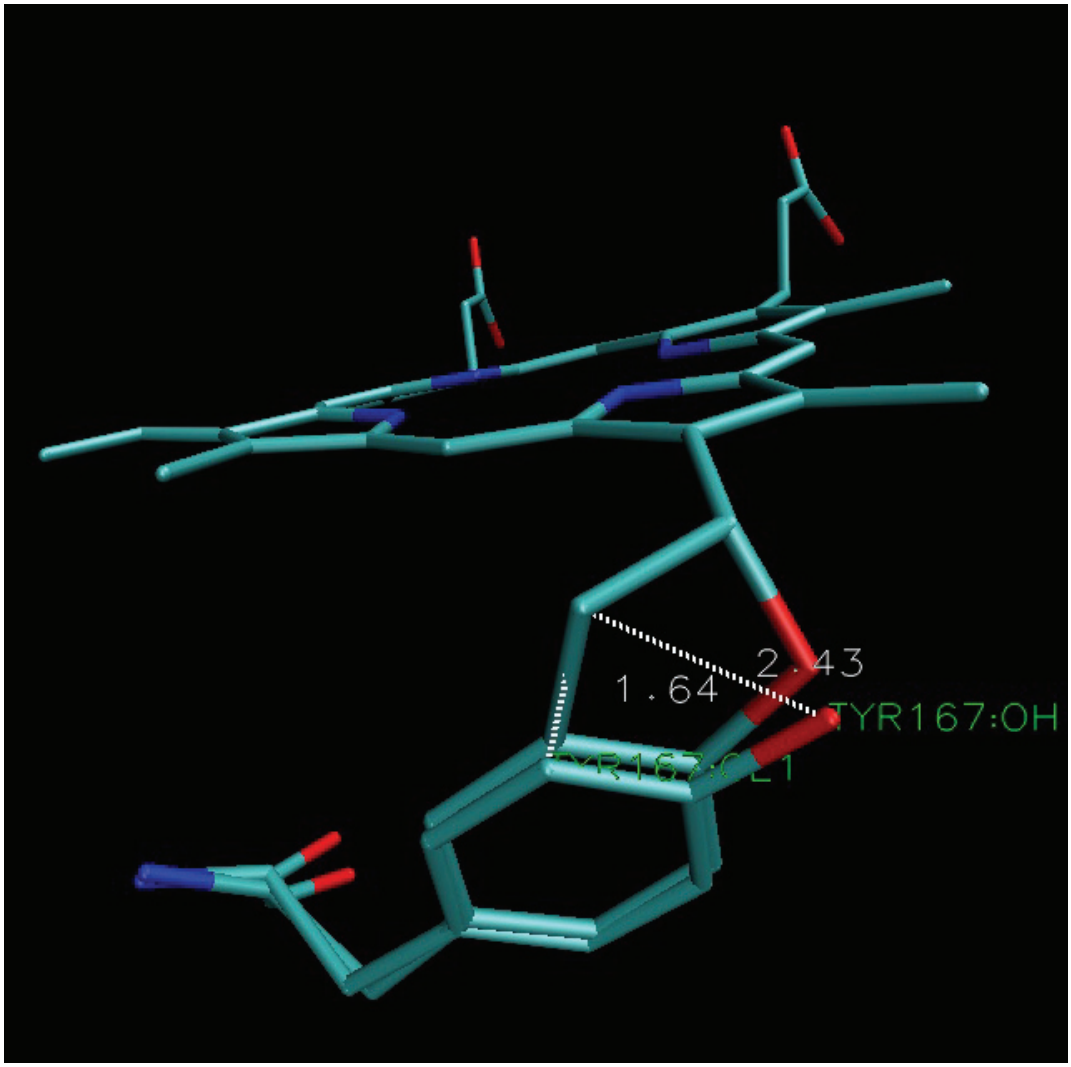

Figure 7.2: Five member ring linkage between Tyr167 and the haem vinyl group in the structure of the [S167Y] HRP-C* mutant. The figure shows the positions of Tyr167 molecules both unlinked and covalently linked to the haem vinyl group. The distance between the engineered Tyr167 hydroxyl and the haem vinyl β carbon is 2.43 Å, and the distance between the *O*-carbon of the phenyl ring of Tyr167 and haem vinyl β carbon is 1.64 Å. The figure was constructed by **VMD** molecular visualization programme using the molecular coordinates of the X-ray crystal structure of [S167Y] HRP-C* mutant, accession code 2YLJ.

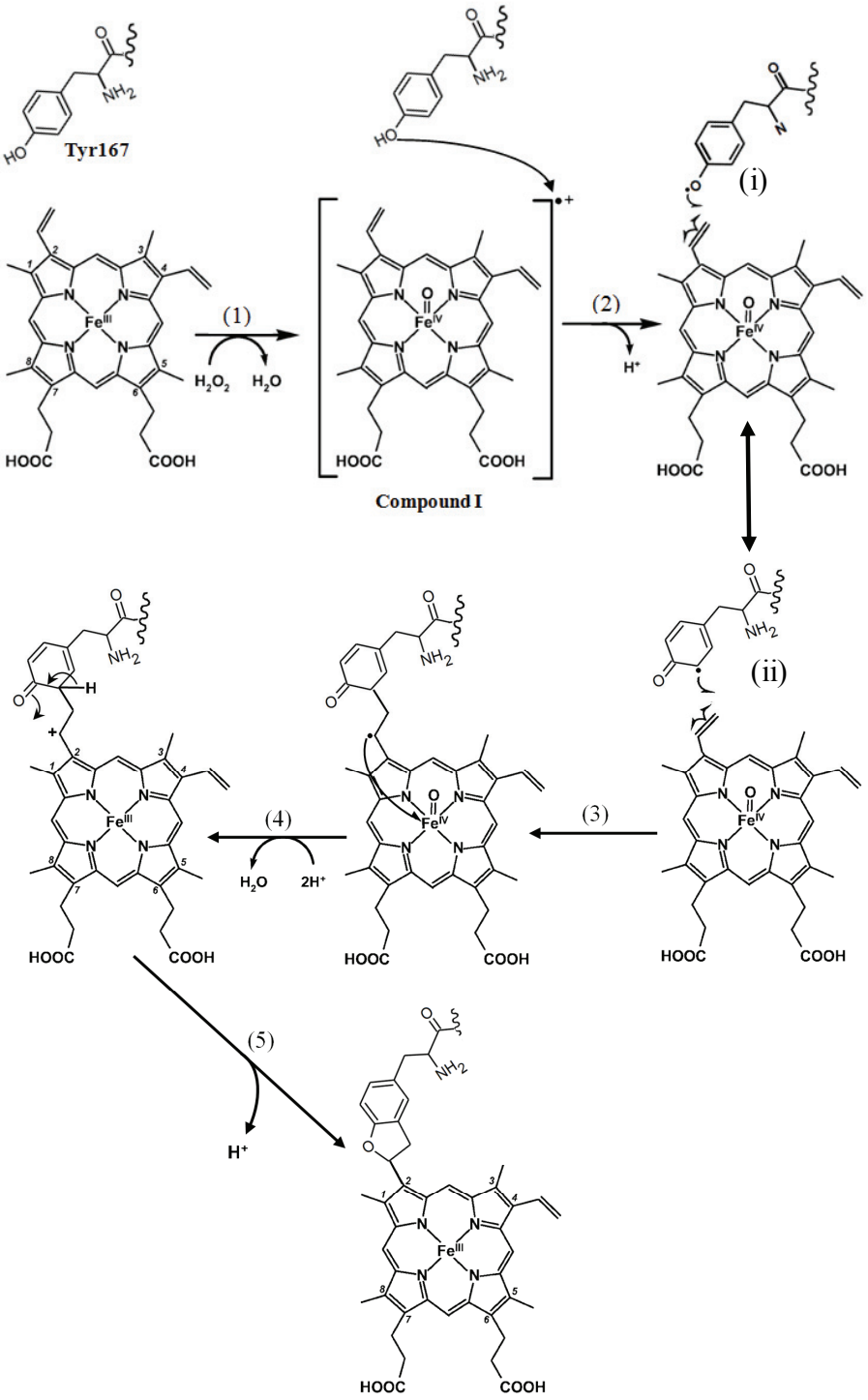

Scheme 7.1: Proposed mechanism for formation of a five member ring linkage between Tyr167 and 2-vinyl haem group in HRP-C*. Reactions 1-5 are described in the text. The results also indicate that the linkage is formed even before treatment with H_2O_2. Therefore, another possible route to initiating the reaction is that during catalysis a 2-vinyl radical species appears transiently on the haem, and this (and not Compound I) is responsible for hydrogen abstraction from the tyrosine side chain to initiate the covalent link formation.

References:

Ackermann, B. L., Berna, M. J., Eckstein, J. A., Ott, L. W. and Chaudhary, A. K. (2008). Current applications of liquid chromatography/mass spectrometry in pharmaceutical discovery after a decade of innovation. Annual Review of Analytical Chemistry. **1:** 357-396.

Adam, W., Hoch, U., Lazarus, M., Saha-Moller, C. R. and Schreier, P. (1995). "Enzyme-catalyzed asymmetric synthesis: Kinetic resolution of racemic hydroperoxides by enantioselective reduction to alcohols with horseradish peroxidase." Journal of the American Chemical Society **117**(48): 11898-11901.

Aliaga, C. and Lissi, E. A. (1998). "Reaction of 2,2′-azinobis (3-ethylbenzothiazoline-6-sulfonic acid) (ABTS) derived radicals with hydroperoxides. Kinetics and mechanism." International Journal of Chemical Kinetics **30**(8): 565-570.

Andersson, L. A., Bylkas, S. A. and Wilson, A. E. (1996). "Spectral analysis of lactoperoxidase: Evidence for a common heme in mammalian peroxidases." Journal of Biological Chemistry **271**(7): 3406-3412.

Andrews, P. C. and Krinsky, N. I. (1981). "The reductive cleavage of myeloperoxidase in half, producing enzymically active hemi-myeloperoxidase." Journal of Biological Chemistry **256**(9): 4211-4218.

Ardrey, R. E. (2003). Liquid Chromatography - Mass Spectrometry: An Introduction, John Wiley & Sons Ltd., Chichester, UK**:** 7-127.

Arnhold, J., Monzani, E., Furtmuller, P. G., Zederbauer, M., Casella, L. and Obinger, C. (2006). "Kinetics and thermodynamics of halide and nitrite oxidation by mammalian heme peroxidases." European Journal of Inorganic Chemistry(19): 3801-3811.

Ashcroft, D. A. E. (2002). "An Introduction to Mass Spectrometry." Web site: http://www.astbury.leeds.ac.uk/Facil/MStut/mstutorial.htm.

Atkins, P. and Paula, J. (2009). Elements of Physical Chemistry. Oxford, W. H. Freeman.

Azevedo, A., Martins, V., Prazeres, D., Vojinovic, V., Cabral, J. and Fonseca, L. (2003). Horseradish peroxidase: A valuable tool in biotechnology. Biotechnology Annual Review. **9:** 199-247.

Baek, H. K. and Van Wart, H. E. (1992). "Elementary steps in the reaction of horseradish peroxidase with several peroxides: Kinetics and thermodynamics of formation of compound 0 and compound I." Journal of the American Chemical Society **114**(2): 718-725.

Baer, B. R., Kunze, K. L. and Rettie, A. E. (2007). "Mechanism of formation of the ester linkage between heme and Glu310 of CYP4B1: ^{18}O protein labeling studies." Biochemistry **46**(41): 11598-11605.

Baker, J. R., Arscott, P. and Johnson, J. (1994). "An analysis of the structure and antigenicity of different forms of human thyroid peroxidase." Thyroid **4**(2): 173-178.

Belding, M. E., Klebanoff, S. J. and Ray, C. G. (1970). "Peroxidase-mediated virucidal systems." Science **167**(3915): 195-196.

Berg, J. M., Tymoczko, J. L. and Stryer, L. (2002). Biochemistry. New York, W. H. Freeman.

Bhandari, A., Kim, W. and Hohn, K. (2010). "Luminol-Based Enhanced Chemiluminescence Assay for Quantification of Peroxidase and Hydrogen Peroxide in Aqueous Solutions: Effect of Reagent pH and Ionic Strength." Journal of Environmental Engineering **136**(10): 1147-1152.

Blair-Johnson, M., Fiedler, T. and Fenna, R. (2001). "Human Myeloperoxidase: Structure of a Cyanide Complex and Its Interaction with Bromide and Thiocyanate Substrates at 1.9 Å Resolution." Biochemistry **40**(46): 13990-13997.

Blodig, W., Smith, A. T., Doyle, W. A. and Piontek, K. (2001). "Crystal structures of pristine and oxidatively processed lignin peroxidase expressed in Escherichia coli and of the W171F variant that eliminates the redox active tryptophan 171. Implications for the reaction mechanism." Journal of Molecular Biology **305**(4): 851-861.

Bosterling, B. and Trudell, J. R. (1981). "Spin trap evidence for production of superoxide radical anions by purified NADPH-cytochrome P-450 reductase." Biochemical and Biophysical Research Communications **98**(2): 569-575.

Bramer, S. E. V. (1998). "An Introduction to Mass Spectrometry." web site: http://science.widener.edu/svb/massspec/massspec.pdf. 1998.

Branden, C. I. and Tooze, J. (1991). Introduction to Protein Structure, Taylor & Francis.

Briheim, G., Stendahl, O. and Dahlgren, C. (1984). "Intra- and extracellular events in luminol-dependent chemiluminescence of polymorphonuclear leukocytes." Infection and Immunity Journal **45**(1): 1-5.

Brill, A. S. and Williams, R. J. (1961). "The Absorption Spectra, Magnetic Moments and the Binding of Iron in some Haemoproteins." Biochemical Journal **78**: 246-253.

Burner, U., Jantschko, W. and Obinger, C. (1999). "Kinetics of oxidation of aliphatic and aromatic thiols by myeloperoxidase compounds I and II." FEBS Letters **443**(3): 290-296.

Burns, P. S., Williams, R. J. P. and Wright, P. E. (1975). "Conformational studies of peroxidase-substrate complexes. Structure of the indolepropionic acid-horseradish

peroxidase complex." Journal of the Chemical Society, Chemical Communications(19): 795-796.

Bus, J. S., Aust, S. D. and Gibson, J. E. (1974). "Superoxide and singlet oxygen catalyzed lipid peroxidation as a possible mechanism for paraquat (methyl viologen) toxicity." Biochemical and Biophysical Research Communications **58**(3): 749-755.

Cali, K. C. (2008). Towards the design of new functional properties in horseradish peroxidase (HRP): Engineering a covalent linke between the haem and the protein. Biochemistry. Brighton, Sussex. **Ph.D:** 185

Cals, M. M., Mailliart, P., Brignon, G., Anglade, P. and Dumas, B. R. (1991). "Primary structure of bovine lactoperoxidase, a fourth member of a mammalian heme peroxidase family." European Journal of Biochemistry **198**(3): 733-739.

Campa, A. (1991). Biological roles of plant peroxidases: known and potential function. Peroxidases in chemistry and biology. J. Everse, K. E. Everse and M. B. Grisham, CRC Press Inc., Boca Raton, USA. **2:** 25-50.

Campbell, M. K. and Farrell, S. O. (2009). Biochemistry, Thomson-Brooks/Cole, United State.

Campos, A. M. and Lissi, E. A. (1997). "Kinetics of the reaction between 2,2′-azinobis (3-ethylbenzothiazoline-6-sulfonic acid) (ABTS) derived radical cations and phenols." International Journal of Chemical Kinetics **29**(3): 219-224.

Capena, X., Vidossich, P., Schrottner, K., Calisto, B. M., Banerjee, S., Stampler, J., Soudi, M., Furtmuller, P. G., Rovira, C., Fita, I. and Obinger, C. (2009). "Essential role of proximal histidine-asparagine interaction in mammalian peroxidases." Journal of Biological Chemistry **284**(38): 25929-25937.

Carlson, M. G., Peterson, C. G. and Venge, P. (1985). "Human eosinophil peroxidase: purification and characterization." Journal of Immunology **134**(3): 1875-1879.

Carr, S. A., Hemling, M. E., Bean, M. F. and Roberts, G. D. (1991). "Integration of mass spectrometry in analytical biotechnology." Analytical Chemistry **63**(24): 2802-2824.

Chance, B. (1952). "The spectra of the enzyme-substrate complexes of catalase and peroxidase." Archives of Biochemistry and Biophysics **41**(2): 404-415.

Chance, B. and Maehly, A. C. (1955). Assay of catalase and peroxidase. Methods in Enzymology. S. P. Colowick and N. O. Kaplan, Academic Press, New York. **2:** 764-775.

Chapman, J. R. (1993). Practical Organic Mass Spectrometry: A Guide for Chemical and Biochemical Analysis, John Wiley & Sons Ltd., Chichester, UK.**:** 1-31.

Chen, Y., Yan, G., Zhou, X. and Yang, P. (2010). "Combination of matrix-assisted laser desorption ionization and electrospray ionization mass spectrometry for the analysis of intact glycopeptides from horseradish peroxidase." Chinese Journal of Chromatography (Se Pu) **28**(2): 135-139.

Childs, R. E. and Bardsley, W. G. (1975). "The steady state kinetics of peroxidase with 2,2'-azino-di-(3-ethylbenzthiazoline-6-sulphonic acid) as chromogen." Biochemical Journal **145**(1): 93-103.

Churin, Y., Schilling, S. and Borner, T. (1999). "A gene family encoding glutathione peroxidase homologues in Hordeum vulgare (barley)." FEBS Letters **459**(1): 33-38.

Cline, J., Braman, J. C. and Hogrefe, H. H. (1996). "PCR fidelity of Pfu DNA polymerase and other thermostable DNA polymerases." Nucleic Acids Research **24**(18): 3546-3551.

Colas, C., Kuo, J. M. and Ortiz de Montellano, P. R. (2002). "Asp-225 and Glu-375 in autocatalytic attachment of the prosthetic heme group of lactoperoxidase." Journal of Biological Chemistry **277**(9): 7191-7200.

Colas, C. and Ortiz de Montellano, P. R. (2003). "Autocatalytic radical reactions in physiological prosthetic heme modification." Chemical Reviews **103**(6): 2305-2332.

Colas, C. and Ortiz de Montellano, P. R. (2004). "Horseradish peroxidase mutants that autocatalytically modify their prosthetic heme group. Insights into mammalian peroxidase heme-protein covalent bonds." Journal of Biological Chemistry **279**(23): 24131-24140.

Cornish-Bowden, A. (2004). Fundamentals of Enzyme Kinetics, Portland Press, London.

Coulet, P. R. and Blum, L. J. (1992). "Bioluminescence/chemiluminescence based sensors." Trends in Analytical Chemistry **11**(2): 57-61.

Critchlow, J. E. and Dunford, H. B. (1972). "Studies on horseradish peroxidase. IX. Kinetics of the oxidation of p-cresol by compound II." Journal of Biological Chemistry **247**(12): 3703-3713.

Daniel, J. M., Friess, S. D., Rajagopalan, S., Wendt, S. and Zenobi, R. (2002). "Quantitative determination of noncovalent binding interactions using soft ionization mass spectrometry." International Journal of Mass Spectrometry **216**(1-2): 1-27.

Davies, K. J. (1987). "Protein damage and degradation by oxygen radicals. I. general aspects." Journal of Biological Chemistry **262**(20): 9895-9901.

Davies, K. J., Lin, S. W. and Pacifici, R. E. (1987). "Protein damage and degradation by oxygen radicals. IV. Degradation of denatured protein." Journal of Biological Chemistry **262**(20): 9914-9920.

de Boer, H. A., Comstock, L. J. and Vasser, M. (1983). "The tac promoter: a functional hybrid derived from the trp and lac promoters." Proceedings of the National Academy of Sciences of the United States of America **80**(1): 21-25.

de Villiers, A., Lestremau, F., Szucs, R., Gelebart, S., David, F. and Sandra, P. (2006). "Evaluation of ultra performance liquid chromatography. Part I. Possibilities and limitations." Journal of Chromatography A **1127**(1-2): 60-69.

DePillis, G. D., Ozaki, S. I., Kuo, J. M., Maltby, D. A. and Ortiz de Montellano, P. R. (1997). "Autocatalytic processing of heme by lactoperoxidase produces the native protein-bound prosthetic group." Journal of Biological Chemistry **272**(14): 8857-8860.

Dolphin, D. and Felton, R. H. (1974). "The biochemical significance of porphyrin π-cation radicals." Accounts of Chemical Research **7**(1): 26-32.

Done, J. N. (1978). Idealized Equipment Design for HPLC. Practical high performance liquid chromatography C. F. Simpson, Heyden in association with the Continuing Education Committee of the Chemical Society, London, UK**:** 69-88.

Doyle, W. A., Blodig, W., Veitch, N. C., Piontek, K. and Smith, A. T. (1998). "Two substrate interaction sites in lignin peroxidase revealed by site- directed mutagenesis." Biochemistry **37**(43): 15097-15105.

Dunford, H. B. (1982). Peroxidases. Advances in Inorganic Biochemistry. G. L. Eichhorn and L. G. Marzilli. New York, Elsevier. **4:** 41-68.

Dunford, H. B. (1991). Horseradish peroxidase: Structural and kinetic properties. Peroxidases in Chemistry and Biology. J. Everse, K. E. Everse and M. B. Grisham, CRC Press Inc., Boca Raton, USA. **2:** 1-24.

Dunford, H. B. (1993). Kinetics of peroxidase reactions: horseradish, barley, coprinus cinereus, liginin and manganese. Plant peroxidases: biochemistry and physiology : III International Symposium 1993 : proceedings. K. Welinder, University of Copenhagen and University of Geneva**:** 113-124.

Dunford, H. B. (1999a). Heme peroxidase nomenclature. Plant Peroxidase Newsletter: Plant Biochemistry and Physiology. C. Penel, T. Gaspar and H. Greppin, University of Geneva, Geneva.**:** 65-71.

Dunford, H. B. (1999b). Heme peroxidase and catalases families and superfamilies: Crystal structures. Heme peroxidases, Joun Wiley & Sons, Inc., New York, USA.**:** 33-57.

Dunford, H. B. (1999c). Lactoperoxidase, Thyroid peroxidase and other Animal peroxidase. Heme Peroxidases, Joun Wiley & Sons, Inc., New York, USA.**:** 414-434.

Dunford, H. B. (1999d). Meyloperoxidase and Eosinophil peroxidase: Phagocytosis and Microbial Killing. Heme Peroxidases, Joun Wiley & Sons, Inc., New York, USA.**:** 349-385.

Dunford, H. B. (1999e). Introduction. Historical Background. Heme Peroxidases, Joun Wiley & Sons, Inc., New York, USA.**:** 1-17.

Dunford, H. B. (1999f). Spectroscopic of Horseradish Peroxisae. I: Optical, Resonanse Raman, Magnetic Circular Dichrosim, X-Ray Absorption and Diffraction. Heme Peroxidases, Joun Wiley & Sons, Inc., New York, USA.**:** 135-174.

Dunford, H. B. (1999g). Horseradish peroxidases. III: Reaction with indole-3-acetic acid , light emission, and quantitative structure-activity realasionships. Heme Peroxidases, Joun Wiley & Sons, Inc., New York, USA.**:** 112-134.

Dunford, H. B. (1999h). Horseradish peroxidases. I: Ligand binding, redox potentials, formation of its compounds, and some of their reactions. Heme Peroxidases, Joun Wiley & Sons, Inc., New York, USA.**:** 58-91.

Dunford, H. B. (1999i). Model Peroxidases from Yeast and Horseradish, cloned enzymes, and comparison to metmyoglobin. Heme Peroxidases, Joun Wiley & Sons, Inc., New York, USA.**:** 18-32.

Dunford, H. B. and Stillman, J. S. (1976). "On the function and mechanism of action of peroxidases." Coordination Chemistry Reviews **19**(3): 187-251.

Eaton, W. A. and Hochstrasser, R. M. (1967). "Electronic spectrum of single crystals of ferricytochrome-c." The Journal of Chemical Physics **46**(7): 2533-2539.

Elliot, R. M. (1963). Ion Sources. Mass Spectrometry. C. A. McDowell, McGraw-Hill, New York, USA.**:** 69-103.

Erman, J. E., Vitello, L. B., Miller, M. A., Shaw, A., Brown, K. A. and Kraut, J. (1993). "Histidine 52 is a critical residue for rapid formation of cytochrome c peroxidase compound I." Biochemistry **32**(37): 9798-9806.

Everse, J. (1998). "The structure of heme proteins compounds I and II: Some misconceptions." Free Radical Biology and Medicine **24**(7-8): 1338-1346.

Farmer, J. B. (1963). Types of Mass Spectrometers. Mass Spectrometry. C. A. McDowell, McGraw-Hill, New York**:** 7-44.

Fayadat, L., Niccoli-Sire, P., Lanet, J. and Franc, J. L. (1999). "Role of Heme in Intracellular Trafficking of Thyroperoxidase and Involvement of H_2O_2 Generated at the Apical Surface of Thyroid Cells in Autocatalytic Covalent Heme Binding " Journal of Biological Chemistry **274**(15): 10533-10538.

Fenn, J. B., Mann, M., Meng, C. K., Wong, S. F. and Whitehouse, C. M. (1989). "Electrospray ionization for mass spectrometry of large biomolecules." Science **246**(4926): 64-71.

Fenna, R., Zeng, J. and Davey, C. (1995). "Structure of the green heme in myeloperoxidase." Archives of Biochemistry and Biophysics **316**(1): 653-656.

Fiedler, T. J., Davey, C. A. and Fenna, R. E. (2000). "X-ray crystal structure and characterization of halide-binding sites of human myeloperoxidase at 1.8 ^{o}A resolution." Journal of Biological Chemistry **275**(16): 11964-11971.

Fifield, F. W. and Kealey, D. (1995). Principles and Practice of Analytical Chemistry, Chapman & hall, Glasgow, UK**:** 55-183.

Floris, R., Moguilevsky, N., Puppels, G., Jacquet, A., Renirie, R., Bollen, A. and Wever, R. (1995). "Heme - protein interaction in myeloperoxidase: Modification of spectroscopic properties and catalytic activity by single residue mutation." Journal of the American Chemical Society **117**(14): 3907-3912.

Fountoulakis, M. and Langen, H. (1997). "Identification of proteins by matrix-assisted laser desorption ionization-mass spectrometry following in-gel digestion in low-salt, nonvolatile buffer and simplified peptide recovery." Analytical Biochemistry **250**(2): 153-156.

Fridovich, I. (1986). "Biological effects of the superoxide radical." Archives of Biochemistry and Biophysics **247**(1): 1-11.

Fridovich, I. (1998). "Oxygen toxicity: A radical explanation." Journal of Experimental Biology **201**(8): 1203-1209.

Fuhrhop, J. H. and Smith, K. M. (1975). "Hemes: Determinations as pyridine hemochromes, in Laboratory Methods in Porphyrin and Metalloporphyrin Research." Elsevier Scientific Publishing(Oxford): 48-50.

Fulop, V., Ridout, C. J., Greenwood, C. and Hadgu, J. (1995). "Crystal structure of the di-heme cytochrome c peroxidase from Pseudumonas aeroginosa." Structure **3**(11): 1225-1233.

Furtmuller, P. G., Burner, U. and Obinger, C. (1998). "Reaction of myeloperoxidase compound I with chloride, bromide, iodide, and thiocyanate." Biochemistry **37**(51): 17923-17930.

Furtmuller, P. G., Zederbauer, M., Jantschko, W., Helm, J., Bogner, M., Jakopitsch, C. and Obinger, C. (2006). "Active site structure and catalytic mechanisms of human peroxidases." Archives of Biochemistry and Biophysics **445**(2): 199-213.

Furtmuller, P. O., Obinger, C., Hsuanyu, Y. and Dunford, H. B. (2000). "Mechanism of reaction of myeloperoxidase with hydrogen peroxide and chloride ion." European Journal of Biochemistry **267**(19): 5858-5864.

Gajhede, M., Schuller, D. J., Henriksen, A., Smith, A. T. and Poulos, T. L. (1997). "Crystal structure of horseradish peroxidase C at 2.15 A^{o} resolution." Nature Structural Biology **4**(12): 1032-1038.

Garguilo, M. G., Huynh, N., Proctor, A. and Michael, A. C. (1993). "Amperometric sensors for peroxide, choline, and acetylcholine based on electron transfer between horseradish peroxidase and a redox polymer." Analytical Chemistry **65**(5): 523-528.

Ghiladi, R. A., Knudsen, G. M., Medzihradszky, K. F. and Ortiz de Montellano, P. R. (2005a). "The Met-Tyr-Trp cross-link in Mycobacterium tuberculosis catalase-peroxidase (KatG): Autocatalytic formation and effect on enzyme catalysis and spectroscopic properties." Journal of Biological Chemistry **280**(24): 22651-22663.

Ghiladi, R. A., Medzihradszky, K. F. and Ortiz de Montellano, P. R. (2005b). "Role of the Met-Tyr-Trp cross-link in Mycobacterium tuberculosis catalase-peroxidase (KatG) as revealed by KatG(M255I)." Biochemistry **44**(46): 15093-15105.

Gilbert, M. T. (1987). High Performance Liquid Chromatography, IOP Publishing Limited, Bristol, UK**:** 12-52.

Gleich, G. J., Ottesen, E. A., Leiferman, K. M. and Ackerman, S. J. (1989). "Eosinophils and human disease." International Archives of Allergy and Applied Immunology **88**(1-2): 59-62.

Goodin, D. B. and McRee, D. E. (1993). "The Asp-His-iron triad of cytochrome c peroxidase controls the reduction potential electronic structure, and coupling of the tryptophan free radical to the heme." Biochemistry **32**(13): 3313-3324.

Gutfreund, H. (1999). "Rapid-flow techniques and their contributions to enzymology." Trends in Biochemical Sciences **24**(11): 457-460.

Halliwell, B. and Gutteridge, J. M. (1989). Free radicals in biology and medicine, Clarenden Press, Oxford, UK.**:** 466-493.

Harrison, J. E. and Schultz, J. (1976). "Studies on the chlorinating activity of myeloperoxidase." Journal of Biological Chemistry **251**(5): 1371-1374.

Haschke, R. H. and Friedhoff, J. M. (1978). "Calcium-related properties of horseradish peroxidase." Biochemical and Biophysical Research Communications **80**(4): 1039-1042.

Hasinoff, B. B. and Dunford, H. B. (1970). "Kinetics of the oxidation of ferrocyanide by horseradish peroxidase compounds I and II." Biochemistry **9**(25): 4930-4939.

Heering, H. A., Smith, A. T. and Smulevich, G. (2002). "Spectroscopic characterization of mutations at the Phe41 position in the distal haem pocket of horseradish peroxidase C: Structural and functional consequences." Biochemical Journal **363**(3): 571-579.

Henderson, W. and McIndoe, J. S. (2005). Mass Spectrometry of Inorganic and Organometallic Compounds, John Wiley & Sons Ltd., Chichester, UK.**:** 1-21.

Henne, K. R., Kunze, K. L., Zheng, Y. M., Christmas, P., Soberman, R. J. and Rettie, A. E. (2001). "Covalent linkage of prosthetic heme to CYP4 family P450 enzymes." Biochemistry **40**(43): 12925-12931.

Henriksen, A., Schuller, D. J., Meno, K., Welinder, K. G., Smith, A. T. and Gajhede, M. (1998a). "Structural interactions between horseradish peroxidase C and the substrate

benzhydroxamic acid determined by X-ray crystallography." Biochemistry **37**(22): 8054-8060.

Henriksen, A., Smith, A. T. and Gajhede, M. (1999). "The structures of the horseradish peroxidase C-ferulic acid complex and the ternary complex with cyanide suggest how peroxidases oxidize small phenolic substrates." Journal of Biological Chemistry **274**(49): 35005-35011.

Henriksen, A., Welinder, K. G. and Gajhede, M. (1998b). "Structure of barley grain peroxidase refined at 1.9 ^{o}A… Resolution: A plant peroxidase reversibly inactivated at neutral pH." Journal of Biological Chemistry **273**(4): 2241-2248.

Higson, S. P. J. (2004). Analytical Chemistry, Oxford University PressInc., New York, USA.**:** 207-283.

Hillenkamp, F., Karas, M., Beavis, R. C. and Chait, B. T. (1991). "Matrix-assisted laser desorption/ionization mass spectrometry of biopolymers." Analytical Chemistry **63**(24).

Hiraga, S., Sasaki, K., Ito, H., Ohashi, Y. and Matsui, H. (2001). "A large family of class III plant peroxidases." Plant and Cell Physiology **42**(5): 462-468.

Hoch, U. and Ortiz de Montellano, P. R. (2001). "Covalently Linked Heme in Cytochrome P4504A Fatty Acid Hydroxylases." Journal of Biological Chemistry **276**(14): 11339-11346.

Hosoya, Y. (1960). "Turnip peroxidase. I. Purification and physiochemical properties of multiple components in turnip peroxidase." Jornal of Biochemistry **47**(3): 369-381.

Howes, B. D., Feis, A., Raimondi, L., Indiani, C. and Smulevich, G. (2001a). "The Critical Role of the Proximal Calcium Ion in the Structural Properties of Horseradish Peroxidase." Journal of Biological Chemistry **276**(44): 40704-40711.

Howes, B. D., Heering, H. A., Roberts, T. O., Schneider-Belhadadd, F., Smith, A. T. and Smulevich, G. (2001b). "Mutation of residues critical for benzohydroxamic acid binding to horseradish peroxidase isoenzyme C." Biopolymers **62**(5): 261-267.

Howes, B. D., Veitch, N. C., Smith, A. T., White, C. G. and Smulevich, G. (2001c). "Haem-linked interactions in horseradish peroxidase revealed by spectroscopic analysis of the Phe-221 Met mutant." Biochemical Journal **353**(2): 181-191.

Hunt, D. F., Shabanowitz, J., Yates, J. R., Griffin, P. R. and Zhu, N. Z. (1988). Protein sequence analysis by tandem mass spectrometry: New methods and instrumentation. The analysis of peptides and proteins by mass spectrometry. C. J. McNeal, John Wiley and Sons Ltd., Chichester, UK.**:** 151-166.

Jacquet, A., Garcia-Quintana, L., Deleersnyder, V., Fenna, R., Bollen, A. and Moguilevsky, N. (1994). "Site-directed mutagenesis of human myeloperoxidase: Further identification of residues involved in catalytic activity and heme interaction." Biochemical and Biophysical Research Communications **202**(1): 73-81.

Jantschko, W., Furtmuller, P. G., Allegra, M., Livrea, M. A., Jakopitsch, C., Regelsberger, G. and Obinger, C. (2002). "Redox intermediates of plant and mammalian peroxidases: A comparative transient-kinetic study of their reactivity toward indole derivatives." Archives of Biochemistry and Biophysics **398**(1): 12-22.

Jennings, S. P. (1998). The properties of [H42E]HRP-C*, a horseradish peroxidase variant in which histidine 42, a proton acceptor, is replaced by a glutamate. Biochemistry. Brighton, Sussex. **Ph.D.:** 149.

Job, D. and Dunford, H. B. (1976). "Substituent Effect on the Oxidation of Phenols and Aromatic Amines by Horseradish Peroxidase Compound I." European Journal of Biochemistry **66**(3): 607-614.

Johnstone, R. A. W. and Rose, M. E. (1996). Mass Spectrometry for Chemists and Biochemists Cambridge University Press, Cambridge, UK.**:** 1-112.

Karas, M. and Hillenkamp, F. (1988). "Laser desorption ionization of proteins with molecular masses exceeding 10 000 daltons." Analytical Chemistry **60**(20): 2299-2301.

Kay, E., Shannon, L. M. and Lew, J. Y. (1967). "Peroxidase isozymes from horseradish roots. II. Catalytic properties." Journal of Biological Chemistry **242**(10): 2470-2473.

Kealey, D. and Haines, P. J. (2002). Instant Notes in Analytical Chemistry, BIOS Scientific Publisher Limited, Oxford, UK**:** 109-282.

Kenten, R. H. (1955). "The oxidation of indolyl-3-acetic acid by waxpod bean root sap and peroxidase systems." Biochemical Journal **59**(1): 110-121.

Kimura, S., Kotani, T., McBride, O. W., K Umeki, K., Hirai, K., Nakayama, T. and S Ohtaki, S. (1987). "Human thyroid peroxidase: Complete cDNA and protein sequence, chromosome mapping, and identification of two alternately spliced mRNAs." Proceedings of the National Academy of Sciences of the United States of America **84**(16): 5555-5559.

Klebanoff, S. J. (1970). "Myeloperoxidase: Contribution to the microbicidal activity of intact leukocytes." Science **169**(3950): 1095-1097.

Klebanoff, S. J. (1991). Myeloperoxidase: Occurrance and biological function. Peroxidases in chemistry and biology. J. Everse, K. E. Everse and M. B. Grisham, CRC Press, Boca Rotan, Florida, USA. **1:** 1-36.

Klibanov, A. M., Berman, Z. and Alberti, B. N. (1981). "Preparative hydroxylation of aromatic compounds catalyzed by peroxidase." Journal of the American Chemical Society **103**(20): 6263-6264.

Kooter, I. M., Koehler, B. P., Moguilevsky, N., Bollen, A., Wever, R. and Johnson, M. K. (1999c). "The Met243 sulfonium ion linkage is responsible for the anomalous magnetic circular dichroism and optical spectral properties of myeloperoxidase." Journal of Biological Inorganic Chemistry **4**(6): 684-691.

Kooter, I. M., Moguilevsky, N., Bollen, A., Sijtsema, N. M., Otto, C., Dekker, H. L. and Wever, R. (1999a). "Characterization of the Asp94 and Glu242 mutants in myeloperoxidase, the residues linking the heme group via ester bonds." European Journal of Biochemistry **264**(1): 211-217.

Kooter, I. M., Moguilevsky, N., Bollen, A., Sijtsema, N. M., Otto, C. and Wever, R. (1997a). "Site-directed mutagenesis of Met243, a residue of myeloperoxidase involved in binding of the prosthetic group." Journal of Biological Inorganic Chemistry **2**(2): 191-197.

Kooter, I. M., Moguilevsky, N., Bollen, A., Van Der Veen, L. A., Otto, C., Dekker, H. L. and Wever, R. (1999b). "The sulfonium ion linkage in myeloperoxidase. Direct spectroscopic detection by isotopic labeling and effect of mutation." Journal of Biological Chemistry **274**(38): 26794-26502.

Kooter, I. M., Pierik, A. J., Merkx, M., Averill, B. A., Moguilevsky, N., Bollen, A. and Wever, R. (1997b). "Difference fourier transform infrared evidence for ester bonds linking the heme group in myeloperoxidase, lactoperoxidase, and eosinophil peroxidase [5]." Journal of the American Chemical Society **119**(47): 11542-11543.

Korfmacher, W. A. (2005). "Foundation review: Principles and applications of LC-MS in new drug discovery." Drug Discovery Today **10**(20): 1357-1367.

Kricka, L. J., Cooper, M. and Ji, X. (1996). "Synthesis and Characterization of 4-Iodophenylboronic Acid: A New Enhancer for the Horseradish Peroxidase-Catalyzed Chemiluminescent Oxidation of Luminol." Analytical Biochemistry **240**(1): 119-125.

Kricka, L. J., Stott, R. A. W. and Thorpe, G. H. G. (1988). Enhanced chemiluminescence enzyme immunoassays. Complementary Immunoassay. W. P. Collins. Chichester, J. Willey & Sons**:** 169-179.

Langbakk, B. and Flatmark, T. (1989). "Lactoperoxidase from human colostrum." Biochemical Journal **259**(3): 627-631.

Lebrun, L. A., Hoch, U. and Ortiz de Montellano, P. R. (2002a). "Autocatalytic mechanism and consequences of covalent heme attachment in the cytochrome P4504A family." Journal of Biological Chemistry **277**(15): 12755-12761.

Lebrun, L. A., Xu, F., Kroetz, D. L. and Ortiz de Montellano, P. R. (2002b). "Covalent attachment of the heme prosthetic group in the CYP4F cytochrome P450 family." Biochemistry **41**(18): 5931-5937.

Lewis, J. K., Wei, J. and Siuzdak, G. (2000). Matrix-assisted Laser Desorption/Ionization Mass Spectrometry in Peptide and Protein Analysis Encyclopedia of Analytical Chemistry. R. A. Meyers, John Wiley & Sons Ltd, Chichester, UK.**:** 5880–5894

Limburg, J., LeBrun, L. A. and Ortiz de Montellano, P. R. (2005). "The $P450_{cam}$ G248E mutant covalently binds its prosthetic heme group." Biochemistry **44**(10): 4091-4099.

Lindsay, S. (1992). High Performance Liquid Chromatography. J. Barnes, Joun Wiley & Sons Ltd., Chichester, UK**:** 43-62.

Loschen, G., Azzi, A., Richter, C. and Flohe, L. (1974). "Superoxide radicals as precursors of mitochondrial hydrogen peroxide." FEBS Letters **42**(1): 68-72.

Lundberg, K. S., Shoemaker, D. D., Adams, M. W. W., Short, J. M., Sorge, J. A. and Mathur, E. J. (1991). "High-fidelity amplification using a thermostable DNA polymerase isolated from Pyrococcus furiosus." Gene **108**(1): 1-6.

Lundqvist, H. and Dahlgren, C. (1996). "Isoluminol-enhanced chemiluminescence: A sensitive method to study the release of superoxide anion from human neutrophils." Free Radical Biology and Medicine **20**(6): 785-792.

Mader, M. and Fussl, R. (1982). "Role of Peroxidase in Lignification of Tobacco Cells." Plant Physiological **70**: 1132-1134.

Maidan, R. and Heller, A. (1992). "Elimination of electrooxidizable interferant in glucose electrodes." Jornal of the American Chemical Society **113**(23): 9003-9004.

Marquez, L. A. and Dunford, H. B. (1995). "Kinetics of oxidation of tyrosine and dityrosine by myeloperoxidase compounds I and II: Implications for lipoprotein peroxidation studies." Journal of Biological Chemistry **270**(51): 30434-30440.

Marquez, L. A., Huang, J. T. and Brian Dunford, H. (1994). "Spectral and kinetic studies on the formation of myeloperoxidase compounds I and II: Roles of hydrogen peroxide and superoxide." Biochemistry **33**(6): 1447-1454.

McCord, J. M. and Fridovich, I. (1968). "The reduction of cytochrome c by milk xanthine oxidase." Journal of Biological Chemistry **243**(21): 5753-5760.

Meno, K., Jennings, S., Smith, A. T., Henriksen, A. and Gajhede, M. (2002). "Structural analysis of the two horseradish peroxidase catalytic residue variants H42E and R38S/H42E: implications for the catalytic cycle." Acta Crystallogr D Biol Crystallogr **58**(2): 1803-1812.

Metcalfe, C. L., Daltrop, O., Ferguson, S. J. and Raven, E. L. (2007). "Tuning the formation of a covalent haem-protein link by selection of reductive or oxidative conditions as exemplified by ascorbate peroxidase." Biochemical Journal **408**(3): 355-361.

Metcalfe, C. L., Ott, M., Patel, N., Singh, K., Mistry, S. C., Goff, H. M. and Raven, E. L. (2004). "Autocatalytic formation of green heme: Evidence for H_2O_2-dependent formation of a covalent methionine-heme linkage in ascorbate peroxidase." Journal of the American Chemical Society **126**(49): 16242-16248.

Meunier, B. (1991). *N*- and *O*-Demethylations catalyzed by peroxidases. Peroxidases in chemistry and biology. J. Everse, k. Everse and M. B. Grisham, CRC Press Inc., Boca Raton, USA. **2:** 201-217.

Michaelis, L. and Menten, M. (1913). "Die Kinetik der Invertinwirkung." Biochem. Z.(49): 333-369.

Milne, G. W. A. (1991). The applications of Mass spectrometry to proplems in medicine and biochemistry. Mass spectrometry: techniques and applications. G. W. A. Milne, Wiley-Interscience, New York, USA.**:** 327-371.

Mo, W. and Karger, B. L. (2002). "Analytical aspects of mass spectrometry and proteomics." Current Opinion in Chemical Biology **6**(5): 666-675.

Montaudo, G., Montaudo, M. S. and Samperi, F. (2002). Matrix-Assisted Laser Desorption Ionization/Mass Spectrometry of Polymers (MALDI-MS). Mass Spectrometry of Polymers. G. Montaudo and R. P. Lattimer, CRC Press, New York, USA.**:** 428-530.

Morishima, I. (1978). "Proton nuclear magnetic resonance spectra of compounds I and II of horseradish peroxidase." Biochemistry **17**(21): 4384-4388.

Mousty, C., Therias, S., Aboab, B., Molinie, P., Queignec, M., Leone, P., Rossignol, C. and Palvadeau, P. (1997). "Single crystal structure refinement and physical characterization of 2,2'-azinobis(3-ethylbenzothiazoline-6-sulfonate) diammonium salt (ABTS)." New journal of chemistry **21**(12): 1321-1330

Munir, I. Z. and Dordick, J. S. (2000). "Soybean peroxidase as an effective bromination catalyst." Enzyme and Microbial Technology **26**(5-6): 337-341.

Nagano, S., Tanaka, M., Ishimori, K., Watanabe, Y. and Morishima, I. (1996). "Catalytic Roles of the Distal Site Asparagine-Histidine Couple in Peroxidases." Biochemistry **35**(45): 14251-14258.

Nagano, S., Tanaka, M., Watanabe, Y. and Morishima, I. (1995). "Putative hydrogen bond network in the heme distal site of horseradish peroxidase." Biochemical and Biophysical Research Communications **207**(1): 417-423.

Nakayama, T. and Amachi, T. (1999). "Fungal peroxidase: Its structure, function, and application." Journal of Molecular Catalysis - B Enzymatic **6**(3): 185-198.

Nelson, D. P. and Kiesow, L. A. (1972). "Enthalpy of decomposition of hydrogen peroxide by catalase at 25 °C (with molar extinction coefficients of H_2O_2 solutions in the UV)." Analytical Biochemistry **49**(2): 474-478.

Newmyer, S. L. and Ortiz de Montellano, P. R. O. (1995). "Horseradish peroxidase His-42 Ala, His-42 Val, and Phe-41 Ala mutants. Histidine catalysis and control of substrate access to the heme iron." Journal of Biological Chemistry **270**(33): 19430-19438.

Newmyer, S. L. and Ortiz de Montellano, P. R. O. (1996a). "Rescue of the catalytic activity of an H42A mutant of horseradish peroxidase by exogenous imidazoles." Journal of Biological Chemistry **271**(25): 14891-14896.

Newmyer, S. L., Sun, J., Loehr, T. M. and Ortiz de Montellano, P. R. (1996b). "Rescue of the horseradish peroxidase His-170 Ala mutant activity by imidazole: Importance of proximal ligand tethering." Biochemistry **35**(39): 12788-12795.

Nishikawa, T., Rapoport, B. and McLachlan, S. M. (1994). "Exclusion of two major areas on thyroid peroxidase from the immunodominant region containing the conformational epitopes recognized by human autoantibodies." Journal of Clinical Endocrinology and Metabolism **79**(6): 1648-1654.

Olsson, I., Persson, A. M., Stromberg, K., Winqvist, I., Tai, P. C. and Spry, C. J. (1985). "Purification of eosinophil peroxidase and studies of biosynthesis and processing in human marrow cells." Blood **66**(5): 1143-1148.

Ortiz de Montellano, P. R. (1992). "Catalytic Sites of Hemoprotein Peroxidases." Annual Review of Pharmacology and Toxicology **32**(1): 89-107.

Ortiz de Montellano, P. R. and Grab, L. A. (1987). "Cooxidation of styrene by horseradish peroxidase and phenols: A biochemical model for protein-mediated cooxidation." Biochemistry **26**(17): 5310-5314.

Oxvig, C., Thomsen, A. R., Overgaard, M. T., Sorensen, E. S., Hojrup, P., Bjerrum, M. J., Gleich, G. J. and Sottrup-Jensen, L. (1999). "Biochemical Evidence for Heme Linkage through Esters with Asp-93 and Glu-241 in Human Eosinophil Peroxidase." Journal of Biological Chemistry **274**(24): 16953-16958.

Ozaki, S. I. and Ortiz de Montellano, P. R. (1995). "Molecular engineering of horseradish peroxidase: Thioether sulfoxidation and styrene epoxidation by Phe-41 leucine and threonine mutants." Journal of the American Chemical Society **117**(27): 7056-7064.

Paul, K. G. (1958). "Die Isolierung von Meerrettichperoxydase." Acta. Chem. Scand. **12**: 1312-1318.

Peter, K. V. (2004). Handbook of Herbs and Spices, CRC Press LLC, Boca Raton, USA. **2:** 69-74.

Pipirou, Z., Bottrill, A. R., Metcalfe, C. M., Mistry, S. C., Badyal, S. K., Rawlings, B. J. and Raven, E. L. (2007a). "Autocatalytic formation of a covalent link between tryptophan 41 and the heme in ascorbate peroxidase." Biochemistry **46**(8): 2174-2180.

Pipirou, Z., Bottrill, A. R., Svistunenko, D. A., Efimov, I., Basran, J., Mistry, S. C., Cooper, C. E. and Raven, E. L. (2007b). "The reactivity of heme in biological systems: Autocatalytic formation of both tyrosine-heme and tryptophan-heme covalent links in a single protein architecture." Biochemistry **46**(46): 13269-13278.

Pipirou, Z., Guallar, V., Basran, J., Metcalfe, C. L., Murphy, E. J., Bottrill, A. R., Mistry, S. C. and Raven, E. L. (2009). "Peroxide-dependent formation of a covalent link between Trp51 and the heme in cytochrome c peroxidase." Biochemistry **48**(16): 3593-3599.

Polce, M. J. and Wesdemiotis, C. (2002). Introduction to mass spectrometry of polymers. Mass Spectrometry of Polymers. G. Montaudo and R. P. Lattimer, CRC Press, New York, USA.**:** 1-40.

Poulos, T. L. and Kraut, J. (1980). "The stereochemistry of peroxidase catalysis." Journal of Biological Chemistry **255**(17): 8199-8205.

Prokai, L. (2002). Electrospray Ionization (ESI-MS) and On-Line Liquid Chromatography/Mass Spectrometry (LC/MS). Mass Spectrometry of Polymers. G. Montaudo and R. P. Lattimer, CRC Press, New York, USA.**:** 159-190.

Pryde, A. and Gilbert, M. T. (1979). Applications of high performance liquid chromatography Chapman and Hall Ltd., London, UK 13-23.

Puppo, A., Rigaud, J., Job, D., Ricard, J. and Zeba, B. (1980). "Peroxidase content of soybean root nodules." Biochimica et Biophysica Acta **614**(2): 303-312.

Radi, R., Cosgrove, T. P., Beckman, J. S. and Freeman, B. A. (1993). "Peroxynitrite-induced luminol chemiluminescence." Biochemical Journal **290**(15): 51-57.

Rae, T. D. and Goff, H. M. (1996). "Lactoperoxidase heme structure characterized by paramagnetic proton NMR spectroscopy." Journal of the American Chemical Society **118**(8): 2103-2104.

Rajagopalan, K. V., Fridovich, I. and Handler, P. (1962). "Hepatic aldehyde oxidase. I. Purification and properties." The Journal of Biological Chemistry **237**: 922-928.

Reeder, B. J., Svistunenko, D. A., Sharpe, M. A. and Wilson, M. T. (2002). "Characteristics and mechanism of formation of peroxide-induced heme to protein cross-linking in myoglobin." Biochemistry **41**(1): 367-375.

Roboz, J. (1968). Introduction to Mass Spectrometry Instrumentation and Techniques John Wiley & Sons Inc., New York, USA.**:** 115-148.

Rodriguez-Lopez, J. N., Smith, A. T. and Thorneley, R. N. F. (1996a). "Recombinant horseradish peroxidase isoenzyme C: the effect of distal haem cavity mutations (His42→Leu and Arg38→Leu) on compound I formation and substrate binding." Journal of Biological Inorganic Chemistry **1**(2): 136-142.

Rodriguez-Lopez, J. N., Smith, A. T. and Thorneley, R. N. F. (1996b). "Role of arginine 38 in horseradish peroxidase: A critical residue for substrate binding and catalysis." Journal of Biological Chemistry **271**(8): 4023-4030.

Roepstorff, P. (1997). "Mass spectrometry in protein studies from genome to function." Current Opinion in Biotechnology **8**(1): 6-13.

Sakamaki, K., Tomonaga, M., Tsukui, K. and Nagata, S. (1989). "Molecular cloning and characterization of a chromosomal gene for human eosinophil peroxidase." Journal of Biological Chemistry **264**(28): 16828-16836.

Sambrook, J., Fritsch, E. F. and Maniiaties, T. (1989). "Molecular Cloning: A Laboratory Manual." Cold Sold Harbour Laboratory Press(USA).

Savenkova, M. I., Kuo, J. M. and Ortiz de Montellano, P. R. (1998). "Improvement of Peroxygenase Activity by Relocation of a Catalytic Histidine within the Active Site of Horseradish Peroxidase." Biochemistry **37**(30): 10828-10836.

Savenkova, M. I., Newmyer, S. L. and Ortiz de Montellano, P. R. (1996). "Rescue of His-42 Ala horseradish peroxidase by a Phe-41 His mutation. Engineering of a surrogate catalytic histidine." Journal of Biological Chemistry **271**(40): 24598-24603.

Schejter, A., Lanir, A. and Epstein, N. (1976). "Binding of hydrogen donors to horseradish peroxidase: a spectroscopic study." Archives of Biochemistry and Biophysics **174**(1): 36-44.

Schonbaum, G. R. (1973). "New complexes of peroxidases with hydroxamic acids, hydrazides, and amides." Journal of Biological Chemistry **248**(2): 502-511.

Schuller, D. J., Ban, N., Van Huystee, R. B., McPherson, A. and Poulos, T. L. (1996). "The crystal structure of peanut peroxidase." Structure **4**(3): 311-321.

Scott, S. L., Chen, W. J., Bakac, A. and Espenson, J. H. (1993). "Spectroscopic parameters, electrode potentials, acid ionization constants, and electron exchange rates of the 2,2'-azinobis(3-ethylbenzothiazoline-6-sulfonate) radicals and ions." The Journal of Physical Chemistry **97**(25): 6710-6714.

Shannon, L. M., Kay, E. and Lew, J. Y. (1966). "Peroxidase isozymes from horseradish roots. I. Isolation and physical properties." Journal of Biological Chemistry **241**(9): 2166-2172.

Shin, J. H. C., Shannon, L. M., Kay, E. and Lew, J. Y. (1971). "Peroxidase isozymes from horseradish roots. IV. Structural realationships." The Journal of Biological Chemistry **246**(14): 4546-4551.

Shiro, Y., Kurono, M. and Morishima, I. (1986). "Presence of endogenous calcium ion and its functional and structural regulation in horseradish peroxidase." Journal of Biological Chemistry **261**(20): 9382-9390.

Sievers, G. (1980). "Structure of milk lactoperoxidase. A study using circular dichroism and difference absorption spectroscopy." Biochimica et Biophysica Acta **624**(1): 249-259.

Singh, A. K., Singh, N., Sharma, S., Singh, S. B., Kaur, P., Bhushan, A., Srinivasan, A. and Singh, T. P. (2008). "Crystal Structure of Lactoperoxidase at 2.4 Å Resolution." Journal of Molecular Biology **376**(4): 1060-1075.

Skoog, D. A., Holler, F. J. and Nieman, T. A. (1998). Principles of Instrumental Analysis, Saunders College Publishing/Harcourt Brace College Publishers, Philadelphia, USA**:** 674-767.

Skoog, D. A., West, D. M. and Holler, F. J. (1996). Fundamentals of Analytical Chemistry, Saunders College Publishing, Philadelphia, USA**:** 660-724.

Smith, A. T., Sanders, S. A., Sampson, C., Bray, R. C., Burke, J. F. and Thorneley, R. N. F. (1993). Folding and activation of recombinant horseradish peroxidase from E.Coli and analysis of protein variants by side-directed mutagenesis. Plant Peroxidases, Biochemistry and Physiology, III International symposium proceedings. K. G. Welinder, S. K. Rasmussen, C. Penel and H. Greppin. University of Geneva, Geneva, Switzerland.**:** 159-168.

Smith, A. T., Sanders, S. A., Thorneley, R. N. F., Burke, J. F. and Bray, R. R. C. (1992). "Characterisation of a haem active-site mutant of horseradish peroxidase, Phe41 Val, with altered reactivity towards hydrogen peroxide and reducing substrates." European Journal of Biochemistry **207**(2): 507-519.

Smith, A. T., Santama, N., Dacey, S., Edwards, M., Bray, R. C., Thorneley, R. N. F. and Burke, J. F. (1990). "Expression of a synthetic gene for horseradish peroxidase C in Escherichia coli and folding and activation of the recombinant enzyme with Ca^{2+} and heme." Journal of Biological Chemistry **265**(22): 13335-13343.

Smith, A. T. and Veitch, N. C. (1998). "Substrate binding and catalysis in heme peroxidases." Current Opinion in Chemical Biology **2**(2): 269-278.

Smulevich, G., English, A. M., Mantini, A. R. and Marzocchil, M. P. (1991). "Resonance Raman Investigation of Ferric Iron in Horseradish Peroxidase and Its Aromatic Donor Complexes at Room and Low Temperatures." Biochemistry **30**: 772-779.

Smulevich, G., Paoli, M., Burke, J. F., Sanders, S. A., Thorneley, R. N. F. and Smith, A. T. (1994). "Characterization of recombinant horseradish peroxidase C and three site-directed mutants, F41V, F41W, and R38K, by resonance Raman spectroscopy." Biochemistry **33**(23): 7398-7407.

Sundaramoorthy, M., Terner, J. and Poulos, T. L. (1995). "The crystal structure of chloroperoxidase: A heme peroxidase-cytochrome P450 functional hybrid." structure **3**(12): 1367-1377.

Suriano, G., Watanabe, S., Ghibaudi, E. M., Bollen, A., Pia Ferrari, R. and Moguilevsky, N. (2001). "Glu375Gln and Asp225Val mutants: about the nature of the covalent linkages between heme group and apo-Protein in bovine lactoperoxidase." Bioorganic and Medicinal Chemistry Letters **11**(21): 2827-2831.

Tanaka, M., Ishimori, K. and Morishima, I. (1996). "The distal glutamic acid as an acid-base catalyst in the distal site of horseradish peroxidase." Biochemical and Biophysical Research Communications **227**(2): 393-399.

Tanaka, M., Ishimori, K. and Morishima, I. (1998). "Structural roles of the highly conserved Glu residue in the heme distal site of peroxidases." Biochemistry **37**(8): 2629-2638.

Tanaka, M., Ishimori, K. and Morishima, I. (1999). "Luminol activity of horseradish peroxidase mutants mimicking a proposed binding site for luminol in Arthromyces ramosus peroxidase." Biochemistry **38**(32): 10463-10473.

Tanaka, M., Nagano, S., Ishimori, K. and Morishima, I. (1997). "Hydrogen Bond Network in the Distal Site of Peroxidases: Spectroscopic Properties of Asn70-Asp Horseradish Peroxidase Mutant." Biochemistry **36**(32): 9791-9798.

Taurog, A. (1970). "Thyroid peroxidase and thyroxine biosynthesis." Recent Progress in Hormone Research **26**: 189-247.

Taurog, A. (1999). "Molecular evolution of thyroid peroxidase." Biochimie **81**(5): 557-562.

Thomas, E. L., Bozeman, P. M. and Learn, D. B. (1991). Lactoperoxidase: structure and catalytic properties. Peroxidases in chemistry and biology. J. Everse, K. E. Everse and M. B. Grisham, CRC Press, Boca Raton, Florida, USA. **1:** 123-142.

Thorpe, G. H. G. and Kricka, L. J. (1986). Enhanced chemiluminescent reactions catalyzed by horseradish peroxidase. Methods in Enzymology. M. A. Deluca and W. D. McElory. Orlando, Florida, Academic Press **133:** 331-353.

Tijssen, P. and Kurstak, E. (1984). "Highly efficient and simple methods for the preparation of peroxidase and active peroxidase-antibody conjugates for enzyme immunoassays." Analytical Biochemistry **136**(2): 451-457.

Ueda, T., Sakamaki, K., Kuroki, T., Yano, I. and Nagata, S. (1997). "Molecular Cloning and Characterization of the Chromosomal Gene for Human Lactoperoxidase." European Journal of Biochemistry **243**(1-2): 32-41.

Van Dalen, C. J., Whitehouse, M. W., Winterbourn, C. C. and Kettle, A. J. (1997). "Thiocyanate and chloride as competing substrates for myeloperoxidase." Biochemical Journal **327**(2): 487-492.

Veitch, N. C. (2004). "Horseradish peroxidase: A modern view of a classic enzyme." Phytochemistry **65**(3): 249-259.

Veitch, N. C., Gao, Y., Smith, A. T. and White, C. G. (1997). "Identification of a critical phenylalanine residue in horseradish peroxidase, Phe179, by site-directed mutagenesis and ^{1}H-NMR: Implications for complex formation with aromatic donor molecules." Biochemistry **36**(48): 14751-14761.

Veitch, N. C., Gilfoyle, D. J., White, C. G. and Smith, A. T. (1996). Plant Peroxidases: Biochemistry and Physiology. C. Obinger, U. Burner, E. R., C. Penel and H. Greppin University of Geneva: Geneva, Switzerland**:** 1-6.

Veitch, N. C. and Smith, A. T. (2001). Horseradish peroxidase. Advances in Inorganic Chemistry. A. G. Sykes. London, UK., Academic Press. **51:** 107-162.

Veitch, N. C. and Williams, R. J. P. (1995). "The use of methyl-substituted benzhydroxamic acids as structural probes of peroxidase substrate binding." European Journal of Biochemistry **229**(3): 629-640.

Wada, N., Kinoshita, S., Matsuo, M., Amako, K., Miyake, C. and Asada, K. (1998). "Purification and molecular properties of ascorbate peroxidase from bovine eye." Biochemical and Biophysical Research Communications **242**(2): 256-261.

Wang, R. Y. (2007). Rapid Scan, Stopped-Flow Kinetics. Applications of physical methods to inorganic and bioinorganic chemistry. R. A. Scott and C. M. Lukehart. Chichester, Wiley-Interscience**:** 469-488.

Welinder, K. G. (1976). "Covalent structure of the glycoprotein horseradish peroxidase (EC 1.11.1.7)." FEBS Letters **72**(1): 19-23.

Welinder, K. G. (1979). "Amino acid sequence studies of horseradish peroxidase. Amino and carboxyl termini, cyanogen bromide and tryptic fragments, the complete sequence, and some structural characteristics of horseradish peroxidase C." European Journal of Biochemistry **96**(3): 483-502.

Welinder, K. G. (1991). The plant peroxidase superfamily. Biochemical, Molecular and Physiological Aspects of Plant Peroxidases. J. Lobarzewski, H. Greppin, C. Penel and T. Gaspar, University M. Curie-Sklodowska, Lublin, Poland and University of Geneva, Switzerland.**:** 3-13.

Welinder, K. G. (1992). "Superfamily of plant, fungal and bacterial peroxidases." Current Opinion in Structural Biology **2**(3): 388-393.

Welinder, K. G., Mauro, J. M. and Norskov-Lauritsen, L. (1992). "Structure of plant and fungal peroxidases." Biochemical Society Transactions **20**(2): 337-340.

Welinder, K. G. and Mazza, G. (1975). "Similarities and differences of five peroxidases from turnip and horseradish. Peptide mapping studies on glycoproteins." European Journal of Biochemistry **57**(2): 415-424.

Wever, R. and Plat, H. (1981). "Spectral properties of myeloperoxidase and its ligand complexes." Biochimica et Biophysica Acta - Enzymology **661**(2): 235-239.

Wolfenden, B. S. and Willson, R. L. (1982). "Radical-cations as reference chromogens in kinetic studies of ono-electron transfer reactions: pulse radiolysis studies of 2,2[prime or minute]-azinobis-(3-ethylbenzthiazoline-6-sulphonate)." Journal of the Chemical Society, Perkin Transactions 2(7): 805-812.

Wu, N. C. and Schultz, J. (1975). "The prosthetic group of myeloperoxidase." FEBS Letters **60**(1): 141-144.

Yamashita, M. and Fenn, J. B. (1984). "Electrospray ion source. Another variation on the free-jet theme." Journal of Physical Chemistry **88**(20): 4451-4459.

Yamazaki, I. (1974). Molecular mechanisms of oxygen activation. O. Hayaishi, Academic Press, New York, USA**:** 535-558.

Zederbauer, M., Furtmuller, P. G., Bellei, M., Stampler, J., Jakopitsch, C., Battistuzzi, G., Moguilevsky, N. and Obinger, C. (2007a). "Disruption of the aspartate to heme ester linkage in human myeloperoxidase: Impact on ligand binding, redox chemistry, and interconversion of redox intermediates." Journal of Biological Chemistry **282**(23): 17041-17052.

Zederbauer, M., Furtmuller, P. G., Brogioni, S., Jakopitsch, C., Smulevich, G. and Obinger, C. (2007b). "Heme to protein linkages in mammalian peroxidases: Impact on spectroscopic, redox and catalytic properties." Natural Product Reports **24**(3): 571-584.

Zederbauer, M., Jantschko, W., Neugschwandtner, K., Jakopitsch, C., Moguilevsky, N., Obinger, C. and Furtmuller, P. G. (2005). "Role of the covalent glutamic acid 242-heme linkage in the formation and reactivity of redox intermediates of human myeloperoxidase." Biochemistry **44**(17): 6482-6491.

Zeng, J. and Fenna, R. E. (1992). "X-ray crystal structure of canine myeloperoxidase at 3 Å resolution." Journal of Molecular Biology **226**(1): 185-207.

Zhu, M., Huang, X. and Shen, H. (2001). "Aromatic azo compounds as spectrophotometric kinetic assay substrate for HRP." Talanta **53**(5): 927-935.